Project no.:	**637268**
Project full title:	**Robust Internal Thermal Insulation of Historic Buildings**
Project Acronym:	**RIBuild**
Deliverable no.:	**D2.2 (not yet approved by the European Union)**
Title of the deliverable:	**Threshold values for failure, linked to types of building structures and failure modes**

Contractual Date of Delivery to the EC	**31.12.2018 (M50)**
Actual Date of Delivery to the EC	**29.03.2019 (M51)**
Organisation name of lead contractor for this deliverable	**RISE**
Authors	***Pernilla Johansson (RISE), Lukas Lång (RISE), Carl-Magnus Capener (RISE), Eva Møller (AAU), Enrico Quagliarini (UNIVPM), Marco D'Orazio (UNIVPM), Andrea Gianangeli (UNIVPM), Hans Janssen (KUL), Chi Feng (KUL), Jelle Langmans (KUL), Nickolaj Feldt Jensen (DTU), Ernst Jan de Place Hansen (AAU), Ruut Peuhkuri (AAU), Tessa Kvist Hansen (AAU)***
Participants	***AAU, DTU, KUL, RISE, UNIVPM***
Internal reviewers	***Peggy Freudenberg (TUD), Enrico Quagliarini (UNIVPM), Ernst Jan de Place Hansen (AAU)***
Work package contributing to the deliverable	***WP2.***
Nature	**R**
Version	**1.0**
Total number of pages	**155**
Start date of project	**01.01.2015**
Duration of project	**31.12.2019**

Abstract:

This report comprises a study of material threshold values, failure modes and related failure prediction models to enable an evaluation of adding internal insulation in historic brick buildings. Threshold values and prediction models have been investigated both within literature and through laboratory study, by for instance comparing prediction models to real field results and by testing threshold values in laboratory. The aim of this report is to find threshold values and suitable and reliable prediction models to be included in the decision guidelines and the web tool, which are the final outcomes of the RIBuild project. Failure modes included in the report are mould growth on building materials, rot and wood decay, frost damage and discoloration of facades.

Keyword list: mould, frost, rot, fungi, algae, cyanobacteria, threshold values, failure modes, predictive models, laboratory testing

Table of Contents

Abbreviations

AAU	Aalborg University Copenhagen
DTU	Technical University of Denmark
HAM	Heat, Air and Moisture
KUL	Katholieke Universiteit Leuven
RH	Relative Humidity [%]
RH_{crit}	Critical Relative Humidity for mould growth [%]
RISE	Research Institutes of Sweden
TUD	Technische Universität Dresden
UNIVPM	Università Politecnica delle Marche
WP	Work Package

1 Executive Summary

This deliverable presents the findings on threshold values for failure within RIBuild, linked to types of building structures and failure modes, as defined in WP1. Threshold values for failure will be very important to develop decision guidelines for eligible renovation measures (WP6).

Failure in the construction related to overrun of a limit state are related to those occurring as a result of changed hygro-thermal conditions in the structures as a result of introducing internal insulation. The project has identified and investigated the following failure modes and concluded on;

Mould
Threshold values for mould has been derived as part of the project for a large number of products/materials that will be used in WP6 for the guidelines. Several mould models have been evaluated and the conclusion is not to overestimate the results from dynamic models since they may underestimate the risk and produce varying results. The PJ-model, however, shows reliable results and will be modified for further use in WP6. Mould is important to consider when evaluating materials containing organic substance within the wall and on interior surfaces, but also joints connecting to the exterior wall.

Rot
In general, the threshold values are higher than for those for mould growth. Therefore, although the consequences of rot attack are severe, the threshold values for mould growth is more likely to be the limiting factor in the critical positions where mould is not accepted. Examples of rot threshold values are presented related to fungal species. Rot is especially important to evaluate for beam-ends in the exterior wall. Several models have been evaluated and RIBuild has selected the most suitable prediction model for evaluation of performance by relative comparisons, since the model has in more than one case shown to generate too conservative results with regard to mass loss.

Frost
Three conditions must be fulfilled for frost damage to occur; sufficient wetness, phase change in the material, and the material must be sensitive to frost. Frost damage can typically occur at the façade surface if the material is sensitive to frost and exceeds its critical saturation degree due to changes in hygrothermal conditions. In order to evaluate material sensitivity to frost, a high degree of experimental effort is required. Existing frost damage models have been investigated and laboratory experiments on brick frost sensitivity has been performed. However, to this date, no frost model exist that can translate the exceedance of the first two parameters to an initiation of mechanical stress and strain, to be weighed against the frost damage sensitivity of the material.

Algae
Algae can become an aesthetical problem on the façade surface. Conducted laboratory studies on algae growth shows that important and limiting material parameters are commonly porosity and roughness. Free water must be available, too. That is, from a conservative standpoint, a water content greater than that corresponding to about RH=98% is needed. The laboratory studies also show that the developed model on algae prediction is working, although at this stage only for constant conditions.

2 Introduction

Before deciding whether external walls in a historic building are eligible for internal insulation it is necessary to point out;

- the critical areas in the construction (based on the survey and screening performed in WP1)
- what can go wrong when installing internal insulation (failure modes based partly on WP1)
- the criticality at failure (related to risk assessment, as part of WP4)

This deliverable presents the findings on threshold values for failure within RIBuild, linked to types of building structures and failure modes. Threshold values for failure will be very important to develop decision guidelines for eligible renovation measures (WP6). Threshold values for failures related to the specific building materials need to be translated to threshold values for specific compositions of external walls as the inter-relation between the different building materials in external walls and the adjoining elements is one of the most important factors that determines whether internal insulation is possible and under which conditions. Threshold values for failure for specific composition of external walls need further to be developed into threshold values for the building as such, e.g. internal RH and temperature values, induced by the insulation intervention, as it often is difficult or even impossible to measure the conditions in the wall itself. Threshold values also need to be linked to types of building structure and thermal bridges.

Failure in the construction related to overrun of a limit state are related to those occurring as a result of changed hygrothermal conditions in the structures as a result of introducing internal insulation, given that internal insulation may increase the moisture content in the wall structure. All identified failure modes are dependent on moisture; it is the access to and level of moisture that controls the failure modes. Failure is for instance expressed as freeze-thaw damage of stone and brick used for the external wall or mould growth or rot in wooden parts of a suspended floor that rest on the inner part of the external wall.

Outline of deliverable structure

Section 3 describes the identified failure modes, which materials that are at risk for each failure mode and what part of the building that is at risk for exposure to the failure mode.

Section 4 describes threshold values from literature; how they can be derived by laboratory studies and gives a state-of-the-art on what is published to date.

Section 5 gives an overview of models for predicting failure mode.

Section 6 describes the laboratory testing of threshold values conducted within RIBuild on mould, frost and algae.

Section 7 presents the evaluation of and advance on existing and new prediction models. It also gives recommendations on the use of models and their strengths and weaknesses.

Sections 8 and 9 presents the deliverable conclusion and recommendations and give an outline for recommended future work.

The Appendices give references for algae, cyanobacterial and mould growth, presents the detailed outcome of a round-robin comparison on dynamic and static mould models with field results. The

appendices also give an introduction to salt in walls and the failure mode salt efflorescence, in particular related to the occurrence of this in Denmark. Finally, Appendix 5 presents early results from a study conducted by DTU on control and prevention of mould growth for post-insulation: Laboratory based investigations of the materials' water activity and pH related to mould growth.

3 Failure modes

The identified failure modes to study were mould growth within the building structure (excluding the outer facades), rot, discoloration of facades due to microbial growth and frost. At the beginning of the project, it was discussed if also salt efflorescence would count as a failure mode. It was decided to be excluded, since salt complicates DELPHIN simulations by affecting the moisture content. In addition, it was not possible to get a clear picture of the number of damages related to presence of salt or locate it to specific types of buildings. Therefore, to be on the safe side, it was decided not to recommend the use of internal insulation if visual inspection could detect (unwanted) presence of salt, which is also described in the WP6 web tool. However, it is of interest to summarise the knowledge about this phenomenon. In Appendix 4 a report on this is presented.

In this section of the report, the different failure modes are described, which materials that are at risk for each failure mode and which part of the building that is at risk for exposure to the failure mode.

The positions for where the failure modes take place are illustrated in Figure 3.1.

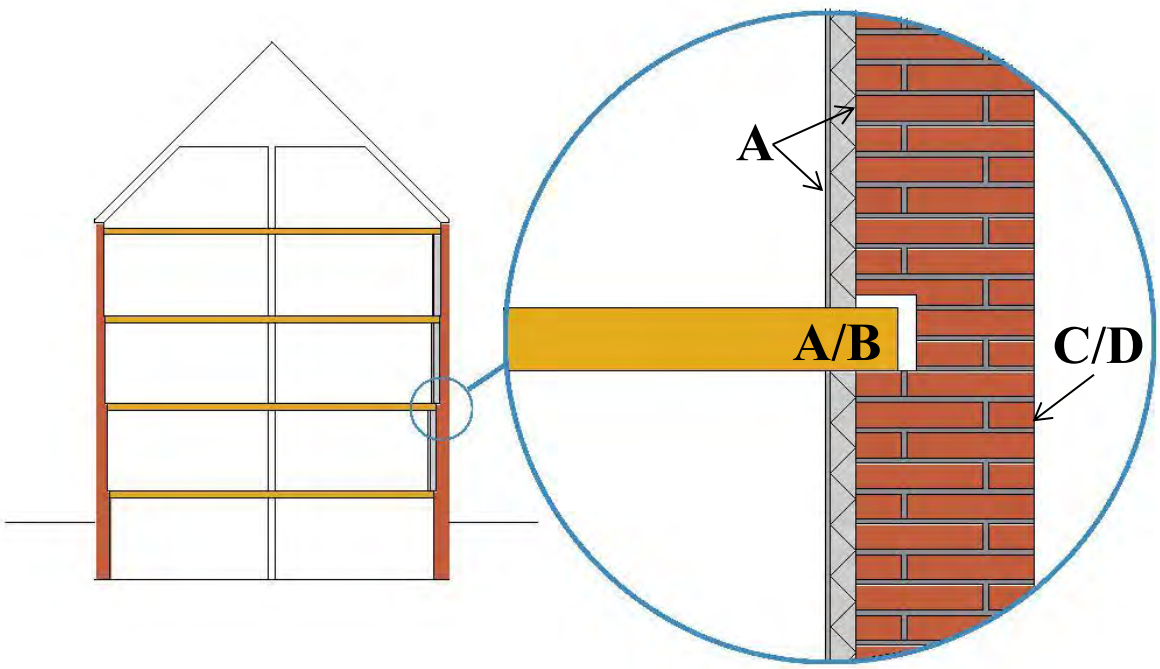

Figure 3.1: Failure modes in the construction. (A) Mould at the surface and within the construction, (B) Rot, (C) Frost, (D) Discolouration by fungi and algae

3.1 Mould within the building

3.1.1 Introduction

Mould is microscopic fungi, belonging to different biological groups and consisting of many species. In some respects, they share common traits. They live on the surfaces of materials, use easily assimilated nutrients for growth and produce airborne spores.

Mould fungi are widely spread across different environments on the Earth and there is no natural place where air and materials are free from spores. When favourable conditions are present, the spores (also called conidia) will germinate and a small germ tube will develop; if the favourable conditions prevail, a hypha will be formed. A hypha is a tubular cell structure, which extends at the tip. By continuously branching during growth, the hyphae form a mycelium. Eventually, specialized structures (conidiophores) develop from the hyphae and from them; the spores are produced and dispersed. A schematic illustration of the life cycle is presented in Figure 3.2.

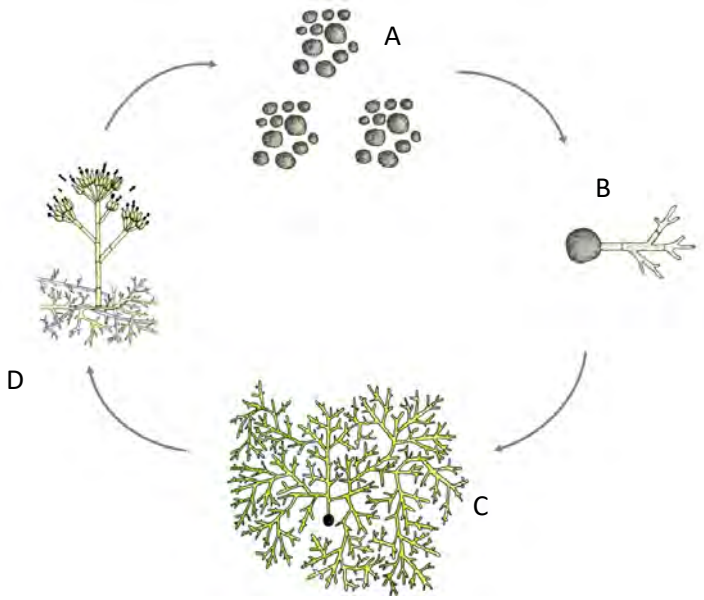

Figure 3.2:Schematic overview of the asexual life cycle of a typical mould fungus. When suitable conditions are present, spores (A) at the material surface germinate into a germ tube that grows into a hypha (B), which then extends and branches into a mycelium (C). From some of the hyphae, conidiophores are developed (D) and from them, masses of spores are released into the air. Illustration: Agneta Olsson- Jonsson

The main environmental factors affecting mould growth in building structures are humidity and temperature; moisture being the crucial factor. Suitable conditions for the growth and reproduction of different mould fungi vary. Some thrive at relatively low relative humidity (RH = 75%), while most fungi require higher values of RH (90-95 %) for optimal growth in room temperature. Different building materials vary in their susceptibility to mould growth; some can withstand high moisture content better than others.

Mould growth is the result of a complex interaction between all these factors; environmental factors and duration, material properties and the characteristics of mould fungi present (Blackburn 2000). To prevent mould growth in buildings, these interactions must be considered during the design, construction and maintenance of a building.

Adding internal insulation to the building façade will make the original wall structure colder, reducing the drying potential. This in turn may increase RH locally and thereby the risk for mould growth and

condensation. An increased RH level increases the risk for mould growth on existing, historical materials and on new materials. The risk of high moisture levels may increase further if the internal insulation admits air leakage of humid indoor air into the wall construction, especially if the ventilation is unbalanced (internal overpressure). In time, problems with rot may also develop if access to moisture increases (see Section 3.2).

Mould in buildings may have negative effect on the perceived indoor environment, for example, by the production of odorous substances. In addition, human health may be adversely affected due to the spread of particles, toxins and volatile organic compounds from the mould fungi to the indoor air. The costs associated with this growth, i.e. due to renovation, are substantial. Therefore, both economy and health can be used as arguments for reducing the risk of mould growth in buildings.

3.1.2 Material at risk for mould growth and critical position in the building envelope

For mould to grow on a material there must be nutrients in the form of simple carbohydrates present in the material. All materials with organic compounds are therefore at risk for mould growth. However, the susceptibility for mould growth varies; some materials can withstand higher moisture loads than other. This can be described as the critical moisture value, RH_{crit} (further discussed in section 4.1). In addition, materials may be contaminated by organic substances during production and construction, for example by dust, soil, surface treatments etc. and the susceptibility may then be changed.

Extended mould growth on building materials may be visible to the naked eye. However, often this fouling cannot be seen by the naked eye, see example in Figure 3.3A. Some fungi produce pigments in their hyphae and spores that can cause discolouration of surfaces on which they grow, while others lack this pigment. The production of pigments by fungi is a species-specific trait, but can also be dependent on the nutrients available, or the growth phase of the fungus (Gadd 1980),(Eagen, Brisson et al. 1997, Fleet, Breuil et al. 2001). In addition, especially in houses in Northern Europe, mould usually grows inside sealed building structures, see Figure 3.3B. Therefore, extensive mould growth may be present in buildings without anything unusual can be seen. Growth not visible to the naked eye and growth inside building structures may be problematic, as there is a risk of negative effects on the indoor environment, which can pose health risks to those in the building. Mould can theoretically grow anywhere in a building, provided the conditions for growth are suitable. Some types of structures are more favourable than others for mould growth, and some materials are more susceptible to mould growth than others.

The original external wall in historic buildings often consists of inorganic building material and may therefore be considered as robust from a mould perspective. However, there are also adjoining frames, beams, windows, doors, added insulation and surfaces containing organic compounds. For further discussion on critical positions, see section 3, and for material susceptibility in section 4.1.

(A) (B)

Figure 3.3: (A) Illustration of how the visible impression of mould growth varies. On all samples in this example there is the same extent of mould growth(rating 4 according to the rating scale described in Table 6.3), although the growth on samples to the right is not visbile to the naked eye. (B) Example on how the mould growth may be hidden within the building structure. In this example the interior surface materials and insulation have been removed. Note that although the growth is visible in this example, the growth is most often not visible to the naked eye.

3.2 Rot or wood decay

3.2.1 Introduction

Rot or wood decay caused by fungal growth is a failure mechanism for wooden constructions that is closely linked to moisture, as water activity is a prerequisite for fungal growth (Al-Omari, Beck et al. 2015). Consequently, fungal growth starts when the moisture content in wood exceeds a threshold value. The threshold value depends on different factors:

- Time of wetness, i.e. time above the certain threshold value
- Previous attacked wood has a lower threshold value than sound wood
- Temperature

In general, the threshold value is higher than for mould growth. Therefore, the threshold value for mould growth is more likely to be the limiting factor in critical positions where mould growth is not accepted. Some fungal species (dry rot) are able to transport moisture over several meters enabling rot attack far away from the moisture source.

In historic masonry facades, wood is mostly used for half-timbering in external walls. Although structural floors are not a part of the wall, wooden beam-ends and supporting laths may be placed in the external walls and therefore in direct contact with bricks or stones in the external wall. Consequently, the moisture content of the embedded timber will be dependent of the moisture conditions in the wall. For most fungal species the threshold value is in the over-hydroscopic range; condensation or liquid water sources e.g. penetrating rain are therefore usually a prerequisite for fungal growth (Nevander and Elmarsson 1994).

When an external wall with wooden elements as half-timbering or beam-ends is insulated internally, the temperature and the heat flux through the wall will decrease. Consequently, the relative humidity will increase and therefore the moisture content is expected to increase in the wall including the wooden elements.

The consequences of rot attack are severe: The most severe is the reduction of the structural strength of the wooden construction but it may also have serious consequences for the indoor air quality (Singh 1999).

3.2.2 Material at risk

Rot can attack all wooden constructions. Some species need lime as well as moisture to grow (Bech-Andersen 1995). Lime is often used in historic buildings and therefore present for fungal growth.

If the building is internally insulated with systems that contain wooden materials e.g. wooden framing, there is a risk of rot if condensation can occur due to insufficient vapour barrier or if water from driving rain is trapped in the internal insulation.

A rot attack causes wood decay, resulting in reduced strength and ultimately collapse of the wooden construction. How fast a rot attack develops depends on the available moisture. If moisture supply is stopped the attack stops but will return if moisture again becomes available. Some fungal species need long time exposure to high moisture content before the wooden construction weakens substantially, other species can weaken the wooden constructions fast if the conditions especially favours these species (Munck, Koch et al. 2003). Damages caused by the first kind of attack could be seen as lack of maintenance, as a slowly developing attack should be discovered before it becomes critical.

Fungal growth can - depending of the species - result in unpleasant odour and emissions, which must be considered as an indoor climate problem. Depending on the exposure and the immunological reactivity of the inhabitants the inhalation of airborne micro-organisms and their metabolites of some species may cause respiratory symptoms (Singh 1999).

3.2.3 Critical position in the building envelope

The critical positions in the building envelope are where wood is present and especially where the moisture load is high. This is illustrated in Figure 3.4 and based on RIBuild deliverable D1.1 *Report on historical building types and combinations of structural solutions* (Blumberga, Blumberga et al. 2015). Not only is the position in the envelope critical: The moisture load on wooden constructions is highly dependent on the structural details and material composition of the detail as well as the characteristics of the materials, including also the wooden species and quality. These factors determine e.g. the drying potential.

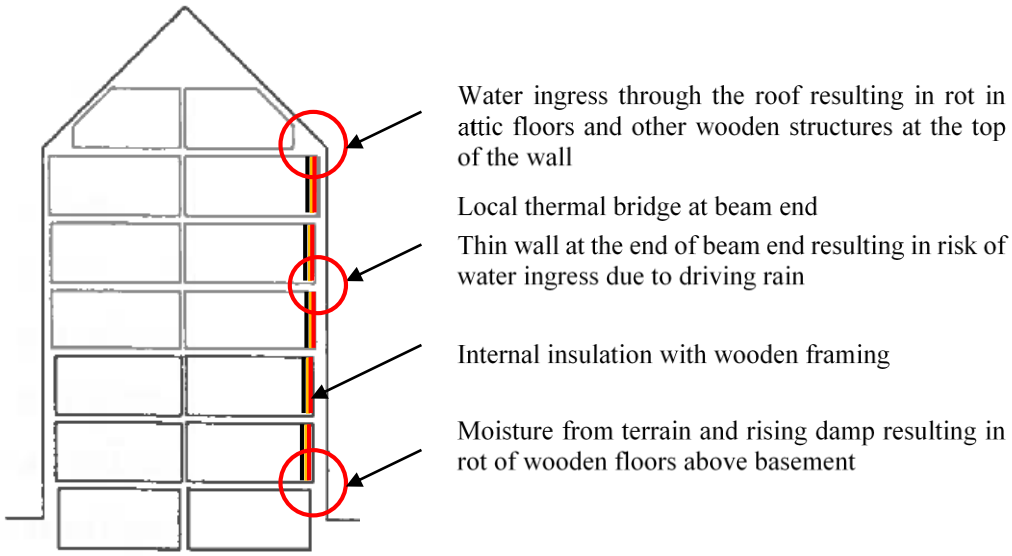

Figure 3.4: Cross section of a multi storey house with markings of areas in the external wall where there is a risk of rot. A prerequisite is the presence of wood. Water ingress or high moisture content in materials in contact with wood can cause rot. Figure 3.5 is a photo of wood damage near the roof.

Figure 3.5: Rot fungi attack on beam end near the roof

3.3 Frost damage

3.3.1 Introduction

Frost damage in porous building materials can originate from a variety of physical frost impacts, of which the volume increase of the water-to-ice phase change is the most widely known. Three conditions must be fulfilled for frost damage to occur:

- The material must be sufficiently wet
- Phase change must happen in the material
- The material must be sensitive to frost damage

Adding internal insulation to a massive masonry wall may give important alterations of the first two conditions. Firstly, by adding internal insulation, the temperatures in the wall generally decline, and the occurrences of freezing conditions in the wall become more frequent and more intense. Furthermore, the freezing conditions will also penetrate deeper into the wall. Secondly, the drying potential of the wall diminishes because of the internal insulation, which commonly gives increased moisture levels. If the material is not significantly sensitive to frost damage though – see the third condition – then these alterations of the first two conditions will of course have negligible impact.

Frost damage is commonly solely related to aesthetical problems, particularly scaling of the exterior surface of the masonry wall, which normally not lead to structural problems except for very extreme cases. Given the more frequent and intense freezing conditions that penetrate deeper into the wall, the risk for structural damage may rise when adding internal insulation, if the material is significantly sensitive to frost damage.

3.3.2 Material at risk

Porous building materials experiencing high moisture contents and low frost temperatures are at risk for frost damage. The ‘Frost damage’ sections of this report primarily emphasise ceramic brick, and by extension natural stone, as RIBuild focuses on external walls in historic buildings. Frost damage may though similarly occur in concrete building elements, clay roof tiles, but these materials are not addressed.

3.3.3 Critical position in the building envelope

The outer surface layers of historic masonry walls are normally exposed to the highest risk for frost damage, mainly manifested through scaling of the outer surfaces. If water can infiltrate in layered massive wall systems (e.g. covered by tiles), the zone at risk may shift towards the interior of the wall, where often materials of lower quality are used.

Both the moisture and temperature levels of porous building materials depend of course on the wall orientation. The prevailing direction for wind-driven rain in Europe is South-West while the lowest facade temperatures occur in North-faced facades. It is subsequently difficult to predict the most exposed orientation with respect to frost damage.

3.4 Discoloration of facades

3.4.1 Introduction

It is well known that the hygrothermal conditions in the original wall could change and get worse, as reported in the following, after the application of internal insulation (Morelli, Nielsen et al. 2010, Morelli and Svendsen 2013, Steskens, Loncour et al. 2013). This new configuration can lead to condensation behind the insulation panels (Künzel 1998, Straube and Schumacher 2007, Vereecken and Roels 2014), reducing temperature and increasing the moisture content inside the original masonry (Künzel 1998, Saïd and Demers LL McSheffrey 2003, Vereecken and Roels 2014, Vereecken and Roels 2015, Abdul Hamid and Wallentén 2017, De Mets, Tilmans et al. 2017). Moreover the drying potential towards the room inside is reduced, since, the implementation of an internal insulation system could act as a barrier, which makes the water inside the masonry migrate only towards the external side, thus increasing the water content in that layer (Harrestrup and Svendsen 2015, Abdul Hamid and Wallentén 2017, Biseniece, Žogla et al. 2017, Odgaard, Bjarløv et al. 2018). Thus, the consequences are not only inside the masonry, for instance causing a possible decay of embedded wooden beams (Morelli and Svendsen 2013, Harrestrup and Svendsen 2015), but also on the external side of the wall leading more favourable conditions for the biological growth (Künzel 1998, Holm, Zillig et al. 2004, Künzel 2007, Straube, Ueno et al. 2012).

In section 3.4 discolouration caused by algae as well as fungal growth are discussed. In section 4-7, only algal growth is discussed, as fungal growth on facades is not further studied in the project.

In Appendix 1 a number of references to research articles have been categorized according to a number of parameters that may affect the growth of facades. The tables in Appendix 1 are taken from (Johansson and Capener 2015).

3.4.1.1 Biodeterioration of the building envelope caused by algae colonization

In addition to a possible increased moisture content on building façades after internally insulated, the building envelope is continuously exposed to open air and to weather conditions. For this reason, façades are inevitably subject to the deterioration due to natural causes and biological growth of microorganisms (biodeterioration), too (Johansson 2005a, Venzmer, Von Werder et al. 2008).

Algae and cyanobacteria are the main colonizers of building façades, and they can adapt to a large variety of substrates, on which a suitable condition for growth as combination of dampness, warmth and light (Kastien 1999, Gaylarde, Ribas Silva et al. 2003, Hofbauer, Breuer et al. 2003, Gaylarde and Gaylarde 2005, Johansson 2005a, Miller, Sanmartín et al. 2012). Algal biofouling could also become a habitat for other species like mould, lichens and fungi. However, in this report, only the phenomenon of growth related to algae and cyanobacteria is investigated, since they are the first responsible of the formation of the biofilm matrix that permits the consequent growth of other microorganisms (Crispim, Gaylarde et al. 2003, Escadeillas, Bertron et al. 2009b). On the contrary, the development of ferns, creepers and higher plants are not addressed here, since their growth can be avoided by ordinary maintenance and cleaning of the external walls.

Green algae, belonging to the division Chlorophyta, are a polyphyletic group of eukaryotic organisms, and they are very ancient living organisms. They belong to several orders in the kingdoms of Plants and Protists. Some algae, called terrestrial algae, can live in terrestrial environments as, for instance,

on tree trunks or on building façades (Hoffmann 1989, Crispim, Gaylarde et al. 2003, Johansson 2005a, Lopez-Arce and Garcia-Guinea 2005, Barberousse, Lombardo et al. 2006, Flores-Colen, de Brito et al. 2008, Venzmer, Von Werder et al. 2008, Amaro, Saraiva et al. 2013).

Cyanobacteria, belonging to the division Cyanophyta, also known as blue-green algae, can survive in the biofilm even during summer months when the temperature on a building façades exceeds 60 °C coupled with high light intensity and extreme dryness (Imre Friedmann and Ocampo-Friedmann 1995, Pattanaik and Adhikary 2002, Billi 2010).

Biofouling on building facades caused by algae and cyanobacteria can lead to the appearance of stains, which induces aesthetic degradation on the façades. Algal communities are usually readily recognizable on building exposed surfaces, because they form patina or sheets varying in extent, thickness, consistency, and colour. In well-lit and relatively dry environments, patinas are thin, tough, sometimes green, and very often grey or black, depending on the different-coloured pigments of the algae (Saiz-Jimenez 1994, Kumar and Kumar 1999, Flores-Colen, de Brito et al. 2008).

Apart from the aesthetic deterioration, algae may also cause biochemical deterioration (Saiz-Jimenez 1994). It has been reported that the presence of a microbial layer may facilitate the production of acids and the biochemical deterioration of the material through the etching of mineral components and dissolution of binding minerals, especially in carbonates (Tiano 2001). Biophysical deterioration of the materials may also occur. Considerable force may be exerted through repeated shrinking and relaxing of the slimy sheath of the cyanobacteria during their cycle of drying and moistening. This eventually loosens mineral grains of the stone surface (Tiano 2001).

Another effect of the presence of biofilm on exposed surfaces is the acceleration of the accumulation of atmospheric pollutants. The slimy surfaces of these microorganism facilitate adherence of airborne particles of dust, pollen, oil, and coal ash, giving rise to hard crusts and patinas that are difficult to eliminate (Tiano 2001).

3.4.1.2 Biodeterioration of the building envelope caused by fungal colonization

In addition to discoloration of facades caused by algal and cyanobacterial growth (section 3.4.1.1), also micro-fungi can cause discoloration. Micro-fungi consist of the same group of mould fungi that grow inside building structures (section 3.1). However, although a vast range of those fungi can grow on facades, only a few causes discoloration. Most of the mould fungi have dematiaceous, “colourless”, cells while the fungi causing discoloration has dark pigment in their cells.

The general conditions discussed for mould growth within buildings are the same for microbial growth on the facades: available nutrients, access to moisture and a favourable temperature. Access to water is the limiting factor for life to exist at all. If a façade is sufficiently dry, no organisms will cause discoloration to grow. The minimum level of amount of water required varies. Generally, fungi can live at lower moisture levels than cyanobacteria and most algae (section3.4.1.1), although moisture requirements are also connected to temperature.

Water is supplied to the façade through rain and humid air. Temperature and RH at facades vary highly during the day and during the year. In addition, the facades are exposed to UV-radiation. The fungi growing in these environments must therefore be adapted to such conditions. For example, the pigment in the cells can provide protection against UV radiation and dehydration.

In contrast to algae and cyanobacteria (section 3.4.1.1), fungi cannot produce their own carbon source but are dependent on available nutrients within the material they grow on. Environmental factors are therefore more crucial than the nutrient content of the material for algae to grow (Tanaca, Dias et al. 2011), while the façade material may also have an important impact on the establishment of fungi.

3.4.2 Material at risk

3.4.2.1 Algae

The biological colonization on building surfaces is highly dependent on the material substrate: a large variety of porous building materials (e.g. bricks, stones, mortar, paints) was found to be colonized by algae (Tomaselli, Lamenti et al. 2000, Dubosc, Escadeillas et al. 2001, Crispim, Gaylarde et al. 2003, Gaylarde and Gaylarde 2005, Barberousse, Lombardo et al. 2006, Ruot and Barberousse 2007, Flores-Colen, de Brito et al. 2008, Miller, Sanmartín et al. 2012).

Furthermore, the presence of moisture in large and enough quantities mainly trigger algae development (Di Giuseppe 2013). Considering that the more porous a material is, the more moisture it can contain, historic masonry walls, that are generally built by porous bricks and natural stones, are greatly exposed to moisture impact (Bjarløv, Finken et al. 2015, Uranjek and Bokan-Bosiljkov 2015, Biseniece, Žogla et al. 2017). Moreover, roughness affects the flow of water on the surface and favours the adhesion of algae cells and organic material blown by the wind or brought by water flow on the substrate (Figure 3.6). Consequently, rough building facades are more subject to biofouling than smooth ones (Tomaselli, Lamenti et al. 2000, Tran, Govin et al. 2014).

Figure 3.6: Growth of green algae on a wall (Johansson 2005a)

3.4.2.2 Fungal discolouration

Microfungal growth on facades is primarily an aesthetic problem, causing discolouration that will not affect the strength of the façade elements. The appearance of discolouring is a complex phenomenon. Climatic factors such as the structure and properties of the façade material affect the growth, as well as other factors such as surrounding vegetation and contamination. Given the complexity behind the emergence of microbiological growth on facades, it is not easy to reduce the problem of discolouring growth and there is not a single general solution to the problem (Johansson and Capener 2015).

Water is supplied to a building's façade mainly through rain and humid air. In addition, water left in the material from the manufacturing or from the construction site can contribute to increased moisture

at the surface during the time the material dries out. The possible enhanced risk for discolouration on the facades of internal insulated buildings is linked to increased RH at the surface of the façade.

The temperature, and hence the moisture level, at the façade surface is affected by the wall structure. The surface temperature will be higher, and moisture conditions lower on a poorly insulated wall than on a well-insulated, as the heat loss through the wall is higher. Additional insulation of an outer wall can therefore increase the risk of fungal growth on the new façade surface. This effect has been observed by, for example (Becker 2003, Krus, Fitz et al. 2013).

On relatively cold walls, there may be sections that are locally warmer, and thus drier. An example is where the ceiling joints connect to external walls, promoting heat transport to the façade (thermal bridges). This can give rise to patterns on facades, with growth only on cold parts (Figure 3.7) (Becker 2003, Johansson 2011). The temperature difference between areas with growth and surfaces without growth was not very large, only a few °C. It is not surprising that small differences can give effect because each degree's rise in temperature causes a greater reduction of RH, an effect even more apparent at lower temperatures.

Figure 3.7: (A) A facade with growth of discoloured organisms (right part). In the light circles, there is no growth. Behind these are fasteners (B) that conduct heat from the inner part of the wall. Such attachment was lacking in areas where there was growth (C). Where there were fasteners under the pad, the surface became somewhat warmer, and therefore drier than surrounding surfaces. From (Johansson 2011)

3.4.3 Critical positions in the building envelope

Several factors such as the local environment, the building design and the material substrate influence the algal biofouling on building materials (Guillitte 1995).

The growth of algae is also influenced by orientation of the facade. Indeed, the north-facing facades, which are wetter for longer time and less irradiated by the sun, are faster colonized (Ortega-Calvo, Ariño et al. 1995, Barberousse, Lombardo et al. 2006). Similarly, a facade exposed to dominant winds seems to be colonized more easily than the other sides of the same building. The wind can transport both rain and biological propagules on the facades promoting the biofouling. A façade, which is often wet by rainfall, promotes the growth of algae. However, a high temperature caused by direct irradiation induces water evaporation by heating the materials. Similarly, exposed façades to the wind are more subject to drying phenomenon (Ortega-Calvo, Ariño et al. 1995).

The geometry of the building may offer preferential routes where the water could stagnate after a rain event, creating the ideal conditions for the proliferation of algae and cyanobacteria. If balconies or roof overhangs reduce the wind driven rain on the walls, a light inclination of the façade increase the surface exposed to the water (Di Giuseppe 2013). Once the algae have grown, the run-off rain water contributes to replacing the old cells with new cells, and favours the spread of spots of biofilm to other non-contaminated building components (Künzel 2007).

Parts of building often moistened for long periods, or easily covered by propagules, are highly sensitive to the biological colonization. Biofouling often increases at the foot of walls, junctions of different coatings, and overhanging elements (cornices, mouldings, balconies, etc.) (Barberousse 2007, Tran, Govin et al. 2014).

4 Threshold values from literature

4.1 Threshold values for mould growth

Mould fungi can grow on building materials in the range of RH 75 -100%. Each fungal species has a minimum moisture requirement in order to grow (Flannigan and Miller 2001). Xerophilic fungi can grow in the lower range of RH, while hydrophilic fungi need RH above 90 % for growth (Figure 4.1A). However, the majority of fungi will grow well at high moisture conditions, at room temperature. Moisture requirements are also related to temperature; at lower temperatures, fungi require a higher RH to germinate and grow (Sedlbauer 2001b) see Figure 4.1B.

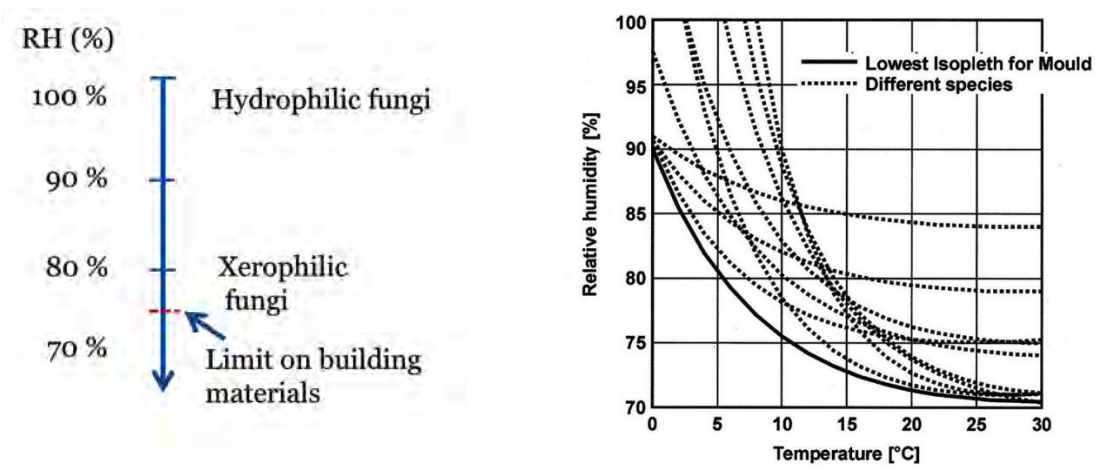

(A) (B)

Figure 4.1: Moisture requirements of mould fungi. (A) Limits for growth of different groups on mould fungi on building materials (at room temperature). (B) Curves defining the limiting conditions for different species of mould growth. Note that the growth limits are valid for optimal nutrient media. (Sedlbauer 2001b)

As stated in section 3.1.2, materials containing organic compounds are at risk for mould growth when exposed to the favourable conditions for mould growth. However, different materials vary in their susceptibility for mould growth. The differences between materials can be explained by differences in the concentration of organic compounds, which are essential nutrients for mould fungi, as well as by differences in other characteristics that may affect growth (such as pH, surface structure, etc.).

(Block 1953) conducted one of the earliest studies of mould growth on different types of building materials at different moisture levels. Numerous researchers e.g. (Ritschkoff, Viitanen et al. 2000, Hofbauer, Kreuger et al. 2008, Johansson, Ekstrand-Tobin et al. 2012) have since studied mould growth at different conditions, some with the aim of identifying the climates in which different types of building materials begin to mould, other with the aim to compare the susceptibility for mould growth at high RH.

The ability to withstand mould growth at RH above 90-95 % is often called mould resistance. Several standardised tests methods are available for evaluating the mould resistance of building materials. Mould resistance is evaluated by exposing test specimens of a material to spores of mould fungi and then incubating the specimens at a relative humidity and temperature favourable to mould growth. Some of the test methods are presented and discussed in (Adan 1994, Johansson 2014, Johansson, Ekstrand-Tobin et al. 2014).

Another way to describe and test the susceptibility for mould growth is the critical moisture level for different building materials, RH_{crit}, i.e., the lowest RH at which mould growth can grow on a certain material. RH_{crit} is also dependent on the temperature, at lower temperatures RH_{crit} is higher. RH_{crit} can also be tested with a standardised test method (SIS 2014).

In Figure 4.2 the difference and connection between RH_{crit} and mould resistance is described. While being able to discriminate between materials in a "worst case scenario", the mould resistant test methods do not provide any information on how a material will perform in a part of a building where the moisture conditions are not as high as in the test. Therefore, it may be possible to use materials that showed mould growth in the 'mould resistance tests', in buildings in which the RH is expected to be lower, without risk of mould growth.

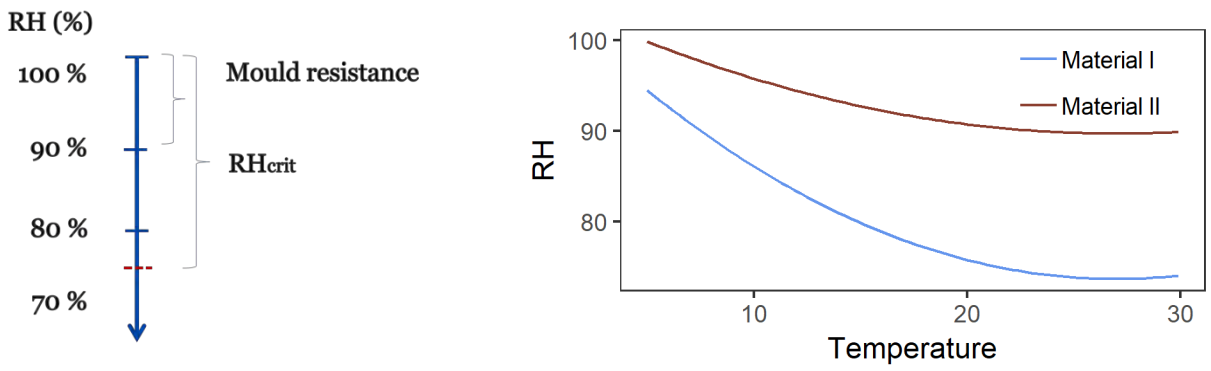

(A) (B)

Figure 4.2: (A) Comparison of range of mould resistance and RH_{crit}; mould resistance is tested at optimal growth conditions (see Figure 4.1A) while RH_{crit} represents the lowest RH that makes mould growth possible. (B) RH_{crit} as a function of temperature for two different materials (schematic)

In general, when there is a high content of organic compounds in a substrate, the RH requirement for mould growth is lower, and the biodiversity of fungi may be higher than if the concentration of these compounds is low. (Hyvärinen, Meklin et al. 2002) found that mould growth was highest on wooden materials and paper materials, which are rich in organic compounds, and lowest in samples of mineral insulation, ceramic products, and paints and glues, in which the content of organic compounds is expected to be low (Pietarinen, Rintala et al. 2008) found the highest diversity of microbes on wooden materials.

Attempts has previously been made to place different products in specific groups of materials, such as "wood based boards", "gypsum boards" etc. However, it was shown not to be possible, as it is difficult to know how these groups should be defined (Johansson 2014). Different brands of one type of material, that is a specific product, may have different susceptibility for mould growth, for example due to additives. In addition, new products are constantly being developed. Therefore, each product needs to be tested and this report will not provide any list of the threshold values for building materials in general.

4.1.1 Control actions

Mould fungi are a natural part of the organic lifecycle, and spores are present everywhere, both in the air and on material surfaces. It is therefore not possible to protect building materials from contamination by mould spores. It is the germination and growth of these spores (see also Figure 3.2) that must be prevented. In practice, there are two fundamental ways of preventing the growth of

mould in buildings. Either the moisture and temperature conditions should be such that mould growth is not possible, or materials on which mould cannot grow under the prevailing conditions should be chosen.

To avoid mould growth, it is important to be able to estimate or calculate the expected microclimates in different layers of the wall construction before retrofitting, both for existing construction parts and new materials, and to know the critical moisture level (RH_{crit}) for each of these materials. Control parameters include for example verified RH_{crit} value of the materials, relevant values of RH and temperature in the different parts of the wall and, in some cases, air tightness performance testing. A condition that might occur when applying internal insulation is the risk of elevated humidity load from the indoor moisture content in the air leaking out through convection into the colder parts of the wall construction. Insufficient airtightness of the added internal insulation must, as generally for new constructions, be considered as a potential risk of damage.

Following the above reasoning, the control actions below are recommended:

- estimate/calculate the expected humidity conditions for building material layers in the wall construction after applying internal insulation
- choose materials/applications with higher RH_{crit} than the estimated actual conditions
- choose clean, dry materials to eliminate additional building moisture and if storing material outdoors, use weatherproof cover to avoid excess moisture from precipitation.
- ensure air tight mounting to circumvent additional moisture content leakage from indoor air into the wall

To treat surfaces and mix materials with mould inhibitors such as e.g. asphalt or fungicides is not recommended as these products can fortify the development of an odour and/or health hazard to the indoor air. The precautionary principle is recommended as an approach.

4.2 Threshold values for Rot

Decay in wood can be initiated by three types of rot fungi: brown rot, soft rot and white rot. Brown rot fungus is more likely to appear earlier than white and soft rot and develop faster than the other types of rot fungi. The decay process initiated by brown rot fungi causes around 50% more weight and strength loss compared with white and soft rot fungi (Curling, Clausen et al. 2002, Brischke and Meyer-Veltrup 2015). Moisture content and temperature are the overriding parameters for development and survival of rot fungi (Low, Palfreyman et al. 1999), although humidity also play a role (Singh 1999). Through sorption curves, humidity and moisture content are correlated. In addition, decay and degradation of wood is highly dependent on the wood species; e.g. larch and pine are more likely to decay than fir (Brischke and Meyer-Veltrup 2015). Furthermore wood used in historic buildings is more favourable for fungal attacks than new wood (Low, Palfreyman et al. 1999). Finally, threshold values of moisture content and temperature also depend on the fungi species as illustrated in Figure 4.3.

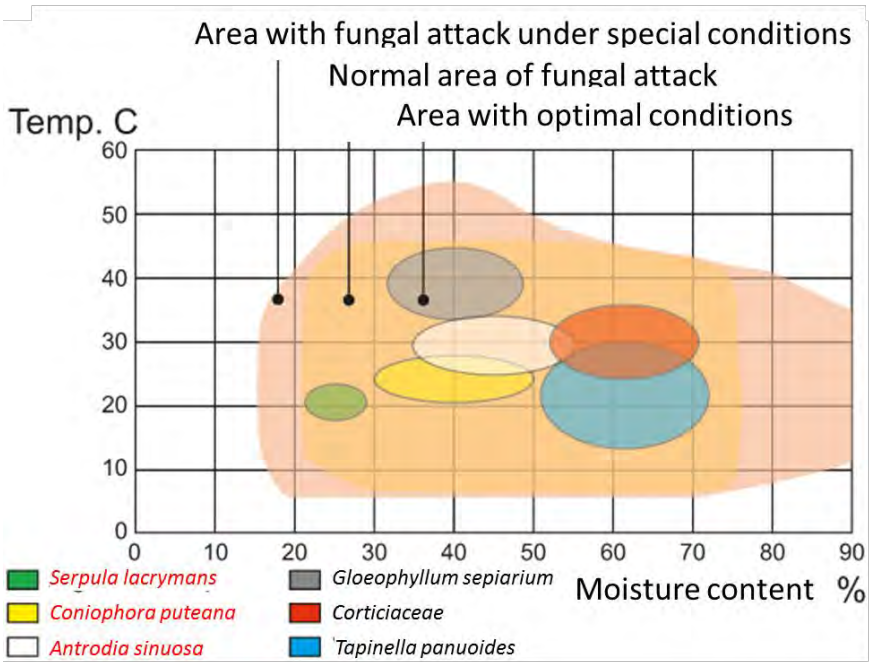

Figure 4.3: Example of threshold values depending on fungi species, the most relevant fungi for beam ends are written in red (Koch 2014)

Although the threshold values for environmental factors for enabling rot fungi growth determined in different studies vary significantly. Table 4.1 gives an overview of the obtained threshold values across the literature. Table 4.2 includes a more detailed list that shows the variety of test methods and resulting different threshold values, determined in different studies including the reference and more info.

Table 4.1: Typical threshold values for rot found in literature

Environmental factors	Typical threshold values found in literature
Temperature	• The critical temperature for decay caused by rot fungi is between 20 ºC and 30 ºC • The optimum temperature for dry rot is 23 ºC (critical value) • No fungi growth is initiated or developed at temperatures between 40 ºC-65 ºC • At temperatures below 5 ºC the fungi are dormant
Relative humidity	• The optimum RH for rot is 98 % • At 30 ºC the lowest level of decay is above 90-92 % RH • Between 0 ºC and 5 ºC the lowest level of decay is 97 % RH
Water activity (equivalent to RH)	• The critical value for water activity is between 0,97 and 0,98, which is the optimal condition for fungi growth provided that RH and temperature are not limiting conditions
Moisture content	• The ideal condition for rot fungi growth is when the moisture content in wood is between 20 and 30 weight %. However, this threshold is lower for already infected wood. Above 70 weight-% there is no fungi growth (Traeportal 2019)
pH	• At 20 ºC, the minimum pH value for fungi growth is between 1 and 3, the optimum value is pH = 4,1, while no fungi growth occurs above pH = 8,2

Table 4.2: Summary of threshold values for rot

Source	Material/ product	Age of material H: historical N: New	Test results	Test method used
(Low, Palfreyman et al. 1999)	Pine sapwood	H	Slight decay 76 % < RH_{slight} < 86 %	Small-scale models & larger-scale models
(Boddy 1983)	Beech & oak	N	20º < $T_{optimal}$ < 30º No growth below 5º and above 35º	
(Curling, Clausen et al. 2002)	Southern pine sapwood	H	No threshold values but results after exposure: Brown-rot: 80-100 % strength loss and 25-40 % weight loss. White-rot: 20-40% strength loss	Biological exposure method with infected soil in contact with wood
(Saito, Fukuda et al. 2012)	Japanese red pine	N	Mass loss 0.4 at 100% RH and 20 º < T < 30º, no mass loss at 97% RH at any temp.	
(Morris and Winandy 2002)	Southern pine sapwood - oriented strand board (OSB)	H	Moisture content (mass) ≤ 20% - no decay 20 < MC < 30% - grey area MC ≥ 30 % - decay RH_{crit} = 27 % for OSB	FPL soil pan decay technique
(Maurice, Coroller et al. 2011)	Beech	H	Min. growth T = 1,5º No growth above 25º Min. growth temp -2,3º , optimal growth temperature 20,6º, max growth temperature 25,7º Optimum growth at water activity rate 0,993 (99,3% RH) Min. pH = 1-3 at 20º optimal pH=4,1 max pH=8,2 (no growth)	
(Fuhr, Schubert et al. 2011)	Norway spruce		Mean hyphal growth μ relates to water activity rate 0,972 (equivalent to 97,2 %RH) at T=22º and pH=5	
(Viitanen 1997b)	Pine and spruce sapwood	N (samples cut out from trees aged 80-90 years)	Conditions for fungal activation and mass loss: RH >94-96%, moisture content around 25-28% at 20º (for weeks) and at 5º (for months). Lowest RH >90-92% at T=30º. Lowest RH≥97% at 0º<T<5º	Mathematical model

Some of the primary methods to determine threshold values and detection methods for fungi in wood are listed below. However, the basic methods for experimental determination of temperature, moisture content, pH, etc. are not included.

- Moisture meter, ultrasonic hammer, endoscopes and genetics (Singh 1999)
- Immunodiagnostic (Immuno-dot blot) and enzyme-linked immunosorbent assay (ELISA), developed in late 80's to early 90's are effective serological methods that can be applied to detect fungi in early stages (Clausen, Green III et al. 1991)
- Biological exposure methods (strength test, weight loss test and chemical analysis): basic feeder strip and direct inoculation. Four-point bending test can be used to determine strength and weight loss (Curling, Clausen et al. 2002)
- Terminal restriction fragment length polymorphism (T-RFLP), to identify the occurrence of fungi species (Råberg, Brischke et al. 2007)

In addition, a number of assessment algorithms have been developed to predict the risk of rot based on measured values for governing environmental conditions like moisture content and temperature:

- Mathematical model for predicting wood decay and service life (de Freitas, Molina et al. 2010).
- Durability assessment: Hygrothermal analysis model that can predict hygrothermal conditions and decaying process in the wood. The model can be applied to foresee wood decay progress under dynamic conditions (Saito, Fukuda et al. 2012).
- Mathematical model: Combination of exponential model and cardinal model (CM) to predict growth conditions of various fungi species (Maurice, Coroller et al. 2011)
- Fungal growth model (FGM) – to predict the hyphal growth of white rot fungi

4.2.1 Control action

The most important measures to minimize or prevent rot attacks are:

- Controlling the moisture through design of construction, ensuring the moisture level will not exceed the threshold value, coupled with a temperature threshold
- Prevent water ingress into the wall; e.g. make sure joints in brick walls are filled, and avoid leaks from rainwater drainage systems or through roofs
- Limit the use of wood in critical parts of the envelope, especially less robust species

Moisture content and moisture ingress is the most important factor in limiting the risk of wood decay in existing constructions containing wood. If parts of the original structure are renewed e.g. due to rot attack in the existing construction it is possible to choose other materials. Replacing wooden beam-ends with concrete beams is one possibility. When parts of the construction are replaced, not only the damaged wood is removed; sound wood must also be removed to create a safety zone. How much sound wood that should be removed depends on the fungi species. Recommended safety zones are described in Table 4.3.

Table 4.3: Safety zone of apparently sound wood when replacing wood with fungi attack (Koch 2014)

Fungi	Safety zone
Serpula lacrymans (dry rot)	100 cm
Coniophora puteana (brown rot)	20 cm
Antrodia sinuosa and *Antrodia vaillantii* (brown rot)	30 cm
Gloeophyllum sepiarium (brown rot)	10 cm
Other fungi	10 cm

When installing new internal insulation, wood-based materials should be avoided if it is difficult to control the moisture content or moisture ingress.

Dependent on the measures to minimize or prevent rot attack it is important to know the coupled threshold values for moisture and temperature for different wood species.

4.3 Threshold values for Frost damage

Frost damage presupposes three conditions to be fulfilled (section 3.3.1):

- The material must be sufficiently wet
- Phase change must happen in the material
- The material must be sensitive to frost damage

Threshold values for these conditions are not easily established. Frost damage may initiate when the moisture content in the building material exceeds its 'critical saturation degree' during an interval of 'freezing conditions' (Fagerlund, 1977). When these criteria are fulfilled, a pressure will build up in the material, possibly leading to frost damage, if the 'mechanical resistance' of the material is insufficient. All three parameters (critical saturation degree, freezing conditions, mechanical resistance) are highly material dependent, and formulating generally valid threshold values is impossible. Maage (1984), among others, shows that the critical saturation degree is strongly related to porosity and pore size distribution, see section 4.3.1. Additionally, the temperature at which the freezing conditions occur also depends on the pore size distribution, see section 4.3.2. Finally, the mechanical resistance of building materials is equally linked to porosity and pore size distribution, see section 4.3.3.

Complementarily, there is no clear definition on what is considered (un)damaged in relation to frost damage. Often, a mere visual inspection is used to determine the final state of the materials, see e.g. NBN B23-002/A2 , (NBN 1986), only capturing the very severe damage. EN 12371 on the other hand stipulates a 30 % reduction of the Young's modulus as criterion, again hinging the threshold on the material involved (EN 2010). Moreover, it is not clear how this relative criterion pertains to the absolute performance criteria with respect to the mechanical properties of the facade materials.

Moreover, much of our current knowledge on frost damage in building materials results from direct accelerated freeze-thaw tests at very low frost temperatures and very high moisture contents. These tests can be deemed binary: if the material successfully endures the extreme conditions, it will most likely also perform reasonably under milder conditions; if not successful, it is commonly considered

inapt for exterior applications. While there are general concerns on the dependability of this method (P. Ingham 2005) more subtle but fundamentally crucial flaw is present when considering internally insulated retrofitted facades. These retrofits lower the facades' temperatures and raise their moisture contents to a certain degree only, generally not down or up to the extreme conditions applied during freeze-thaw testing.

Even if it were possible to establish valid threshold values from the current literature, these would not necessarily apply to the usually milder conditions found in masonry facades with(out) internal insulation. To correct for that issue, Section 6.2 presents and employs a novel test method, wherein a spectrum of frost temperatures and moisture contents is investigated. The results there validate though that the occurrence and intensity of frost damage in building materials is highly material dependent, again impeding determination of generally valid threshold values. Nevertheless, the current state-of-the-art on the three conditions is summarised in the sections below.

4.3.1 Must be sufficiently wet

In most of the frost testing, as e.g. described in NBN B23-002/A2, (NBN 1986), fully saturated samples are used, inhibiting the definition of a threshold moisture content or saturation level for the (non-)occurrence of frost damage. Experience has demonstrated though that a lower limit for these does exist, below which no frost damage will occur. This is typically expressed as the 'critical saturation degree', in which the saturation degree quantifies the relative occupancy of the pore space by water. Theoretically, if frost damage would exclusively originate from the volume increase of water upon freezing, this critical saturation degree would be 0.917. However, among others Fagerlund (1977) has shown that the critical saturation degree is typically far lower than this value Table 4.4: collects values for the critical saturation degrees of common building materials. This table indicates that large variations within the same material category may occur. Therefore, it is commonly recommended to use a conservative value (lowest value in Table 4.4:) or to judge the critical saturation degree for the material involved by laboratory measurement. Below the two main measuring techniques for that property are briefly outlined.

Table 4.4: Critical saturation degree of building materials

Material	Critical saturation degree (%)	References
Natural stone	65-96	(Hens 2014)
Concrete	60-90	(Fagerlund 1972, Litvan 1973, Hens 2014)
Cellular concrete	40-47	(Fagerlund 1972)
Brick	25-87	(Fagerlund 1972, Mensinga 2010, Hens 2014)
Sand lime stone	65-80	(Fagerlund 1972, Hens 2014)
Cement mortar	60-90	(Fagerlund 1972, Hens 2014)
Lime mortar	45-70	(Fagerlund 1972, Hens 2014, Kočí, Maděra et al. 2017)
Limestone	58-100	(Prick 1997, Al-Omari, Beck et al. 2015)
Sandstone	88-96	(Wessman 1997)

The critical saturation degree is measured by evaluating a material response, like Young's modulus or the dilatation, at various degrees of saturation. Young's modulus is often determined with ultrasonic wave propagation or vibration frequency methods. An exemplary result of the experiment based on vibration frequencies is illustrated in Figure 4.4. That method was originally used in this context to determine the critical saturation degree of concrete (Fagerlund 1977) but has later been employed for all kinds of building materials.

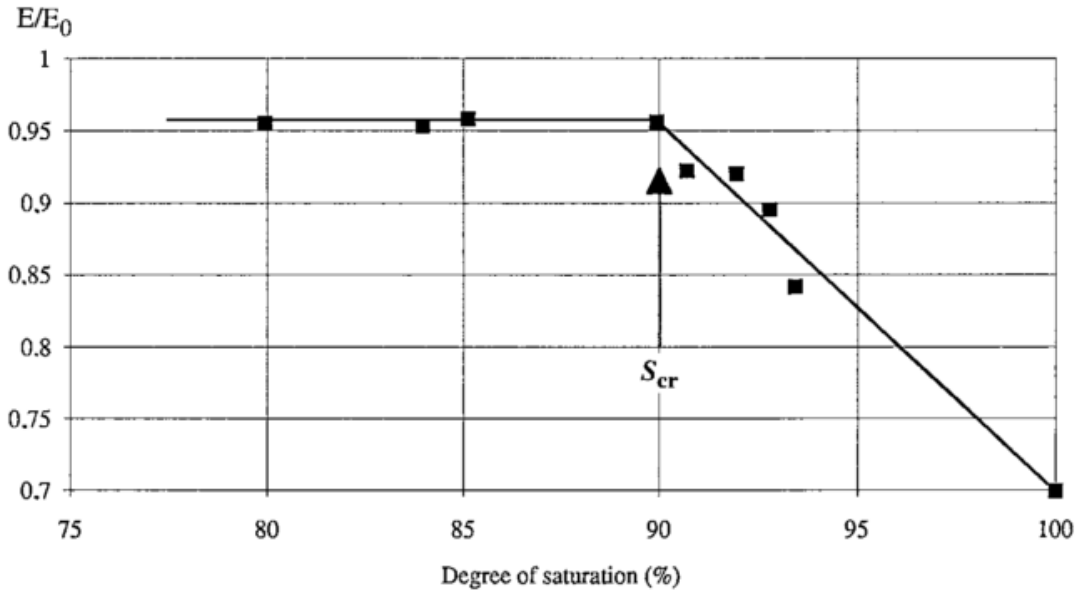

Figure 4.4: Example of Young's modulus after freeze/thaw cycles as a function of degree of saturation, for limestone, with S_{cr} indicating the critical saturation degree (Prick 1997).

The second method, based on the material dilatation, was equally developed more than 30 years ago (e.g. (Mamillan 1984)), and is normalized via ASTM C671-86 (ASTM 1986). The method recently regained interest in Canada to assess the risks for frost damage in renovation projects with brick facades with internal insulation (Mensinga et al., 2010). In that same research group, (Van Straaten 2014) further elaborated this method, and established a measurement protocol, which should allow to apply the technique in practice. Figure 4.5 illustrates exemplary results from dilatation testing, as well as the experimental apparatus to execute such measurements.

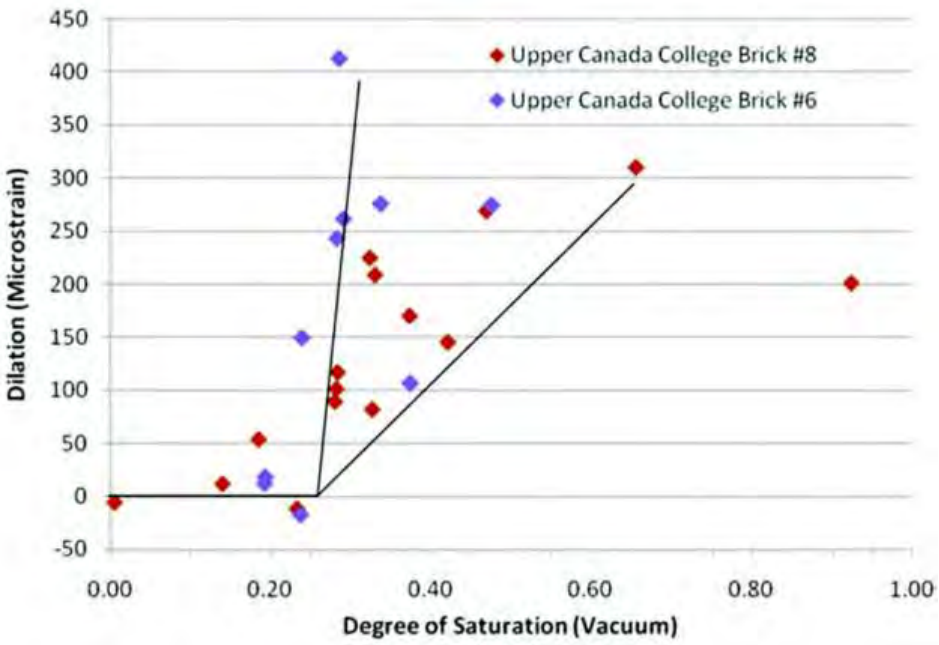

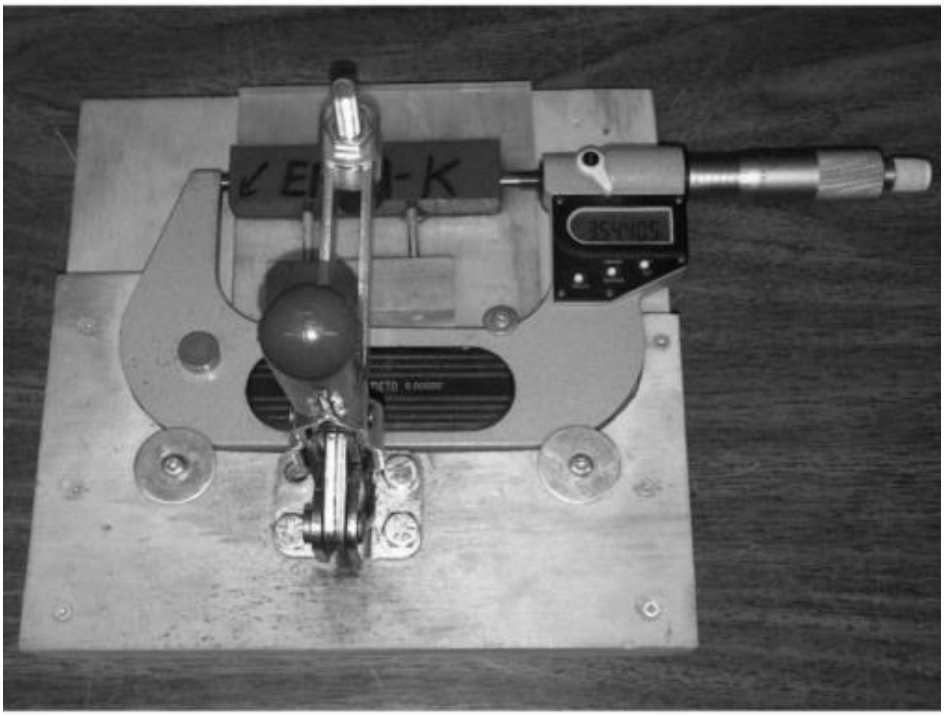

Figure 4.5: Top: Example of dilatation as a function of saturation degree for 'Upper Canada brick' (Mensinga 2010); Bottom: developed measuring apparatus to determine dilatation (Van Straaten 2014)

4.3.2 Phase change must happen

In unconfined and unpolluted water, the phase change from water to ice occurs at 0 °C. In confined state, like in the pores of a building material, that freezing temperature T_L (K) is below the standard 0 °C, and depends on the pore size. The relation between the freezing point depression ΔT_f (K) and the pore radius r (m) is given by Gibbs-Thomson equation (Kočí et al. 2017):

$$\Delta T_f = \frac{2T_0\gamma_{sl}v_l}{\Delta h_b r} \quad (1)$$

where γ_{sl} (J/m²) is the surface energy of water/ice interface, v_l (m³/mol) the molar volume of water, Δh_b (J/mol) the melting enthalpy in the bulk state and T_0 (K) the reference freezing temperature. Figure 4.6 illustrates this relation, which implies that the freezing point depression only becomes really significant for small pores (< 100 nm).

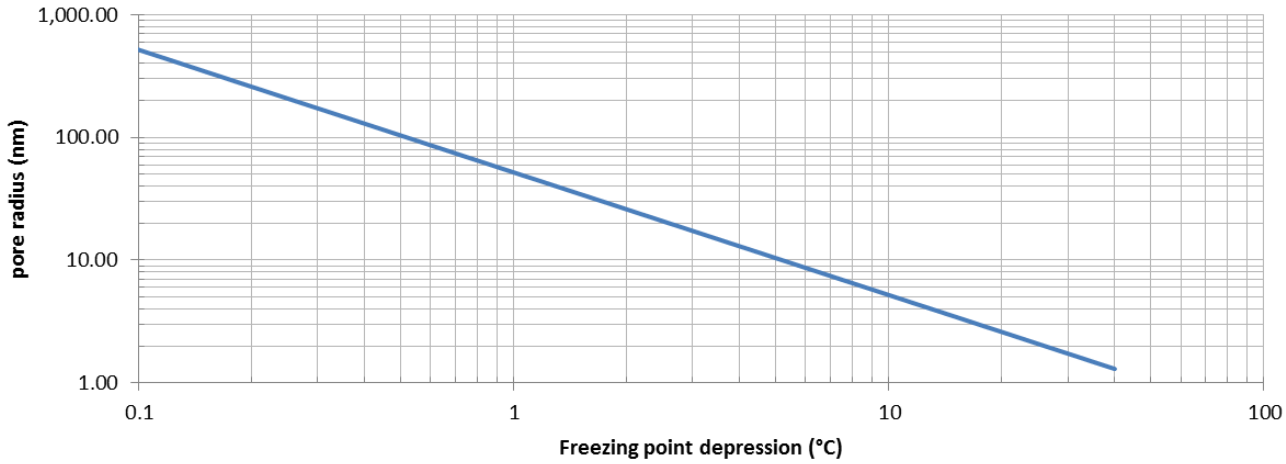

Figure 4.6: Freezing point depression as function of the pore radius (logarithmic scales)

However, most building materials have wide pore size distributions, including a large share of pores bigger than 100 nm. The process of ice formation in these materials is not yet fully understood (Sun and Scherer 2010, De Kock, Boone et al. 2015). Both these authors discuss detailed experiments on ice formation in building materials, which reveal, for example, that the freezing point depression is also influenced by the size of the test sample. Furthermore, the exact location of ice formation in heterogeneous building materials as well as the propagation of the ice front are still points of discussion in these articles.

4.3.3 The material must be sensitive

Notwithstanding the occurrences of sufficient moisture levels and frost temperatures, if the building material is not significantly sensitive for the resultant pore pressures, no frost damage develops. The sensitivity for frost damage can be determined with various direct or indirect methods, see below. It should be noted again though that the conditions imposed in these direct and indirect approaches are typically severe, in comparison with reality, because very high moisture contents and very low temperatures are applied. Consequently, it can be safely assumed that no frost damage will occur in real life if the building material passes the test positively. Of course, the severe conditions in the method may result in false positive errors: building materials not passing the frost damage sensitivity evaluation but without risk for actual frost damage for milder conditions met in practice.

4.3.3.1 Direct methods

Direct test methods expose samples at an elevated moisture content to freeze-thaw cycling with low frost temperatures, after which the frost damage is investigated. Examples of such direct approaches are NBN B-23-002/A2, EN 771-1 , CSA Standard A82-06 (clause 14), and ASTM Standard C67-07 (clause 9). As an example of such protocols, the Belgium standard NBN B-23-002/A2 (NBN 1986) prescribes to impregnate at least five full bricks to nearly vacuum-saturated conditions. After that, the wet brick samples are positioned in a bed of sand and are exposed to 20 freeze/thaw cycles from 15 °C to -15 °C, after which the frost damaging of the samples is evaluated visually.

While most other standards maintain the same critical principles, numerous differences exist with relation to the uni- or omnidirectional frost ingress, the temperatures levels and time profiles, the moisture contents and conditioning, the number of freeze-thaw cycles, the evaluation of the frost damage etc. Illustratively, the European standard for natural stone EN 12371 imposes the freezing

and thawing on all six surfaces of the sample, leading to an omnidirectional test, while its counterpart for clay masonry units CEN/TS 772-22 exposes just one surface to the conditions, giving a unidirectional test. In addition, the frost temperature in EN 12371 is about -10 °C against -15 °C in CEN/TS 772-22. Furthermore, one full cycle in EN 12731 lasts minimally half a day, whereas CEN/TS 772-22 restricts the cycle to a few hours. In addition, EN 12371 prescribes an interval of full immersion of the samples as initial moisture conditioning, while CEN/TS 772-22 on the other hand adds cyclic spraying of the exposed surface as further continuous moisture conditioning. EN 12371 moreover does not implement a preset number of freeze-thaw cycles but tests until failure, CEN/TS 772-22 in contrast imposes 100 cycles – whereas other authors go as low as 6 cycles (Mensinga et al., 2010). Finally, EN 12371 characterizes the damage via quantitative measurements, CEN/TS 772-22 on the other hand applies visual evaluations.

It is clear that no agreement has been reached on a generally accepted methodology for accelerated freeze-thaw testing. Nonetheless, these experiments are widely accepted as the standard approach to assess the sensitivity to frost damage of building materials.

4.3.3.2 Indirect methods

The indirect methods, on the other hand, are based on correlation studies between directly measured frost damage sensitivities and simple material parameters (capillary absorption coefficient, capillary and saturated moisture contents, porosity, pore volume distribution, …), enabling an indirect evaluation of the frost damage sensitivity of building materials. However, due to the complexities of frost damage and the large variety of porosities and pore volume distributions of building materials, these methods are not always reliable, and may lead to false negative or false positive errors. Examples of such methods are described below.

Durability factor (Maage 1984)

Based on a large-scale lab and field investigation (Maage 1984) defines a Durability Factor (DF) for clay brick materials:

$$DF = \frac{3{,}2}{PV} + 2{,}4.P3 \qquad (2)$$

wherein *PV* (cm³/gram) corresponds to the total porosity and *P3* (%) to the percentage of pores with radii bigger than 3µm, properties which can both be obtained from e.g. mercury intrusion porosimetry. Materials with a *DF* over 70 are classified as frost resistant, while *DF* values below 55 are classified as sensitive for frost damage. This method has been validated by several authors (e.g. Bajare (2000); Dondi, Fabbri et al. (1993)) with satisfying results.

Further attempts to evolve this method have been equally discussed in the literature (Koroth, Fazio et al. 1998). Illustratively, their DIAP(S) methods are solely based on the total porosity and the absorption properties, and are thus an alternative if no mercury intrusion equipment is available. Furthermore Dondi, Fabbri et al. (1993) also compare the DF-method (Maage 1984) to the 'Critical diameter method' (Italian standard UNI 8635/12) for 144 Italian clay bricks (UNI 1984). The authors deduce that Maage's method should be preferred.

GC-method (NBN B27-010)

This test is based on a simple free water uptake experiment, from which the GC-value is calculated:

$$GC = -14.53 - 0.309 \cdot \frac{100 \cdot \sqrt{60} \cdot A_{cap}}{w_{sat}} + 0.203 \cdot \frac{100 \cdot w_{cap}}{w_{sat}} \qquad (3)$$

where A_{cap} is the capillary absorption coefficient (kg/ms$^{0.5}$), w_{sat} and w_{cap} (kg/m³) the saturated and capillary moisture content (kg/m³) and the values 100 and $\sqrt{60}$ are there for unit conversion. Table 4.5: gives the frost resistance classification based on this GC-factor:

Table 4.5: GC-based material classes

G_c	Frost resistance
$G_c < -2.5$	Material is frost resistant even under most severe exposure
$-2.5 < G_c < -0.95$ $-0.95 < G_c < 0$ $0 < G_c < 4.5$	Usage of the material subjected to increasingly severe limitations
$4.5 < G_c$	Material is not frost resistant

ASTM Standard C62-05 & C216-07a, CSA Standard A82-06

This American classification method is also purely based on the total porosity and the water absorption parameters and is therefore similar to the GC-method Table 4.6: summarizes the upper limits of these parameters in order to be classified as a frost-resistant brick (Mensinga et al., 2010).

Table 4.6: Exterior grade/Severe weathering acceptance criteria (Mensinga et al., 2010)

	Compressive strength		Max. Boiling Absorption	Max. Saturation coefficient	Max. 24-hour cold absorption
	MPa	psi	5-hour, %	(-)	24-hour, %
CSA individual brick	17.2	-	17.0	0.78	8.0
Five-brick average	20.7	-	-	-	-
ASTM individual brick	17.2	2500	20.0	0.80	8.0
Five-brick average	20.7	3000	17.0	0.78	-

4.3.4 Control actions

Of the three conditions to be fulfilled to induce frost damage (section 3.3.1):

- The material must be sufficiently wet
- Phase change must happen in the material
- The material must be sensitive to frost damage

The first and second conditions can primarily be affected by the type and thickness of the insulation material. However, only material with very low thermal resistance will not affect the moisture and temperature conditions, nullifying the desired impact of the thermal retrofit via internal insulation.

The third condition cannot be altered in the design or the application of the internal insulation thermal retrofit. However, it can be evaluated whether it applies for the masonry material involved. As a first step, a visual inspection of the existing facade may reveal evidence of frost damage from the past,

which logically is an indicator of potential future frost damage. In these cases, the application of internal insulation cannot be recommended. If there is no visual evidence, one should secondly consider a direct or indirect evaluation of the masonry material, based on the methods from section 4.3.3. If these (extreme) evaluations give a negative result, it should thirdly be considered to assess the sensitivity to frost damage at milder conditions with the methodology set forward in section 6.2. One should keep in mind though that this requires an extensive experimental effort, wherein a large number of material samples has to be available

4.4 Threshold values for Algae and Cyanobacteria

A building façade is characterized by extreme fluctuations of temperature, repeated desiccation and high UV-radiation, so any organism living here must be able to tolerate these variations, maintaining a metabolic activity. Different algal species have very different appearances, life-styles and tolerance of variations in temperature, moisture etc. and they are metabolically active when appropriate combinations of dampness, warmth and light are present (Ortega-Calvo, Ariño et al. 1995, Saiz-Jimenez 1997, Tiano 2001). Algae and cyanobacteria growth combined with the dissolutive effect of water may also result in micro-cavities, or micro-indentation of the stone. This effect facilitates algae and cyanobacteria growth by providing to the cells much more asperities to anchor themselves.

In general, there is a lack of knowledge about conditions which influence algae and cyanobacteria growth, but some common demands can be specified. For photosynthesis process, the combination of sufficient light, water, temperature, carbon dioxide and some mineral nutrients must be present. Algae can find also nutrients in some trace elements (Fe, Mn, Si, Zn, Cu, Co, Mo, B, V) for growth, which are normally available in the environment (rain, dust, material substrate), so that the local micro climate is the determining factor for biological growth on façades (Zillig, Lenz et al. 2003).

However, humidity and temperature are the most important environmental conditions. Water is fundamental for algae growth, as it is needed for photosynthesis. The water uptake must occur directly through the cell wall by osmosis and the growth limit for green and for blue algae is about 100% RH (liquid water) (Lengsfeld and Krus 2001). Wind driven rain and dew water are the main causes for wetting of façades with liquid water (Miller, Dionísio et al. 2009). However, algae and cyanobacteria can survive dry periods and can restart their growth when enough humidity is available. Therefore, the drying of façades during the day is not sufficient to prevent algae growth (Moon and Augenbroe 2004).

For each species of microorganism, there is an optimal temperature for growth and a range between a minimum and a maximum outside of which growth is not possible (Singh and Singh 2015). According to literature, for most algae and cyanobacteria an optimal temperature for growth was estimated within the range of 20 °C and 30 °C (Konopka and Brock 1978, Mai, Militz et al. 2004, Serra-Maia, Bernard et al. 2016), while the range of suitable growth is usually considered between 5 °C and 40 °C (Raven and Geider 1988, Lengsfeld and Krus 2001). However, the resistance to high temperatures (above 50 °C) or low temperatures (below 0°C) appreciably varies from one type of microorganism to another (Imre Friedmann and Ocampo-Friedmann 1995, Billi 2010, Shukla, Kvíderová et al. 2013).

The influence of pH action on algae is not well known and depends on their tolerance. Microorganism can be classified into acidiphiles, neutrophiles and basiphiles, but there also exist indifferent microorganisms which normally develop in a wide range of pH, such as bacteria whose growth is

satisfactory between pH values equal to 6.0 and 9.0. Most algae and cyanobacteria found on building façades can normally develop at a pH equal to 8.0 (Verhoef 1988, Singh and Singh 2015).

Finally, as photosynthetic organisms, algae and cyanobacteria need light and carbon dioxide to permit photosynthesis biochemical process and produce energy needed for maintenance, growth and reproduction.

It was found that the physical phenomenon of growth and multiplication of algal cells generally follow a trend similar to a sigmoid curve (Tran, Govin et al. 2013). Indeed, the growth of a micro-algae culture is characterized by three phases: an initial lag phase during the so-called "latency time" (when algal stains are not still visible), a phase of rapid growth and a final stagnation phase, when the covered surface by microorganisms become constant over the time (Figure 4.7) (Tran, Govin et al. 2012, Tran, Govin et al. 2014).

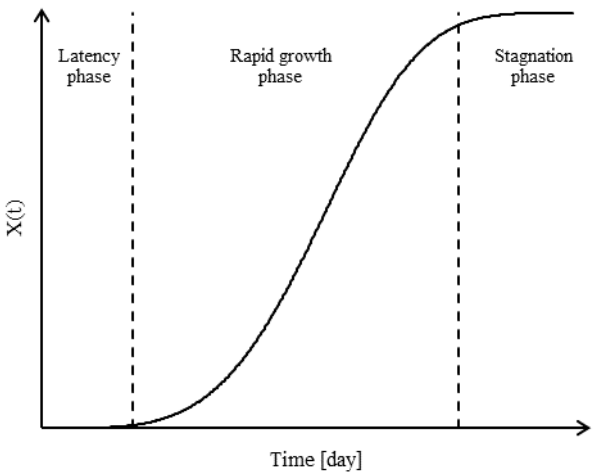

Figure 4.7: Typical growth of a micro-algae culture

4.4.1 Control actions

To induce algae growth the material surface must be sufficiently wet. Since it is not possible to control the outdoor environmental conditions, the most recommended measure to prevent or minimize algal development is to avoid the presence of free water on the material surface. In fact, water is the most important factor to consider when limiting the risk of algal growth, and the consequent building material decay. The use of high porous and rough materials in the critical parts of the envelope should also be limited, especially where wind driven rain and leaks from rainwater drainage systems or from the roof can occur.

However, once the building materials' surface is affected by the presence of algae, mechanical methods can be used to remove stains and patinas from contaminated elements either by hand or with tools such as scalpels, spatulas, scrapers, etc. These methods have the advantage of not adding any substance that might cause further deterioration, but mechanical actions could physically damage the substrate (Tiano 2001). Anyhow, a preliminary biocide treatment (applied before the mechanical intervention) is advantageous to facilitate the removal of biofilm (Hofbauer, Breuer et al. 2003), but some chemical substances can enter in contact with the substrate in any case.

Among the physical interventions, one of the most widespread method against algal and cyanobacteria growth is ultraviolet (UV) radiation treatments. The germicidal activity is obtained

with the part of the UV spectrum between 300-200 µm (Tiano 2001). However, UV radiation does not have a deep penetration power and sometimes they can modify the material of the substrate, changing the colours of the surface (Tiano 2001). Thus, it is not always appropriate in cultural heritage or similar applications.

Other possibilities are related to chemical methods, which use biocide agents of synthetic origin like pesticides and disinfectants (Tiano 2001). A side problem with chemical methods is related to the use of pesticides that persist in the soil or water (Bester and Lamani 2010). In addition, all the methods described above require re-application over time because they are not able to create a permanent film on the treated surface. In this field, some recent works investigated remediations against the biofouling process by novel techniques as TiO2 nano-coatings (Fonseca, Pina et al. 2010, La Russa, Ruffolo et al. 2012, Graziani, Quagliarini et al. 2013, Maury-Ramirez, De Muynck et al. 2013, Radulovic, MacMullen et al. 2013, Graziani, Quagliarini et al. 2014a, Martinez, Bertron et al. 2014).

5 Overview of models for predicting failure mode

5.1 Mould growth in buildings

Mould growth is expected on a certain material if the actual RH conditions exceed the limit value for mould growth at the present temperature (section 4.1). However, RH and temperature are seldom constant, instead they are varying both in the long and short term and hence the critical limit may be exceeded only occasionally, see Figure 5.1 for an example. Favourable conditions for mould growth are therefore replaced by unfavourable conditions by time, as shown schematically in in Figure 5.2.

There is always a time before mould growth begin also at the most favourable conditions. This is called the lag phase. This varies among different materials, levels of RH and temperature (Viitanen 1997a, Fog Nielsen, Nielsen et al. 2000, Johansson, Ekstrand-Tobin et al. 2012). Also, the length of periods with unfavourable or favourable conditions effects mould growth (Viitanen and Bjurman 1995, Johansson, Bok et al. 2013). The long-term cycling affects mould growth more than the short-term.

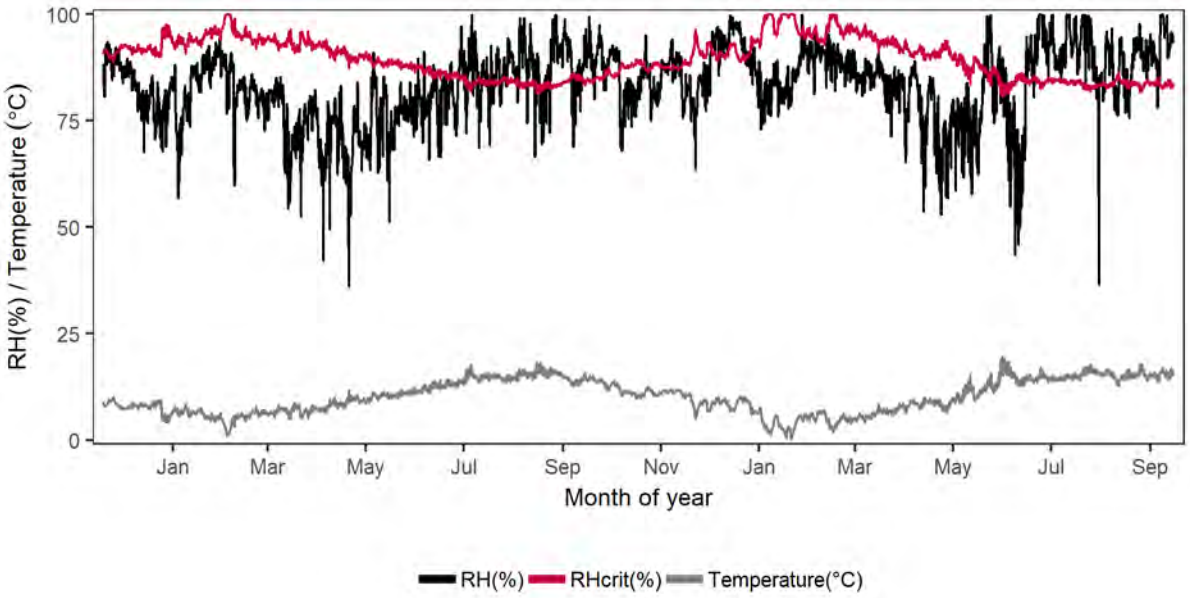

Figure 5.1: Example on how RH and temperature vary by time in a crawl space, showing the actual RH for some periods exceeding the limit values for mould growth

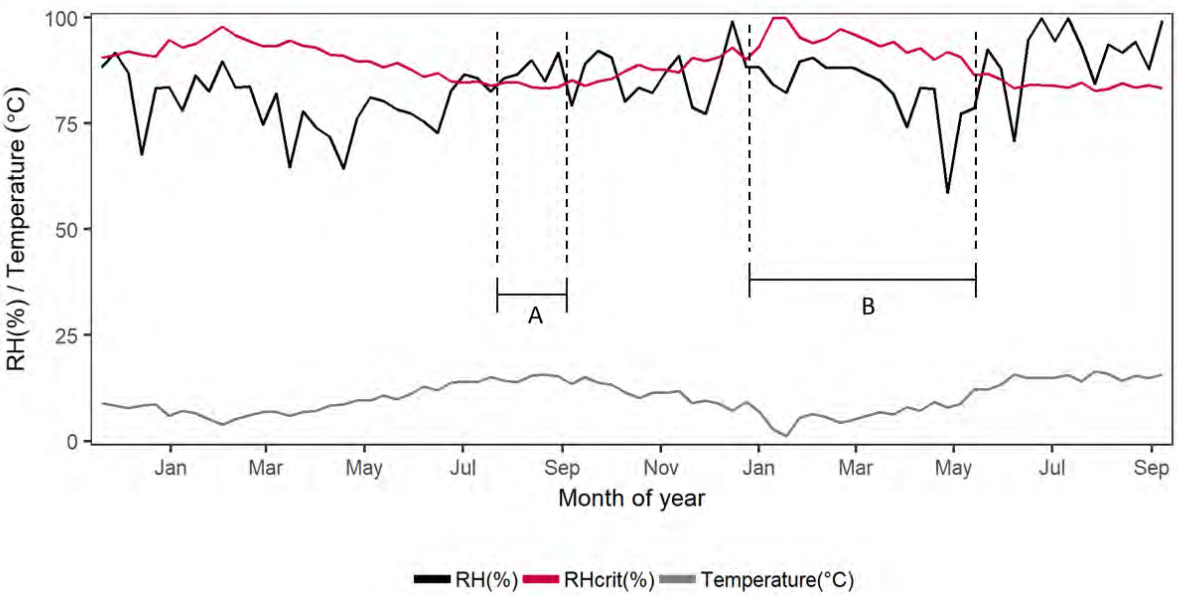

Figure 5.2: Illustration on variations of RH and temperature by time. Periods of favourable conditions for mould growth appears when actual RH is above the limit value for growth (RH_{crit}) (A) and unfavourable when RH is below this limit (B). RH_{crit} varies over time as it is dependent on the temperature

In order to avoid mould growth, different mould prediction models may be used in the design phase of new buildings, including moisture safety design. Several such models have been developed during the last 20-25 years, aiming to estimate the "risk" for mould growth at given conditions of RH and temperature. Some models are presented in (Sedlbauer 2002, Ojanen, Viitanen et al. 2010, Vereecken and Roels 2012, MRD 2016, Gradeci, Labonnote et al. 2018). The models are available as part of hygrothermal simulation tools, as stand-alone programs or have been described and published as journal or conference papers.

The simplest models consider only the situation if the actual RH_{crit} values exceeds the limit values for mould growth (A in Figure 5.2), while more complex models also consider length of time of unfavourable and favourable conditions. A general overview and description of several mould models is given in (Vereecken and Roels 2012) and (Gradeci, Labonnote et al. 2018). Some of the models are also described in Section 7.1, where a round robin test comparing different models is presented.

5.2 Rot

There are several models for predicting rot or phenomena associated to rot. Table 5.1: presents a compilation of some of the most relevant models and what parameters they include in the modelling. Very specialized models e.g. for wood in contact with soil are omitted. However, most of the models are based on a limited number of experiments or very specific cases e.g. growth of a specific fungi or a specific wood species. Therefore, the equations describing the models may not be applicable in cases relevant for internal insulation in historic buildings. Instead, Table 5.1: is illustrating the hygrothermal factors that are needed in models that are relevant for the RIBuild project. Material parameters describing e.g. water uptake in sound and damaged wood respectively, would be relevant as well, but difficult to determine. In case of simulations where these parameters are relevant, general assumptions must be made.

In Table 5.1 below, models for predicting rot are presented. Moisture conditions are described differently in the models. They can be Relative Humidity, Moisture Content (MC) or water activity, as these terms are correlated, they are only described as moisture conditions in this table. Most of the models are based on studies of specific wood species, see Table 4.2.

Table 5.1: Models for predicting rot.

Reference	Modelled parameter	Needed parameters			
		Moisture conditions	Temperature	Time	Others
(Saito, Fukuda et al. 2012)	Mass loss	X*	X	X	
(Maurice, Coroller et al. 2011)	Radiant growth rate inoculated fungi	X	X	X	pH
(Fuhr, Shcubert et al. 2011)	Hyphal growth	X	X	X	pH
(Rapp, Peek et al. 2000)	Moisture induced risk of decay	X*			Liquid absorption at MC_{crit} Vapour desorption at MC_{crit}
(Brischke and Meyer-Veltrup 2015) and (Isaksson, Brischke et al. 2012)	Decay rate	X	X	X	
(van de Kuilen 2006)	Service life	X	X	X	Load
(Viitanen, T. et al. 2010)	Mass loss	X	X	X	

*) Moisture dependency is simply described as above a given critical value independent of e.g. temperature

Of the presented models the model given by (Viitanen, T. et al. 2010), seems to be the most applicable for the use in RIBuild, as it describe a relevant parameter (mass loss) by using hygrothermal parameters in a nuanced way, instead of e.g. defining a general critical value for moisture content independently of temperature.

5.3 Frost damage

In section 4.3, the three prime parameters for frost damage have been introduced: critical saturation degree, critical frost temperature and frost damage sensitivity. However, to the authors' knowledge, no real models exist that translate the exceedances of the first two parameters to an initiation and development of mechanical stresses and strains, to be weighed against the frost damage sensitivity of the material. For mould growth or wood rot, on the other hand, dynamic models exist that transform

the occurring hygrothermal conditions to the evolution of mould and rot. For frost damage, most of the models available to judge frost damage are limited to hygrothermal damage indicators, quantifying exceedances of the critical saturation degree and critical frost temperature. Kočí, Maděra et al. (2017) provide this overview of the indexes put forward in the literature:

- Modified Winter Index: $MWI = \sum_{i=1}^{8760}(T_L - T_i)(w_i - w_L)[T_i < T_L \,\&\, w_i > w_L\,]$;
- Amount of Frozen Water: $AFW = \sum_{i=1}^{8760} w_i[T_i < T_L \,\&\, w_i > w_L\,]$;
- Time Of Freezing: $TOF = \sum_{i=1}^{8760}[T_i < T_L \,\&\, w_i > w_L\,]$;
- Indicative freeze/thaw cycles: *IFTC = number of frost periods > 2h with* $w_i > w_L$

in which T_i (K) and w_i (kg/m³) are hourly values for temperature and moisture content at the considered location, and T_L and w_L refer to the critical frost temperature and moisture content (deduced from the critical saturation degree).

Such simple indexes aim at providing indications of the risk for frost damage. They are comparable thus to the Time Of Wetness for the prediction of wood rot. However, they do not provide information on the damage evolution itself as for example the VTT-model does for wood rot. In addition, it should be stressed again that there is a lack of info on the critical saturation degrees of building materials, since the mentioned frost indexes are only relevant if detailed w_L values are available. These values are very material specific, with large differences amongst materials within the same building material group, see Table 4.4:. Finally, it must be noted that these indexes are cumulative, increasing with increasing exposure. Evidence from the literature and from our own measurements, see section 6.2, does indicate though that there is no linear link between damage and the length, the intensity or the frequency of the exposure.

In contrast to other damage phenomena like mould growth or wood rot, for which predictive models can be applied as decoupled post-processing tools around the basic HAM-calculation, quantification of frost damage actually necessitates an extension of the current HAM-models, firstly with freezing and thawing physics and secondly with mechanical analyses. The level of detail with which the two aspects are implemented in HAM-models will affect the results of the frost damage evaluation. The latter aspect is considered out of reach still – there are first attempts however, see (Gawin, Pesavento et al. 2016) below –, and in what follows primarily the integration of freeze and thaw phenomena is described. Mainly three approaches can be distinguished in the literature:

1: No ice formation included

The simplest way of dealing with freezing and thawing in hygrothermal simulation is of course their exclusion from the model. In doing so, the effects of freezing point depression or latent heat conversion are not considered. The actual ice formation is hence not directly quantified with this approach, but tentative information can still be obtained by using the abovementioned frost indexes.

Examples:

- WUFI (Fraunhofer) (Sedlbauer and Kunzel 2000)
- HAMFEM (KU Leuven) (Vereecken, Van Gelder et al. 2015)
- COMSOL based model (TU/e) (Van Aarle, Schellen et al. 2015)

2: Ice formation included, assuming instantaneous equilibrium between all phases and components

To the authors' knowledge only two existing models in this category can be distinguished: DELPHIN 5.9 (Nicolai and Sontag 2013), and an EMPA COMSOL-model (Zhou, Derome et al. 2017). For the DELPHIN software, a first step toward implementing freezing and thawing phenomena has been taken. Currently, DELPHIN takes ice formation into account by assuming the instantaneous equilibrium between the three phases (vapour, liquid and ice), by applying a freezing point depression under the assumption that the pore space fills from the smallest to the largest pore, and presuming that ice crystalizes outside of the liquid phase (Nicolai and Sontag 2013). Basically, this model investigates, based on the concept of freezing point depression, whether the moisture content is sufficiently high to fill pores wherein water could freeze. In this way, DELPHIN takes into account that low moisture content levels will require much lower temperatures. In addition, DELPHIN incorporates latent heat effects connected to freezing and thawing.

First attempts to account for the impacts of ice formation on the heat and moisture transport properties in the DELPHIN-framework have also been documented (Sontag, Nicolai et al. 2014). A very similar approach is applied by Zhou, Derome et al. (2017). These authors report on the impressive impact on the moisture distribution when taking freezing into account. Figure 5.3 below is adopted from Zhou, Derome et al. (2017) and it illustrates that the moisture content is consistently higher in winter for a brick facade with internal insulation when freezing is considered. The authors link this effect to moisture migration towards the freezing front. They also provide a validation of the model with experimental results (Zhou, Zhou et al. 2014), confirming the importance of this effect within soils. However, preliminary numerical investigations by the authors with the DELPHIN 5.9 model could not identify similar levels of moisture migration towards the freezing front within bricks.

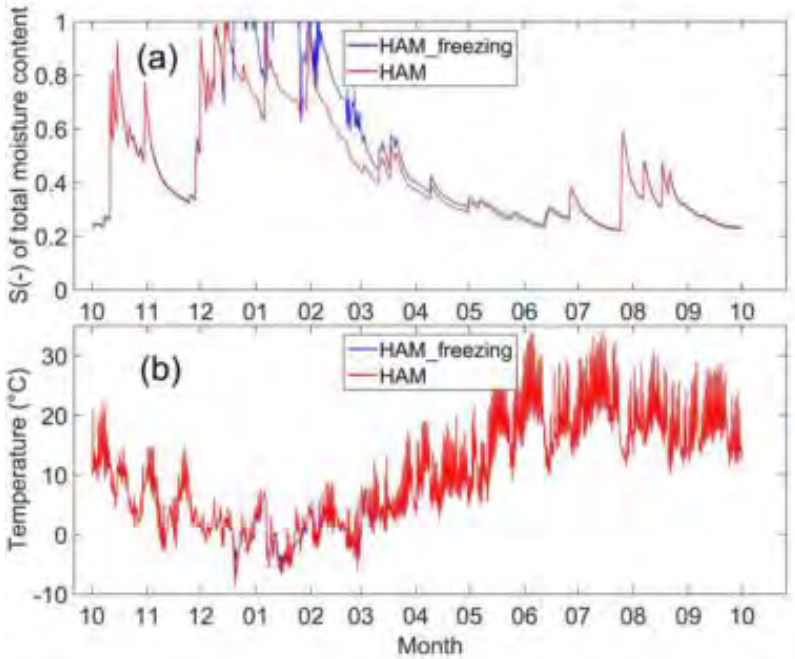

Figure 5.3: Simulation results on the impact of taking freezing process into account (Zhou, Zhou et al. 2014)

In addition, it must also be mentioned that a global assumption in both models – pores filling from the smallest to the biggest pore with a subsequent quantification of the freezing point depression for the smallest filled pore (see section 4.3.2) – is probably overly simplified. Such assumption is based on completely redistributed moisture in porous media. In dynamic conditions though, this may not

(always) hold. Bigger pores may (temporarily) be filled before this moisture is redistributed to smaller pores. As a consequence, this handling of the freezing point depression might result in an underestimation of frost damage processes under dynamic conditions.

Examples:

- DELPHIN 5.9 (TUD) (Sontag, Nicolai et al. 2014)
- COMSOL based model (EMPA) (Zhou, Derome et al. 2017)

3: Ice formation included, considering non-equilibrium between all phases and components

Gawin, Pesavento et al. (2016) implemented a model (HMTRA-FREEZE) wherein a non-equilibrium approach considers the thermodynamics of the freezing and thawing processes. This model also takes the resulting mechanical stresses and strains into account, permitting the prediction of damage patterns. The first validations of the model with the experiments of (Sun and Scherer 2010) are promising. More research is required though to verify the need to implement kinetic effects of freezing and thawing in the overall simulation of frost's and frost damage's initiation and development.

5.4 Algae on the facades

Only a few studies have attempted to model biofouling on building materials (Ruot and Barberousse 2007, Tran, Govin et al. 2013, D'Orazio, Cursio et al. 2014, Graziani, Quagliarini et al. 2016a, Graziani, Quagliarini et al. 2016b) and further research is needed to predict the growth of algae and cyanobacteria. The biofouling process was numerically simulated and it was found that Avrami's theory allows to suitably model biofouling under accelerated laboratory growth conditions (Tran, Govin et al. 2013, Graziani, Quagliarini et al. 2016a, Graziani, Quagliarini et al. 2016b). Avrami's theory was developed as an exponential equation (Avrami 1939, Johnson and Mehl 1939, Avrami 1940, Avrami 1941) and was originally used to describe the allotropic phase transformation in solids (M.Fanzoni and M.Tomellini 1998, Khawam and Flanagan 2006). Currently it is used in many domains: crystallization of polymers, heat treatment, decomposition of solids (Hay 1971, Slovácek 2004).

Two processes are at the base of this theory: the nucleation, which corresponds to the appearance of nuclei of a new phase, and the growth, which represents the increase in the size of the nuclei during time. The algal colonization can be described by two processes: attachment and growth of algal cells. The biofouling starts by attachment of algae on the material surface which creates many spots and the colonization rate follows a sigmoid curve for the surface fraction colonized as function of time. The colonization can be simulated considering the algal spots as nuclei. The extension of the fouling results from the increase in the size of the first algal spots by the growth of algal filament as a function of time.

In order to represent the growth process also in case of a surface not totally covered by the biofouling, the original Avrami's law was improved into a modified model (Graziani, Quagliarini et al. 2016a, Graziani, Quagliarini et al. 2016b, Graziani and Quagliarini 2018) described by the equation 4.:

$$X(t) = (1 - \exp^{-K(t-t_1)^n}) \cdot \frac{A_c}{A_t} \qquad (4)$$

where the covered area by algae $X(t)$ [-] is given as a function of time t [day]. The rate coefficient K [-] is a parameter related to the growth rate and it is constant for each material. The time t_1 [day]

represents the latency time before a chromatic alteration occurs on the material surface. The Avrami's exponent n [-] is a coefficient which can be reasonably assumed equal to 4 in case of algae growth: three dimensions represents the growth and one represents nucleation rate assumed as constant (Jena and Chaturvedi 1992, Tran, Govin et al. 2013, Graziani and Quagliarini 2018). Lastly, the final covered area ratio, indicated as A_c/A_t [-], expresses the percentage of covered area at the end of the growth process. A_c is the covered area by algae at the end of the accelerated growth test, and A_t is the total area of the sample exposed to biofouling (Graziani and Quagliarini 2018).

The parameter K depends on the nucleation rate of algal cells and it is related to material properties. It can be calculated from equation 5.

$$K = \Lambda \cdot k_g \cdot k_c^{\,2} \tag{5}$$

where k_g [spot/μm^2 day^2] is the specific attachment rate constant, indicating the rate of the nucleation of new particles, and k_c [μm/day] is the specific growth rate constant. The Avrami's constant Λ [-] can be determined by equation 6.

$$\Lambda = \frac{2}{(q+1)\cdot(q+2)\cdot(q+3)} \tag{6}$$

with:

$$q = n - 3 = 1 \tag{7}$$

The specific attachment rate constant k_g can be obtained by linear regression from the specific attachment rate dγ/dt [spot/μm^2 day], which defines the number of algal spots that appears on a surface unit per time unit (equation 8):

$$\frac{d\gamma}{dt} = k_g \cdot (t - t_1)^q \tag{8}$$

where γ is the number of algal spots at time t per unit area [Spot/μm^2].

The growth rate constant k_c can be experimentally determined by calculating the equation 9:

$$k_c = \frac{\sqrt{S_{t+\Delta t}} - \sqrt{S_t}}{((t+\Delta t) - t)} \tag{9}$$

where S_t [μm^2] represents the area of an algal spot at time t, and $S_{t+\Delta t}$ [μm^2] is the area of the same algal spot at time $t+\Delta t$.

The modified Avrami's model (equation 1) for the biofouling modelling was validated by (Graziani, Quagliarini et al. 2016a, Graziani, Quagliarini et al. 2016b, Graziani and Quagliarini 2018).

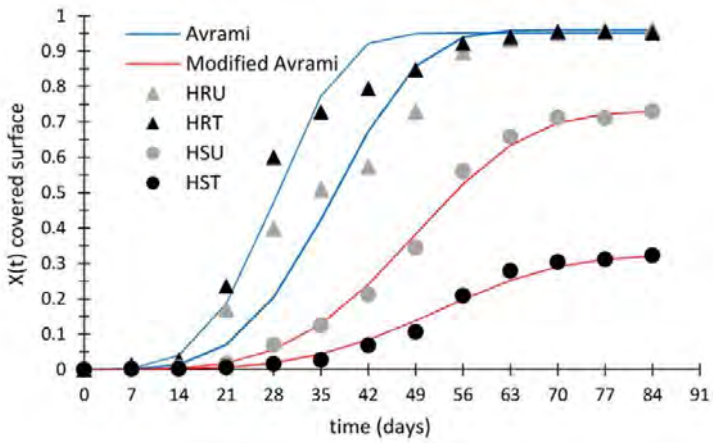

Figure 5.4: Example of algae growth on fired bricks, overlapping the analytical curve (red and blue lines) on the experimental data from (Graziani, Quagliarini et al. 2016a, Graziani, Quagliarini et al. 2016b, Graziani and Quagliarini 2018)

6 Laboratory testing of threshold values in RIBuild

6.1 Determination of RH_{crit} for mould growth on new insulation materials

6.1.1 Aim of the study

The aim of the study was to determine the critical moisture value, $RH_{crit,}$ for mould growth on different insulation materials commercially used in Europe. Some of the products are used in RIBuild WP3 case study buildings. The results may be used in the evaluation tool developed in WP6, to determine if there is a risk for mould growth on the tested products during given conditions of RH and temperature.

The laboratory tests of threshold values for mould were performed at RISE, Division Built Environment – Building Technology in Borås, Sweden.

6.1.2 Materials and method

6.1.2.1 Test method

The test was performed according to 'Laboratory method for assessment of the lowest hygrothermal conditions required for mould growth' (SIS 2014), also named the CML-method (Critical Moisture Level-method) (Johansson, Ekstrand-Tobin et al. 2014). It is based on different standardised methods for determining the mould resistance of building materials and on laboratory testing (Johansson, Ekstrand-Tobin et al. 2012) and is validated in field studies (Johansson, Svensson et al. 2013). The method is also described and discussed in (Johansson, Ekstrand-Tobin et al. 2014) and is published in (Johansson 2014).

6.1.2.2 Materials

The partners in the RIBuild project were asked to select products used for internal insulation in their own country or used in RIBuild test stands (Freudenberg, Ruisinger et al. 2018). Samples of products, clean and unused, were sent to RISE (Borås, Sweden). The samples were packaged moisture open to avoid mould growth during transport and were also dry and clean before wrapping. Twelve different insulation boards and one loose fill insulation material was tested. In addition, one gypsum board and seven different kinds of mortars were tested.

At RISE, the samples of board materials were divided into test specimens, sizing 50x100 mm. Test specimens of loose-fill insulation were prepared by placing samples of the material in a cage of fine stainless-steel mesh (autoclaved) with an internal volume of approximately 0.05 litres. The mortars were prepared according the instructions for each product and was partitioned in petri dishes with a diameter of 90 mm. The thickness of each sample was approximately 7-10 mm

The tested products are shown in Figure 6.1and Figure 6.2. In some cases, the product was made of two or three different materials. In those cases, each facing was evaluated separately during the test.

In this report the professional product name is not given, as this would conflict with the impartiality of RISE. Instead, the names are decoded in the result section, see Table 6.7.

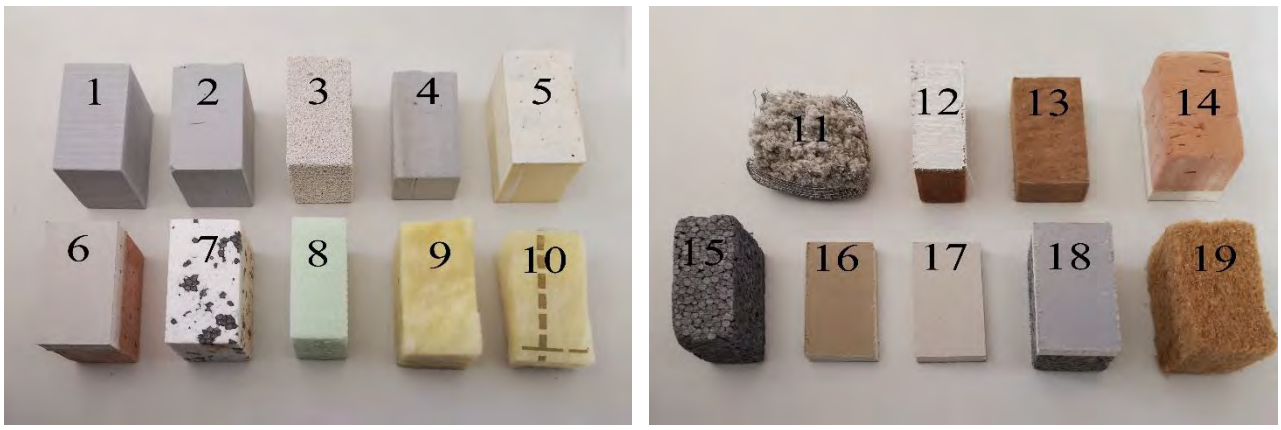

Figure 6.1. The building materials tested. The numbers refer to material name presented in Table 6.2. Note that there may be two different faces of the same product

Figure 6.2. Tested mortars

Table 6.1: Materials referring to Figure 6.1 . Note that the numbers extend in two columns

Number according to Figure 6.1	Material	Number according to Figure 6.1	Material
1	CaSi board 3	11	Loose fill cellulose
2	CaSi board 1	12	Aluminium foil
3	CaSi board 4	13	Wood fibre board
4	CaSi board 2	14	PUR
5	Foil on PUR*	15	Polystyrene 2
6	Gypsum board 4	16	Gypsum board 3
7	Polystyrene 1	17	Gypsum board 2
8	Polystyrene 3	18	Gypsum board 1
9	Mineral wool	19	Wood fibre board 2
10	Soft tissue on mineral wool board		

*The core consists of PUR. The tested surface is the outer foil

6.1.2.3 Laboratory test

A spore suspension consisting of six different kinds of mould spores, according to Table 6.2, was prepared under sterile conditions. The concentration of spores was counted, diluted and mixed to 10^6 spores per ml of each species in the solution. 0.4 ml of the spore suspension was sprayed evenly onto one surface of each test specimens.

Table 6.2: Test fungi

Test fungus	CBS number
Eurotium herbariorum	115808
Aspergillus versicolor	117286
*Penicillium rubens**	401.92
Aureobasidium pullulans	101160
Cladosporium sphaerospermum	122.63
Stachybotrys chartarum	109292

*This was previously named as Penicillium chrysogenum

Following this inoculation, the test specimens were incubated horizontally in the dark in four different climate test chambers (CTS C-20/350, CTS GmbH, Hechningen, Germany) for 12 weeks, inoculated side of the specimen was faced up. The chambers are calibrated once a year from an accredited laboratory. The set RH in the chambers was 80%, 85 %, 90 % and 95 % respectively. The temperature was 22°C. Air with the desired RH and temperature streamed over the test pieces at a velocity of 0.3-0.5 m/s, which ensured that the microclimate at the surface of each test specimen was the same (Johansson, Ekstrand-Tobin et al. 2012). Temperature and RH were recorded every 12 minutes with calibrated integrated sensors in the chambers.

Every 14 days, the test specimens were removed from the chambers for a short time. Mould growth on the inoculated surface of each test sample, excluding the edges, was assessed. Both mould growth visible to the naked eye and that which was only visible under the microscope at 10–40x magnification were rated according to a five-point rating scale according to Table 6.3.

Table 6.3: Rating scale for the assessment of mould

Rating	Description of extent of growth	Schematic illustration*
0	No mould growth.	
1	Initial growth; one or a few hyphae and no conidiophores.	
2	Sparse, but clearly established, growth; often conidiophores are beginning to develop.	
3	Patchy, heavy growth with many well-developed conidiophores.	
4	Heavy growth over more or less the entire surface.	

*Note that the pictures are only schematic for guidance and that the growth may not be visible to the naked eye.

6.1.2.4 Determination of RH_{crit} at 22°C

An individual test specimen is defined as having failed when the mould growth equals or exceeds rating 2. The critical moisture level is considered reached at the RH level where at least two test specimens have failed (RH_{up}) at the end of the test (12 weeks) and no growth is detected on the test specimens at the next lower RH level tested (RH_{Low}). The actual critical moisture level is then expected between these two values or at the RH level when the test specimen is positive. The value is therefore reported as a range $RH_{Low} < RH_{crit} \leq RH_{up}$. This principle, with examples, is shown in Figure 6.3. If mould is detected at 80% RH, then the critical moisture level is estimated to 75% ≤ RH_{crit} ≤ 80%RH, since the lowest RH for mould growth on building materials is 75 %.

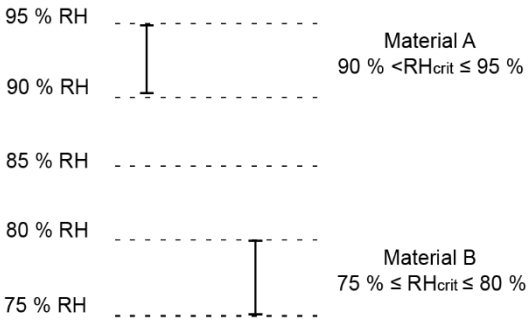

Figure 6.3: Principle of determination of critical moisture level. The numbers of RH represent the tested RH, except for 75% which is used as the lowest limit for mould growth based on literature. On material A, there is mould growth at 95% RH but not at 90% RH and the critical moisture level is therefore 90% < RHcrit ≤ 95%. on material B there is mould growth at 80% RH and the critical moisture level will consequently be established as 75% ≤ RHcrit ≤ 80%. (From Johansson et al 2014).

The mean RH and temperature in the test chamber will not always be equivalent to the set value, due to measurement uncertainties. The expanded measurement uncertainty, *U*, for each chamber was calculated according to equation 10 and 11.

$$u_c = \sqrt{s^2 + u_{cal}^2} \tag{10}$$

where u_{cal} the measurement uncertainty from calibration of the test chamber
s the standard deviation from the measurements

$$U_c = k * u_c \tag{11}$$

where k=2 and corresponds to a coverage probability of 95 %

Simply expressed, this means that there is 95% probability that the true mean value of the measured RH in the test chamber is in the interval mean RH ± U. To ensure that the various incubation RH level differ from each other, the intervals cannot overlap. For the test to be valid, mean values with uncertainties must fall into specified limits for the test to be valid, see Figure 6.4.

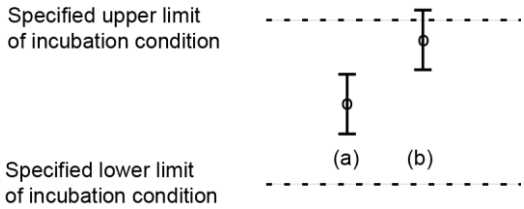

Figure 6.4: Illustration of the evaluation of incubation criteria. The specified limits of incubation condition are described in

Table 6.4:. The dots represent mean measured values of RH or temperature and the whiskers represent the calculated expanded uncertainty. In (a) the mean value with uncertainties fall into allowed limits. In (b) it does not, since the upper limit is exceeded. Therefore, in this case, the test is not valid

Table 6.4: Set points of each incubation condition of the test method

Incubation condition	Set point	Specified lower limit	Specified upper limit
T	22.0°C	20.0°C	24.0°C
RH 1	80.0	77.5%	82.5%
RH 2	85.0	82.5%	87.5%
RH 3	90.0	87.5%	92.5%
RH 4	95.0	92.5%	97.5%

The product tested will belong to one out of five material classes, according to Table 6.5.

Table 6.5: Material classes

Class	RH_{crit} at 22°C
A	$75\% \leq RH_{crit} \leq 80\%$
B	$80\% < RH_{crit} \leq 85\%$
C	$85\% < RH_{crit} \leq 90\%$
D	$90\% < RH_{crit} \leq 95\%$

E	$RH_{crit} > 95\%$

6.1.2.5 RH_{crit} at other temperatures

As RH_{crit} is temperature-dependent, the test results are only valid for the temperature tested, that is, 22°C. RH_{crit} is assessed also for other temperatures by using equation 12. The equation is based on the shape in Sedlbauers LIMcurves and extensive testing of mould growth on different temperatures and RH (Johansson, Ekstrand-Tobin et al. 2012). A value is produced for the lower as well as the higher level in the RH_{crit} expression $RH_{low} < RH_{crit} \leq RH_{up}$.

$$RH_{critT} = 105 + c(T^2 - 54 * T) \quad (12)$$

Where c takes values according to Table 6.6.

Table 6.6: Values of c

Class	*RHlow*	*RHup*
A	0.043	0.036
B	0.036	0.028
C	0.028	0.021
D	0.021	0.017
E	0.017	-

If calculations are repeated for a series of temperatures common in buildings, the critical moisture levels can be expressed as growth limit curves, see Figure 6.5.

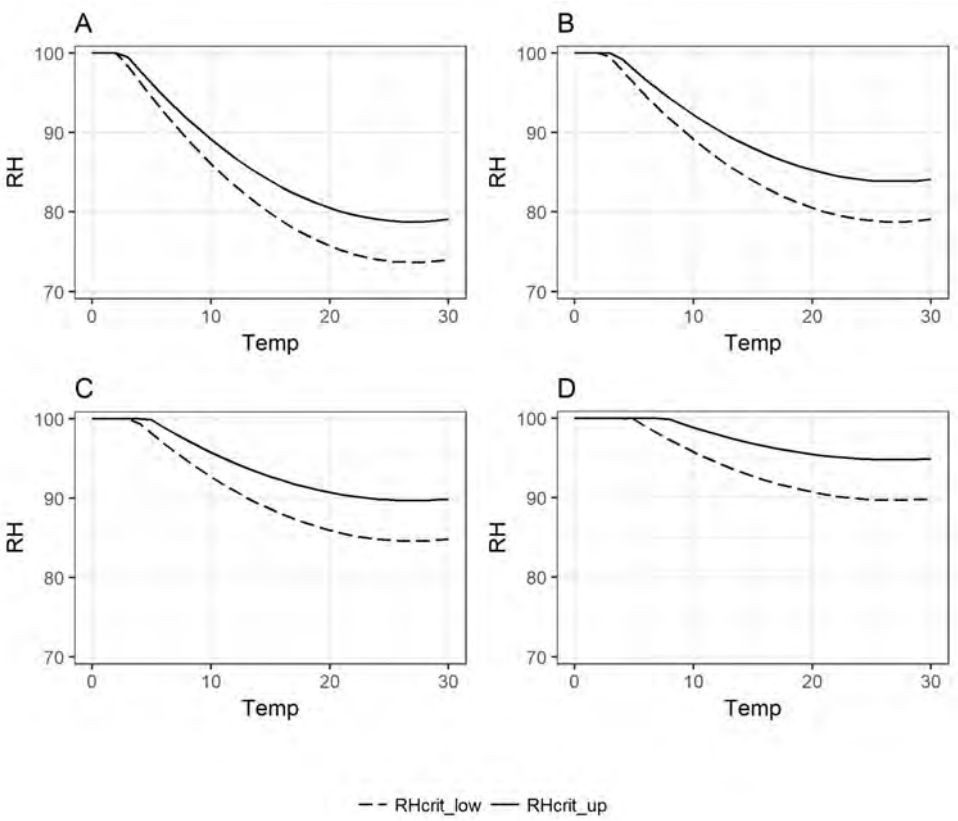

Figure 6.5: Growth limit curves for the different material classes according to equation 12

6.1.3 Results

The results, RH_{crit}, for each product, facing of the product or component of a product, is shown in Table 6.7.

The incubation RH of one of the chambers did not fulfil the criteria. This was not found until after the test ended, in connection with the annual calibration of the climate cabinet. The prior calibration result, on which the test relied, was proven wrong. The test in this chamber therefore had to be restarted and is not yet finished at the time of writing this report. The results for some materials are therefore preliminary, marked with * in. In addition, the testing of mortars started close to the writing of this report and there are still no results for products in this group. The final results will be included in WP6 as the final outcome of RIBuild.

Table 6.7: Determined RH_{crit} Cells marked with grey: Cases where specific product differ from other products in the same material group. Some products contain different kind of material, e.g. product "l" containing gypsum, PUR and aluminium foil

Group	Material	Product id	RH_{crit} (%)	Class RHcrit
CaSi board	CaSiboard1	b	$RH_{crit} > 95$	E
	CaSiboard2	r	$90 > RH_{crit} \leq 95$	D
	CaSiboard3	a	$90 > RH_{crit} \leq 95$*	D
	Casiboard4	o	$90 > RH_{crit} \leq 95$	D
Gypsum board	Gypsumboard1	e	$85 > RH_{crit} \leq 90$	C
	Gypsumboard2	h	$90 > RH_{crit} \leq 95$	D
	Gypsumboard3	h	$90 > RH_{crit} \leq 95$	D
	Gypsumboard4	l	$90 > RH_{crit} \leq 95$	D
Mineral wool	Mineral wool board	c	$90 > RH_{crit} \leq 95$	E
	Membrane on mineral wool board	c	$RH_{crit} > 95$	E
Mortar	Mortar1	n	No results yet	No results yet
	Mortar2	i	No results yet	No results yet
	Mortar3	j	No results yet	No results yet
	Mortar4	v	No results yet	No results yet
	Mortar5	q	No results yet	No results yet
	Mortar6	m	No results yet	No results yet
	Mortar7	d	No results yet	No results yet
PUR	PUR	l	$RH_{crit} > 95\%$	E
	Foil on PUR	k	$90 > RH_{crit} \leq 95$	D
	Aluminium foil on PUR	l	$85 > RH_{crit} \leq 90$	D
Polystyrene board	Polystyrene1	g	$RH_{crit} > 95$	E
	Polystyrene2	e	$RH_{crit} > 95$	E
	Polystyrene3	s	$RH_{crit} > 95$	E
Wood fibre insulation	Loose fill cellulose	f	$RH_{crit} > 95$	E
	Woodfibreboard1	p	$75 > RH_{crit} \leq 80$*	A
	Woodfibreboard2	u	$75 > RH_{crit} \leq 80$*	A

*Preliminary results. The final results will be included in WP6.

6.1.4 Discussion

RH_{crit} varied among the different products included in this study. Conventional tests for mould resistance are performed at high RH generally above 95 % (section 4.1). Many of the products in this study would have failed such a test. However, a product not fulfilling the mould resistance test, could still be used in building parts were the RH are not expected to be as high.

From the results above it is confirmed, as have been previously stated (Johansson, Ekstrand-Tobin et al. 2012) that it is not possible to predict RH_{crit} for one specific product, or mark, from the result from another product belonging to the same group of materials. For example, different CaSi boards in the study belong to two different classes of RH_{crit} (D respectively E). Some of the products (CaSi-boards) with the lowest RH_{crit} contains wood fibres, which might have affected the mould susceptibility.

In the building sector, it is sometimes argued that building materials with high pH are inert to mould growth and therefore may be used in building parts with high expected RH without risk for mould growth. Even though the pH of the CaSi boards of this study was not measured, it is expected to be high. Mould growth was still growing on three out of the four products, indicating that it is not the pH that govern if there will be growth or not on a product (although it may affect the mould growth rate).

During production, different batches of a product may vary in their quality that possibly can affect RH_{crit}. Therefore, the test method description prescribes that test samples should be "preferably from different batches in production. This is particularly important if the quality is expected to vary between batches." In this study, RIBuild partners were asked to send materials from different boards of the same product. However, it is suspected that, in most cases, the board samples of a specific product belonged to the same board. If there were samples from different boards, there is no traceability and it is not possible to identify if they come from different batches. The results from the study is therefore valid for the specific samples tested and there might be different results if the same product from another batch are tested.

Contamination of the materials with dirt etc. may affect the susceptibility for mould growth. At the RISE laboratory, the specimens were handled with clean gloves and the partners had previously been asked to handle the samples to minimize the risk for contamination. However, it cannot be ensured that they were totally clean. However, as seven samples from each product was used for each RH tested, the possible risk of contamination affecting the results was reduced as much as possible.

6.1.5 Conclusion

The results verify previous findings that mould susceptibility, in this study determined as RH_{crit}, cannot be estimated based on which group of material it belongs to, supposed contents of organic compounds or pH. Instead, each product must be tested.

Even different faces of a material may vary in susceptibility for mould growth. If a product has two different facings, each facing should be tested separately. In addition, all individual components of a composite product should be tested.

Testing of RH_{crit} widens the use of materials comparing with mould resistance test that only evaluates the resistance to mould growth in a "worst case scenario", i.e. at levels limited to relatively high RH and temperature.

6.2 Frost damage

6.2.1 Aim of the tests

The physical phenomena governing frost damage make it clear that the actual frost temperature and moisture content are important parameters with respect to the occurrence and magnitude of frost damage in building materials. In regular frost damage experiments, only a single extreme combination of frost temperature and moisture content is evaluated, leading to a binary finding on the sensitivity of the material for frost damage. Given that these binary outcomes are irrelevant with respect to the impact of thermal retrofits (e.g. by internal insulation), the experimental campaign aims at widening that sole combination into a spectrum of frost conditions. In this analysis, we examine frost damage in four types of ceramic bricks for frost temperatures ranging from -2 °C to -20 °C and for moisture saturation degrees going from 0.1 to 1.0. The dilatation and ultrasonic methods are employed as damage assessment techniques. In the section below, the material and experimental details are put forward. Then, the experimental results are presented and discussed in detail. Finally, conclusions concerning the impact of frost temperature and moisture content on frost damage are drawn.

6.2.2 Materials and methods

In this section, we first characterize the building materials used for our study. After that, the freeze-thaw cycling is explained as well as both the dilatation and the ultrasonic testing applied to quantify the frost damage.

6.2.2.1 Materials

As a typical facade material, ceramic bricks are chosen as target materials in this study. Concretely, four types of ceramic bricks are used. The Vandersanden brick is a frost-resistant brick, thus appropriate for exterior use, while the Vogelensangh brick is frost-sensitive, and hence limited to interior purposes, both commercially available. In addition, Wienerberger has produced two types of bricks specifically for the investigation, with firing temperatures of 925 and 970 °C in an attempt to obtain frost-sensitive bricks. Table 6.8 summarizes some fundamental properties of these bricks: bulk density (ρ_{bulk}, kg/m^3), open porosity (ϕ, -), capillary absorption coefficient (A_{cap}, kg·m^{-2}s$^{-0.5}$) and capillary moisture content (w_{cap}, kg·m^{-3}). The Vandersanden brick clearly has a similar bulk density and open porosity as the others, but deviates strongly on capillary absorption coefficient and capillary moisture content. This may subsequently give it a relatively stronger frost resistance, see section 4.3.3.2.

Table 6.8: Fundamental properties of the four types of ceramic bricks

Brick type	ρ_{bulk} (kg·m^{-3})	ϕ (%)	A_{cap} (kg·m^{-2}s$^{-0.5}$)	w_{cap} (kg·m^{-3})
Vandersanden	1838	31.4	0.487	176
Vogelensangh	1704	35.4	0.143	244
Wienerberger (925 °C)	1750	33.5	0.145	248
Wienerberger (970 °C)	1778	32.0	0.165	229

Evaluating these properties with the GC-factor (section 4.3.3.2), we obtain -3.5, -0.6, 0.4 and -0.1 respectively, classifying all bricks except for the Vandersanden brick as sensitive to frost damage.

6.2.2.2 Freeze-thaw cycles

In preparation for the test, raw bricks are first cut into samples with the same dimension of 17×10×5 cm^3 and then preconditioned to various moisture contents. After this the moist samples are wrapped with plastic film to avoid evaporation, and then they are placed vertically in the climate chamber on top of an insulation board, Figure 6.6. This gives an omnidirectional test, with frost conditions at all surfaces except for the bottom. Although this protocol is open to discussion, see section 4.3.3.1, the relative comparison between the different brick samples and the various frost conditions is possible.

The execution of the actual freeze-thaw cycling is based on a prior Belgian standard for freeze-thaw testing, NBN B05-203, and the resulting temperature evolution is illustrated in Figure 6.7. The freezing process starts at an ambient air temperature of 15 °C and cools down to 0 °C within 2 h. After that, the targeted frost temperature is approached at a rate of -4 °C/h and maintained for 8~14 h. For the thawing process, the ambient temperature rises rapidly to 15 °C in about 1 h, and remains at that level for 6 h. The variable interval at the actual frost temperature is motivated by imposing a full 24 h cycle in all measurements. In all experiments, 10 freeze-thaw cycles are executed.

In total seven saturation degrees (S) and six frost temperatures (T) have been applied in the test campaign, specifically 0.10, 0.25, 0.40, 0.55, 0.70~0.75, 0.85, 1.0 for S and -2, -4, -6, -8, -14, -20 °C for T. Given the extensive number of frost conditions and the restricted volume of the climate chamber used, only a single sample of each type of brick is tested at each set of frost temperature and saturation degree.

Figure 6.6: Wrapped brick samples (left) and samples positioned in climate chamber (right)

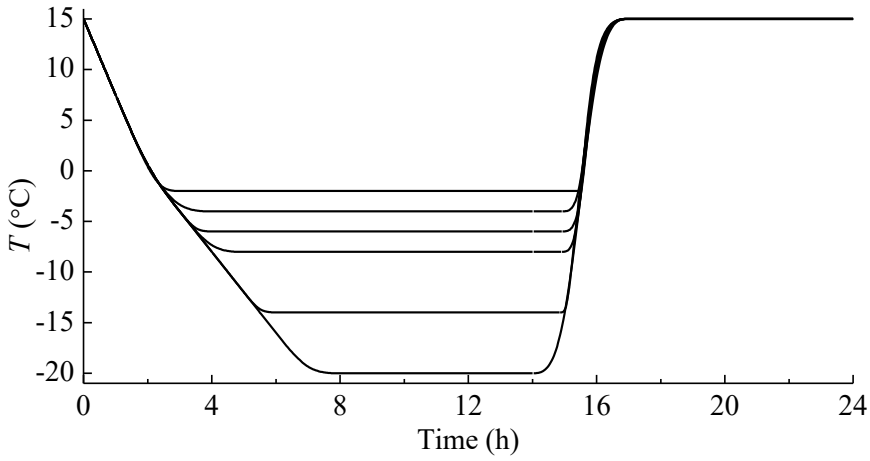

Figure 6.7: The 24-hour freeze-thaw cycle imposed in all experiments, with the different frost temperatures used

6.2.2.3 Damage evaluation

The frost damage is examined via dilatometric and ultrasonic testing, wherein the responses of each sample before and after 5 and 10 freeze-thaw cycles is compared. To perform the dilatometric tests, the dimension of the sample along the longitudinal and transversal axis is measured before and after the freeze-thaw cycling, at the same positions, via calipers with a resolution of 0.01 mm, Figure 6.8 left. A damage index ε (-) is then calculated as the relative dimension change:

$$\varepsilon = \frac{l - l_0}{l_0} \tag{13}$$

with l_0 and l (m) the original and final dimension. For all values of l_0 and l, an average of two measurements is taken.

For the ultrasonic test, a C373N high performance ultrasonic tester emitting a pulse with a frequency of 55 kHz is used. The time needed for the pulse to travel through the sample is measured along the longitudinal and transversal axes, before and after freeze-thaw cycling, at the same sensor locations, Figure 6.8 right. A damage index Ω (-) is calculated as (Løland 1980, Li, Pour-Ghaz et al. 2012).

$$\Omega = 1 - \left(\frac{t_0}{t}\right)^2 \tag{14}$$

with t_0 and t (s) the original and final pulse travel time. It should be mentioned that preliminary testing proves that the plastic film wrapped around the samples has a negligible impact on our results; it is therefore kept throughout the whole study to prevent evaporation.

Figure 6.8: The set-ups for the dilatometric (left) and ultrasonic (right) testing

6.2.3 Results and discussion

In this section, we first report the results obtained from the dilatometric test and analyse them briefly. Next, the ultrasonic test results are presented and studied more deeply. The impact of the measurement direction, the freeze-thaw cycle number, and most importantly, the frost temperature and saturation degree, is examined profoundly.

6.2.3.1 Dilatometric test

The dilatometric test is first performed on samples having experienced the -20 °C frost cycles. The results after five freeze-thaw cycles are brought together in Figure 6.9. A general tendency can be

seen: when the saturation degree S increases then also the damage index ε increases, indicating that moisture content does indeed contribute to frost damage. A closer look disappointingly reveals that even for fully saturated samples ($S = 1$) the ε values remain very limited, never exceeding 0.4%. At lower moisture contents, ε is generally below 0.2%. This minor amount of dimension change can easily be affected by experimental errors, and is thus deemed insufficiently accurate for quantitative analysis, as for freeze-thaw cycling at milder frost temperatures; the results are presumed to be even less discernable. Consequently, we conclude that dilatometric tests are not reliably applicable for our purpose, and we instead restrict the further analysis to the ultrasonic test.

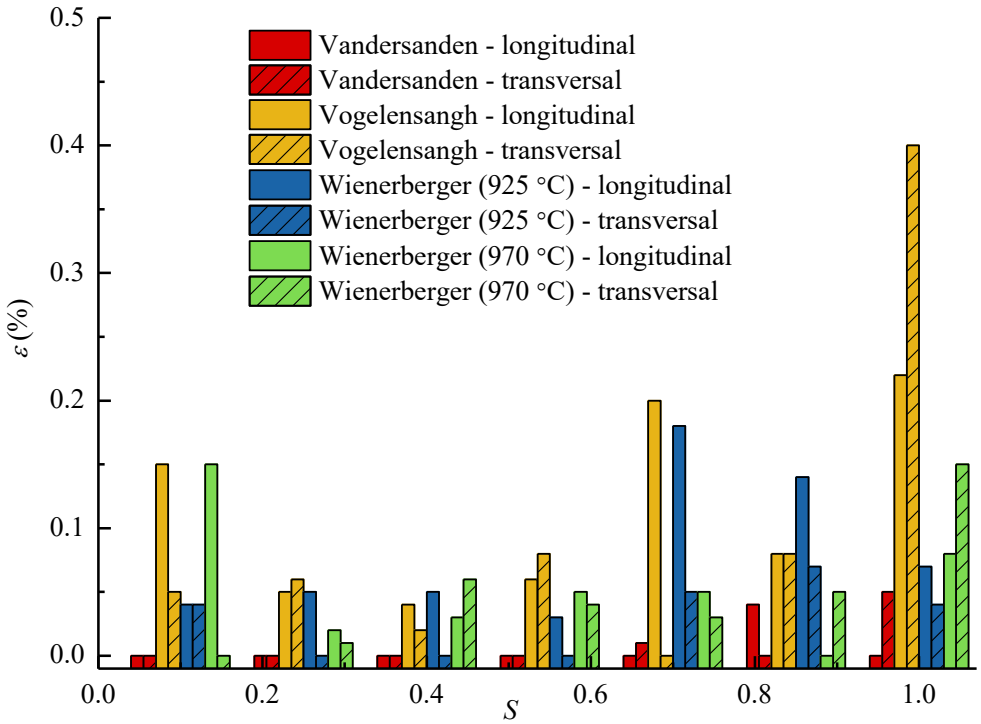

Figure 6.9: Results from the dilatometric evaluation, after 5 freeze-thaw cycles at -20 °C

6.2.3.2 Ultrasonic test

Effect of measurement direction and cycle number

As mentioned previously, the ultrasonic tests are performed after 5 and 10 freeze-thaw cycles along both the longitudinal and the transversal axis. To use Ω as a reliable frost damage index, we first investigate the impact of the measurement direction and the freeze-thaw cycle number. Figure 6.10 and Figure 6.11 illustrate their respective impacts.

It is clearly reflected in Figure 6.10 that different measurement directions do not necessarily produce similar results. However, as observed before, it is generally established that higher moisture contents (larger S values) lead to more severe frost damage. When the ultrasonic tests are executed along the longitudinal direction, this trend is always observable, whatever the material or temperature. On the contrary, the transversal measurements often lead to irregular damage quantifications, rendering the longitudinal measurement direction more dependable. In addition, the ultrasonic technique itself advocates a longer measurement length for better accuracy. Therefore, in the analyses below, only the outcomes from the longitudinal direction are included.

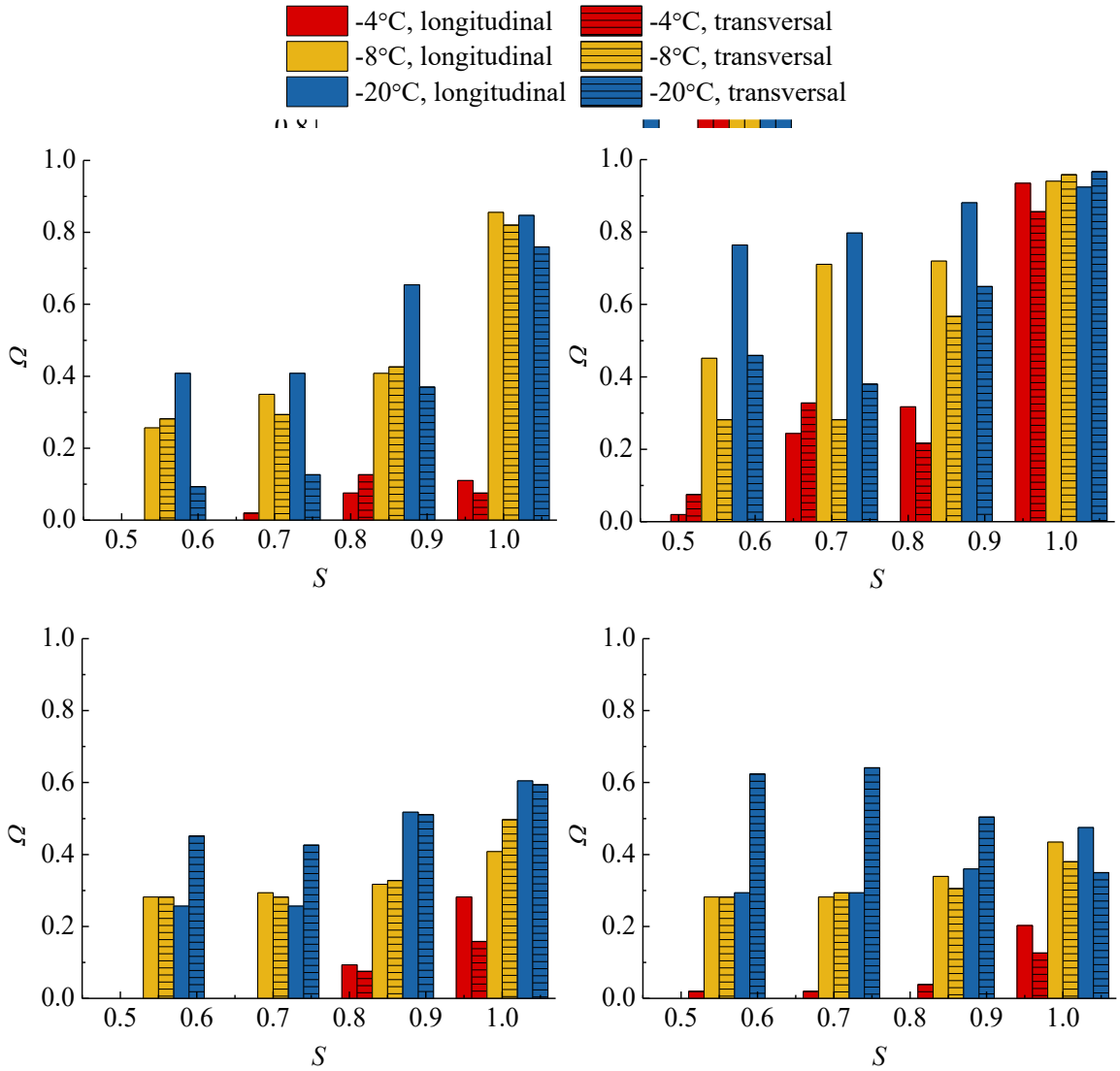

Figure 6.10: Influence of measurement direction on the ultrasonic evaluation, after 10 freeze-thaw cycles; top left: Vandersanden, top right: Vogelensangh, bottom left: Wienerberger (925), bottom right: Wienerberger (970)

From Figure 6.11 it can easily be noted that the freeze-thaw cycle number has a systematic impact: a larger freeze-thaw cycle number always produces a larger Ω. This is a reasonable trend approved by other studies (P. Ingham 2005, Zhou, Derome et al. 2017). Some researchers even claim that mainly the first few freeze-thaw cycles cause the frost damage, i.e. the result not being heavily influenced by the number of cycles (Al-Omari, Beck et al. 2015). This appears to be confirmed by Figure 6.11. In our investigation, the impact of cycle number is in most cases limited, and we therefore limit our evaluation to the outcomes after 10 cycles.

It should be noted that for the ultrasonic test there are in total six applied frost temperatures, while we only show results for -4 °C, -8 °C and -20 °C in Figure 6.10 and Figure 6.11, in order to present 'mild', 'intermediate' and 'harsh' conditions respectively. Moreover, the saturation degrees in both figures start from 0.55 rather than 0.10. This is partly because not all tests combining mild frost temperatures and mild moisture contents have been executed for all four types of bricks – since only minimal damage is expected – and partly because higher moisture levels tend to cause more damage, where measurement uncertainties interfere less and experimental tendencies appear more clearly. Despite the frost temperature and saturation degree spectra in Figure 6.10 and Figure 6.11 being restricted, the general conclusions should still be valid.

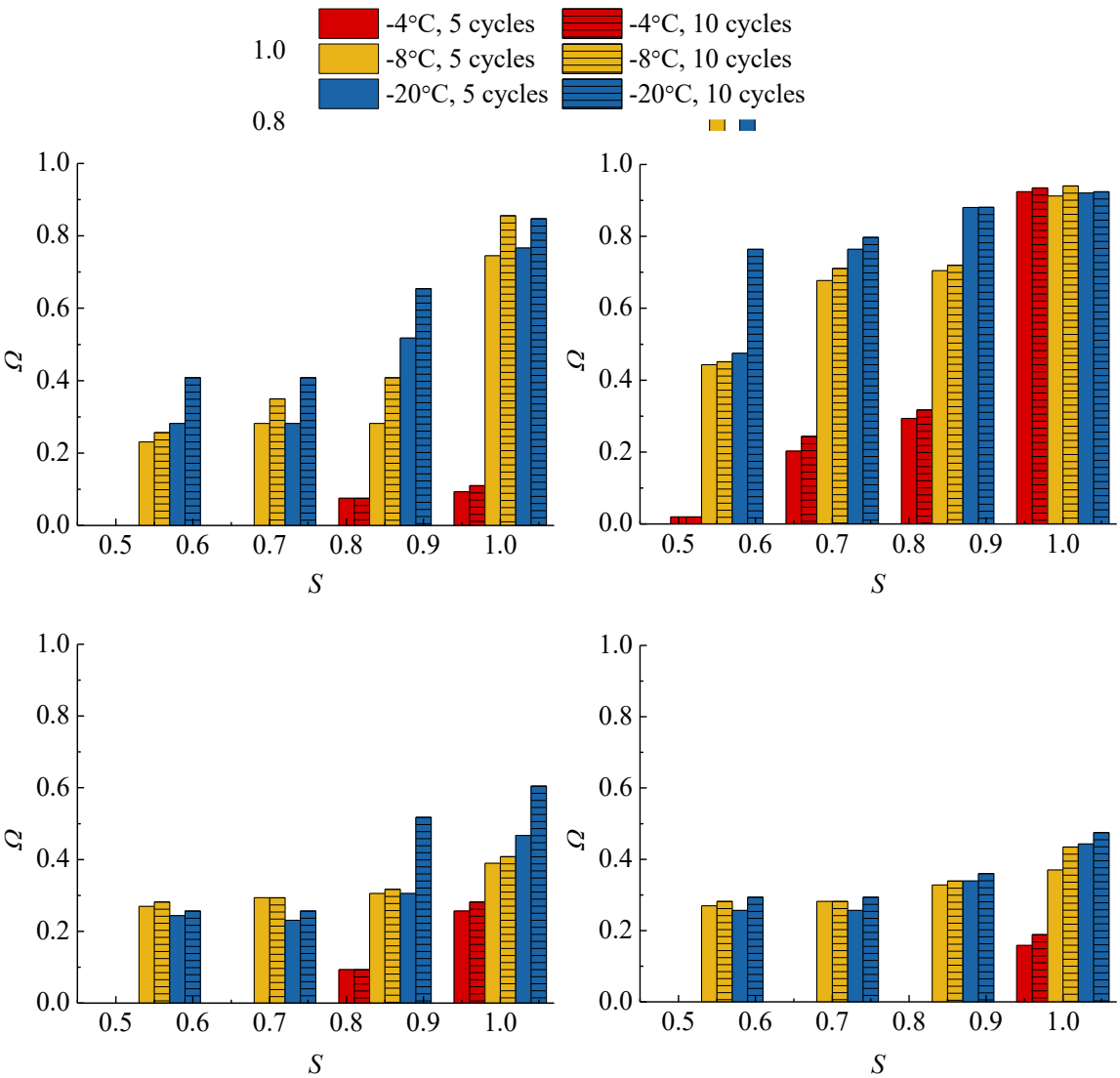

Figure 6.11: Influence of the freeze-thaw cycles on the ultrasonic evaluation along the longitudinal axis; top left: Vandersanden, top right: Vogelensangh, bottom left: Wienerberger (925), bottom right: Wienerberger (970)

Impact of frost temperature and moisture content

Having fixed the measurement direction and the freeze-thaw cycle number, it is time to compare the frost resistance of the four types of ceramic bricks, as well as quantifying the impact of the frost temperature and the moisture content. We furthermore identify their respective critical saturation degrees S_{cr} (-), with the EN 12371 limit of 30% change of Young's modulus translating to Ω equal to 0.3 as critical value. These results are illustrated in Figure 6.12 and Figure 6.13. It should be reiterated that only one single sample is applied for each test condition, which yields occasional irregularities due to experimental uncertainties. The general trends are however reasonably reflected.

A first glance at Figure 6.12 tells that both the frost temperature and the moisture content are positive contributing factors to frost damage: at the same moisture contents a lower frost temperature causes a greater Ω, while at the same frost temperatures a higher moisture content incurs a larger Ω. Resultantly, the most extreme condition (S = 1 and T = -20 °C) is accompanied by the largest Ω values. It is also clearly illustrated in Figure 6.12 that the interior-application-oriented Vogelensangh brick has the largest red-yellow-green area, implying that this brick is most sensitive to frost damage. Contrarily, the Vandersanden brick shows to be less sensitive to frost damage, in agreement with its exterior-application purpose. The two types of Wienerberger bricks are, surprisingly, the least

sensitive to frost damage, contrary to their original purpose. It can also be observed that the Wienerberger brick fired at 970 °C is slightly less sensitive than its counterpart fired at 925 °C. This can be attributed to the fact that a higher firing temperature tends to result in larger pore sizes and smaller porosity, both contributing positively to the resistance to frost damage (Netinger, Vracevic et al. 2014).

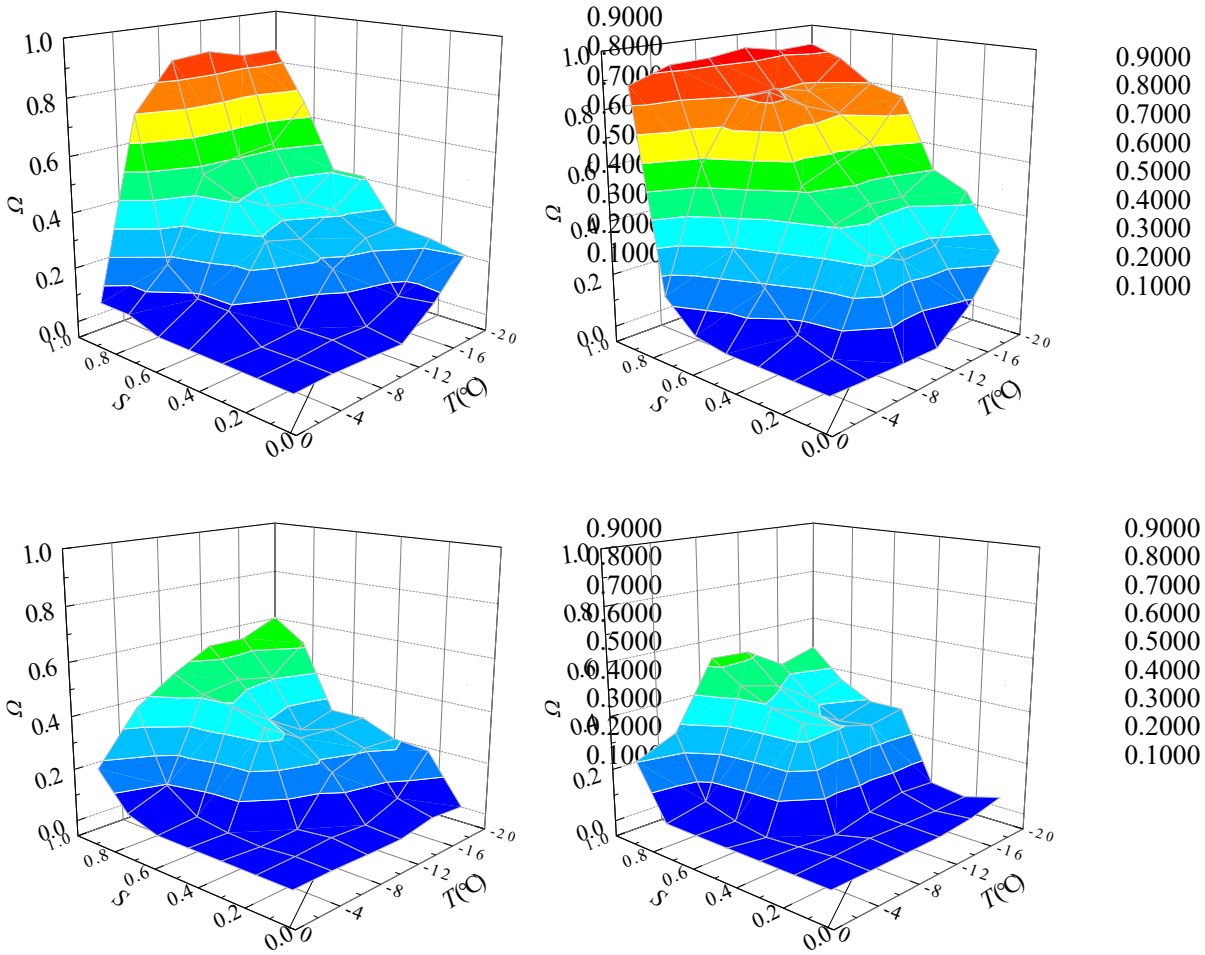

Figure 6.12: Influence of frost temperature and moisture content on the ultrasonic evaluation along the longitudinal axis after 10 freeze-thaw cycles; top left: Vandersanden, top right: Vogelensangh, bottom left: Wienerberger (925), bottom right: Wienerberger (970)

Figure 6.13 illustrates this trend from another angle, as a larger S_{cr} value implies a greater frost resistance, when keeping all other conditions the same. Figure 6.13 furthermore demonstrates that S_{cr} depends on the frost temperature, rather than the usually assumed single value. It is hence more reasonable to express S_{cr} as an isopleth. In addition, the *S* values at the capillary moisture content S_{cap} (-) are 0.72 and 0.74 for the Wienerberger bricks fired at 970 °C and 925 °C, respectively, just around or smaller that their S_{cr}. This implies the moisture content of these two types of bricks would hardly ever go above S_{cr} in common facade applications. They can therefore be considered as virtually fully frost-resistant, as long as the frost temperature does not drop below -20 °C. By the same argument the Vandersanden brick, whose S_{cap} is 0.56, would generally be frost-resistant when the frost temperature does not go below -17 °C. On the other hand, the Vogelensangh brick with S_{cap} 0.69 starts to deteriorate at a mild frost temperature of -6 °C when saturated up to its capillary moisture content.

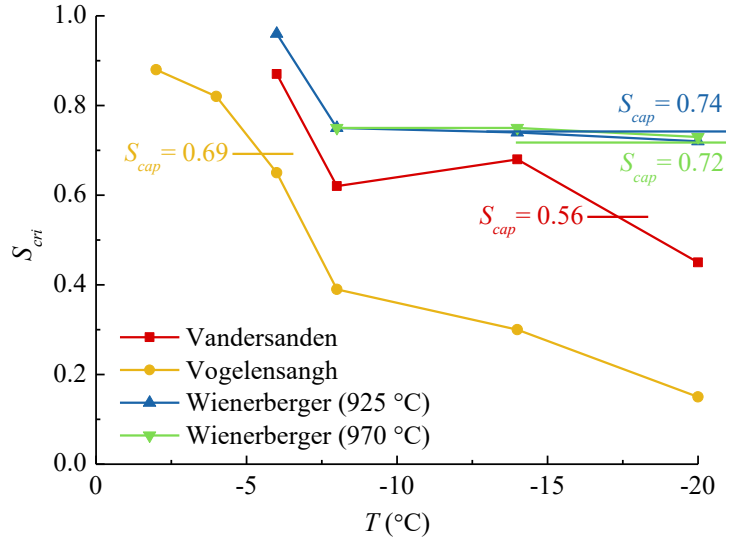

Figure 6.13: The critical saturation degree in function of the applied frost temperature for all four bricks

6.2.3.3 Towards a practical application

Frost damage to building materials and structures have been a central aspect in the arena of building physics for years. There are currently multiple hygrothermal damage indicators to quantify potential frost damage, see section 5.3, like the Modified Winter Index, Time of Frost, ... These damage indicators functions are however restricted to the climatic exposure and do not comprise the mechanical resistance of the material to frost damage. It is however straightforward that different materials have different sensitivities to frost damage, and hence respond differently when exposed to the same climatic exposure. Consequently, to predict and prevent frost damage in real world situations, both the climatic exposure and the mechanical resistance of the material should be considered. One approach towards this integration is to combine hygrothermal simulation outcomes with the material frost damage characteristics. Illustratively, we assume the Vandersanden brick is applied as facade material in a building and convert its three-dimensional Ω profile in Figure 6.12 into a two-dimensional contour (for visual simplicity) in Figure 6.14.

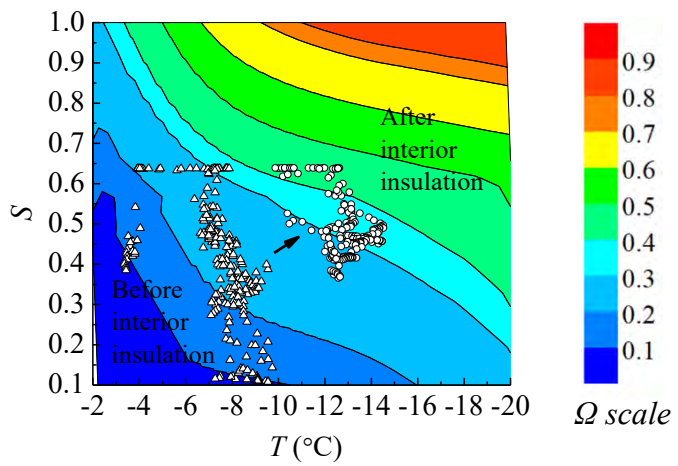

Figure 6.14 Damage isopleths of the Vandersanden brick and the imaginary frost temperature and saturation degree variations of a masonry wall without and with internal insulation

Before and after the application of internal insulation, hygrothermal simulations can predict the respective temperature and moisture content levels. These can be added to the damage contour plot for the Vandersanden brick, as shown in Figure 6.14 with imaginary hygrothermal simulation results for a winter situation. It is clearly illustrated that without the internal insulation most points stay within the range of $\Omega < 0.3$, meaning that the facade does not suffer from significant frost damage. On the contrary, the retrofit with internal insulation moves the data cloud to Ω values of 0.3~0.5, increasing the frost damage. These frost damage isopleths hence perform a similar function as the well-known mould growth isopleths. They are however more rich in information, as they do not just contain one single boundary curve, but instead signal the actual damage potentials at the resulting hygrothermal states. However, while these frost damage isopleths are a major step forward from the binary freeze-thaw testing that is generally applied, it is still unclear how the superposition of the different damage potentials should be accumulated towards a real frost damage development over time. Much more research is needed to that purpose.

6.2.4 Conclusion

This section studies the frost damage to four types of ceramic bricks (Vandersanden, Vogelensangh, and two Wienerberger, fired at 925 and 970 °C). Accelerated freeze-thaw tests at frost temperatures ranging from -2 °C to -20 °C and moisture saturation degrees going from 0.1 to 1.0 were performed. Dilatation and ultrasonic measurements were carried out to assess the frost damage. The following conclusions have been drawn:

- The ultrasonic test along the longitudinal direction after 10 freeze-thaw cycles is most reliable for our purpose, with the relative decrease of the elasticity modulus as the damage index;
- The Wienerberger brick fired at 970 °C is most frost-resistant, followed by the Wienerberger brick fired at 925 °C, the Vandersanden brick and finally the Vogelensangh brick;
- Both the frost temperature and the moisture content are positive contributing factors to frost damage, meaning that a lower frost temperature and a higher moisture content tend to cause more severe frost damage;
- The critical saturation degree is not a constant but a function of the frost temperature;
- Damage isopleths are put forward as a means to assess the risk of frost damage when milder frost temperature and moisture contents are to be evaluated. However, these are not the optimal damage model yet, as the superposition of the different damage potentials towards a development of damage remains unclear still.

6.3 Algae

6.3.1 Aim of the tests

A better understanding of biodeterioration mechanisms that generally happen on façades due to the proliferation of algae and cyanobacteria is necessary in order to define a reliable prediction model. However, the study of bioreceptivity, which is related to the aptitude of a certain material to be colonised by organisms, may raise some methodological problems regarding its expression as readily observable and measurable phenomena (Guillitte and Dreesen 1995). Since the first visible biological developments generally begin after a 1-year or more of natural exposure (Dubosc 2000, Barberousse 2007), the studies carried out on algae colonization of the façades require the implementation of accelerated tests.

Laboratory experiments were carried out in order to investigate the influence of substrate properties and evaluate how different environmental conditions could affect the biofouling process on building materials.

6.3.2 Materials and methods

6.3.2.1 Materials

The microbial cultures chosen for the experimental tests were a green alga (*Chlorella mirabilis* strain ALCP 221B) and a cyanobacterium (*Chroococcidiopsis fissurarum* strain IPPAS B445), since they can be commonly found on building façades, especially in European countries (Tomaselli, Lamenti et al. 2000, Dubosc, Escadeillas et al. 2001, Crispim, Gaylarde et al. 2003, Gaylarde and Gaylarde 2005, Barberousse, Lombardo et al. 2006, Barberousse 2007, Lupan and Popescu 2012, Miller, Sanmartín et al. 2012). The microbial strains were cultivated as pure cultures in 5 l glass flasks containing Bold's Basal medium (BBM), prepared in accordance with ASTM D5589-09 (ASTM 2009).

Algae biofouling was evaluated on ceramic bricks, since this type of building material is usually found on façades, and especially in Cultural Heritage (Giuseppe 1990, Giuliani 1993). Five different types of bricks were selected, considering their different total porosity *P*, as reported in Table 6.9. The tested bricks can be considered representative of the variety of bricks in terms of porosity found in literature, with values mostly ranging between about 16% and 45% (Cultrone, Sebastián et al. 2004, Cultrone and Madkour 2013, Coletti, Cultrone et al. 2016b, Coletti, Cultrone et al. 2016a, Viani, Cultrone et al. 2018). In addition to the porosity, different roughness *R* was examined. A smoothing treatment with sand paper was manually applied on some samples. Smoothed samples were identified with "S", while samples with original surface roughness were named with "R" at the end of the acronym.

Table 6.9:Properties of the tested brick types (mean value ± standard deviation)

Sample	Total porosity [%]	Roughness [μm]
AS	19.24 ± 0.37	4.50 ± 0.27
AR	19.24 ± 0.37	5.54 ± 0.42
B	24.62 ± 1.02	2.95 ± 0.63
CS	44.09 ± 1.63	6.60 ± 0.49
CR	44.09 ± 1.63	7.60 ± 0.57

The brick materials were preliminarily characterized before the tests. Total porosity *P* [%] of each material was determined onto three samples by mercury intrusion porosimetry (Micromeritics Autopore III) following ASTM D4404-10 (ASTM 2010). The surface roughness, as arithmetical mean roughness R_a [μm], was determined according to UNI EN ISO 4287:2009 (UNI 2009), by using a Taylor Hobson CCI 3D Optical Profiler.

6.3.2.2 Experimental set up and test apparatus

As preliminary investigations before the accelerated tests, the effect of five different temperatures were analysed, evaluating the growth rate of algae cultures, without considering the material substrate. The aim was to understand the suitable temperatures to set during the accelerated tests on brick samples, in order to obtain useful results for the implementation of the failure model, and not to waste time in non-favourable environmental conditions for growth.

According to the available literature, algae and cyanobacteria can live in a wide range of temperature, which are usually comprised between 5° and 40°C (Raven and Geider 1988, Lengsfeld and Krus 2001). Considering this range, algal cultures were incubated at the following temperatures: 5°C, 10°C, 27.5°C, 35°C and 40°C. The set temperatures were maintained with the accuracy of ± 2.5°C. Growth tests were carried out on both pure and mixed cultures of *Chlorella mirabilis* and *Chroococcidiopsis fissurarum*, using glass bottles containing 100 ml of each culture incubated at constant temperature. Since algal cells need sun light to reproduce, a 39 W neon (5000 K light temperature) was provided for day/night cycles of 14/10 h (Johansson 2005b). Every week the cultures were sampled and a microscopy count was carried out using a Thoma-Zeiss hemocytometer (Gwo, Chiu et al. 2005): the results were expressed in logarithmic scale as number of cells/ml. All the tests were performed in duplicate.

Subsequently, accelerated growth tests, for the evaluation of biological defacement of building materials, were performed at different controlled environmental conditions (temperature and relative humidity). The behaviour of samples in each environment was investigated until the end of the biofouling process (stagnation phase). For each tested material three prismatic samples (8×8×3 cm^3) were placed inside the climatic chambers (100×40×53 cm^3), positioned on aluminium-glass racks inclined at 45°. All the three growth chambers were placed in a dark room to avoid the influence of the external environment (daily light, outdoor temperature and relative humidity). Each test apparatus was equipped with two neon lamps (Sylvania TopLife 39W) to provide an adequate illumination to simulate a day/night cycles of 14/10 h (Johansson 2005a). The lamps were positioned on the top of the chamber at a constant distance from the sample surface.

In order to evaluate the influence of relative humidity on the growth of algae on fired brick surfaces, three different relative humidity (RH_i) conditions were reproduced inside three separate climatic chambers (Figure 6.15a). Saturated solutions were used to condition the indoor environment of three glass chambers, according to EN ISO 12571:2013 (UNI 2013). RH_1 (75 ± 2%) was obtained using a saturated solution of NaCl, RH_2 (about 87 ± 2%) using a saturated solution of Na_2CO_3, and RH_3 (about 98 ± 2%) using deionized water (Perry 1942). To exclusively evaluate the effect of relative humidity, during all the tests temperature was constantly controlled and maintained at 27.5 ± 2.5°C. This temperature was selected considering the results of the preliminary tests and in accordance with literature about the optimal temperature for algae growth (Konopka and Brock 1978, Singh and Singh 2015, Serra-Maia, Bernard et al. 2016). Once at the beginning of each test, samples were inoculated on nine different points on their surface with 5 µl of the mixed culture per point.

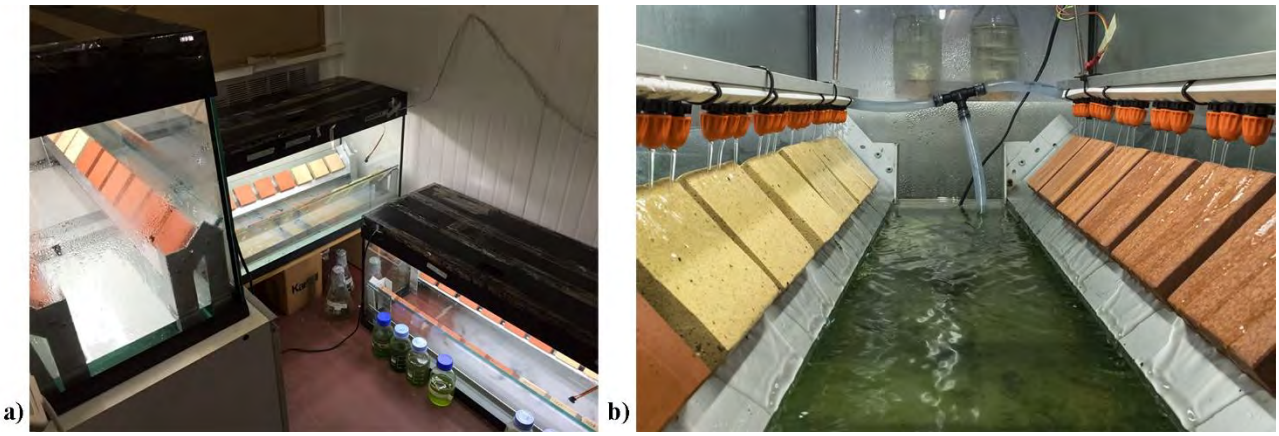

Figure 6.15: View of the glass chambers used to maintain different constant relative humidities; b) View of the inside growth chamber used for the evaluation of temperature influence on algae biofouling

Investigations on the effect of temperature on algae growth were carried out following the methodology adopted in previous research (Graziani, Quagliarini et al. 2013, Graziani, Quagliarini et al. 2014b, Graziani, Quagliarini et al. 2016a, Graziani, Quagliarini et al. 2016b). The method well simulates the behaviour of roof or external wall surfaces exposed to bad weather, or leaky parts of a building or design defects. It consists in accelerated tests with periodical water spray on the material surface.

Different growth chambers were filled with 35 l of BBM and microbial suspension, composed by a mix of the two algal strains, in a concentration of about 4 mg of algal cells per litre. A PVC tube, with three holes drilled every 20 mm in correspondence of each sample, was connected to a 500 l/h water pump (Blupower) submerged in the broth culture. By doing so, the algal suspension was sprinkled on sample surfaces, with run/off cycles of 15 minutes, for a total duration of 6 hours per day (3 hours run and 3 hours off). The distance from the samples to the rails to was approximately 50 mm and designed to allow water to run on the entire sample surfaces Figure 6.15b).

According to the results from the preliminary experiments using different temperatures (section 6.3.3.1) and considering the available literature (Konopka and Brock 1978, Raven and Geider 1988, Guillitte and Dreesen 1995, Lengsfeld and Krus 2001, Escadeillas, Bertron et al. 2009a, Singh and Singh 2015, Graziani, Quagliarini et al. 2016b, Serra-Maia, Bernard et al. 2016), the accelerated tests were set under two different temperatures. A temperature of 27.5 ± 2.5°C was selected to be within the range of the optimal growth conditions comprised between 20°C and 30°C (Konopka and Brock 1978, Guillitte and Dreesen 1995, Escadeillas, Bertron et al. 2009b, Singh and Singh 2015, Graziani, Quagliarini et al. 2016b, Serra-Maia, Bernard et al. 2016), and a lower temperature of 10 ± 2.5°C, within the range of suitable growth for both the studied strains (Raven and Geider 1988, Lengsfeld and Krus 2001). A modified refrigerator Electrolux RC 5200 AOW2 was used to set the lower test temperature. In these experiments, relative humidity was assumed equal to 100%, since the wet and dry cycles allow keeping the sample surface wet during the test time.

6.3.2.3 Measurement and evaluation of algae growth

During the accelerated growth test, both quantitative and qualitative analyses were performed to evaluate the biofouling process on the samples' surface (Graziani, Quagliarini et al. 2013, Graziani, Quagliarini et al. 2014b, Quagliarini, Graziani et al. 2018).

Qualitative analyses were performed by chromatic investigations during the tests. Colorimetric measurements for the evaluation of the chromatic variation (ΔE) were carried out using a portable spectrophotometer (Konika Minolta CM-2600d), in accordance with UNI EN 15886:2010 and UNI 1602371:2018 (UNI 2010) (UNI 2018). On each sample surface, nine measurements were repeated weekly on the same points. Results were expressed in CIELab colour space (Gwo, Chiu et al. 2005) and averaged to obtain a representative value for each material. Colour variations were calculated in terms of total colour difference ΔE, following the equation (15):

$$\Delta E = \sqrt{(L_0^* - L^*)^2 + (a_0^* - a^*)^2 + (b_0^* - b^*)^2} \qquad (15)$$

where L_0^*, a_0^* and b_0^* indicate the colour coordinates of samples before the start of the test, and L^*, a^*, b^* the coordinates periodically measured during the tests. According to standard methods (UNI 2018) and researches (Franzoni, Fregni et al. 2014), a total colour difference $\Delta E<1$ can be considered not visible by naked human eyes, while a ΔE ranging between 1 and 2 can be detectable only with a close observation. From an engineering point of view, a $\Delta E=1$ could be assumed as the acceptable lowest limit for algae growing. In case of average $\Delta E>1$, the term a_0^*-a^* was evaluated to verify if the colour change was actually due to the presence of algae. In fact, the variation Δa indicates to a colour difference in a red/green scale. That way, it permits to associate the colour variation to the appearance of algae as green stains: the amount of red is indicated by positive values ($\Delta a>0$), while a green toning by negative values ($\Delta a<0$). Thus, in case of average $1<\Delta E<2$ but at the same time average $\Delta a>0$, it can be reasonably assumed that the colour variation is not due to the presence of algae.

The colorimetric analyses were associated to the quantification of the biofouling extension, evaluated by a (quantitative) Digital Image Analysis (DIA) (De Muynck, Ramirez et al. 2009, Giovannacci, Leclaire et al. 2013, Graziani, Quagliarini et al. 2014b, Quagliarini, Graziani et al. 2018), which is a non-destructive test and whose effectiveness has been confirmed in previous studies (Escadeillas, Bertron et al. 2009b, Giovannacci, Leclaire et al. 2013).

In particular, to calculate the extension of colonized area the threshold method was adopted (De Muynck, Ramirez et al. 2009, Giovannacci, Leclaire et al. 2013, Graziani, Quagliarini et al. 2014b, Quagliarini, Graziani et al. 2018). Sample surfaces were digitalized weekly with a scanner HP Scanjet G3010 (600 dpi resolution). The scanned images were elaborated to calculate the algal coverage, expressed as a percentage of the total sample area. To identify the colonized area, the acquired images were processed with ImageJ software (Tiago and Wayne 2011, Schneider, Rasband et al. 2012): once set the threshold values in CIELab colour space, images were binary converted to consider only the contaminated pixels by algal cells (Figure 6.16). The covered area by microalgae was represented as the percentage of the black pixels on the total area of the sample (De Muynck, Ramirez et al. 2009). Measurements were carried out once a week during the accelerated growth tests and results were reported as average values and standard deviations of three samples for each fired brick material. The samples were tested in the accelerated growth environment until their maximum coverage was reached and maintained after two subsequent measurements defining a stabilization point.

Figure 6.16: An example of binarization process; from left to right: scanned images from the original sample were elaborated by a filtering process (threshold method) to obtain binary images

6.3.3 Results and discussion

6.3.3.1 Preliminary investigations on growth rate of algae cultures

The results of the preliminary investigations at different constant temperatures and wet conditions, without the influence of the substrate are expressed as growth curves of the pure (CM or CF) and mixed (MIX), in Figure 6.17. Regarding Chlorella mirabilis (CM) (Figure 6.17a), an increasing number of cells was counted at both 10 and 27.5 °C. The growth process was in accordance with observations reported in (Shukla, Kvíderová et al. 2013), that studied the growth of Chlorella mirabilis in low-temperature environments. On the contrary, at T=5 °C the number of cells was constant over the time (attested at about 10^5 cells per ml). The higher tested temperatures (35 °C and 40 °C) leaded to a remarkable decrease in the cell numbers of the tested strains, with a considerable reduction after 14-21 days of test. Regarding the growth of Chroococcidiopsis fissurarum (CF) (Figure 6.17b), no particular effect of the tested temperatures was observed at the end of the monitoring, thus confirming the high adaptation of this blue algal species to extreme environments (Billi 2010). Finally, the growth curves of the mixed cultures (Figure 6.17c) substantially reflected the trends of the growth curves related to the two pure cultures.

In order to assure the presence of both the two microorganism species during the tests on the building materials, the growth temperatures of the accelerated tests were chosen following these results. Thus, T=10 °C and T=27.5 °C were selected, as the most suitable temperatures to allow the growth of both *Chlorella mirabilis* and *Chroococcidiopsis fissurarum*. The chosen temperatures correspond to what is reported into the available literature (Raven and Geider 1988, Lengsfeld and Krus 2001).

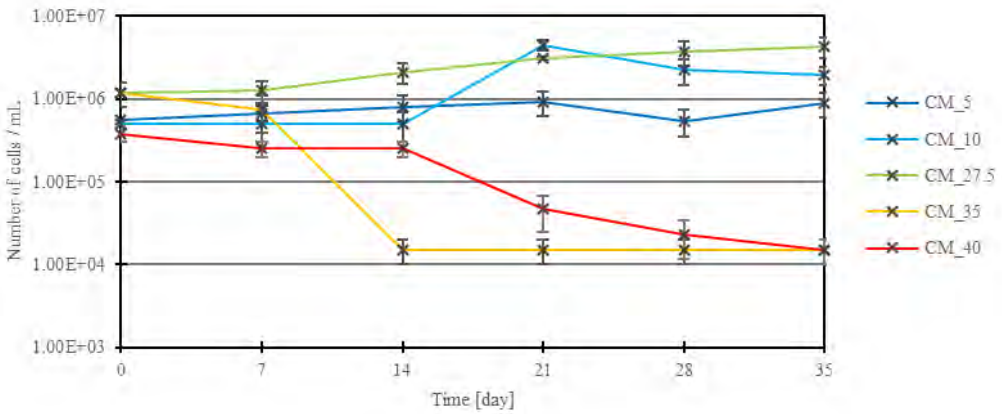

a)

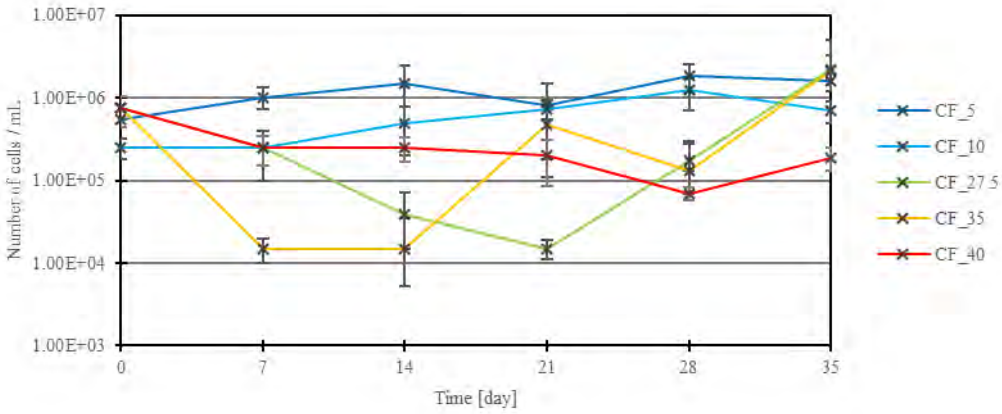

b)

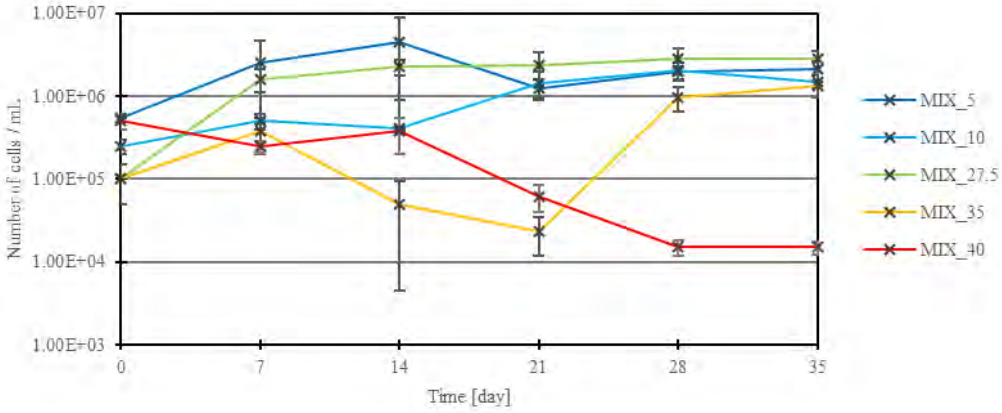

c)

Figure 6.17: Growth curves of: a) Chlorella mirabilis CM; b) Chroococcidiopsis fissurarum CF; c) mixed culture MIX. The growth of the microbial species was tested at five different temperatures

6.3.3.2 Accelerated tests on types of brick

Figure 6.18 (a, b, c) shows the total colour difference ΔE of the brick samples exposed to different relative humidities (RH_1=75%, RH_2=87%, RH_3=98%). During the 36 weeks of test, all the samples AR and B showed an average colour variation ΔE < 1 at all the tested RHs, thus under the limit of human perception. Average colour variations higher than 1 (but lower than 2) were registered only on samples CR from 9th week and onward when exposed to RH_3=98%, while an average ΔE<1 was always measured at RH_1 and RH_2. However, the red/green difference Δa^*, investigated to check a

possible chromatic change to green due to the presence of chlorophyll, gave always positive average values (Figure 6.19). Therefore, it can be assessed that at RH ≤ 98% no (qualitative) signs of algae growth was present.

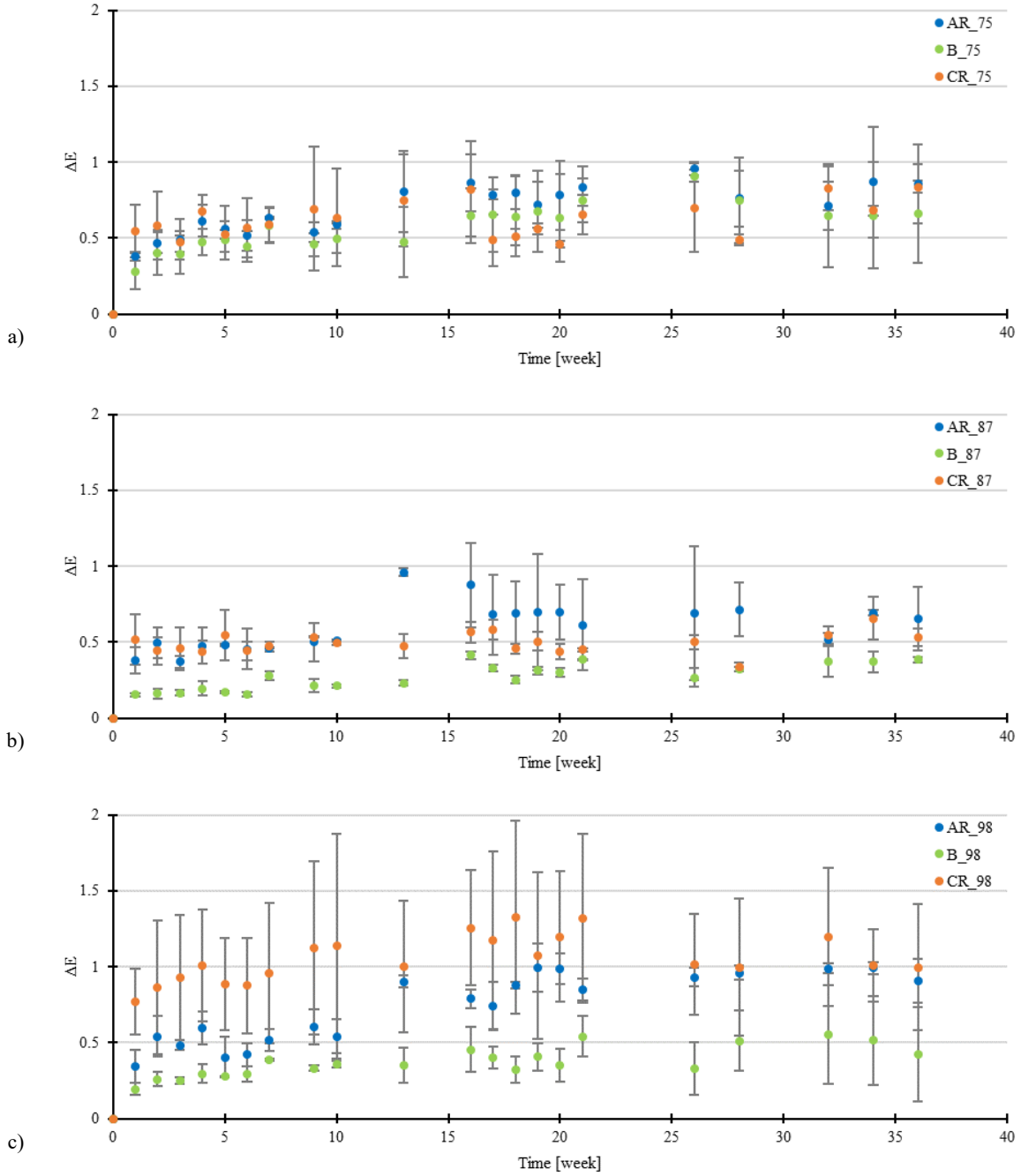

Figure 6.18: Total colour difference ΔE of samples AR, B and CR: a) RH1=75%; b) RH2=87%; c) RH3=98%. Results are reported weekly; vertical line bars indicate standard deviations

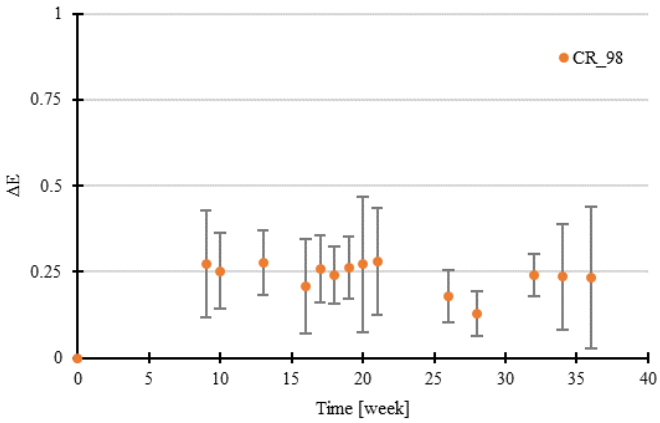

Figure 6.19: Red/green colour difference Δa of sample CR_98 (98 % RH). Results are reported weekly; vertical line bars indicate standard deviations

Digital Image Analysis results on bricks exposed to constant relative humidities confirmed the previous qualitative colorimetric analysis. Measurements are not reported, since the covered area during all the tests was always equal to 0 for each sample. This quantitatively demonstrated that the exposure to RH ≤ 98% does not seem to allow algae growth on the tested brick samples.

Figure 6.20 reports the results, obtained by DIA, about the quantification of the covered area by algae, during the accelerated run-off tests on brick materials at two different temperatures: 10°C and 27.5°C (i.e. moisture conditions comparable with 100 % RH according to section 0. Samples AR and AS showed similar growth processes after the exposure under 27.5 °C (Figure 6.20 a-b). A very slow growth was observed until the 27th day, and after 140 days, the maximum covered areas in both cases reached about 80%. Concerning the results from tests at T=10 °C, it is noticeable that biofouling was significantly affected by the lower temperature. Indeed, the measured covered areas were less than 10% of the total area during the stagnation phase of growth after 182 days of test (Figure 6.20 a-b).

A similar behaviour was observed on brick type B. The tested samples at T=27.5 °C were covered on average up to 65% of the total area after 63 days, while at T=10°C samples reached on average 12% of coverage after about 70 days (Figure 6.20 c). Considering brick type C, both rough (CR) and smoothed (CS) surfaces showed green coverage equal to 90% of the total area at T=27.5°C (Figure 6.20 d-e). After 42 days, the trend of the measured data reached the stagnation phase. On the contrary, at T=10 °C (Figure 6.20 d-e), CR and CS samples showed on average 35 % of algal coverage after 49 days.

Moreover, comparing the measurements of the two accelerated tests performed at T=27.5°C and T=10°C, it is possible to assess that the covered area decreased when the samples were exposed to a colder temperature (T=10°C).

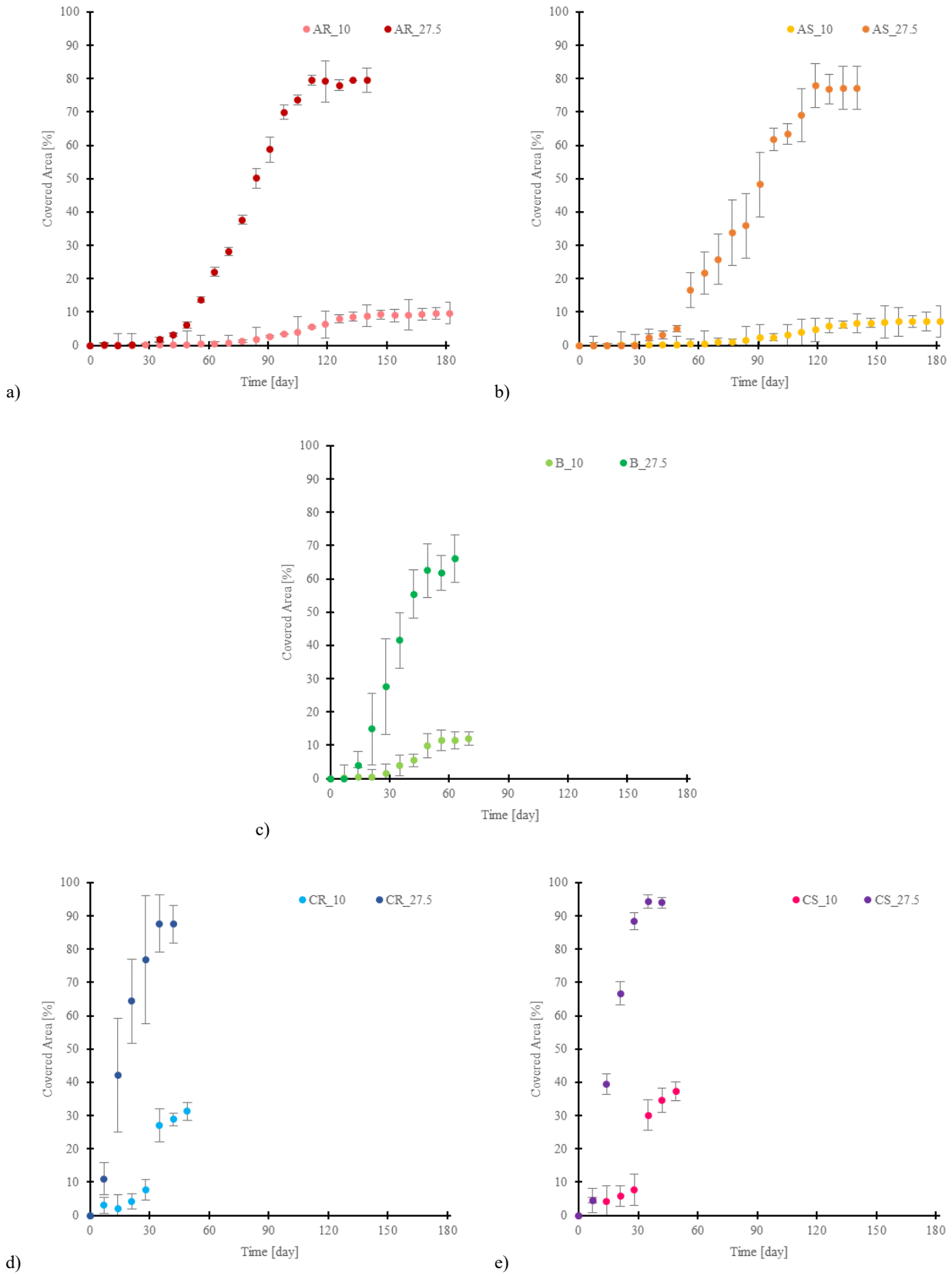

Figure 6.20: Average area coverage on fired bricks: a) samples AR; b) samples AS; c) samples B; d) samples CR; e) samples CS, at the temperatures of T=10°C and T=27.5°C

Finally, the role of the substrate was accounted, by evaluating the differences in terms of maximum covered area by algae at the end of the tests and the time to reach it Figure 6.21 (a) reports the number of days until the stagnation phase was reached in relation to the porosity of each sample. However, it is evident how a brick type with a high porosity (type C, P=44%) accelerated the coverage process compared to a brick type with a low porosity (type A, P=19%). Porosity also influenced the effect of temperature, having a higher effect on the duration of the biofouling process at low porosity (duration 30 % longer at 10 °C than at 27.5 °C) than at high porosity (duration 15 % longer).

The effect of roughness on the average covered area at the end of the tests is reported in Figure 6.21 (b). A roughness higher than 6 µm favoured algae growth, compared to samples with lower roughness. Roughness influenced the effect of temperature, too. On samples with high roughness the average algal coverage decreased by 60%, while on samples with low roughness it was decreased up to 80%.

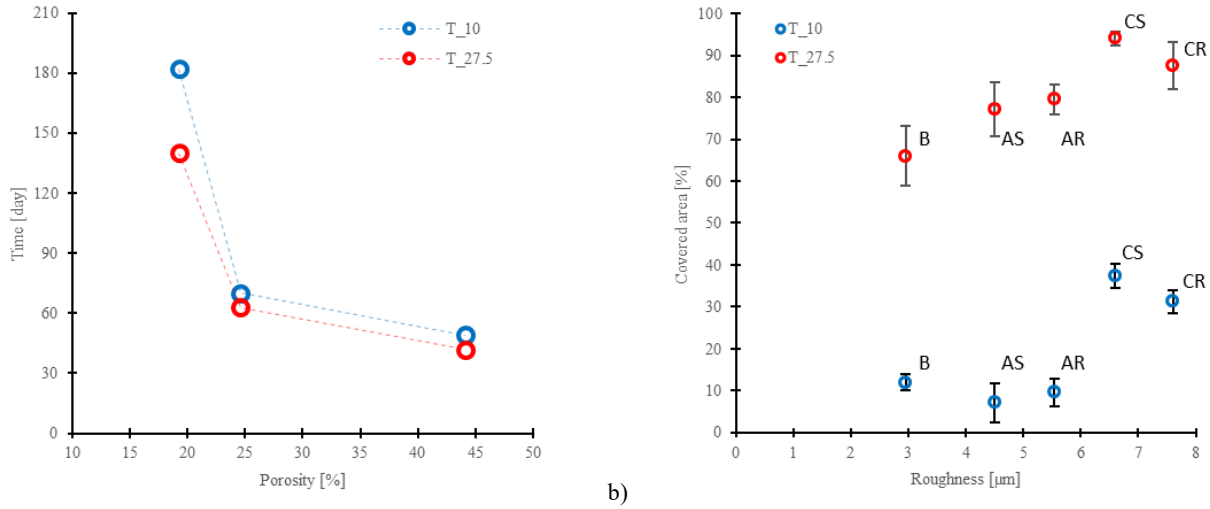

a) b)

Figure 6.21: a) Duration of the accelerated biofouling process on the tested brick types (having different porosities); b) Average covered area by algae at the end of the tests depending on the surface roughness

6.3.4 Conclusion and future work

The biofouling processes of a green alga *Chlorella mirabilis* and a cyanobateria *Chroococcidiopsis fissurarum* were investigated on five types of brick, through accelerated growth tests at different relative humidity and temperature.

Concerning the tests evaluating the effect of relative humidity, colorimetric variations detected on samples' surfaces were generally lower than the perceptible threshold for the human eye. Quantitative analysis (DIA) confirmed this result, since no covered area by algae was detected on any sample at RH ≤ 98%. Results are independent on substrate properties such as total porosity and roughness. An eventual presence of algae and cyanobacteria at the microscopic level, not detectable by the instruments used in this work, could be also acceptable since it corresponds to a non-visible algae growth on a façade from an engineering point of view. Thus, from an engineering standpoint, RH < 98% can be assumed as a safety limit not to exceed.

In accelerated growth tests performed at T=10°C and T=27.5°C (optimal growth temperature), the algal biofouling was highly influenced by the temperature conditions. 10°C slightly reduced the rate

of the biofouling process and significantly the total covered area on samples at the end of the test compared to 27.5°C. Experimental results confirmed the role of the substrate on algae growth: high porosity and high roughness favoured colonization, by influencing it in terms of growth rate and covered area at the end of the process.

Finally, it can be pointed out that porosity strongly influences the rate of biofouling process: a higher value of porosity corresponds to a faster algae growth. At the same time, roughness seems to affect the covered area reached at the end of the biofouling: the percentage of algal coverage has an increasing trend from smoother to rougher surfaces. Moreover, the biofouling is significantly reduced by the effect of a substrate characterized by low porosity and/or low roughness combined with a low temperature.

7 Evaluation of and advance on prediction models

7.1 Round robin of mould prediction models

7.1.1 Aim of the study

As described in section 5.1, several models for predicting mould in buildings are available. Previously, comparisons of the design and/or results of the models have been performed. In some cases, suggestions on how to improve the models have been presented. However, to the best of our knowledge, the results from the most commonly used prediction models have not previously been compared to real outcome. In the present study, we aimed to evaluate the models in relation to actual mould growth in different building parts.

In all models, choices of input parameters need to be made by the person performing the simulation. One such parameter is related to a material's susceptibility to mould growth. Therefore, there is a possibility that the outcome of the model will be different depending on who is performing the simulation. To map this possibility, the study was performed as a round robin test. The design or the in-depth equations and assumptions on which the different models are based, were not evaluated. In addition, not all possibly available models have been evaluated, instead the models to be used were chosen by each partner in the round robin.

7.1.2 General description of the study

In a previous field study, samples of different building materials were exposed in different crawlspaces and attics for up to three years. The development of mould growth on the samples was studied by time and RH and temperature was continuously logged (Johansson, Wadsö et al. 2018). In the present study, mould models were used to predict the "risk" for mould growth on building materials in five test sites by using the measured climate data.

Different partners in RIBuild performed simulations and predictions independently of each other on the same data. The outcome was compared between performers and to results from analysis of mould growth on test specimens. The procedure is schematically described in Figure 7.1.

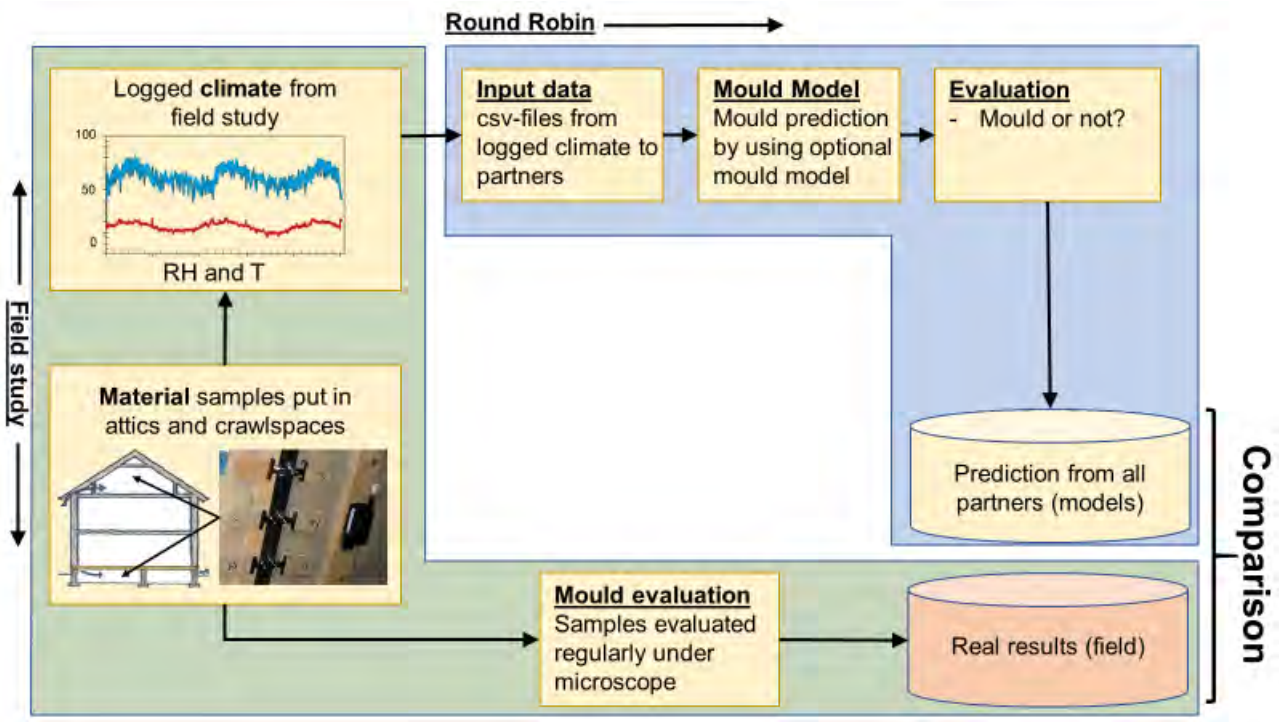

Figure 7.1: Schematic overview of the design of the study. The green area represents the field study previously performed. The blue area represents the round robin presented in this report

7.1.3 Input data from field study

Field study data that formed the basis for the round robin in the study is described in (Johansson, Wadsö et al. 2018). Below is a brief description of the test.

Test specimens, sized 5x10 cm, of five different building materials (gypsum board, plywood, thin hardboard, chipboard and spruce) were placed in crawlspaces and attics in different parts of Sweden in up to 3 years. In each test site, seven replicates of each material were mounted in clips of stainless steel on the inner roof or blind floor. A data logger with internal sensors (Testo 175H1) was placed near to the specimens to ensure that the conditions logged were as close as possible to those that the specimens were exposed to. The temperature and RH at each test site was registered hourly.

The loggers were calibrated at several temperatures and RH before and after exposure. In many cases, the loggers had drifted, so that they showed higher values after exposure than before exposure in the field. The measured values of the loggers were therefore adjusted both according to calibration and drift, as described in (Johansson, Svensson et al. 2013). The expanded measurement uncertainty for each logger was calculated.

The original study included 12 different test sites. In the present round robin, results from five of the test sites, four attics and one crawlspace, was used. Note that the numbering is not the same as in the original report (Johansson, Wadsö et al. 2018). In this study, the different test sites are denominated “Climate1”, “Climate2”, “Climate3”, “Climate5” and “Climate6”. The measured RH and temperature (adjusted according to calibration) in each test sites are shown in Figure 7.2 and Figure 7.3.

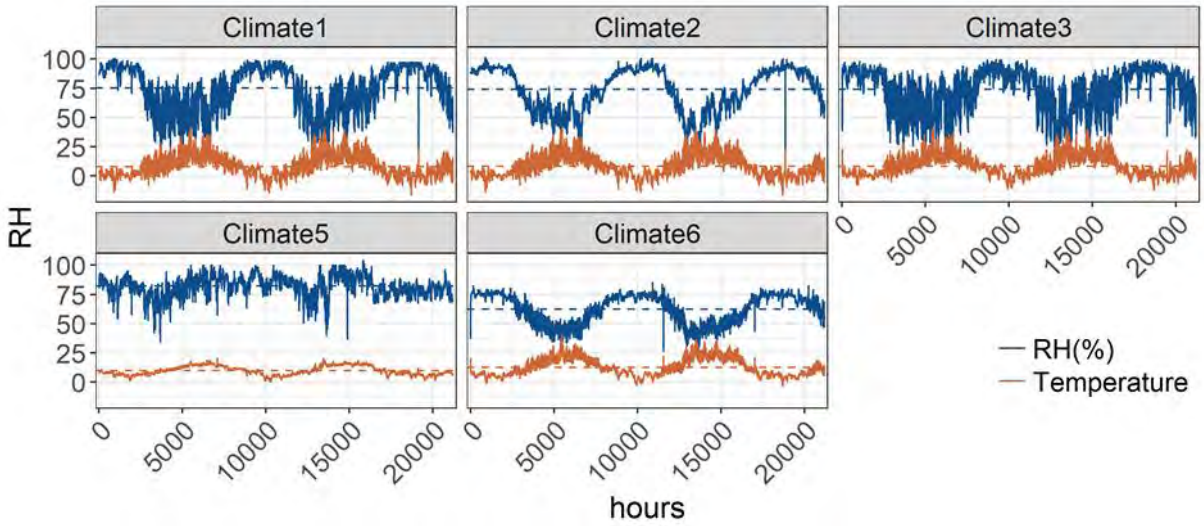

Figure 7.2: Measured RH (%) and temperature (°C) by time (hours). The blue and red dotted horizontal lines is the mean value of RH and temperature respectively

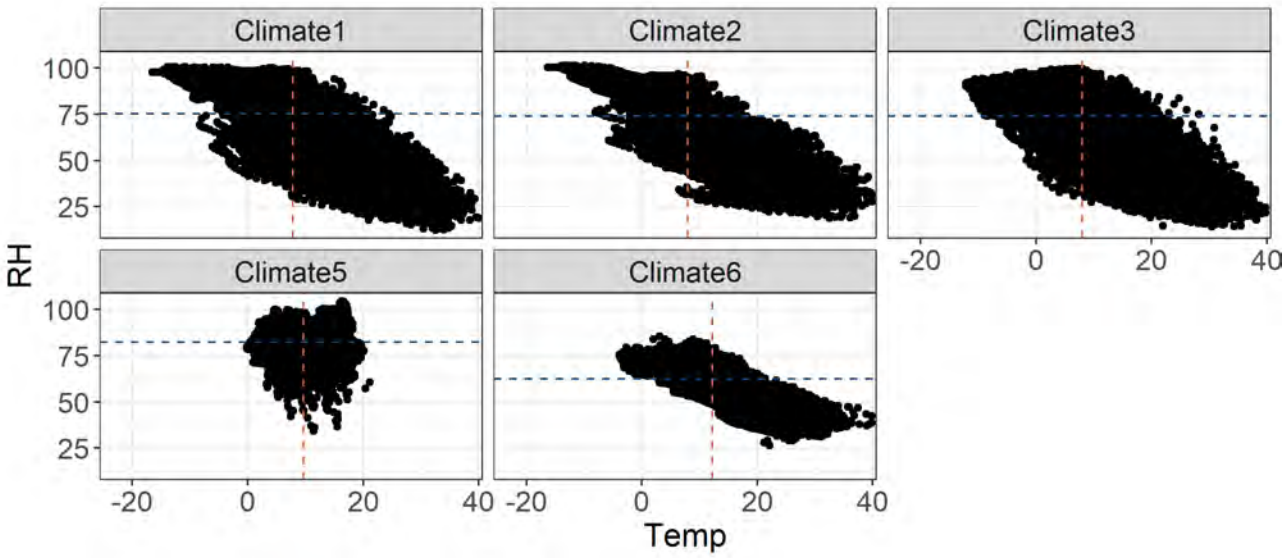

Figure 7.3: Measured RH (%) and temperature (°C). Each dot is hourly measurements. The blue, horisontal, and red, vertical, dotted line shows the mean value of RH and temperature respectively

The surface exposed to open air in the attics and crawl spaces was examined for mould growth at 10-40x magnification under the microscope at irregular intervals of three to six months. Both mould growth visible to the naked eye and mould growth only visible under the microscope was included and rated according to a five-point rating scale (Johansson, Ekstrand-Tobin et al. 2014), see section 6.1.2.3 and Table 6.3. Observe that the numbers of the rating scale cannot directly be translated to other, similar rating scales.

Mould growth was considered established at each test specimen when the rating was at least 2 for the first time and for the material group when the median value of ratings of all seven test specimens were ≥ 2. The rating scale and the definition of established growth has been thoroughly estimated and validated (Johansson, Ekstrand-Tobin et al. 2012, Johansson, Svensson et al. 2013, Johansson, Wadsö et al. 2018).

The results from the mould growth analyses at the end of the test period are presented in Figure 7.4 and for each analysis time and climate in Appendix 2 and Appendix 3.

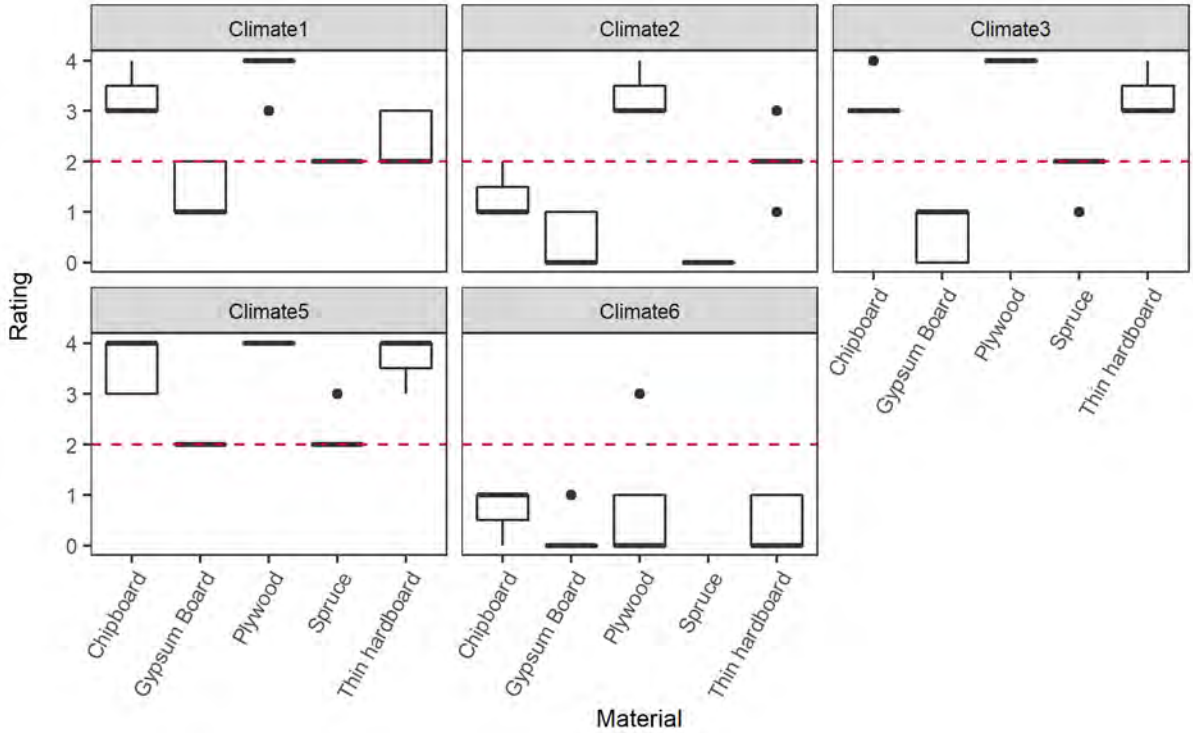

Figure 7.4: Results from the analysis of mould growth on seven test specimens of each material at the end of the evaluated test period

7.1.4 Prediction using mould growth models

Field measurement data were sent to five different RIBuild partners as separate .csv files for each climate. The file contained hourly values of calibrated RH, temperature and time stamp. The partners were asked to use the data in the model(s) commonly used in their organisation to predict mould growth on the five different materials: plywood, chipboard, pine, gypsum board and thin hardboard. No other information than photos and description was given to the partners.

The models used was the updated VTT model, Sedlbauers LIMcurves, WUFI®-Bio, MRD-model, m-model version 2.0 (in this paper denominated as the m-model) and the PJ-model. The models are presented in short below. For a more thorough description of each model, we refer to the references given for each model respectively. Some of the models are also described in (Vereecken and Roels 2012, Gradeci, Labonnote et al. 2018).

To illustrate the outcome and evaluation of models and to compute statistics on agreement of prediction of models and real outcome, each of the models used was programmed and conducted by RISE in R (R Core Team 2018), also using packages dplyr (Wickham, Francois. et al. 2017), lubridate (Grolemund and Wickham 2011) and ggplot2 (Wickham 2009). To ensure that the programming of the models agreed with the original model, the outcome was compared to the outcome from each partner's simulation. As the algorithms for WUFI®-Bio are not public, simulation was made in the program and the results, .csv files, were used.

7.1.4.1 VTT model

General description

This model was first presented in a version aiming to predict mould growth on wood (Hukka and Viitanen 1999). It was later modified to handle also other materials. The latter version is often referred to as "the new VTT model" (Ojanen, Viitanen et al. 2010). The model is available as a postprocessor in the hygrothermal simulation programs DELPHIN and WUFI. In this study, the partners used either DELPHIN or excel files, programmed after published version

Parameters in the model

The material susceptibility parameters to be chosen in the model are shown in Table 7.1. The description differ slightly between the published description (Ojanen, Peuhkuri et al. 2011) and DELPHIN. Two additional parameters linked to material properties can be chosen in the model; Wood species (W=0 for pine or W=1 for spruce) and surface quality (SQ=0 for sawn surfaces, SQ=1 for kiln dried surfaces). In addition, a parameter (C_{mat}) is used in the model in relation to the effect of the duration of unfavourable conditions, see Table 7.2.

Table 7.1: Sensitive classes in the VTT model. The descriptions vary some between the model as it is described in the published model (Ojanen, Peuhkuri et al. 2011) and in DELPHIN (Bauklimat-Dresden 2019). M is the value of mould resistance parameter in the m-model (Section 7.1.4.4)

Mould Sensitivity Class	Material description according to (Ojanen, Peuhkuri et al. 2011)	Material description in DELPHIN	M in m-model (Section 7.1.4.4)
Very sensitive	Pine sapwood	Untreated wood; includes lot of nutrients for biological growth	0.58
Sensitive	Glued wooden boards, PUR with paper surface, Spruce	Planed wood, paper-coated products, wood-based boards	1
Medium resistant	Concrete, aerated and cellular concrete, glass wool, polyester wool	Cement or plastic based materials, mineral fibers	8
Resistant	PUR polished surfaces	Glass and metal products, materials with efficient protective compound treatments	18

Table 7.2: Description of C_{mat}

Ceff/Cmat	Description
1.0	Pine in original model, short periods
0.5	Significant relevant decline
0.25	Relatively no decline
0.1	Almost no decline

Outcome of the VTT model and evaluation of results
The outcome of the model is a dimensionless value, denominated Index. It describes the mould growth intensities, with values between 0 (no growth) and 6 (heavy and tight growth, coverage about 100%). The partners in this study used the index 1 as limit values, according to (Ojanen, Viitanen et al. 2010). However, in other publications other limit values can be used.

7.1.4.2 WUFI®-bio

General description
The WUFI®-Bio model is an add-on tool to the hygrothermal simulation program WUFI (WUFI 2019) . It is either used directly in the hygrothermal WUFI simulation program or as a separate model with input data from other simulation tools or from measurements.

The idea behind the model and its' design is described in (Sedlbauer 2001b, Gradeci, Labonnote et al. 2016), however the equations are not published. In this project output from the program in the form of .csv files are used.

Parameters in the model
The model is based on isopleth system curves. The isopleths for the different material groups are presented graphically in the description within the program. The model includes the material classifications seen in Table 7.3.

Table 7.3: Classes in WUFIbio and Sedlbauer Isopleths (WUFI 2005)

Material classification	Materials
Class 0	Optimal culture medium (e.g. full medium). This represent the maximum growth possible for any mould found in buildings
Class I	Bio-utizable substrates, such as wall paper, plaster board, building products made of biologically degradable materials, materials for permanent joints, strongly contaminated surfaces
Class II	Less bio-utizable substrates with porous structure, such as plaster, mineral building materials, certain woods, insulating materials not belonging to Class I

Outcome of WUFI®-Bio and evaluation of results
Results are presented as graphs showing either mould growth in mm by time or mould growth index by time during one year at a time. The index corresponds to the index in the VTT model (see section 7.1.4.1). The results are also presented in a so-called signal light system according to Table 7.4.

The limit for mould growth corresponds to an index of 2, this was also used as the limit criteria by the partner performing the simulation. In Table 7.4, it says that green light corresponds to a mould index of approx. 0.5. In (Viitanen, Krus et al. 2015) it is stated that it is only a negligible risk for mould growth and the traffic light remains green. In the "yellow light" field, it is up to the user of the model to decide on what is accepted in the specific case.

In this project, the logged climates span over more than one year. The results are evaluated for the whole logged period (approximately 2.5 years). The threshold limit for mould growth was set to 2 ("red light") and 1 ("yellow light").

Table 7.4: Description of evaluation according to traffic light signal in WUFIBio (WUFI 2005)

Light	Description
Red	Mould growth exceeds 200 mm/year, which corresponds to a mould index of approximately 2. Usually not acceptable
Yellow	Mould growth is between 50 mm/year and 200 mm/year. Additional criteria or investigations are needed.
Green	Mould growth is below 50 mm/year, which corresponds to a mould index of approximately 0,5. Usually acceptable

7.1.4.3 MRD model

General

The MRD model is presented in (Isaksson, Thelandersson et al. 2010), as a stand-alone program and as a postprocessor in WUFI (MRD 2016).

The model uses mean values of RH and temperature in a time interval of 12 h as input, and the input data must start at hours 8:00 or 20:00.

Material parameter

The model is based on a critical dose (D_{crit}) which represents the number of days before mould growth is initiated on a material at 90 % RH and 20 °C. In the description of the model, it is stated that D_{crit} should be tested in the laboratory and no values for different materials are presented. In an information document to the model (MRD 2016), some examples of D_{crit} for different materials are presented, see Table 7.5. One of the partners using this model has interpreted that this could be used to estimate RH_{crit} also for other materials and this was used as input in the study, see section 7.1.5. D_{crit} is defined as ”the number of days it takes before mould growth starts on a specific material during constant climate exposure, 20 °C and 90 % RH.” In this table only the first four values are shown, as these were chosen in the study. Dcrit of five other materials, all impregnation or modifications of wood, are presented in the full table

Table 7.5: Values of the material parameter in MRD modelling the tool (reference).

Material	Dcrit,d (Days)
Norway spruce, planed, commercial quality	17
Scots pine, planed	12
Norway spruce, sawn surface1	10
Scots pine, sawn surface1	8
…	…

Outcome of the MRD-model and evaluation of results

In the model, a dose, D, is produced by time. The output is the MRD index, calculated by dividing D with the critical dose D_{crit}. When the MRD-index exceeds 1 it is assumed that mould growth can occur.

7.1.4.4 M-model version 2.0

General description
The m-model was originally developed by Skanska to be used as an internal tool that could be used both to predict if a building part could get mould growth and to make rational choices between different design options (Togerö, Svensson Tengberg et al. 2011). The model is also described in (Gradeci, Labonnote et al. 2018)

In 2013, it was decided to release the model to the public domain. Before making the m-model public the model was investigated in a research project (Johansson, Wadsö et al. 2018). The model was slightly simplified, and the nomenclature and symbols have been revised. The new version is called the m-model version 2.0 and a postprocessor program is available at (Fuktcentrum 2019)

Material parameter
The choices of material parameters for group of building materials are the same as in the VTT model, Table 7.1. To each group, there is a corresponding value M. This value is based on values in the first version of the m-model, however the values will be updated in the future. For now, these are the values available when evaluating the model.

Outcome of the m-model and evaluation of results
The result of the m-model is a parameter *m*, by time. Six different values are calculated based on different time scales, τ (1 d, 1 w, 2 w, 4 w, 8 w, 12 w). If the m-value for any of the time scales exceeds M of a certain material, the model predicts mould growth.

7.1.4.5 The Sedlbauer´s LIMcurves

General
The Sedlbauer´s LIMcurves is an Isopleth model taking into account the temperature and RH at a material surface. The curves used in the model is further described in (Sedlbauer 2001a).

Material parameters
There are 3 different substrate classes according to Table 7.3.

Evaluation of results from the Sedlbauer´s LIMcurves
To evaluate the results there are different curves for different duration of the temperature and RH, e.g. 2 days, 4 days etc. (Sedlbauer 2001a). However, in most of the cases in this round robin only the lowest LIMcurve was used.

7.1.4.6 The PJ-model

General
The PJ-model is a static Isopleth model. The model has not previously been described as a model. It is a part of the application of a standard test method for assessing the critical moisture level for mould growth on building materials, appendix B, in (SIS 2014) also described in section 6.1.2.5. In this study, version 1.0 is used. However, the PJ-model is under development and later version may be published.

Material parameters

The material parameter input to the model is RH_{crit}, which is the tested critical moisture level for a material. A specific product can belong to one of five material classes according to

Table 6.5. From these, growth limit curves are constructed according to equations in section 6.1.2.5 and Figure 6.5.

The RH_{crit} according to the method/model has been published for some materials (Johansson, Ekstrand-Tobin et al. 2012). However, as different products have their specific RH_{crit}, according to the model material data needs to be provided for each product through testing.

If the RH_{crit} is not known, it is recommended to use Class A. This is also in line with recommendations from the Swedish National Board of Housing (Boverket Swedish National Board of Housing 2014). It is recommended that the material producers provide and communicate data of RH_{crit}. Some producers in Sweden have performed tests at RISE. As this is commercial information, it is not referred to in this study. We have no knowledge about whether testing have been performed at other laboratories for other materials.

Outcome of the PJ-model and evaluation of results

If RH values are below the lower growth curve in Figure 6.5 no mould growth is expected. If it exceeds the upper limit growth curve, mould growth is predicted. Values in the zone between the upper and lower curve represent a “yellow-light case”. However, the model also predict mould in these cases to be on the safe side. (Johansson 2012, Johansson, Svensson et al. 2013).

7.1.5 Selected parameter values for different models in the study

Different partners chose different parameter values in the round robin study. In the VTT model, there are many choices and hence many possible combinations of parameters. The different combinations chosen by different partners are shown in Table 7.6. The parameters chosen for the other models are presented in Table 7.7.

Table 7.6: Combinations of parameters for different materials chosen by different RIBuild partners using the VTT model. Each unique combination of parameters corresponds to a letter (ltr), to identify different cases during the evaluation. Note that different materials may belong to the same group (ltr)

Material	Class	Surface	Wood	Cmat	ltr
Chipboard, Gypsum board, Thin hardboard	Sensitive	0	0	0.100	a
Chipboard, Gypsum board, Thin hardboard, Spruce, Plywood	Sensitive	0	0	0.300	b
Chipboard, Gypsum board, Thin hardboard	Sensitive	0	0	0.500	c
Chipboard, Gypsum board, Thin hardboard, Spruce, Plywood	Sensitive	1	1	0.250	d
Plywood, spruce	Very sensitive	0	0	0.100	e
Plywood, spruce	Very sensitive	0	0	0.500	f
Gypsum board, spruce	Very sensitive	0	0	0.250	g
Chipboard, Gypsum board, Thin hardboard, Spruce, Plywood	Sensitive	0	0	0.000	h
Plywood, Thin hardboard, Chipboard	Sensitive	0	0	0.250	i

Table 7.7: Summary of choices of parameters in other models used by different RIBuild partners

	Sensitivity Class WUFI bio and Sedlbauers LIMcurves Table 7.3	D_{crit} MRD model		RH_{crit} PJ-model Table 6.5	m-model Sensitivity class Table 7.1
		Estimated from Table 7.5	(Johansson, Ekstrand-Tobin et al. 2012)		
Plywood	Class I	Dcrit=10	Dcrit =7	A***	Very sensitive, Sensitive
Chipboard	Class I	Dcrit=8	Dcrit =28	B***	Sensitive
Thin hardboard	Class I	Dcrit=17	Dcrit =77	C***	Sensitive
Gypsum board	Class I	Dcrit=8	Dcrit =100*	D***	Very sensitive, Sensitive
Spruce	Class I	Dcrit=10	Dcrit =70**	C**	Very sensitive, Sensitive

*There was no mould growth on this material hence there is no D_{crit} available. The length of the test was 84 days. In the description of the MRDmodel (Thelandersson and Isaksson 2013) it is not specified how long time a test for determining D_{crit} should last.

**Results from laboratory tests in (Johansson, Wadsö et al. 2018)

***Results from laboratory tests according to (SIS 2014) and presented in (Johansson 2012)

7.1.6 Comparison of predications and real outcome

The outcome of the models based on the evaluation criteria of each model were compared to the analysis for mould growth in the previous field study. As the possibility for mould growth vary by time in some models and test climates, the evaluation criteria was to consider if there was predicted mould growth at any point of time. This was then compared to if there was mould growth or not at the end of the exposure in the field study.

The static models (PJ-model and Sedlbauers isopleths) considered the conditions during the whole test period and the mould growth at the end of the period, see an example in Figure 7.6.

7.1.7 Results

Examples on how the comparison between predictions and results of mould growth were performed are presented in Figure 7.5 and Figure 7.6. In the example in Figure 7.5 two cases (VTT model predictions) predicted growth. However, mould growth was established on all samples (after around 10.000 hours). Consequently, most of the predictions were wrong in this example. In Figure 7.6 all samples predicted growth and it agreed with the real results. Comparisons in this case were made in the end of the measured period.

The complete comparison given as the same type of graphs can be found in Appendix 2 for the dynamic models and Appendix 3 for the static models.

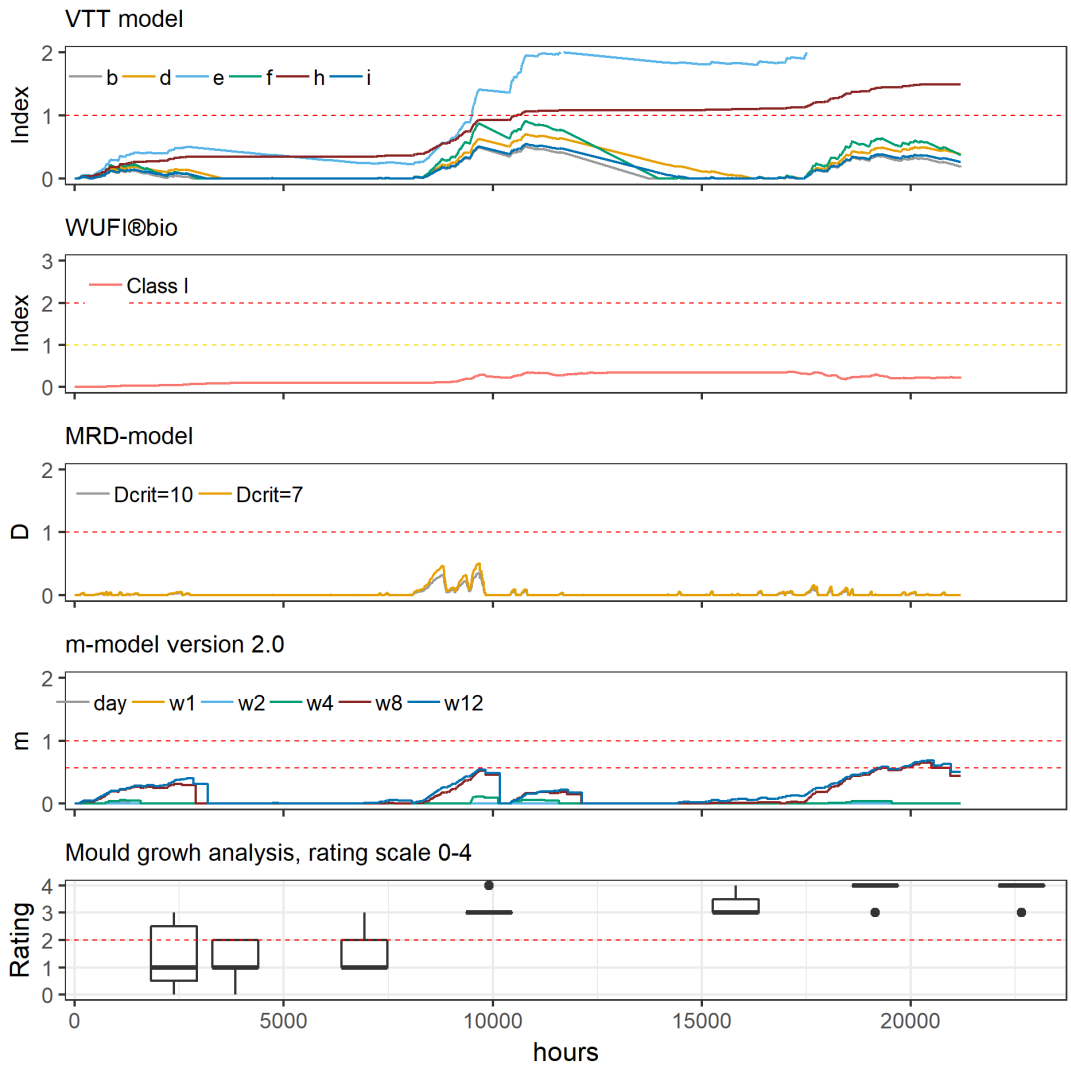

Figure 7.5: Comparison of the outcome of dynamic models (upper four graphs) and mould growth on test specimens, lower graph (Climate 1, material Plywood). Descriptions on how the outcome is evaluated for each model is found in section 7.1.4.
The lower most graph shows real mould growth by time, the thick horizontal line in each box represents the median growth on seven test specimens. Mould growth is established when the median is at or above 2 (horizontal dotted line).

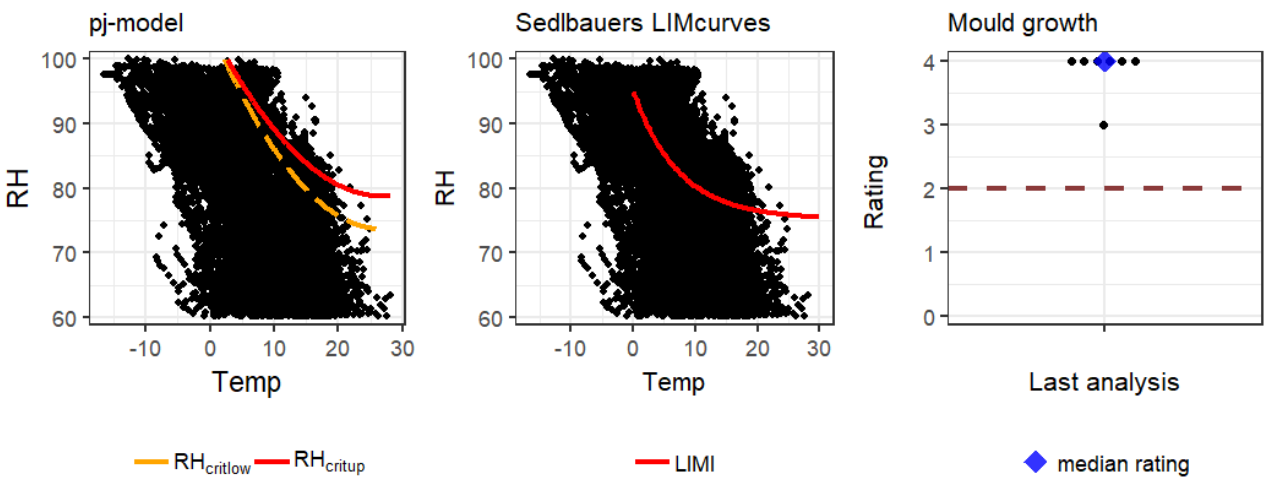

Figure 7.6: Comparison of the outcome of static models (PJ-model and Sedlbauers limcurves) and mould growth on test specimens (Climate 1, material Plywood). If the measured RH is above the red limit curve, mould growth is predicted (both models). If it is above the yellow line, RHcritlow, there is a possible risk for mould growth (PJ-model). The right graph shows the real outcome. When the median is 2 or more (horizontal dotted line) mould growth is considered established.

In Climate5, the conditions for mould growth were favourable as RH is relatively high and the temperature is over 0°C during the entire test period (Figure 7.2). In addition, the variations between higher and lower RH are small. Mould growth was established on all samples of every material. The other extreme is Climate6, where the conditions of RH and temperature were unfavourable and there was no mould growth on any of the samples. In the three other climates, Climate1, Climate2 and Climate3, the RH and temperature varied considerably between unfavourable and favourable conditions during the entire test period. In the comparison between predicted and actual growth, Climate1, Climate2 and Climate3 was evaluated as one group and Climate5 and Climate6 as separate, extreme climates. The results for all models are shown in Table 7.8, Table 7.9 and Table 7.10.

Table 7.8: Summary of comparison of predicted outcome for each model and results from field tests for Climate1, Climate2 and Climate3 treated as one group. Cells that are marked with green represents cases where prediction and actual mould growth agreed and red where it disagreed.

Model	**Predicted mould growth by model**	**Established mould growth on test specimens** (Numbers of observations for each model. percentage of total observations for each model is shown in bracket)	
		No	Yes
m-model version 2.0	No	5 (27%)	13 (72%)
	Yes	0 (0%)	0 (0%)
MRD-model	No	4 (22 %)	14 (78%)
	Yes	0 (0%)	0 (0 %)
VTT model	No	16 (22%)	44 (61 %)
	Yes	2 (3 %)	10 (14 %)
WUFI®-bio, “yellow traffic light”	No	3 (25%)	9 (75%)
	Yes	0 (0%)	0 (0%)
WUFI®-bio, “red traffic light”	No	3 (25%)	9 (75%)
	Yes	0 (0%)	0 (0%)
SedlbauerLIM	No	0 (0 %)	0 (0%)
	Yes	5 (33 %)	10 (67%)
PJ-model $RH_{critlow}$	No	1 (7%)	0 (0 %)
	Yes	4 (26 %)	10 (67%)
PJ-model RH_{critup}	No	4 (26%)	1 (7%)
	Yes	1 (7 %)	9 (60 %)

Table 7.9: Summary of the results from comparison of the predicted outcome for each model and results from field tests for Climate5. Cells that are marked with green represents cases where prediction and actual mould growth agreed and red where it disagreed

Model	**Predicted mould growth by model**	**Established mould growth on test specimens** (Numbers of observations for each model. percentage of total observations for each model is shown in bracket)	
		No	Yes
m-model version 2.0	No	0 (0%)	0 (0%)
	Yes	0 (0%)	6 (100%)
MRD-model	No	0 (0%)	0 (0%)
	Yes	0 (0%)	6 (100%)
VTT model	No	0 (0%)	0 (0%)
	Yes	0 (0%)	24 (100%)
WUFI®-bio, “yellow traffic light”	No	0 (0 %)	0 (0 %)
	Yes	0 (0 %)	15 (100 %)
WUFI®-bio, “red traffic light”	No	0 (0 %)	0 (0 %)
	Yes	0 (0 %)	15 (100 %)
SedlbauerLIM	No	0 (0 %)	0 (0 %)
	Yes	0 (0 %)	15 (100 %)
PJ-model $RH_{critlow}$	No	0 (0 %)	0 (0 %)
	Yes	0 (0 %)	15 (100 %)
PJ-model RH_{critup}	No	0 (0 %)	0 (0 %)
	Yes	0 (0 %)	15 (100 %)

Table 7.10: Summary of the results from comparison of the predicted outcome for each model and results from field tests for Climate6. Cells that are marked with green represents cases where prediction and actual mould growth agreed and red where it disagreed

Model	Predicted mould growth by model	Established mould growth on test specimens (Numbers of observations for each model. percentage of total observations for each model is shown in bracket)	
		No	Yes
m-model version 2.0	No	6 (100%)	0 (0%)
	Yes	0 (0%)	0 (0%)
MRD-model	No	6 (100%)	0 (0%)
	Yes	0 (0%)	0 (0%)
VTT model	No	24 (100%)	0 (0%)
	Yes	0 (0%)	0 (0%)
WUFI®-bio, “yellow traffic light”	No	15 (100%)	0 (0%)
	Yes	0 (0%)	0 (0%)
WUFI®-bio, “red traffic light”	No	15 (100%)	0 (0%)
	Yes	0 (0%)	0 (0%)
SedlbauerLIM	No	15 (100%)	0 (0%)
	Yes	0 (0%)	0 (0%)
PJ-model $RH_{critlow}$	No	15 (100%)	0 (0%)
	Yes	0 (0%)	0 (0%)
PJ-model RH_{critup}	No	15 (100%)	0 (0%)
	Yes	0 (0%)	0 (0%)

7.1.7.1 Dynamic models

When the extreme climates (Climate5, Climate6) were used as input in the models with the different parameters chosen, there was an 100 % agreement between the prediction of mould growth using the different dynamic models (VTT model, WUFI®-bio, m-model version 2.0 and MRD-model) and the outcome of mould growth analysis (field study). All models predicted mould growth in Climate5 and mould growth was established on all materials. The models predicted no mould growth in Climate6, in agreement with the results from the field study.

In the cases were the RH and temperature varied a lot, both daily and seasonally (Climate1 Climate2, Climate 3), the agreement between the prediction from the models and actual mould growth on test specimens varied. The summary of the predictions and real outcome for those climates is presented for all dynamic models in Table 7.11.

Table 7.11: Summary of comparing predictions for mould growth of the dynamic model and outcome of analysis from the field exposure test for Climate1, Climate2 and Climate3

Predicted growth by models	Established mould growth on test specimens	
	No	Yes
No	31 (23%)	89 (67%)
Yes	2 (2%)	10 (8%)

7.1.7.2 Static models (limcurve models)

In the extreme climates (Climate5 and Climate6), the prediction from static models (PJ-model and Sedlbauers LIMcurves), and actual growth are in 100 % agreement.

For Climate1, Climate2 and Climate3, the agreement between predicted and outcome is in general very good. In the cases where there is no agreement, the models are conservative, that is they predict mould growth when there is no established growth. However, the margin differs between the two models, se example in Figure 7.7.

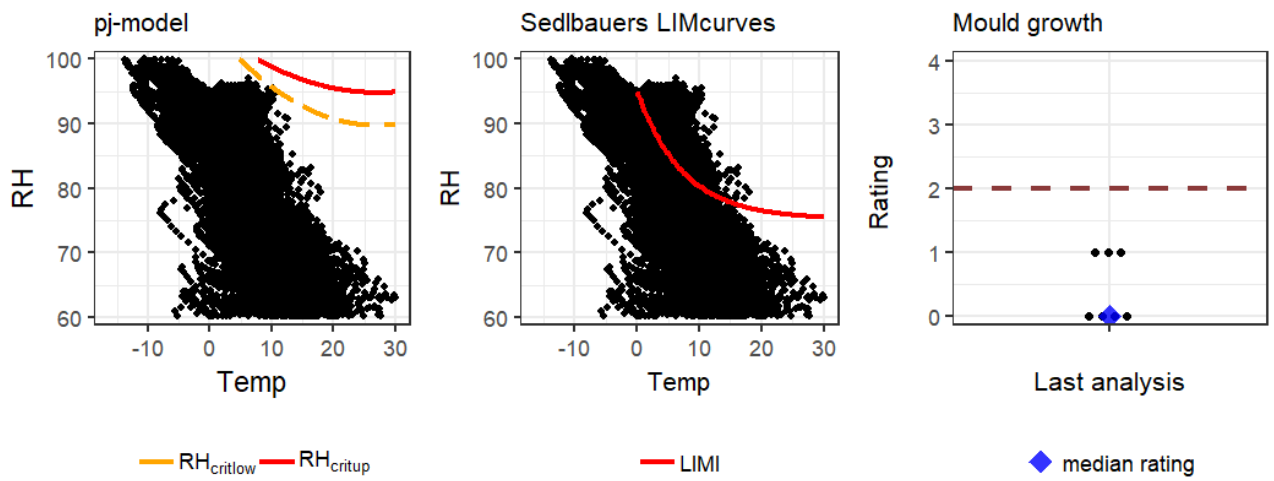

Figure 7.7: Example case of when the static models are conservative (Climate 2, Thin hardboard). If the measured RH is above the red limit curve, mould growth is predicted (both models). If it is above the yellow line, $RH_{critlow}$, there is a possible risk for mould growth (PJ-model). When the median is 2 or more (horizontal dotted line) mould growth is considered established.

7.1.8 Discussion

Mould prediction models aim to predict whether there will be mould growth or not in a building part with known or simulated RH and temperature. Several such models have been developed based on laboratory data. In this study, the prediction of mould growth on different building materials in different building parts were compared to actual mould growth in a round robin study. The models require input choices made by the user of the model. The aim of the study was to assess the performance of the models based on choices and interpretation made by the different partners participating in the round robin.

The results show that the outcome of mould prediction models for mould growth on the same building materials in the same climatic data is dependent on the end user of the model. In addition, the result

showed that in most cases there was a discrepancy between the outcome of the dynamic prediction models and real results of actual mould data. Unfortunately, in some cases the partners did not interpret the results from their simulations, i.e. would there be mould growth or not. However, they did describe how the interpretations should be made and we based the evaluation on these descriptions.

In the "extreme cases", dry conditions (Climate5) or wet conditions (Climate6), with small fluctuations, the outcome of all models was in good agreement with results from field studies of mould growth. For an experienced practitioner, the prediction of possibility for mould growth on materials, in these extreme climates, could possibly have been made without using an advanced prediction model. However, when favourable and unfavourable conditions for mould growth are varying by time, and the difference between these conditions are quite high, it is more complicated to estimate if there would be mould growth or not. The dynamic models used in this study were developed with the purpose to make such predictions also under fluctuating conditions.

In most cases, the results from comparing the outcome of the dynamic models to actual mould growth were false negative (67 % of cases), i.e., the model predicted no growth while there was mould growth on samples exposed to the actual climate. In many cases, the growth was actual even heavy. For the static models, on the other hand, the outcome of the predictions was mostly in agreement with the results from mould analysis. When the results differed, the predictions were false positive, i.e., the models predicted mould growth when there was none. The best agreement to actual mould growth was given using the PJ-model. In the cases where the dynamic VTT model predicted in agreement with the actual mould growth, C_{mat}, the parameter that considers the effect of fluctuating conditions, was chosen to be zero or was very low (C_{mat}=0.1). This indicates that the simpler models only considering the material limit parameters and not the dynamic conditions are useful and reliable.

A perfectly accurate model should predict mould growth when there is growth and no growth when there is none. Although no model could be expected to be perfect, the aim should be that there would be a margin of safety in practical implications. In order to avoid actual mould growth in a building part it means that the models preferably should be conservative, i.e. predicting mould growth when there is none. However, the safety margin should not be too big, as this may lead to big costs when designing a building. Both static models in this study were shown to be conservative, however the safety margin was much bigger for Sedlbauers LIM-curves than in the PJ-model. In the cases where the PJ-model was conservative, only a few measured RH was just above the lower curve.

It could be argued that the rating scale for determining mould growth on the test samples (see Table 6.3) are not the same as the mould index in the VTT model and WUFI®-bio and the criteria for mould growth in the m-model. This would then affect the comparisons of the outcome of the models and the real mould data. However, even though the different descriptions and numerical values of mould growth are not directly comparable, the limit rating value used in the evaluation comprises more extended growth than the limit values in the models. In addition, sometimes the growth was very heavy.

The results show that it is often difficult for the end user of the models to know which input parameters that would be most correct. Different products of the same material group, for example wood based boards, may have different susceptibility for mould growth (Tanaca, Dias et al. 2011, Johansson, Ekstrand-Tobin et al. 2012) as might different qualities of wood (Johansson, Mjörnell et al. 2017, Johansson, Wadsö et al. 2018) and treatments of wood (Bok, Johansson et al. 2012). It is therefore not possible to "guess" the mould resistance of a specific material and hence classify it to a proper material group in the actual model. Instead, the input for the models regarding material data

should be based on laboratory testing of the product. This is the case in the PJ-model, where a standardised test method is used to get the material input data. The material parameter in the MRD-model, D_{crit}, is recommended to be determined by laboratory tests at 90 % RH and 22°C, although the method is not specified. In this study, we used results from testing at the prescribed conditions and following routines in (SIS 2014).

In the study, a discrepancy was identified in documentation on how to interpret the results and which in data to be used in some of the models. The limit value for mould growth in the VTT model varies between different publications and explanations for the model. In this round robin, all partners using the VTT model choose index 1 as the limit value. If a higher value was chosen, the results would have been even more false negative cases. It was also identified in the study that there is a lack of information in the models of how to interpret the cases where the outcome is close to the limits.

The end users of the prediction models should be able to understand how evaluation is done and how to interpret the results. It is worth noticing that in this study, the models were used and interpreted by researchers with good insight in the research area of mould growth in buildings, yet the input parameter choices and interpretation varies.

The input data from measurements in the different climate cases need to be discussed, as these are the basis of the predictions. In the study, the values were adjusted according to calibration at different temperatures and RH. Sometimes the adjustment was several percentages. If there would have been no such adjustment in the input data, the outcome from the models would possibly have been different. Therefore, it is emphasised that data from field studies must always be adjusted according to calibration data. Measurements of RH and temperature are always connected to some measurement uncertainties and the measurement uncertainty were estimated for the different calibrated data. In addition to adjustment to calibration, the data was in some cases also adjusted to the drift of the loggers. The combined measurement uncertainty could in some cases be as high as 2.5 %. In this round robin, the measurement uncertainties are not considered into the mould models, as there is no given way to handle this in the models. Not taking the measurement uncertainties into account may affect those results that are close to the critical limit for mould growth.

Mould growth on a material is governed by the microclimate at the surface. In the field study, the measurement of RH and temperature was performed as close as possible to material surfaces of the test specimens. However, the microclimate at the surface might differ from the measured climate close to the surface. This have been raised as possible explanation for the discrepancy between the outcome of the dynamic models and actual mould growth. However, it does not explain the differences of the outcome between the models.

Even if the round robin shows that dynamic models give false negative results, it should be mentioned that the dynamic models are still useful on a relative basis for comparing and deciding between different constructions during a design phase. However, if a specific construction is to be considered safe or not, the results must be handled with care.

Finally, some words on the design of the models, apart from uncertainties of how the input parameters should be chosen as discussed above. The aim of the study was to compare the outcome of different models based on how different users choose their input parameters, interpret the results etc. and not about the philosophy behind or design of the models. However, some points are worth to mention and discuss. In the dynamic models, the output parameter describing mould growth present on material increase and decrease by time. When mould growth has established, it will not vanish, even though the activity of the fungi may vary by time. However, this is not what the parameters describes.

Another point is that the MRD model assumes a D_{crit} based on testing at 90%, 22 °C but it is impossible to get such a result if the critical moisture state is higher, i.e. that mould will never grow at 90% RH. Another identified issue is that in WUFI®-bio, annual predictions are given. However, in actual situation using the prediction tool longer periods need to be evaluated.

7.1.9 Conclusion and future work

When using models for prediction of mould growth in materials, considering the dynamic conditions of RH and temperature in buildings, the risk of underestimating the potential for mould growth is significant. Therefore, it is important to use caution when interpreting the results.

Static models were shown reliable, as they were in good agreement with the field results. In addition, in the few cases when there was no agreement, the models were conservative, meaning that there is a safety margin. The model using Sedlbauers LIMcurves lead to a big safety margin, as it nearly always predicts mould growth. The PJ-model is more accurate in its prediction as the safety margin is smaller.

In general, there is a need for better manuals and information concerning mould models on how to select parameters and which limit values to be used for the evaluation. This is especially important when the outcome of the models is close to the limit values. This is true for all models used in this study.

It is difficult to “guess” which material group a certain material belongs to and this may lead to differences between users of the same model and to inaccurate predictions. When using laboratory test results, from a standardised test method, the predictions are more accurate and reliable. Material producers should be encouraged to test their products and present the results. In addition, the models should be customized to use such data.

More knowledge is needed to evaluate the complex relationships between fluctuating conditions of RH and temperature encountered in buildings and the risk for mould growth. However, the prediction models should not be too complex. This study shows that simpler models may even be more useful.

In none of the prediction models, the effect of measurement uncertainty of measured data is considered, nor any uncertainties from simulations of expected RH and temperatures. In future versions, the models should also consider this effect for more accuracy, since the uncertainties are especially important when the outcome of the models are close to the limit values.

7.2 Rot

As stated in section 5.2, the VTT model of wood decaying fungi was considered most useful in RIBuild context, as it generates mass loss (%) based on hygrothermal conditions (T and RH) and exposure time in critical conditions. However, the model has in more than one case shown to generate too conservative results with regard to mass loss. Nevertheless, it has proven to be valuable for evaluation of performance, and comparison purposes.

7.2.1 Weakness of the rot model

The inclusion of wood rot models as a RIBuild failure mode was further discussed, due to the following factors;

- Wood rot is initiated at higher moisture levels than mould growth; therefore, if a solution is disregarded due to mould growth, there is no need for modelling wood decay. Furthermore, if a solution is regarded safe in terms of mould growth, likely there is also no wood rot. However, there might be cases, where mould growth might be acceptable, if the indoor climate is not affected, while rot is still not acceptable.
- It can be misleading to include wood rot in 1D simulations, as embedded wood, e.g. beam-ends, are at least a 2D problem. Furthermore, in wood capillary suction is an anisotropic property. The hygrothermal conditions in embedded wood are therefore highly dependent on the direction of the wood, which is not accounted for in the wood rot model or in simulations. Therefore, the 1D simulations do not cover beam-ends sufficiently. Prediction of wood decay based on these could therefore be misleading.
- The wood decay model may be able to provide indication of potential risk of wood decay; however, the model is based on experimental data of decay in only small specimens of pine, and under constant conditions. Furthermore, the embedded wood will not be subjected to driving rain directly, and thus according to (Viitanen, T. et al. 2010) wood decay can be avoided for a longer period. The model merely presents preliminary indications of decay.

7.2.2 Test of rot model on existing building without internal insulation

A way to test if combination of 1D simulations and the VTT rot model gives reliable results, is to perform 1D simulations on an existing building without internal insulation, feed the hygrothermal results over time to the VTT model and see if the results comply with mass loss seen in reality. If the VTT rot model shows high mass loss over few years, while the construction has lasted for decades, the rot model overestimates the risk of rot in this case.

1D simulations were performed on a case building facing renovation including internal insulation. The modelling included a 1D construction of 350 mm brick and 10 mm internal render. The material properties of the bricks in the model were constructed based on “Old Building Brick (Dresden ZH)” from the DELPHIN material database, with alterations due to experimental data (λ, C_p, ρ, A_w) from a brick retrieved from the building. The interior render was of historical lime plaster from the DELPHIN material database. Simulations were performed with constant indoor climate of 20°C and 50% RH. The external climate applied as boundary conditions was projected future climate for Copenhagen 2020-2050, provided by the EU project “Climate for Culture”.

Although the simulations are not based on real weather data, and therefore could be more precise, this kind of simulations would be comparable to how simulations are performed to predict future behaviour. The orientation was SW – corresponding to the orientation most exposed to wind-driven rain in Denmark. In order to assess the conditions in beam ends despite the 1D origin of the models, the hygrothermal conditions generated at a depth of 10 cm from the internal side, were chosen to represent the location of wood, either beams or laths, and the following analysis is based on output from this location.

The VTT model for wood decay was applied to simulated values of temperature and relative humidity in the masonry. The results are illustrated in Figure 7.8.

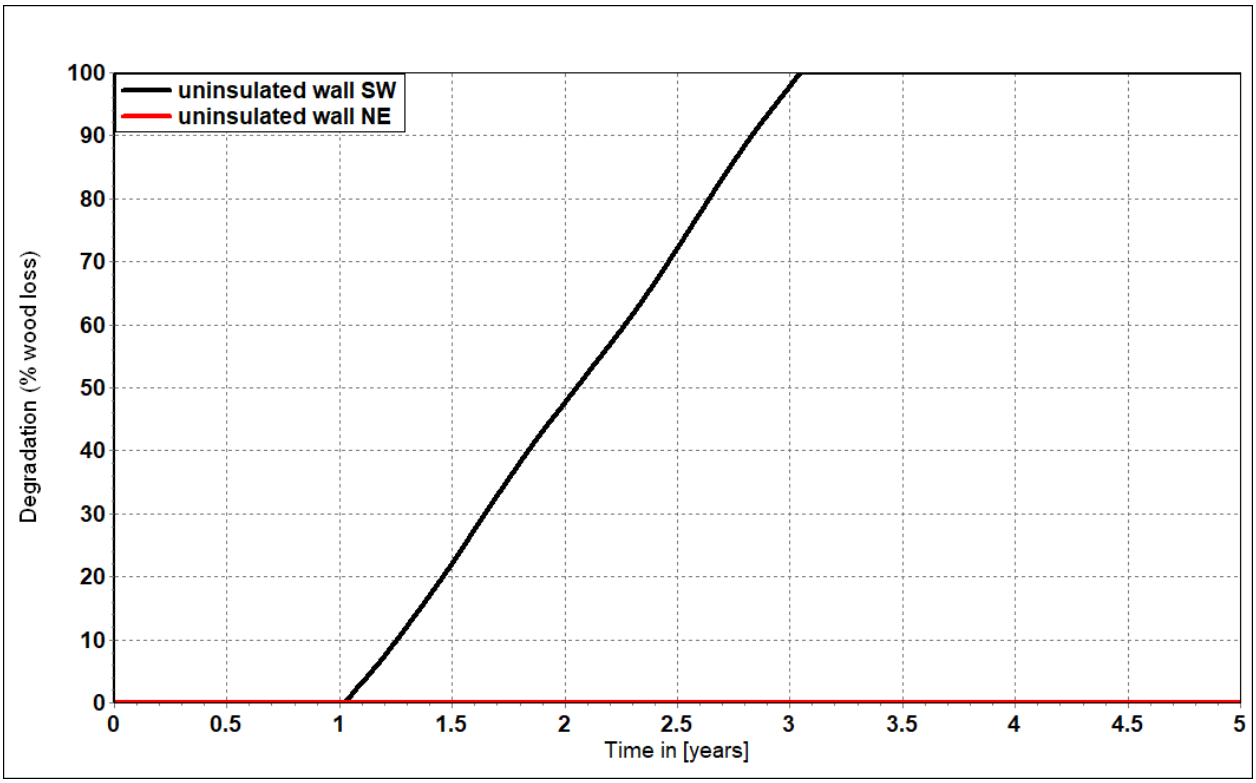

Figure 7.8:Mass loss in uninsulated reference walls with orientations SW and NE

As seen in the figure, it appears that there is no risk of mass loss in the beams facing northeast orientation. On the contrary, beams in the southwestern façade exhibit a risk of extreme mass loss. The mass loss in the southwest façade is initiated after the first year of simulations, and after 3 years of simulation, 100 % mass loss is generated. The case building is from 1928. The construction has not been opened for determination of actual mass loss in the beams, however the significant mass loss generated after 3 years, does not appear to agree with reality. Despite the weather implemented in simulations being forecasted weather, one can imagine that in the past 90 years of the building's service life, there will have been wet and dry years as well, and likely conditions also initiating mass loss according to the model, especially as the wood decay is irreversible. If 100% mass loss could appear after 3 years of simulation, it would have likely appeared during 90 years of service life, whereas there are no actual indications of wood decay.

7.2.3 Test of rot model on experimental data

Measurements of temperature and relative humidity from a large-scale experiment with internally insulated masonry and embedded wood, has been applied to the VTT model. The experimental setup consists of several 1½ brick thick solid masonry walls built into two shipping containers. A variety of internal insulation systems were applied to these walls (including calcium silicate, AAC, PUR foam with calcium silicate channels), and furthermore some external surfaces were hydrophobized. Each of the walls include a wooden beam, and a wooden lath. The walls are subjected to actual outdoor climate, and the interior conditions are kept constant at 20°C and 60% relative humidity.

The experimental setup of each wall is shown in Figure 7.9, and is further described in RIBuild deliverable D3.1 (Freudenberg, Ruisinger et al. 2018). Since 2015, measurements of temperature and relative humidity have been performed at several locations in the masonry, including the wooden beam and lath, as marked in the figure.

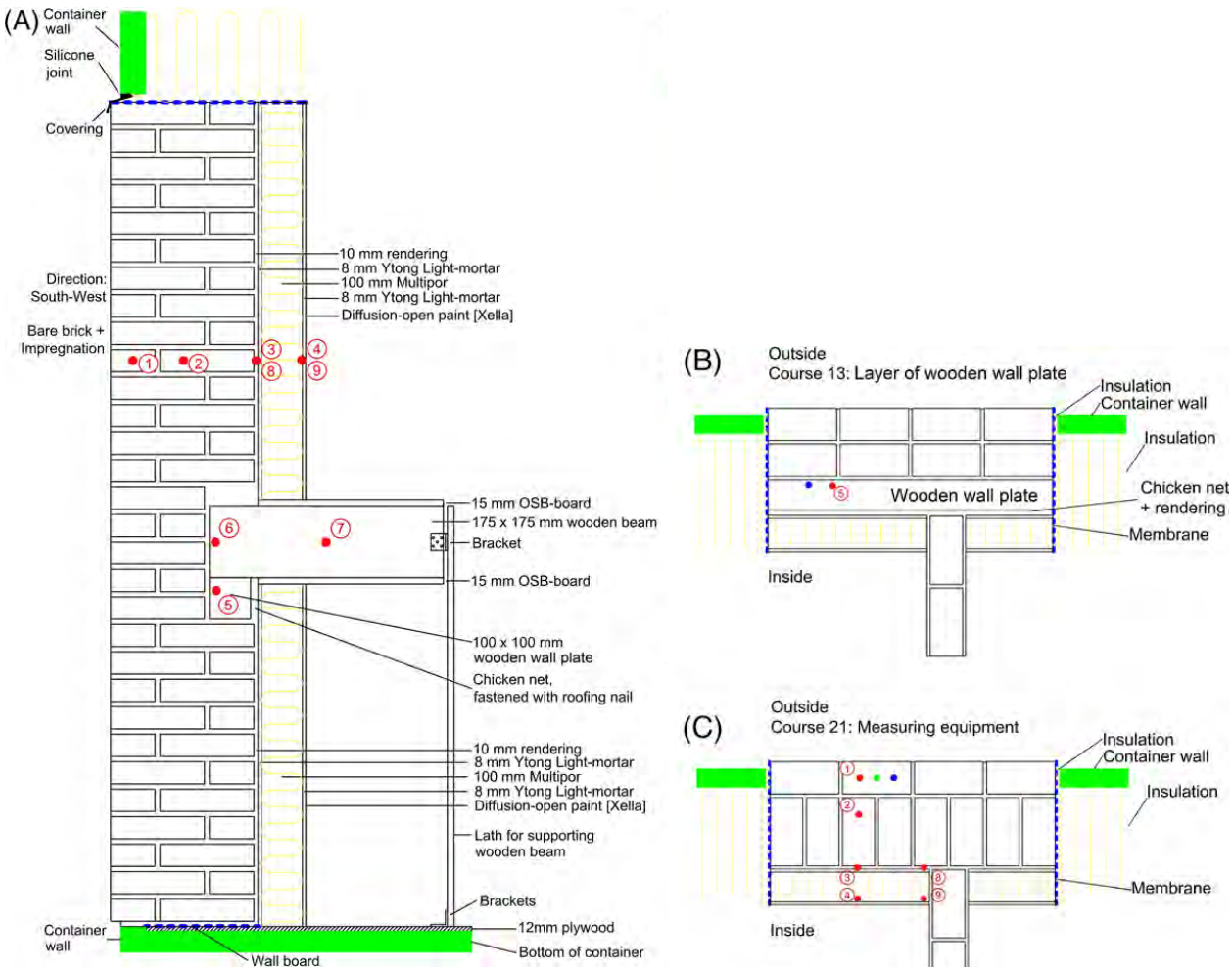

Figure 7.9: Experimental setup of wall configurations, and sensor locations. A) vertical section view, B+C) horizontal section views [Tommy Riviere Odgaard]

Table 7.12 lists a variety of the test walls and their configurations combined with the results from the VTT wood decay model and VTT mould model (mould index) generated for measurements performed in the wooden construction elements. The models were applied to measurements from both the beam-ends (point 6) and the wooden lath (point 5). The mould index was based on very sensitive sensitivity class (untreated wood), and a relatively low decline factor of 0.25. From the table, we can derive that;

- Seven of 28 investigated sensor locations in wood, generated mass loss in the range of 15-108%
- Wood decay is initiated only in the cases of mould index above 5.5
- Higher risk of wood decay in the lath, when compared to the beam end
- Southwest appears to be the dominant orientation for cases with wood decay

Table 7.12: Studied wall configurations with results for wood decay (% mass loss) and mould index with VTT models (wood decay model and mould model). Generated mass loss in rows marked with red.

Wall		Point		Or.	Start	End	Internal insulation system	Exterior surface	Interior surface	Wood decay model, VTT	Mould model, VTT
										% mass loss	Mould index
C3	1	5	**Lath**	SW	01-05-2015	18-01-2018	Mineral wool + vapour barrier	Bare brick	Gypsum + diffusion tighter paint	36.9	6.0
C3	1	6	**Beam**	SW	01-05-2015	18-01-2018	Mineral wool + vapour barrier	Bare brick	Gypsum + diffusion tighter paint	32.1	6.0
C3	2	5	Lath	SW	01-05-2015	18-01-2018	PUR w. CaSi[a]	Hydrophob.	Diffusion open paint	<1	5.5
C3	2	6	Beam	SW	01-05-2015	18-01-2018	PUR w. CaSi[a]	Hydrophob.	Diffusion open paint	0	3.6
C3	3	5	**Lath**	SW	01-05-2015	18-01-2018	Reference wall	Bare brick	Rendering	39.2	6,0
C3	3	6	Beam	SW	01-05-2015	18-01-2018	Reference wall	Bare brick	Rendering	0	4.1
C3	4	5	**Lath**	SW	01-05-2015	18-01-2018	Calcium silicate[b]	Bare brick	Diffusion open paint	**108.0**	6.0
C3	4	6	Beam	SW	01-05-2015	18-01-2018	Calcium silicate[b]	Bare brick	Diffusion open paint	<1	5.6
C3	7	5	Lath	SW	01-05-2015	18-01-2018	PUR w. CaSi[a]	Bare brick	Diffusion open paint	<1	6.0
C3	7	6	Beam	SW	01-05-2015	18-01-2018	PUR w. CaSi[a]	Bare brick	Diffusion open paint	0	5.3
C3	10	5	**Lath**	NE	01-05-2015	18-01-2018	PUR w. CaSi[a]	Bare brick	Diffusion open paint	**52,8**	6.0
C3	10	6	Beam	NE	01-05-2015	18-01-2018	PUR w. CaSi[a]	Bare brick	Diffusion open paint	0	5.5
C3	13	5	Lath	NE	01-05-2015	18-01-2018	Calcium silicate[b]	Bare brick	Diffusion open paint	0	4.9
C3	13	6	Beam	NE	01-05-2015	18-01-2018	Calcium silicate[b]	Bare brick	Diffusion open paint	0	4.9
C3	14	5	Lath	NE	01-05-2015	18-01-2018	Reference wall	Bare brick	Rendering	0	0.1
C3	14	6	Beam	NE	01-05-2015	18-01-2018	Reference wall	Bare brick	Rendering	0	4.4
C3	15	5	Lath	NE	01-05-2015	18-01-2018	PUR w. CaSi[a]	Hydrophob.	Diffusion open paint	0	4.3
C3	15	6	Beam	NE	01-05-2015	18-01-2018	PUR w. CaSi[a]	Hydrophob.	Diffusion open paint	0	2.6
D4	2	5	**Lath**	SW	01-05-2015	24-10-2017	Mineral insulation panels[c]	Bare brick	Diffusion open paint	28.2	6.0
D4	2	6	Beam	SW	01-05-2015	24-10-2017	Mineral insulation panels[c]	Bare brick	Diffusion open paint	0	4.0
D4	3	5	Lath	SW	01-05-2015	24-10-2017	Mineral insulation panels[c]	Hydrophob.	Diffusion open paint	<1	6.0
D4	3	6	Beam	SW	01-05-2015	24-10-2017	Mineral insulation panels[c]	Hydrophob.	Diffusion open paint	0	4.1
D4	4	5	Lath	SW	01-05-2015	24-10-2017	Reference wall	Hydrophob.	Rendering	0	4.8
D4	4	6	Beam	SW	01-05-2015	24-10-2017	Reference wall	Hydrophob.	Rendering	0	3.0
D4	5	5	**Lath**	SW	01-05-2015	24-10-2017	Reference wall	Bare brick	Rendering	15.7	5.9
D4	5	6	Beam	SW	01-05-2015	24-10-2017	Reference wall	Bare brick	Rendering	0	3.3
D4	7	5	Lath	SW	01-05-2015	24-10-2017	Mineral insulation panels w/ T.B.[d]	Bare brick	Diffusion open paint	0	5.5
D4	7	6	Beam	SW	01-05-2015	24-10-2017	Mineral insulation panels w/ T.B.[d]	Bare brick	Diffusion open paint	0	2.7

a) IQ-Therm, PUR foam insulation, with calcium silicate channels in 40x40mm grid
b) SkamoPlus indeklimaplade
c) Multipor, Xella 80kg/m3
d) Multipor, Xella 80 kg/m3 with thermal bridge to beam

Due to the unnaturally high-generated mass loss in several cases, an investigation was initiated to confirm or deny the high levels of wood decay. The two walls with highest generated mass loss, C3-4 (108%) and C3-10 (53%) were opened in January 2019, and samples from the lath removed. The wood samples were all the way through the lath, from the interior side (interface with insulation) to the exterior side (interface with masonry). Moisture content in the laths was registered with a pin type moisture meter after removal of internal insulation, and prior to drilling in the wood. Due to very high heat generation, and water used for cooling of the drill, further moisture measurements in the wood

were not performed. A visual inspection of the wood samples was performed, as well as an awl-test for determination of possible soft areas. Figure 7.10 depicts the removal of the samples; initially the internal insulation was removed, and hard wood. Samples were then removed from the laths.

Figure 7.10: Removal of wood samples from lath beneath wooden beam

Results from the moisture content measurements and the wood samples are seen in Table 7.13:.

Table 7.13: Results from the inspection of wood samples

Wall	Mass loss (VTT)	Moisture content	Pictures of samples
C3-4	108%	12-14%	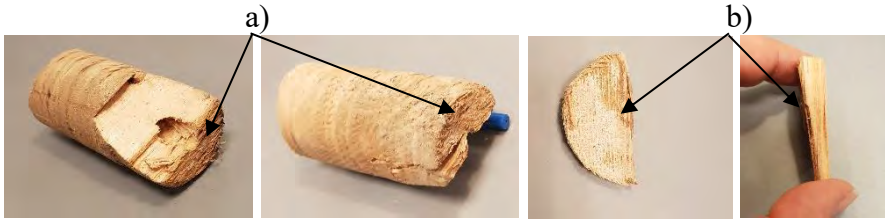 a) Surface towards internal insulation b) Surface towards external masonry
C3-10	53%	14-16%	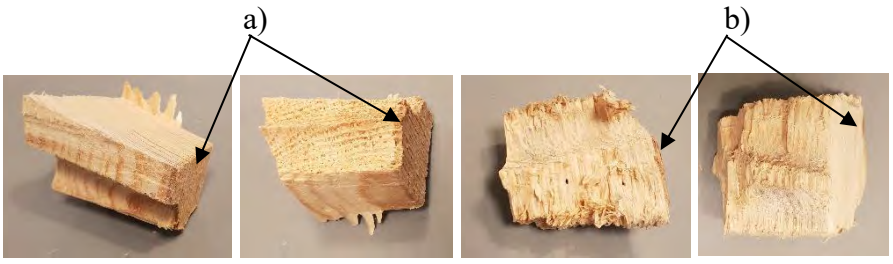 a) Surface towards internal insulation b) Surface towards external masonry

The visual inspection of wood samples from both walls did not indicate any mass loss in the samples. The wood appeared hard and dry, and without discoloration. The wood was hard to remove, and therefore appears in several pieces, and any visual cracks that may appear in pictures, were caused by the removal process. The specimens yielded no smell of mould or rot. It was not possible to visually detect any forms of wood decaying fungi on the specimens. Furthermore, it was not possible to stick an awl in the samples, indicating healthy wood.

In the follow-up period, mycometer tests will be performed on both specimens, and both surfaces. Furthermore, the samples will be visually inspected at certain time intervals. In the event of very high results from mycometer test, further action will follow, however it is not expected.

The model, in these cases, appears to be very conservative. In two cases of high-generated mass loss with the model, no wood decay or mass loss was detected in the specimens. The model can, however, be used to evaluate a variety of solutions relatively, and thus better or worse performance can be established based on comparison. However, whether the solution is suitable or not, cannot be satisfactory determined by the models.

7.3 Frost damage

Given that none of the currently available hygrothermal indicators for frost damage, see section 5.3, allow to actually quantify the frost damage, these have not been explicitly evaluated. Moreover, since the further research required to advance these prediction models is far larger than what is possible within the framework of RIBuild, no further research, besides the activities reported in section 6.2, has been performed.

7.4 Algae

According to the modified Avrami's equation 4, growth curves *X(t)* were analytically modelled with the parameters obtained from the accelerated growth tests at T=27.5 °C and T=10 °C. Results are reported in Figure 7.11.

For all the brick materials, the curves on average tended to slightly underestimate the measurements during the first weeks, and, on the contrary, to slightly overestimate the growth process in the proximity of the last stagnation phase. However, since the Avrami analytical values were generally included within the experimental standard deviations, it can be said that the analytical curves, obtained by the modified Avrami's equation 4, well simulated the experimental measurements, both for the optimal and the non-optimal tested temperatures.

These results confirmed the experimental findings reported in Figure 6.20. The effect of the temperature is well represented, since the curves associated to the lower temperature were clearly lower in terms of covered area and delayed in time respect to the curves related to the optimal temperature.

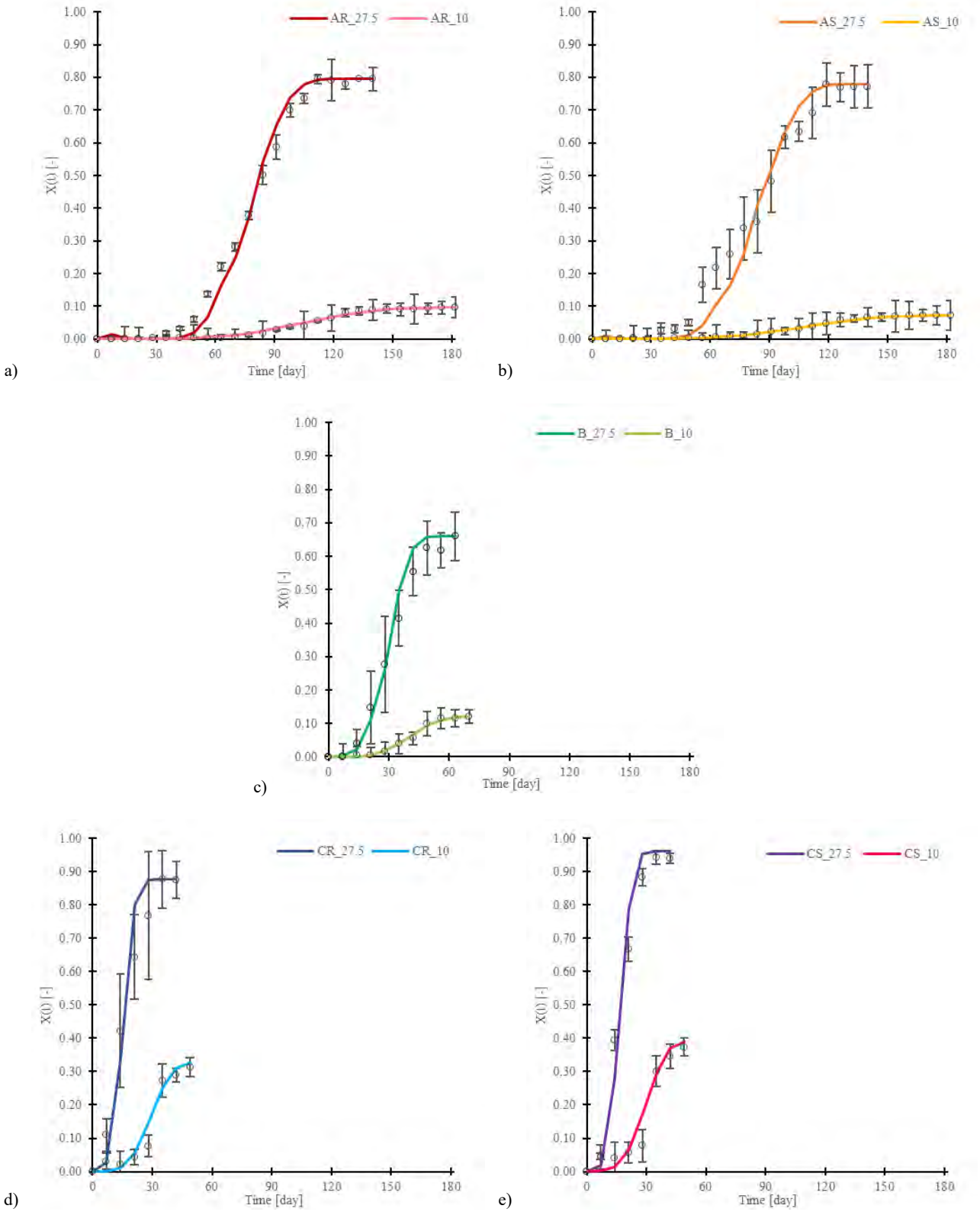

Figure 7.11: Comparison of Avrami's curves (coloured curves) to experimental results (mean values and standard deviation in black) for T=10°C and T=27.5°C . a) samples AR, b) samples AS, c) samples B, d) samples CR and e) samples CS

8 Conclusion and recommendations

This deliverable presents RIBuild findings on threshold values for failure, linked to types of building structures and failure modes. Failures in the construction related to overrun of a limit state are related to those occurring as a result of changed hygrothermal conditions in the structures as a result of introducing internal insulation. The project has identified, investigated (laboratory tests and simulations) and concluded on the following failure modes;

Mould
Threshold values for mould has been derived as part of the project for a large number of products/materials aimed to be used in WP6 for the guidelines. Several mould models have been evaluated and the conclusion is not to overestimate the results from dynamic models since they may underestimate the risk and produce varying results. The PJ-model, however, shows reliable results and will be modified for further use in WP6. Important to emphasise is that the end users of any prediction models should be able to understand how the evaluation is done and how to interpret the results. It is worth noticing that in the performed round-robin study, the models were used and interpreted by researchers with much insight in the questions of mould growth in buildings, yet the input parameter choices and interpretation varies.

Rot
In general, the threshold values for rot are higher than for those for mould growth. Therefore, although the consequences of rot attack are severe, the threshold values for mould growth are more likely to be the limiting factor in the critical positions where mould is not accepted. Examples of rot threshold values are presented related to fungal species. The VTT model of wood decaying fungi was considered most useful in RIBuild context, as it generates mass loss (%) based on hygrothermal conditions (T and RH) and exposure time in critical conditions. However, the model has in more than one case shown to generate too conservative results with regard to mass loss. Nevertheless, it has proven to be valuable for evaluation of performance by relative comparisons.

Frost
Three conditions must be fulfilled for frost damage to occur; the material must be sufficient wet, phase change must happen in the material, and the material must be sensitive to frost. In order to evaluate material sensitivity to frost, an extensive experimental effort is required. Existing frost damage models have been investigated and laboratory experiments on brick frost sensitivity has been performed. Given that none of the currently available hygrothermal indicators for frost damage allow quantifying the frost damage, these have not been explicitly evaluated. In addition, since the further research required advancing these prediction models is far larger than what is possible within the framework of RIBuild, no further research, besides the activities reported in Section 6, has been performed.

Algae
Conducted laboratory studies on algae growth shows that important and limiting material parameters are porosity and roughness in particular. The laboratory studies also show that the developed model on algae prediction is working, although at this stage only for constant hygrothermal conditions.

9 Outlook for future work

9.1 Mould growth

More knowledge on how the dynamic processes of varying RH and temperature affects mould growth is needed to make more precise predictions on mould growth in buildings.

As the PJ-model was shown to make accurate predictions of mould growth, we recommend it to be part of WP6 in the web tool. The model will be further developed, considering measurement uncertainties and recommendations on how to evaluate cases close to the limits, and possibly considering the time at which mould growth is probable to occur.

RH_{crit} for mould growth, tested according to the standardised method, is an effective way to evaluate new, unused products of building materials. However, studies are needed to include the susceptibility of materials already present in buildings (historic materials).

9.2 Rot

Predicting risk of rot or mass loss in beam-ends must be handled in a different way than simply applying the VTT rot model to simulations; either the simulations should be refined, or the model modified for this specific use. The latter is most likely, as the prediction of the model is wrong even when measured values of moisture, temperature and time are used. To modify the model would mean more experiments where rot occurs over time. This is very expensive and time consuming; several monitored constructions must be followed over time, like in the set-up described in Section 7.2.3. This set-up should therefore be followed in many years to come.

9.3 Frost

The study on the failure mode ‘frost’ has demonstrated that none of the currently available frost damage indicators can be considered reliable for the quantification of potential frost damage with respect to massive masonry walls with(out) interior insulation. Future research on this front should focus on the mechanisms for accumulation of frost damage during successive periods of frost conditions and on the relationship between the mechanical properties of the building material and its sensitivity for frost damage.

9.4 Algae

The failure model needs to be improved, in order to confirm the reliability of the model itself and to extend its feasibility to a wider range of building materials’ substrates and environmental conditions. To collect more data, further investigations should be aimed to test:

- different type of building materials (e.g. mortar and plasters, stones etc.)
- different temperatures.

A model which explicitly includes parameters to consider environmental conditions (such as temperature and relative humidity) during the time and the properties of the substrate is needed.

Finally, field studies could be useful to confirm experimental findings and results obtained from accelerated growth tests.

References

Abdul Hamid, A. and P. Wallentén (2017). Hygrothermal assessment of internally added thermal insulation on external brick walls in Swedish multifamily buildings. Building and Environment 123: 351-362.

Adan, O. C. G. (1994). On the fungal defacement of interior finishes PhD-Dissertation, University of Eindhoven.

Al-Omari, A., K. Beck, X. Brunetaud, Á. Török and M. Al-Mukhtar (2015). Critical degree of saturation: A control factor of freeze–thaw damage of porous limestones at Castle of Chambord, France. Engineering Geology 185: 71-80.

Amaro, B., D. Saraiva, J. De Brito and I. Flores-Colen (2013). Inspection and diagnosis system of ETICS on walls. Construction and Building Materials 47: 1257-1267.

ASTM (1986). ASTM Standard C671-86, Standard test method for critical dilation of concrete specimens subjected to freezing. West Conshohocken, PA, American Society for Testing and Materials, International.

ASTM (2007). ASTM Standard C216-07a, Standard Specification for Facing Brick (Solid Masonry Units Made from Clay or Shale). West Conshohocken, PA, American Society for Testing and Materials, International.

ASTM (2008). ASTM Standard C62-05, Standard specification for building brick (solid masonry Units Made From Clay or Shale). West Conshohocken, PA, American Society for Testing and Materials, International.

ASTM (2009). ASTM D5589-09. Standard test method for determining the resistance of paint films and related coatings to algal defacement. American Society for Testing and Materials.

ASTM (2010). ASTM D4404-10. Standard test method for determination of pore volume and pore volume distribution of soil and rock by mercury intrusion porosimetry. American Society for Testing and Materials, American Society for Testing and Materials.

Avrami, M. (1939). Kinetics of phase change. I: General Theory. Journal of Chemical Physics 7: 1103-1112.

Avrami, M. (1940). Kinetics of Phase Change. II Transformation-Time Relations for Random Distribution of Nuclei. The Journal of Chemical Physics 8: 212-224.

Avrami, M. (1941). Granulation, Phase Change, and Microstructure Kinetics of Phase Change. III. The Journal of Chemical Physics 9: 177-184.

Bajare, D. (2000). Restoration of Historical Brick Masonry. In proceedings of the 9th International Congress on Deterioration and Conservation of Stone, Venice

Barberousse, H. (2007). Etude de la diversité des algues et des cyanobactéries colonisant les revêtements de façade en France et recherche des facteurs favorisant leur implantation.

Barberousse, H., R. J. Lombardo, G. Tell and A. Coute (2006). Factors involved in the colonisation of building facades by algae and cyanobacteria in France. Biofouling 22(1-2): 69-77.

Bauklimat-Dresden. (2019). Retrieved 02-15, 2019, from http://www.bauklimatik-dresden.de/delphin/.

Bech-Andersen, J. (1995). Ægte hussvamp og svamp i huse (Translation from Danish: Dry rot and rot in houses).

Becker, R. (2003). Patterned staining of rendered facades: Hygro-thermal analysis as a means for diagnosis. Journal of Thermal Envelope and Building Science 26(4): 321-341.

Bester, K. and X. Lamani (2010). Determination of biocides as well as some biocide metabolites from facade run-off waters by solid phase extraction and high performance liquid chromatographic separation and tandem mass spectrometry detection. Journal of Chromatography A 1217: 5204-5214.

Billi, D. (2010). Genetic tools for desiccation- and radiation-tolerant cyanobacteria of the genus Chroococcidiopsis. Gene: 1517-1521.

Biseniece, E., G. Žogla, A. Kamenders, R. Purviņš, K. Kašs, R. Vanaga and A. Blumberga (2017). Thermal performance of internally insulated historic brick building in cold climate: A long term case study. Energy and Buildings 152: 577-586.

Bjarløv, S., G. Finken and T. Odgaard (2015). Retrofit with Interior Insulation on Solid Masonry Walls in Cool Temperate Climates – An Evaluation of the influence of Interior Insulation Materials on Moisture Condition in the Building Envelope. Energy Procedia 78: 1461-1466.

Blackburn, C. (2000). Modelling shelf-life. The stability and shelf-life of food. D. Kilcast and P. Subramaniam, Woodhead Publishing Limited.

Block, S. S. (1953). Humidity Requirements for Mold Growth. Applied Microbiology 1: 287-293.

Blumberga, A., D. Blumberga, E. Kamendere, A. Kamenders, K. Kristaps Kass, R. Purvins and G. Zogla (2015). RIBuild deliverable D1.1: Report on historical building types and combinations of structural solutions.

Boddy, L. (1983). Effect of temperature and water potential on growth rate of woof-rotting Basidiomycetes. Transactions of the British Mycological Society - Elsevier: 141-149.

Bok, G., P. Johansson and J. Jermer (2012). Mould growth on wood-based materials – a simulated in-service study. IRG – IUFRO Research Sessions International Union of Forest Research Organizations All Division 5 Conference. Estoril, Portugal.

Boverket Swedish National Board of Housing, B. a. P. (2014). Boverket's building regulations-mandatory provisions and general recommendations, BBR. BBR 2014:3.

Brischke, C. and L. Meyer-Veltrup (2015). Modelling timber decay caused by brown rot fungi. Materials and Structures (2016) 49: 3281–3291.

Clausen, C. A., F. Green III and T. L. Highley (1991). Early detection of brown-rot decay in southern yellow pine using immunodiagnostic procedures. Wood Science and Technology: 1-8.

Coletti, C., G. Cultrone, L. Maritan and C. Mazzoli (2016a). Combined multi-analytical approach for study of pore system in bricks: How much porosity is there? Materials Characterization 121: 82-92.

Coletti, C., G. Cultrone, L. Maritan and C. Mazzoli (2016b). How to face the new industrial challenge of compatible, sustainable brick production: Study of various types of commercially available bricks. Applied Clay Science 124-125: 219-226.

Crispim, C. A., P. M. Gaylarde and C. C. Gaylarde (2003). Algal and cyanobacterial biofilms on calcareous historic buildings. Current Microbiology 46: 79-82.

CSA (2006). CSA Standard A82-0, Fired Masonry Brick Made from Clay or Shale. 6. Mississauga, ON, Canadian Standards Association.

Cultrone, G. and F. Madkour (2013). Evaluation of the effectiveness of treatment products in improving the quality of ceramics used in new and historical buildings. Journal of Cultural Heritage 14: 304-310.

Cultrone, G., E. Sebastián, K. Elert, M. J. de la Torre, O. Cazalla and C. Rodriguez–Navarro (2004). Influence of mineralogy and firing temperature on the porosity of bricks. Journal of the European Ceramic Society 24: 547-564.

Curling, S. F., C. A. Clausen and J. E. Winandy (2002). Experimental method to quantify progressive stages of decay of wood by basidiomycete fungi. International Biodeterioration & Biodegradation - Elsevier: 13-19.

D'Orazio, M., G. Cursio, L. Graziani, L. Aquilanti, A. Osimani, F. Clementi, C. Yéprémian, V. Lariccia and S. Amoroso (2014). Effects of water absorption and surface roughness on the bioreceptivity of ETICS compared to clay bricks. Building and Environment 77: 20-28.

de Freitas, R. R., J. C. Molina and C. C. Júnior (2010). Mathematical Model for Timber Decay in Contact with the Ground Adjusted for the State of São Paulo, Brazil. Materials Research. 2010; 13(2): 151-158.

De Kock, T., M. Boone, T. De Schryver, H. Derluyn, J. Van Stappen, D. Van Loo, B. Masschaele and V. Cnudde (2015). Tomography of Materials and Structures. In proceedings of the 2nd International conference, Vancouver

De Mets, T., A. Tilmans and X. Loncour (2017). Hygrothermal assessment of internal insulation systems of brick walls through numerical simulation and full-scale laboratory testing. Energy Procedia 132: 753-758.

De Muynck, W., A. M. Ramirez, N. De Belie and W. Verstraete (2009). Evaluation of strategies to prevent algal fouling on white architectural and cellular concrete. International Biodeterioration & Biodegradation 63(6): 679-689.

Di Giuseppe, E. (2013). Nearly Zero Energy Buildings and proliferation of microorganisms.

Dondi, M., B. Fabbri and I. Venturi (1993). Preliminary Report on the Pore Size Distribution of Italian Heavy-Clay Products. In proceedings of the 3th Euro-ceramics, Madrid

Dubosc, A. (2000). Etude de devellopement de salissures biologiques sur les parements en beton: mise au point d'essais acceleres de viellissement. Laboratoire Matériaux et Durabilité des Constructions.

Dubosc, A., G. Escadeillas and P. J. Blanc (2001). Characterization of biological stains on external concrete walls and influence of concrete as underlying material. Cement and Concrete Research 31: 1613-1617.

Eagen, R., A. Brisson and C. Breuil (1997). The sap-staining fungus Ophiostoma piceae synthesizes different types of melanin in different growth media. Canadian Journal of Microbiology 43(6): 592-595.

EN (2010). 12371 Natural stone test methods - Determination of frost resistance, EN.

Escadeillas, G., A. Bertron, E. Ringot, P. J. Blanc and A. Dubosc (2009a). Accelerated testing of biological stain growth on external concrete walls. Part 1: Quantification of growths. Materials and Structures 42: 937-945.

Escadeillas, G., A. Bertron, E. Ringot, P. J. Blanc and A. Dubosc (2009b). Accelerated testing of biological stain growth on external concrete walls. Part 2: Quantification of growths. Materials and Structures 42: 937-945.

Fagerlund, G. (1972). Critical degrees of saturation at freezing of porous and brittle materials (in Swedish). Lund, Div. of Building Technology, The Lund Institute of Technology.

Fagerlund, G. (1977). The Critical Degree of Saturation Method of Assessing the Freeze-Thaw Resistance of Concrete. Materials and Structures July-Augus Prepared on Behalf of RILEM Committee 4CDC: p217–229.

Flannigan, B. and J. D. Miller (2001). Microbial Growth in Indoor Environments. Mikroorganisms In Home and Indoor Work Environments. Diversity,health impacts, investigation and control. B. Flannigan, R. A. Samson and J. D. Miller. New York, CRC Press LLC: 35-67.

Fleet, C., C. Breuil and A. Uzunovic (2001). Nutrient Consumption and Pigmentation of Deep and Surface Colonizing Sapstaining Fungi in Pinus contorta. Holzforschung 55(4): 371-378.

Flores-Colen, I., J. de Brito and V. P. de Freitas (2008). Stains in facades' rendering – Diagnosis and maintenance techniques' classification. Construction and Building Materials 22(3): 211-221.

Fog Nielsen, K., P. A. Nielsen and G. Holm (2000). Growth of Moulds on Building Materials under Different Humidities. Proceedings of Healthy Buildings 2000, Espoo. Finland.

Fonseca, A. J., F. Pina, M. F. Macedo, N. Leal, A. Romanowska-Deskins, L. Laiz, A. Gómez-Bolea and C. Saiz-Jimenez (2010). Anatase as an alternative application for preventing biodeterioration of mortars: Evaluation and comparison with other biocides. International Biodeterioration and Biodegradation 64: 388-396.

Franzoni, E., A. Fregni, R. Gabrielli, G. Graziani and E. Sassoni (2014). Compatibility of photocatalytic TiO2-based finishing for renders in architectural restoration: A preliminary study. Building and Environment 80: 125-135.

Freudenberg, P., U. Ruisinger, E. Stöcker, S. Roels, N. F. Jensen, T. Odgaard and P. Otiv (2018). RIBuild deliverable D.3.1: Closed Technology Loop of Laboratory Experiments and Simulation Models in the Field of Internal Insulation Testing. Available at www.ribuild.eu.

Fuhr, M. J., M. Schubert, F. W. M. R. Schwarze and H. J. Herrmann (2011). Modelling the hyphal growth of the wood-decay fungus Physisporinus vitreus. Fungal Biology 115, Elsevier: 919-932.

Fuktcentrum. (2019). Retrieved 03-13, 2019, from http://www.fuktcentrum.lth.se/verktyg-och-hjaelpmedel/windows-baserade-datorprogram/m-modellen/.

Gadd, G. M. (1980). Melanin production and differentiation in batch cultures of the polymorphic fungus Aureobasidium pullulans. FEMS Microbiology Letters 9(3): 237-240.

Gawin, D., F. Pesavento and M. Koniorczyk (2016). Numerical modelling of coupled hygrothermal phenomena and frost-induced strains of moist building materials. In proceedings of CESBP2016, Dresden

Gaylarde, C., M. Ribas Silva and T. Warscheid (2003). Microbial impact on building materials: an overview. Materials and Structures 36: 342-352.

Gaylarde, C. C. and P. M. Gaylarde (2005). A comparative study of the major microbial biomass of biofilms on exteriors of buildings in Europe and Latin America. International Biodeterioration and Biodegradation 55: 131-139.

Giovannacci, D., C. Leclaire, M. Horgnies, M. Ellmer, J. D. Mertz, G. Orial, J. Chen and F. Bousta (2013). Algal colonization kinetics on roofing and façade tiles: Influence of physical parameters. Construction and Building Materials 48: 670-676.

Giuliani, C. F. (1993). L'edilizia nell'antichità.

Giuseppe, R. (1990). Istituzioni di restauro dei beni architettonici e ambientali.

Gradeci, K., N. Labonnote, B. Time and J. Köhler (2016). A proposed probabilistic-based design methodology for predicting mould occurrence in timber façades. WCTE 2016 - World Conference on Timber Engineering.

Gradeci, K., N. Labonnote, B. Time and J. Köhler (2018). A probabilistic-based methodology for predicting mould growth in façade constructions. Building and Environment 128: 33-45.

Graziani, L. and E. Quagliarini (2018). On the Modelling of Algal Biofouling Growth on Nano-TiO2 Coated and Uncoated Limestones and Sandstones. Coatings 8: 54.

Graziani, L., E. Quagliarini, F. Bondioli and M. D'Orazio (2014a). Durability of self-cleaning TiO2 coatings on fired clay brick façades: Effects of UV exposure and wet & dry cycles. Building and Environment 71(0): 193-203.

Graziani, L., E. Quagliarini and M. D'Orazio (2016a). The role of roughness and porosity on the self-cleaning and anti-biofouling efficiency of TiO2-Cu and TiO2-Ag nanocoatings applied on fired bricks. Construction and Building Materials 129: 116-124.

Graziani, L., E. Quagliarini and M. D'Orazio (2016b). TiO2-treated different fired brick surfaces for biofouling prevention: Experimental and modelling results. Ceramics International 42: 4002-4010.

Graziani, L., E. Quagliarini, A. Osimani, L. Aquilanti, F. Clementi and M. D'Orazio (2014b). The influence of clay brick substratum on the inhibitory efficiency of TiO2 nanocoating against biofouling. Building and Environment 82: 128-134.

Graziani, L., E. Quagliarini, A. Osimani, L. Aquilanti, F. Clementi, C. Yéprémian, V. Lariccia, S. Amoroso and M. D'Orazio (2013). Evaluation of inhibitory effect of TiO2 nanocoatings against microalgal growth on clay brick façades under weak UV exposure conditions. Building and Environment 64: 38-45.

Grolemund, G. and H. Wickham (2011). Dates and Times Made Easy with lubridate. Journal of Statistical Software 40(3): 1-25.

Guillitte, O. (1995). Bioreceptivity: a new concept for building ecology studies. Science of the Total Environment 167: 215-220.

Guillitte, O. and R. Dreesen (1995). Laboratory chamber studies and petrographical analysis as bioreceptivity assessment tools of building materials. Science of the Total Environment 167: 365-374.

Gwo, J. C., J. Y. Chiu, C. C. Chou and H. Y. Cheng (2005). Cryopreservation of a marine microalga, Nannochloropsis oculata (Eustigmatophyceae). Cryobiology 50: 338-343.

Harrestrup, M. and S. Svendsen (2015). Full-scale test of an old heritage multi-storey building undergoing energy retrofitting with focus on internal insulation and moisture. Building and Environment 85: 123-133.

Hay, J. N. (1971). Application of the modified avrami equations to polymer crystallisation kinetics. British Polymer Journal 3: 74-82.

Hens, H. (2014). Applied building physics: boundary conditions, performance and material properties. Leuven, Acco.

Hofbauer, W., K. Breuer and K. Sedlbauer (2003). Algen, Flechten, Moose und Farne auf Fassaden. Aufsatz 25: 383-396.

Hofbauer, W., N. Kreuger, K. Breuer, K. Sedlbauer and T. Schoch (2008). Mould resistance assessment of building materials – Material specific isopleth-systems for practical application. Indoor Air 2008, Copenhagen, Denmark.

Hoffmann, L. (1989). Algae of terrestrial habitats. The Botanical Review 55: 77-105.

Holm, A., W. Zillig and H. M. Künzel (2004). Exterior Surface Temperature and Humidity of Walls - Comparison of Experiment and Numerical Simulation. Proceedings of Performance of Exterior Envelopes of Whole Buildings IX. ASHRAE. Clearwater.

Hukka, A. and H. A. Viitanen (1999). A mathematical model of mould growth on wooden material. Wood Science and Technology 33: 475-485.

Hyvärinen, A., T. Meklin, A. Vepsäläinen and A. Nevalainen (2002). Fungi and actinobacteria in moisture-damaged building materials - concentrations and diversity. International Biodeterioration & Biodegradation(49): 27-37.

Imre Friedmann, E. and R. Ocampo-Friedmann (1995). A primitive cyanobacterium as pioneer microorganism for terraforming Mars. Advances in Space Research. 15: 243-246.

Isaksson, T., C. Brischke and S. Thelandersson (2012). Development of decay performance models for outdoor timber structures. Materials and Structures - RILEM: 1209–1225.

Isaksson, T., S. Thelandersson, A. Ekstrand-Tobin and P. Johansson (2010). Critical conditions for onset of mould growth under varying climate conditions. Building and Environment 45(7): 1712-1721.

Jena, A. K. and M. C. Chaturvedi (1992). Phase transformation in materials.

Johansson, P. (2012). Critical moisture conditions for mould growth on building materials, Lund University.

Johansson, P. (2014). Determination of the Critical Moisture Level for Mould Growth on Building Materials, Byggnadsfysik,LTH, Lunds Tekniska Högskola.

Johansson, P., G. Bok and A. Ekstrand-Tobin (2013). The effect of cyclic moisture and temperature on mould growth onwood compared to steady state conditions. Building and Environment 65: 178-184.

Johansson, P. and C.-M. Capener (2015). Discolouration of building facades. A knowledge surve, SP Technical Research Institute of Sweden.

Johansson, P., A. Ekstrand-Tobin and G. Bok (2014). An innovative test method for evaluating the critical moisture level for mould growth on building materials. Building and Environment 81: 404-409.

Johansson, P., A. Ekstrand-Tobin, T. Svensson and G. Bok (2012). Laboratory study to determine the critical moisture level for mould growth on building materials. International Biodeterioration and Biodegradation 73: 23-32.

Johansson, P., K. Mjörnell and J. Arfvidsson (2017). Examples of characteristics of wood that affect mould growth: a meta-analysis. European Journal of Wood and Wood Products 75(4): 603-613.

Johansson, P., T. Svensson and A. Ekstrand-Tobin (2013). Validation of critical moisture conditions for mould growth on building materials. Building and Environment 62(0): 201-209.

Johansson, P., L. Wadsö, S. Johansson, T. Svensson and B. BEngtsson (2018). Development and validation of a model to predict mould growth, RISE Research Institutes of Sweden AB.

Johansson, S. (2005a). Biological growth on mineral façades. Licentiate thesis, Lund University.

Johansson, S. (2005b). Biological growth on mineral façades. Lund University. Master Thesis.

Johansson, S. (2011). Biological growth on rendered facades. Lunds Universitet, Lunds Tekniska Högskola, Institutionen för bygg och miljöteknologi.

Johnson, W. A. and R. F. Mehl (1939). Reaction kinetics in processes of nucleation and growth. Transaction of the AIME 135: 416.

Kastien, H. K. (1999). Algen und Pilze an mineralischen Fassaden. 10-11: 57-62.

Khawam, A. and D. R. Flanagan (2006). Solid-state kinetic models: Basics and mathematical fundamentals. Journal of Physical Chemistry B 110: 17315-17328.

Koch, A. P. (2014). Trækonstruktioner – udbedring efter svampe- og insektangreb (Translation from Danish: Wooden constructions – remediation after fungus and insect attacs, BYG-Erfa (99) 14 12 13, Copenhagen.

Kočí, J., J. Maděra, M. Keppert and R. Černý (2017). Damage functions for the cold regions and their applications in hygrothermal simulations of different types of building structures. Cold Regions Science and Technology 135: 1-7.

Konopka, A. and T. D. Brock (1978). Effect of temperature on blue-green algae (Cyanobacteria) in Lake Mendota. Applied and Environmental Microbiology 36: 572-576.

Koroth, S. R., P. Fazio and D. Feldman (1998). Comparative study of durability indices for clay bricks. Journal of Architectural Engineering Volume 4(1) p26–33.

Krus, M., C. Fitz and K. Sedlbauer (2013). Reducing the Risk of Microbial Growth on Insulated Walls by Improving the Properties of the Surface Materials. Hygrothermal Behavior, Building Pathology and Durability. V. P. de Freitas and J. M. P. Q. Delgado, Springer Berlin Heidelberg. 1: 1-21.

Kumar, R. and A. V. Kumar (1999). Biodeterioration of Stone in Tropical Environments. Research in Conservation 20: 85.

Künzel, H. M. (1998). Effect of interior and exterior insulation on the hygrothermal behaviour of exposed walls. Materials and Structures 31: 99-103.

Künzel, H. M. (2007). Factors determining surface moisture on external walls. Buildings X: 6.

La Russa, M. F., S. A. Ruffolo, N. Rovella, C. M. Belfiore, A. M. Palermo, M. T. Guzzi and G. M. Crisci (2012). Multifunctional TiO 2 coatings for Cultural Heritage. Progress in Organic Coatings 74: 186-191.

Lengsfeld, K. and M. Krus (2001). Microorganism on façades – reasons, consequences and measures. 0-7.

Li, W., M. Pour-Ghaz, J. Castro and J. Weiss (2012). Water Absorption and Critical Degree of Saturation Relating to Freeze-Thaw Damage in Concrete Pavement Joints. Journal of Materials in Civil Engineering 24(3): 299-307.

Litvan, G. G. (1973). Pore structure and frost susceptibility of building materials. In proceedings of the international symposium on pore structure and properties of materials, Prague

Lopez-Arce, P. and J. Garcia-Guinea (2005). Weathering traces in ancient bricks from historic buildings. Building and Environment 40: 929-941.

Low, G. A., J. W. Palfreyman, N. A. White and D. C. R. Sinclair (1999). Development of Model Systems for Investigations of the Dry Rot Fungus Serpula lacrymans (Schumach. ex Fr.) Gray: Use for Analysis of the Environmental Sensitivity of the Organism. Holzforschung / Vol. 53 / No. 2: 129-136.

Lupan, I. and O. Popescu (2012). Metagenomics and future perspectives for biodeterioration and biodegradation studies. Annals of the Romanian Society for Cell Biology 17: 37-42.

Løland, K. E. (1980). Continuous damage model for load-response estimation of concrete. Cement and Concrete Research 10(3): 395-402.

M.Fanzoni and M.Tomellini (1998). The Johnson-Mehl-Avrami-Kolmogorov model: A brief review. Il Nuovo Cimento D 20: 1171-1182.

Maage, M. (1984). Frost Resistance and Pore Size Distribution in Bricks. Materials and Structures July-Augus Volume 17(101) p345–350.

Mai, C., H. Militz and U. Kües (2004). Biotechnology in the wood industry. Applied Microbiology and Biotechnology 63(5): 477-494.

Mamillan, M. (1984). Durabilité des pierres tendres. Rapport 102. C. E. d. R. e. d. E. d. B. e. d. T. Publics: p69.

Martinez, T., A. Bertron, G. Escadeillas and E. Ringot (2014). Algal growth inhibition on cement mortar: Efficiency of water repellent and photocatalytic treatments under UV/VIS illumination. International Biodeterioration and Biodegradation 89: 1150-1125.

Maurice, S., L. Coroller, S. Debaets, V. Vasseur, G. Le Floch and G. Barbier (2011). Modelling the effect of temperature, water activity and pH on the growth of Serpula lacrymans. Journal of Applied Microbiology 111: 1436–1446.

Maury-Ramirez, A., W. De Muynck, R. Stevens, K. Demeestere and N. De Belie (2013). Titanium dioxide based strategies to prevent algal fouling on cementitious materials. Cement and Concrete Composites 36: 93-100.

Mensinga, P., Straube J. & Schumacher C (2010). Assessing the Freeze-Thaw Resistance of Clay Brick for Interior Insulation Retrofit Projects. In proceedings of the Performances of Envelopes of Whole Buildings XI

Miller, A. Z., A. Dionísio, L. Laiz, M. F. MacEdo and C. Saiz-Jimenez (2009). The influence of inherent properties of building limestones on their bioreceptivity to phototrophic microorganisms. Annals of Microbiology 59: 705-713.

Miller, A. Z., P. Sanmartín, L. Pereira-Pardo, A. Dionísio, C. Saiz-Jimenez, M. F. Macedo and B. Prieto (2012). Bioreceptivity of building stones: A review. Science of the Total Environment 426: 1-12.

Moon, H. J. and G. L. M. Augenbroe (2004). Towards a practical mould growth risk indicator. Building Services Engineering Research and Technology 25(4): 317-326.

Morelli, M., T. R. Nielsen, G. A. Scheffler and S. Svendsen (2010). Internal Insulation of Masonry Walls with Wooden Floor Beams in Northern Humid Climate. Thermal Performance of the Exterior Envelopes of Whole Buildings XI International Conference.

Morelli, M. and S. Svendsen (2013). Investigation of interior post-insulated masonry walls with wooden beam ends. Journal of Building Physics 36: 265-273.

Morris, P. I. and J. E. Winandy (2002). Limiting Conditions for Decay in Wood Systems. The international research group on wood preservation, Cardiff, South Wales, UK, IRG/WP.

MRD. (2016). Moisture Resistance Design (MRD) model. Retrieved 02-15, 2019, from https://wufi.de/en/2016/04/19/moisture-resistance-design-mrd-model.

Munck, O., A. P. Koch and H. J. Larsen (2003). Trænedbrydende svampe - forekomst i bygninger. BYG-ERFA Copenhagen, Denmark, ERFA Erfaringsblad (29) 03 12 19.

NBN (1983). NBN B27-010 Ceramic products for wall and floor coverings, Frost resistance, Capacity for water absorption by capillarity. Brussels.

NBN (1986). NBN B-23-002/A2 Facade Brick. Brussels.

Netinger, I., M. Vracevic, J. Ranogajec and S. Vucetic (2014). Evaluation of brick resistance to freeze / thaw cycles according to indirect procedures.

Nevander, L. E. and B. Elmarsson (1994). Fukthandbok - Praktik och teori. Stockholm, AB Svensk Byggtjänst.

Nicolai, A. and L. Sontag (2013). Implementation of an efficient numerical solution method to simulate freezing processes in porous media. In proceedings of the 2nd Central European Symposium on Building Physics Vienna, Austria.

Odgaard, T., S. P. Bjarløv and C. Rode (2018). Interior insulation – Experimental investigation of hygrothermal conditions and damage evaluation of solid masonry façades in a listed building. Building and Environment 129: 1-14.

Ojanen, T., R. Peuhkuri and H. Viitanen (2011). Classification of material sensitivity - New approach for mould growth modeling. . 9th Nordic Symposium on Building Physics. Tampere, Finland: 867-874.

Ojanen, T., H. Viitanen, R. Peuhkuri, K. Lähdesmäki, J. Vinha and K. Salminen (2010). Mould growth modelling of building structures useing sensitivity classes of materials. Termal Performance of Exterior Envelopes of Whole Buildings XI. Clearwater Beach, Florida, USA.

Ortega-Calvo, J. J., X. Ariño, M. Hernandez-Marine and C. Saiz-Jimenez (1995). Factors affecting the weathering and colonization of monuments by phototrophic microorganisms. Science of the Total Environment 167: 329-341.

P. Ingham, J. (2005). Predicting the frost resistance of building stone.

Pattanaik, B. and S. P. Adhikary (2002). Blue-green algal flora at some archaeological sites and monuments of India. Feddes Repertorium 113: 289-300.

Perry, J. H., ed. (1942). Chemical Engineers' Handbook. Second edition (Perry, John H., ed.). Journal of Chemical Education 19: 449.

Pietarinen, V. M., H. Rintala, A. Hyvarinen, U. Lignell, P. Kärkkäinen and A. Nevalainen (2008). Quantitative PCR analysis of fungi and bacteria in building materials and comparison to culture-baded analysis. Journal of Environmental Monitoring 10: 655-663.

Prick, A. (1997). Critical degree of saturation as a threshold moisture level in frost weathering of limestones. Permafrost and Periglacial Processes volume 8: p91–99.

Quagliarini, E., L. Graziani, D. Diso, A. Licciulli and M. D'Orazio (2018). Is nano-TiO2 alone an effective strategy for the maintenance of stones in Cultural Heritage? Journal of Cultural Heritage 30: 81-91.

R Core Team (2018). R: A language and environment for statistical computing. Vienna, Austria, R Foundation for Statistical Computing.

Radulovic, J., J. MacMullen, Z. Zhang, H. N. Dhakal, S. Hannant, L. Daniels, J. Elford, C. Herodotou, M. Totomis and N. Bennett (2013). Biofouling resistance and practical constraints of titanium dioxide nanoparticulate silane/siloxane exterior facade treatments. Building and Environment 68: 150-158.

Rapp, A. O., R.-D. Peek and M. Sailer (2000). Modelling the Moisture Induced Risk of Decay for Treated and Untreated Wood Above Ground. Holzforschung 54 (2000) - International Journal of the Biology, Chemistry, Physics, and Technology of Wood: 111–118.

Raven, J. A. and R. J. Geider (1988). Temperature and algal growth. New Phytologist 110: 441-461.

Ritschkoff, A.-C., H. A. Viitanen and K. Koskela (2000). The Response of Building Materials to the Mould Exposure at Different Humidity and Temperature Conditions. Healthy Buildings 2000, Espoo, Finland.

Ruot, B. and H. Barberousse (2007). Quantification and kinetic modelling of the colonisation of façades rendering mortars by algae.

Råberg, U., C. Brischke, A. O. Rapp, N. O. S. Högberg and C. J. Land (2007). External and internal fungal flora of pine sapwood (Pinus sylvestris L.) specimens in above-ground field tests at six different sites in south-west Germany. Holzforschung, Vol. 61, no 1: 104-111.

Saïd, M. and P. R. Demers LL McSheffrey (2003). Hygrothermal performance of a masonry wall retrofitted with interior insulation. Research in Building Physics: 445-454.

Saito, H., K. Fukuda and T. Sawachi (2012). Integration model of hygrothermal analysis with decay process for durability assessment of building envelopes. Building Simulation / Vol. 5, No. 4: 315–324.

Saiz-Jimenez, C. (1994). Biodeterioration of stone in historic buildings and monuments. Biodeterioration Research 4: 587-604.

Saiz-Jimenez, C. (1997). Biodeterioration vs biodegradation: The role of microorganisms in the removal of pollutants deposited on historic buildings. International Biodeterioration and Biodegradation 40: 225-232.

Schneider, C. A., W. S. Rasband and K. W. Eliceiri (2012). NIH Image to ImageJ: 25 years of image analysis. Nature Methods 9: 671-675.

Sedlbauer, K. (2001a). Prediction of mould fungus formation on the surface of and inside building components, Fraunhofer Institute for Building Physics.

Sedlbauer, K. (2001b). Prediction of Mould Growth by Hygrothermal Calculation. Journal of Thermal Env & Bldg Sci 25(4): 321-336.

Sedlbauer, K. (2002). Prediction of Mould Growth by Hygrothermal Calculation. Journal of Building Physics 25(4): 321-336.

Sedlbauer, K. and H. Kunzel (2000). Frost damage of masonry walls - A hygrothermal analysis by computer simulations. Thermal Envelope & Building Science 23: pp 277-281.

Serra-Maia, R., O. Bernard, A. Gonçalves, S. Bensalem and F. Lopes (2016). Influence of temperature on Chlorella vulgaris growth and mortality rates in a photobioreactor. Algal Research 18: 352-359.

Shukla, S. P., J. Kvíderová, J. Tříska and J. Elster (2013). Chlorella mirabilis as a potential species for biomass production in low-temperature environment. Frontiers in Microbiology 4: 1-12.

Singh, J. (1999). Dry Rot and Other Wood-Destroying Fungi: Their Occurrence, Biology, Pathology and Control. Indoor Build Environ 1999;8: 3-20.

Singh, S. P. and P. Singh (2015). Effect of temperature and light on the growth of algae species: A review. Renewable and Sustainable Energy Reviews 50: 431-444.

SIS (2014). Building materials – Laboratory method for assessment of the lowest hygrothermal conditions required for mould growth. S. S. S. Institute. SIS-TS 41:2014.

Slovácek, M. (2004). Application of numerical simulation of heat treatment in industry. Journal de Physique IV France 120: 753-760.

Sontag, L., A. Nicolai and J. Grunewald (2014). Influence of ice formation on thermal conductivity and liquid water conductivity in hygrothermal transport models. Nordic Building Physics Symposium, Lund, Sweden.

Standard, E. (2003). EN 771-1 Specification for masonry. Part 1: masonry brick. Brussels.

Steskens, P., X. Loncour, S. Roels and E. Vereecken (2013). Interior Insulation of masonry walls – An assessment method. Internationaler Innendämmkongress. Vienna: 62-69.

Straube, J. and C. Schumacher (2007). Interior Insulation Retrofits of Load-Bearing Masonry Walls in Cold Climates. Journal of Green Building 2: 42-50.

Straube, J. F., K. Ueno and C. J. Schumacher (2012). Measure Guideline: Internal Insulation of Masonry Walls. Building Science.com. Golden. RR-1105: 1-99.

Sun, Z. and G. W. Scherer (2010). Effect of air voids on salt scaling and internal freezing. Cement and concrete restoration 40: p260–270.

Tanaca, H. K., C. M. R. Dias, C. C. Gaylarde, V. M. John and M. A. Shirakawa (2011). Discoloration and fungal growth on three fiber cement formulations exposed in urban, rural and coastal zones. Building and Environment 46(2): 324-330.

Thelandersson, S. and T. Isaksson (2013). Mould resistance design (MRD) model for evaluation of risk for microbial growth under varying climate conditions. Building and Environment 65(0): 18-25.

Tiago, F. and R. Wayne (2011). The ImageJ User Guide.

Tiano, P. (2001). Biodegradation of Cultural Heritage: Decay Mechanisms and Control Methods. CNR-Centro di Studio Sulle Cause Deperimento e Metodi Conservazione Opere d'Arte 9: 1-37.

Togerö, Å., C. Svensson Tengberg and B. Bengtsson (2011). m-model: a method to assess the risk for mould growth in wood structures with fluctuating hygrothermal conditions. Healthy Buildings. Espoo, Finland. 1: 317-322.

Tomaselli, L., G. Lamenti, M. Bosco and P. Tiano (2000). Biodiversity of photosynthetic micro-organisms dwelling on stone monuments. International Biodeterioration and Biodegradation 46: 251-258.

Traeportal, D. (2019). Nedbrydning af trae. Retrieved 02-15, 2019, from http://www.trae.dk/leksikon/nedbrydning-af-trae.

Tran, T. H., A. Govin, R. Guyonnet, P. Grosseau, C. Lors, D. Damidot, O. Deves and B. Ruot (2014). Influence of the intrinsic characteristics of mortars on their biofouling by pigmented organisms: Comparison between laboratory and field-scale experiments. International Biodeterioration and Biodegradation 86: 334-342.

Tran, T. H., A. Govin, R. Guyonnet, P. Grosseau, C. Lors, D. Damidot, O. Devès and B. Ruot (2013). Avrami's law based kinetic modeling of colonization of mortar surface by alga Klebsormidium flaccidum. International Biodeterioration and Biodegradation 79: 73-80.

Tran, T. H., A. Govin, R. Guyonnet, P. Grosseau, C. Lors, E. Garcia-Diaz, D. Damidot, O. Devès and B. Ruot (2012). Influence of the intrinsic characteristics of mortars on biofouling by Klebsormidium flaccidum. International Biodeterioration & Biodegradation 70: 31-39.

UNI (1984). 8635-12 Edilizia. Prove di prodotti per coperture discontinue. Determinazione della gelività con porosimetro, UNI

UNI (2009). UNI EN ISO 4287:2009. Geometrical Product Specifications (GPS) – Surface texture: Profile Method – Terms, Definitions and Surface Texture Parameters, International Standards Organization.

UNI (2010). UNI EN 15886:2010. Conservation of cultural property - Test methods - Colour measurement of surfaces.

UNI (2013). UNI EN ISO 12571:2013. Hygrothermal performance of building materials and products - Determination of hygroscopic sorption properties.

UNI (2018). UNI 11721:2018. Materiali lapidei - Metodi di prova – Misurazione preventiva della variazione colorimetrica di superfici di pietra.

Uranjek, M. and V. Bokan-Bosiljkov (2015). Influence of freeze–thaw cycles on mechanical properties of historical brick masonry. Construction and Building Materials 84: 416-428.

Van Aarle, M., H. Schellen and J. van Schijndel (2015). Hygrothermal simulation to predict the risk of frost damage in masonry, Effects of Climate Change. Energy Procedia Volume78: p2536-2541.

van de Kuilen, J.-W. G. (2006). Service life modelling of timber structures. Materials and Structures - RILEM: 151–161.

Van Straaten, R. (2014). Improving Access to the frost dilatometry methodology for assessing brick masonry freeze thaw degradation risk. In proceedings of 14th Canadian conference on building science and technology, Toronto.

Venzmer, H., J. Von Werder, N. Lesnych and L. Koss (2008). Algal defacement of facade materials - results of a long term natural weathering tests obtained by new diagnostic tools. Proceedings of 8th Symposium on Building Physics in the Nordic Countries 1: 277-284.

Vereecken, E. and S. Roels (2012). Review of mould prediction models and their influence on mould risk evaluation. Building and Environment 51(0): 296-310.

Vereecken, E. and S. Roels (2014). A comparison of the hygric performance of interior insulation systems: A hot box-cold box experiment. Energy and Buildings 80: 37-44.

Vereecken, E. and S. Roels (2015). Capillary active interior insulation: do the advantages really offset potential disadvantages? Materials and Structures/Materiaux et Constructions 48: 3009-3021.

Vereecken, E., L. Van Gelder, H. Janssen and S. Roels (2015). Interior insulation for wall retrofitting – A probabilistic analysis of energy savings and hygrothermal risks. Energy Buildings Volume 89 p231–244.

Verhoef, L. G. V. (1988). Soiling and cleaning of building facades. London: Chapman and Hall.

Wessman, L. (1997). Studies on the frost resistance of natural stone Studies on the frost resistance of natural stone, Lund University, Sweden.

Viani, A., G. Cultrone, K. Sotiriadis, R. Ševčík and P. Šašek (2018). The use of mineralogical indicators for the assessment of firing temperature in fired-clay bodies. Applied Clay Science 163: 108-118.

Wickham, H. (2009). ggplot2: Elegant Graphics for Data Analysis, Springer-Verlag New York.

Wickham, H., R. Francois., L. Henry and K. Müller (2017). dplyr: A Grammar of Data Manipulation.

Viitanen, H. (1997a). Modelling the time factor in the developement of mould fungi - the effect of critical humidity and temperature conditions on pine and spruce sapwood. Holzforchung 51: 6-14.

Viitanen, H. and J. Bjurman (1995). Mould growth on wood under fluctuating humidity conditions. Material und Organismen 29(1): 27-46.

Viitanen, H., M. Krus, T. Ojanen, V. Eitner and D. Zirkelbach (2015). Mold Risk Classification Based on Comparative Evaluation of Two Established Growth Models. Energy Procedia 78: 1425-1430.

Viitanen, H., T. T., L. Makkonen, R. Peuhkuri, T. Ojanen, L. Ruokolainen and J. Räisänen (2010). Towards modelling of decay risk of wooden materials. Eur. J. Wood Prod. (2010) 68: 303–313.

Viitanen, H. A. (1997b). Modelling the Time Factor in the Development of Brown Rot Decay in Pine and Spruce Sapwood - The Effect of Critical Humidity and Temperature Conditions. Holzforschung 51 (1997): 99-106.

WUFI (2005). WUFI-Bio, Available from http://www.hoki.ibp.fhg.de/wufi/downloads_e.html.

WUFI. (2019). WUFIBio. Retrieved 02-15, 2019, from https://wufi.de/en/2017/03/31/wufi-bio/.

Zhou, X., D. Derome and J. Carmeliet (2017). Hygrothermal simulation and evaluation of frost risk of masonry walls subjected to inside insulation retrofitting. In Proceedings of the XIV DBMC conference, Ghent.

Zhou, X., J. Zhou, W. Kinzelbach and F. Stauffer (2014). Simultaneous measurement of unfrozen water content and ice content in frozen soil using gamma ray attenuation and TDR. Water Resources Research Volume 50: p9630–9655.

Zillig, W., K. Lenz, K. Sedlbauer and M. Krus (2003). Condensation on façades - influences of construction type and orientation. Research in Building Physics: 437-444.

Appendix 1. References for algae, cyanobacterial and mould growth

In this Appendix, a number of references to research articles are categorized according to a number of parameters that may affect the growth of facades. (leftmost column). The references have also been categorized by type of growth (the two middle columns). A third category of articles (the far right to the right) are those that do not describe original research but are summaries of different studies. Note that the table is divided into two pages. The table is taken from (Johansson and Capener 2015).

Table A1.1: Categorization of papers concerning discolouring growth (caused by algae, cyanobacteria and mould fungi). The references for each number are given in Table A1.2

Area of research	Algae/cyanobacteria	Mould fungi	State of the art
Identification of growth on facades or material samples exposed outdoors	1, 4, 6, 20, 27, 29		
Nearby vegetation	1		
Building physics factors	4, 19, 22	4, 19, 22	23
Insulation	19, 22	19, 22	23
Heat storage	22, 19	22, 19	23
Rain and wind driven rain	26	26	5, 23
Building moisture	4	4	
Properties of surface materials	2, 3, 7, 8, 18, 21, 24, 29, 32	13, 14, 19, 21, 29, 32	
Surface structure	3, 7, 24	14, 17	
Water repellence	8, 2		
Absorption	7		
Porosity	3, 7, 24		
Colour	19, 21	19, 21	
Biocides/fungicides	8, 29, 32, 18	13, 29, 32	
Other additives		14	
Orientation of façade	1, 19, 22	19, 22	
Contamination, air pollutants		14	
Geographic location	1, 31-33	27, 32, 33	

Table A1.1 (ctd.)

Area of research	Algae/cyanobacteria	Mould fungi	State of the art
Field or laboratory tests of product groups	6, 7, 8, 21, 22, 29, 30	4, 6, 13, 14, 15, 21, 22, 29, 32, 34, 35	
Plaster	7	4	
Paint	6, 21, 22, 29, 31, 32	6, 13, 15, 21, 22, 29, 32, 34, 35	
Concrete	8, 24	14	
Bricks or stones	7		16
Fibre concrete	33	33	
Cleaning of facades	20, 29, 30	20, 29, 30	11, 16, 28, 36
Multivariate analysis of several parameters	1	15	
Assessment of discoloured facades	9-12, 25		

Table A1.2: References to Table A1.1

1. Barberousse, H., et al., *Factors involved in the colonisation of building facades by algae and cyanobacteria in France.* Biofouling, 2006. 22(1-2): p. 69-77.
2. Barberousse, H., et al., *Capsular polysaccharides secreted by building facade colonisers: characterisation and adsorption to surfaces.* Biofouling, 2006. 22(5-6): p. 361-70.
3. Barberousse, H., et al., *An assessment of façade coatings against colonisation by aerial algae and cyanobacteria.* Building and Environment, 2007. 42(7): p. 2555-2561.
4. Becker, R., *Patterned staining of rendered facades: Hygro-thermal analysis as a means for diagnosis.* Journal of Thermal Envelope and Building Science, 2003. 26(4): p. 321-341.
5. Blocken, B., D. Derome and J. Carmeliet, *Rainwater runoff from building facades: A review.* Building and Environment, 2013. 60: p. 339-361.
6. Colon, I., E.L. Kuusisto and K. Hansen, *Location affects performance of biocide-containing paints.* Paint and Coatings Industry, 2004. 20(11): p. 68-73.
7. D'Orazio, M., et al., *Effects of water absorption and surface roughness on the bioreceptivity of ETICS compared to clay bricks.* Building and Environment, 2014. 77: p. 20-28.
8. De Muynck, W., et al., *Evaluation of strategies to prevent algal fouling on white architectural and cellular concrete.* International Biodeterioration & Biodegradation, 2009. 63(6): p. 679-689.
9. de Oliveira, B.P., et al., *An integrated approach to assess the origins of black films on a granite monument.* Environmental Earth Sciences, 2011. 63(7): p. 1677-1690.
10. Flores-Colen, I. and J. de Brito, *A systematic approach for maintenance budgeting of buildings façades based on predictive and preventive strategies.* Construction and Building Materials, 2010. 24(9): p. 1718-1729.
11. Flores-Colen, I., J. de Brito and V.P. de Freitas, *Stains in facades' rendering – Diagnosis and maintenance techniques' classification.* Construction and Building Materials, 2008. 22(3): p. 211-221.
12. Gaspar, P.L. and J.de Brito, *Quantifying environmental effects on cement-rendered facades: A comparison between different degradation indicators.* Building and Environment, 2008. 43(11): p. 1818-1828.
13. Gaylarde, P.M., et al., *Statistical analysis of fungicide activity in paint films on two buildings.* Surface Coatings International Part B: Coatings Transactions, 2004. 87(4): p. 261-264.
14. Giannantonio, D.J., et al., *Effects of concrete properties and nutrients on fungal colonization and fouling.* International Biodeterioration & Biodegradation, 2009. 63(3): p. 252-259.
15. Gobakken, L.R. and P.K. Lebow, *Modelling mould growth on coated modified and unmodified wood substrates exposed outdoors.* Wood Science and Technology, 2010. 44(2): p. 315-333.
16. Griffin, P.S., N. Indictor and R.J. Koestler, *The biodeterioration of stone: a review of deterioration mechanisms, conservation case histories, and treatment.* International Biodeterioration, 1991. 28(1–4): p. 187-207.
17. Johansson, P. and A. Ekstrand-Tobin, *The effect of surface roughness on mould growth on wood.* , in *10th Nordic Symposium on Building Physics*. 2014.
18. Johansson, S., *Biological growth on rendered facades*. 2011, Institutionen för bygg och miljöteknologi.: Lunds Universitet, Lunds Tekniska Högskola.
19. Johansson, S., L. Wadsö and K. Sandin, *Estimation of mould growth levels on rendered façades based on surface relative humidity and surface temperature measurements.* Building and Environment, 2010. 45(5): p. 1153-1160.

20. Jurado, V., et al., *Recolonization of mortars by endolithic organisms on the walls of San Roque church in Campeche (Mexico): A case of tertiary bioreceptivity.* Construction and Building Materials, 2014. 53(0): p. 348-359.
21. Krus, M., et al., *Prevention of algae and mould growth in facades by coatings with lowered long-wave emissions*. 2006, Fraunhofer Institut Bauphysik.
22. Krus, M., C. Fitz and K. Sedlbauer, *Reducing the Risk of Microbial Growth on Insulated Walls by Improving the Properties of the Surface Materials*, in *Hygrothermal Behavior, Building Pathology and Durability*, V.P. de Freitas and J.M.P.Q. Delgado, Editors. 2013, Springer Berlin Heidelberg. p. 1-21.
23. Kuntzel, H. *Factors determining moisture on external walls*. 2007.
24. Manso, S., et al., *Bioreceptivity evaluation of cementitious materials designed to stimulate biological growth.* Sci Total Environ, 2014. 481: p. 232-41.
25. Marie, I., *Perception of darkening of stone façades and the need for cleaning.* International Journal of Sustainable Built Environment, 2013. 2(1): p. 65-72.
26. Melo Júnior, C.M. and H. Carasek, *Relationship between the deterioration of multi story buildings facades and the driving rain.* Revista de la Construccion, 2014. 13(1): p. 64-73.
27. Nuhoglu, Y., et al., *The accelerating effects of the microorganisms on biodeterioration of stone monuments under air pollution and continental-cold climatic conditions in Erzurum, Turkey.* Science of The Total Environment, 2006. 364(1–3): p. 272-283.
28. Scheerer, S., O. Ortega-Morales and C. Gaylarde, *Chapter 5 Microbial Deterioration of Stone Monuments—An Updated Overview*, in *Advances in Applied Microbiology*, S.S. Allen I. Laskin and M.G. Geoffrey, Editors. 2009, Academic Press. p. 97-139.
29. Shirakawa, M.A., et al., *Mould and phototroph growth on masonry façades after repainting.* Materials and Structures/Materiaux et Constructions, 2004. 37(271): p. 472-479.
30. Shirakawa, M.A., et al., *Resistance of cyanobacterial fouling on architectural paint films to cleaning by water jet.* Current Microbiology, 2012. 64(4): p. 312-316.
31. Shirakawa, M.A., et al., *Biodeterioration of painted mortar surfaces in tropical urban and coastal situations: Comparison of four paint formulations.* International Biodeterioration & Biodegradation, 2011. 65(5): p. 669-674.
32. Shirakawa, M.A., et al., *Climate as the most important factor determining anti-fungal biocide performance in paint films.* Sci Total Environ, 2010. 408(23): p. 5878-86.
33. Tanaca, H.K., et al., *Discoloration and fungal growth on three fiber cement formulations exposed in urban, rural and coastal zones.* Building and Environment, 2011. 46(2): p. 324-330.
34. Van den Bulcke, J., J. Van Acker and M. Stevens, *Assessment of blue-stain resistance according to the EN 152 and a reverse test method using visual and computer-aided techniques.* International Biodeterioration & Biodegradation, 2006. 57(4): p. 229-238.
35. Van den Bulcke, J., J. Van Acker and M. Stevens, *Laboratory testing and computer simulation of blue stain growth on and in wood coatings.* International Biodeterioration & Biodegradation, 2007. 59(2): p. 137-147.
36. Warscheid, T. and J. Braams, *Biodeterioration of stone: a review.* International Biodeterioration & Biodegradation, 2000. 46(4): p. 343-368.

Appendix 2. Comparison of outcome of dynamic mould models and field results

In this appendix, all results from running the dynamic models are presented as graphs. In the upper first three graphs, the lines in the graphs represents the outcome of the models, representing the different choices of the partners in the round robin. The horizontal dotted lines are the limit values. If the curve is crossing the limit value, mould growth is predicted. In the graph presenting the m-model version 2.0, the individual curves are the outcome of the model. The horizontal dotted line is the limit value, which is based on the different choices from different partners and therefore there are sometimes two limit lines in these graphs. The lower most graph describes real mould growth analysis, as boxplots, at different point of times in the filed study. The mould growth was assessed and rated according to Table 6.3. The median in each box is represented with a thick horizontal line. If the median is at or above 2 (represented by the dotted horizontal line) mould growth is considered established.

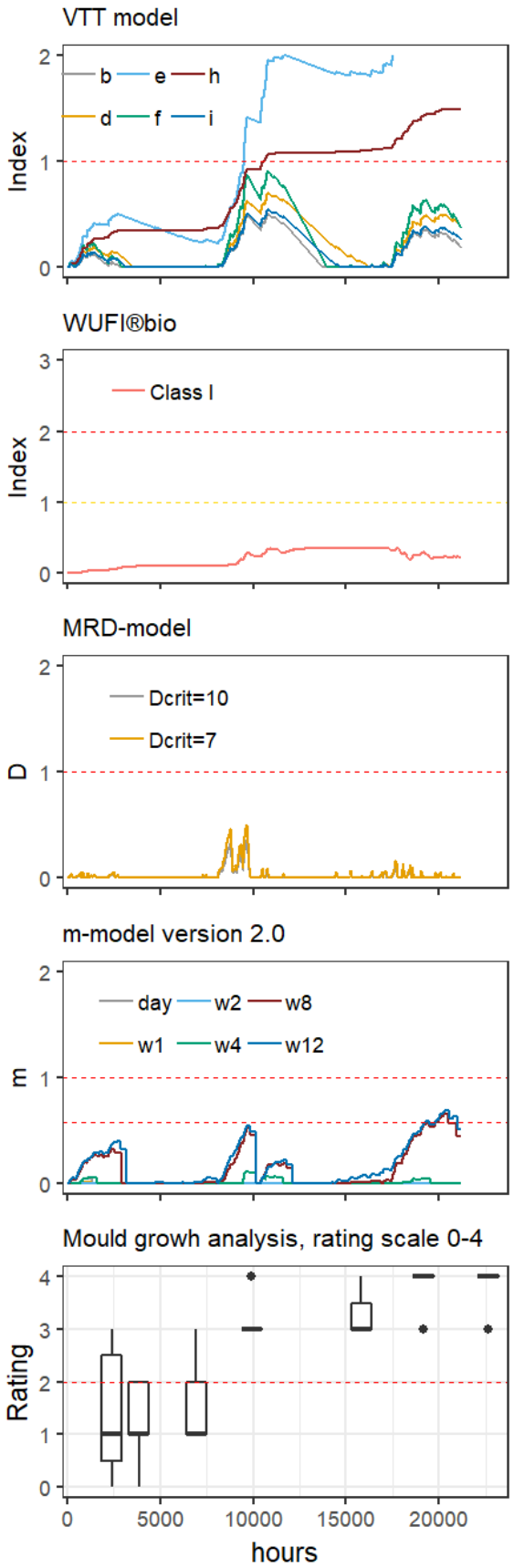

Climate1, Plywood

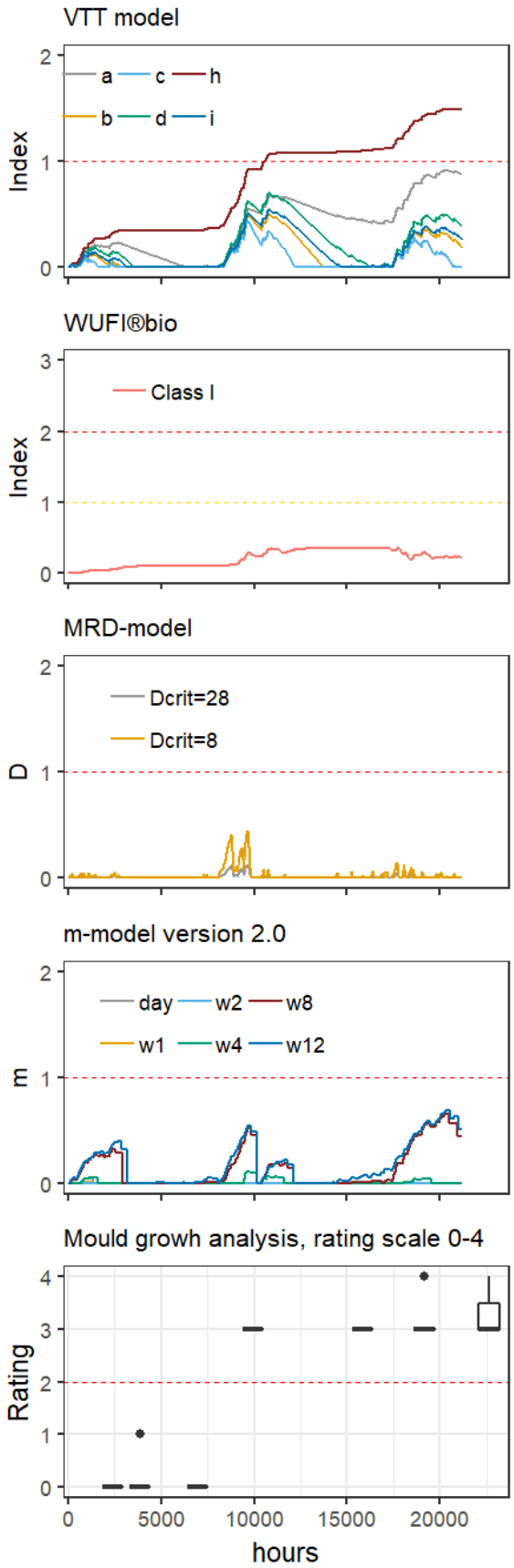

Climate1, Chipboard

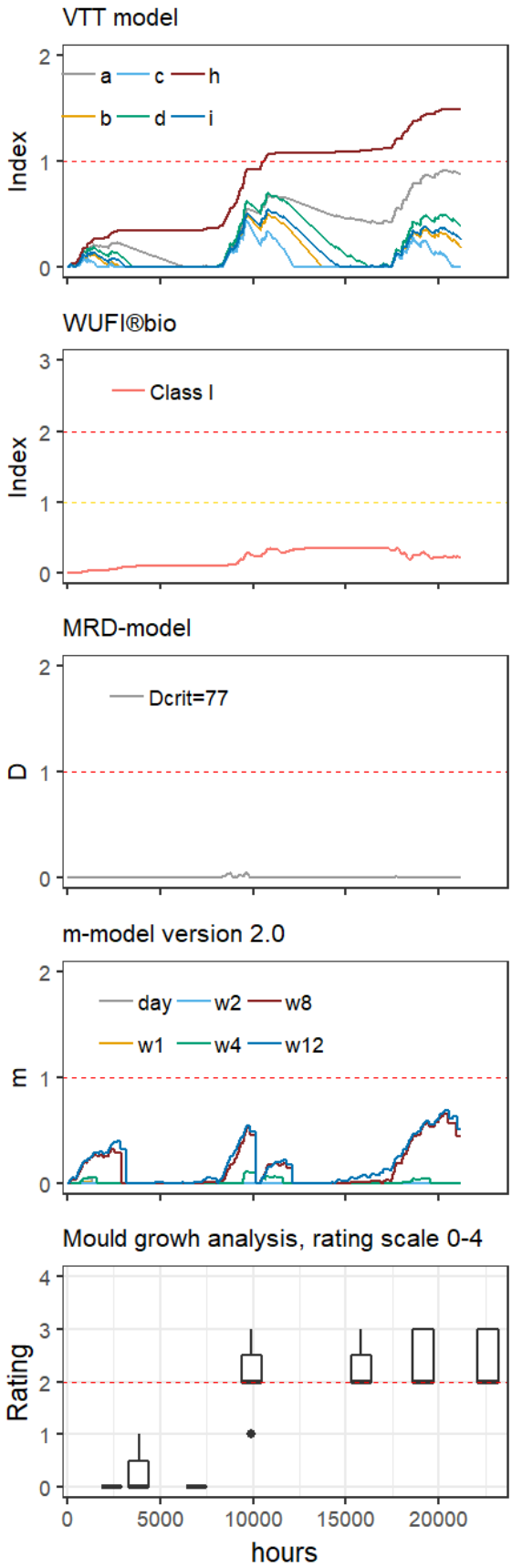

Climate1, Thin hardboard

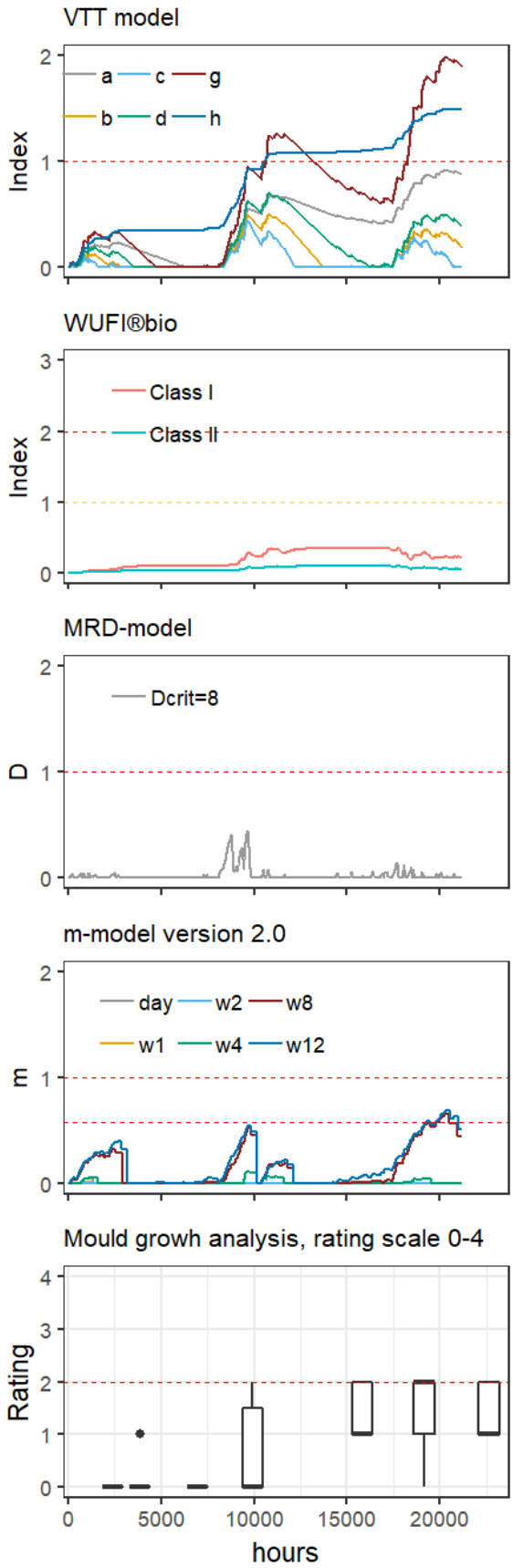

Climate1, Gypsum board

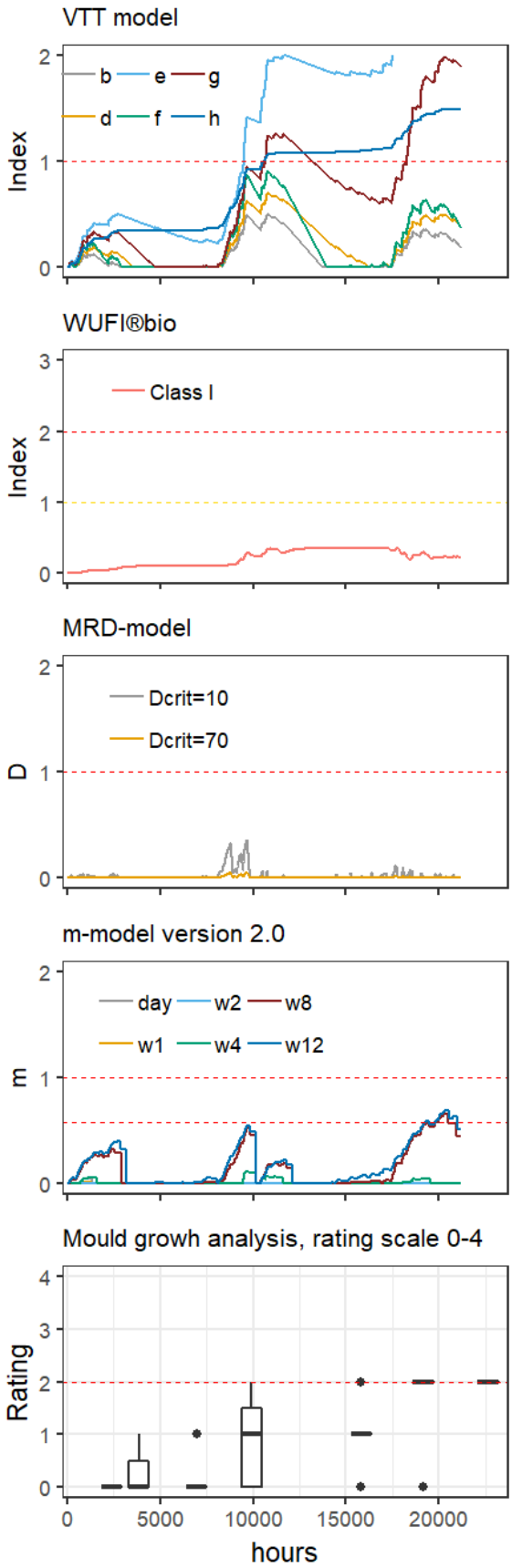

Climate1, Spruce

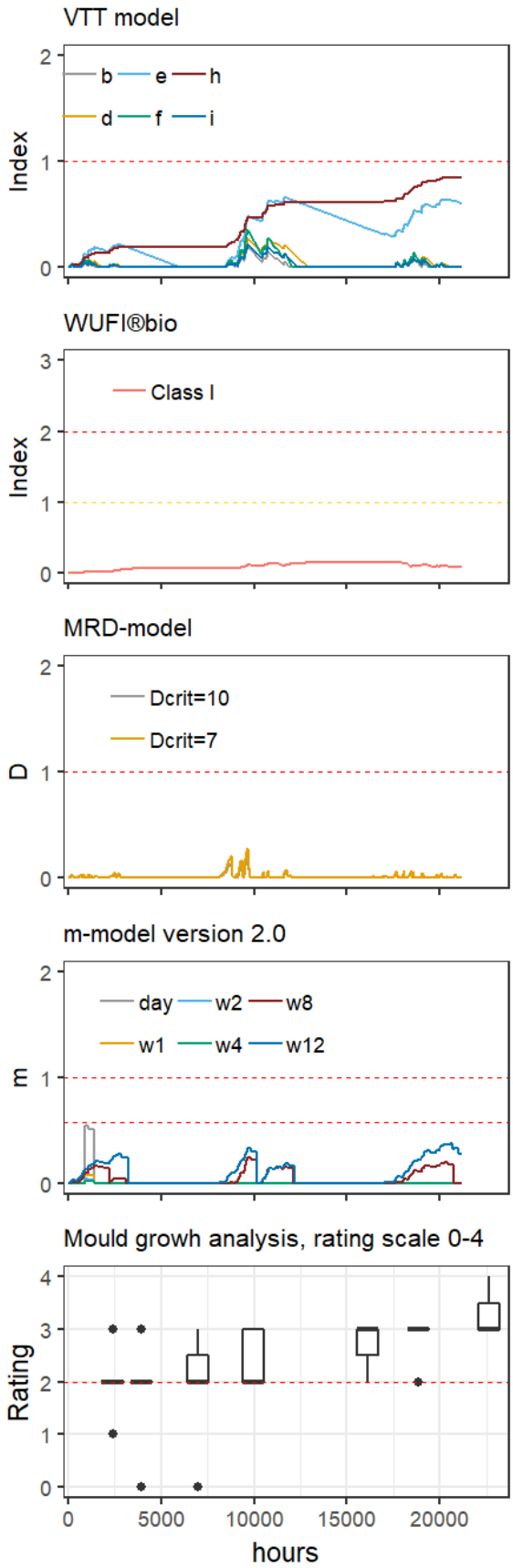

Climate 2, Plywood

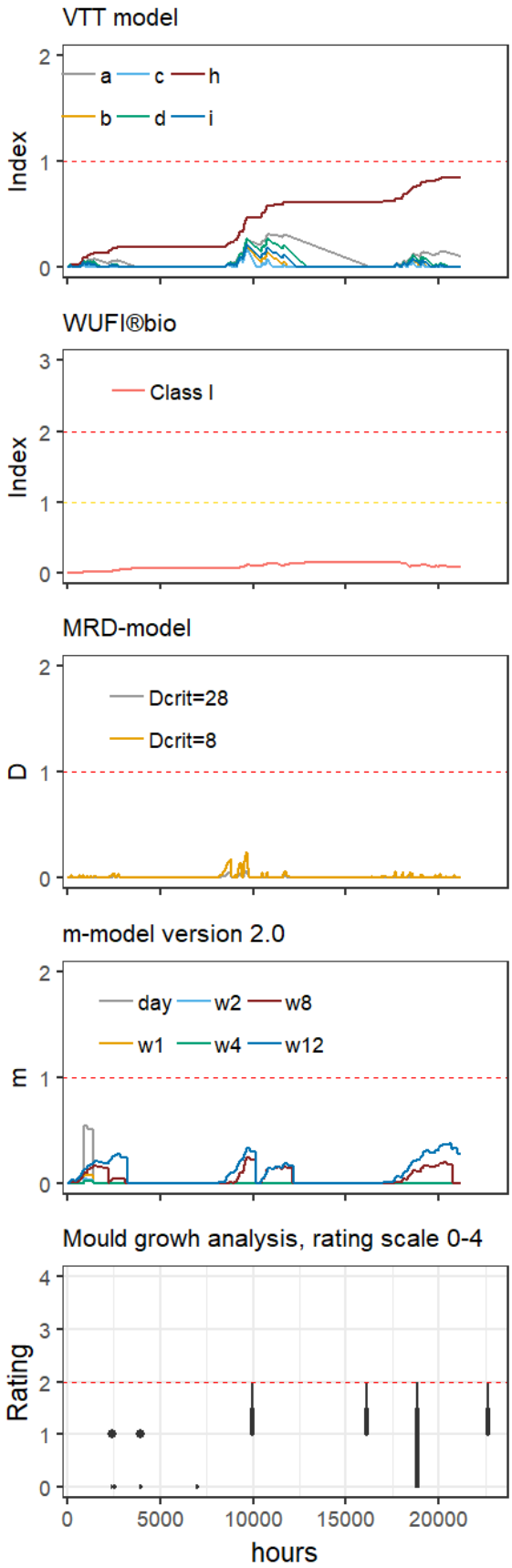

Climate2, Chipboard

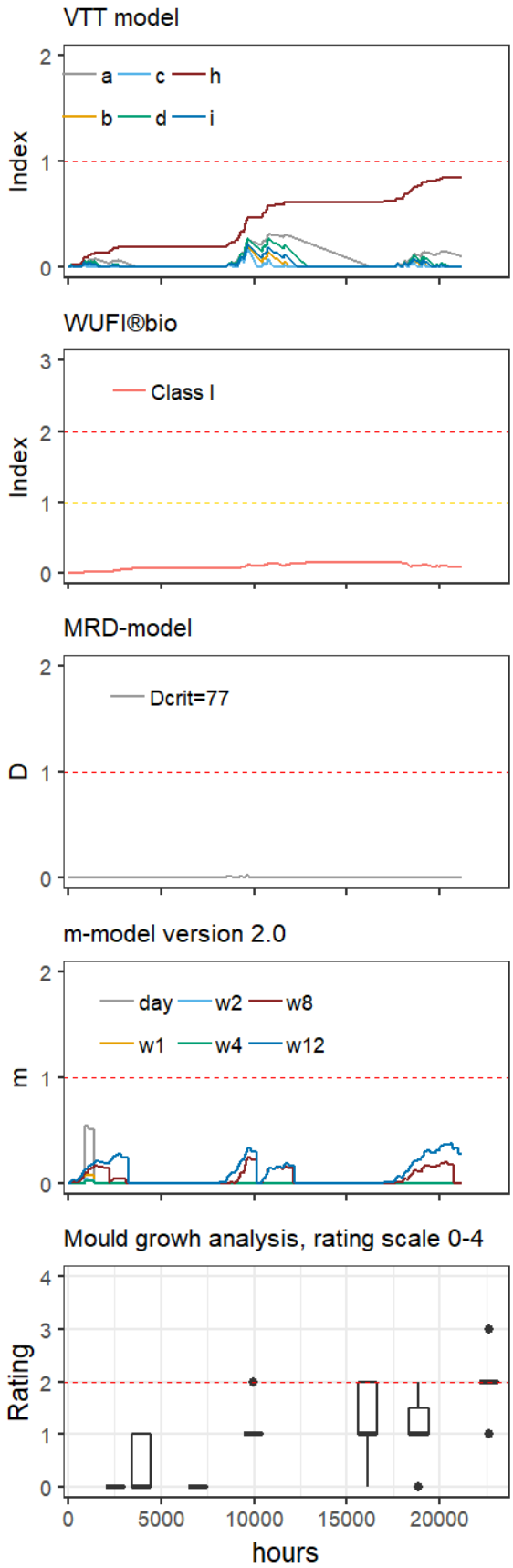

Climate2, Thin hardboard

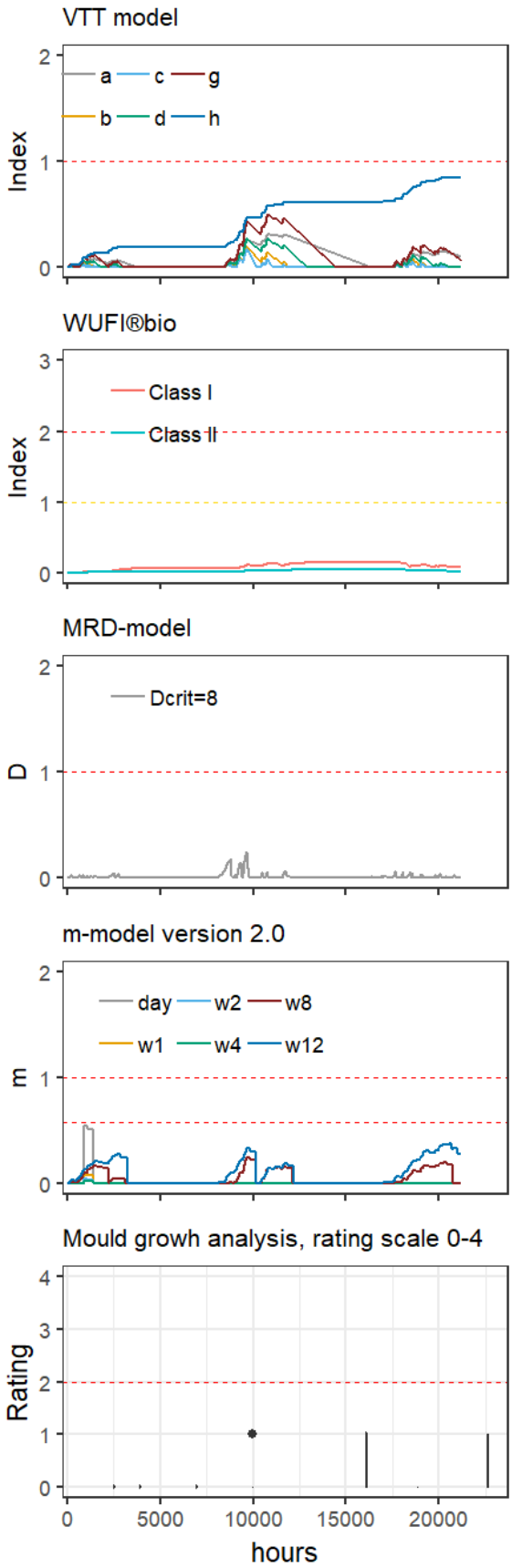

Climate2, Gypsum board

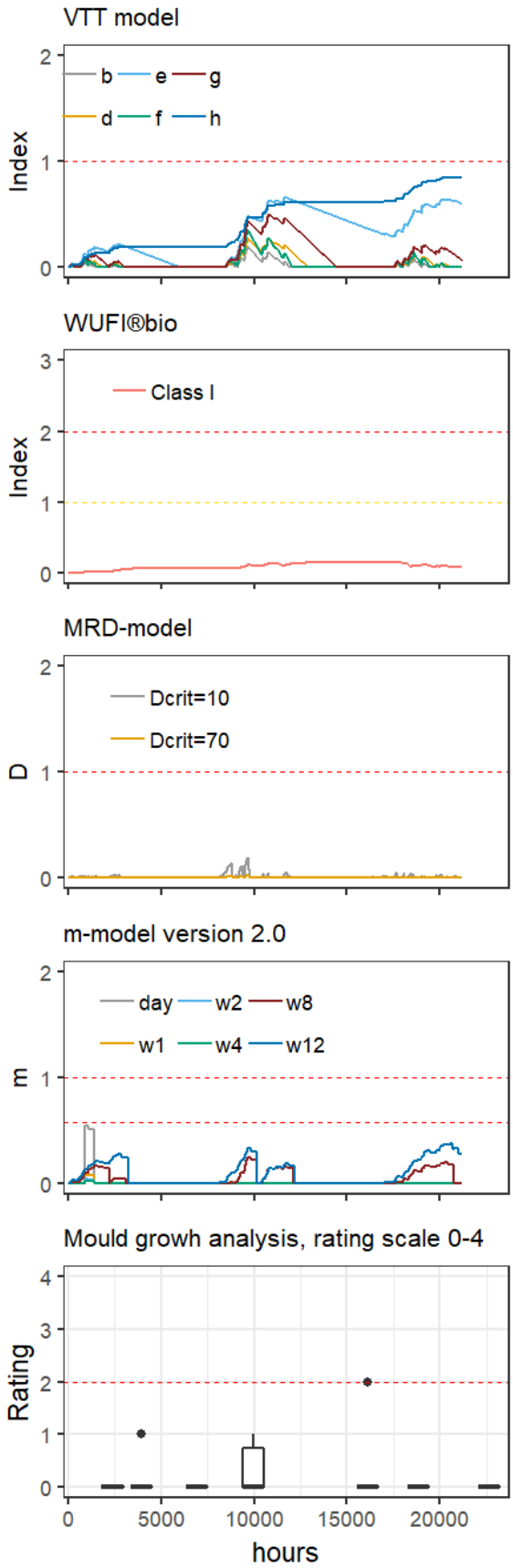

Climate2, Spruce

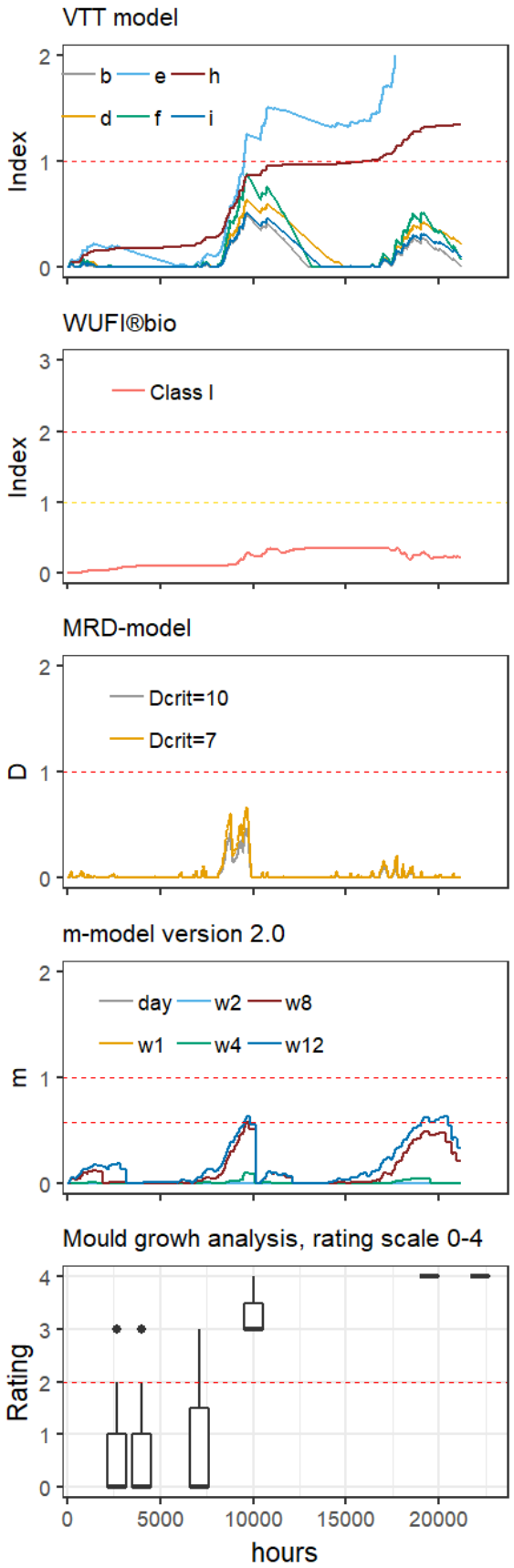

Climate3, Plywood

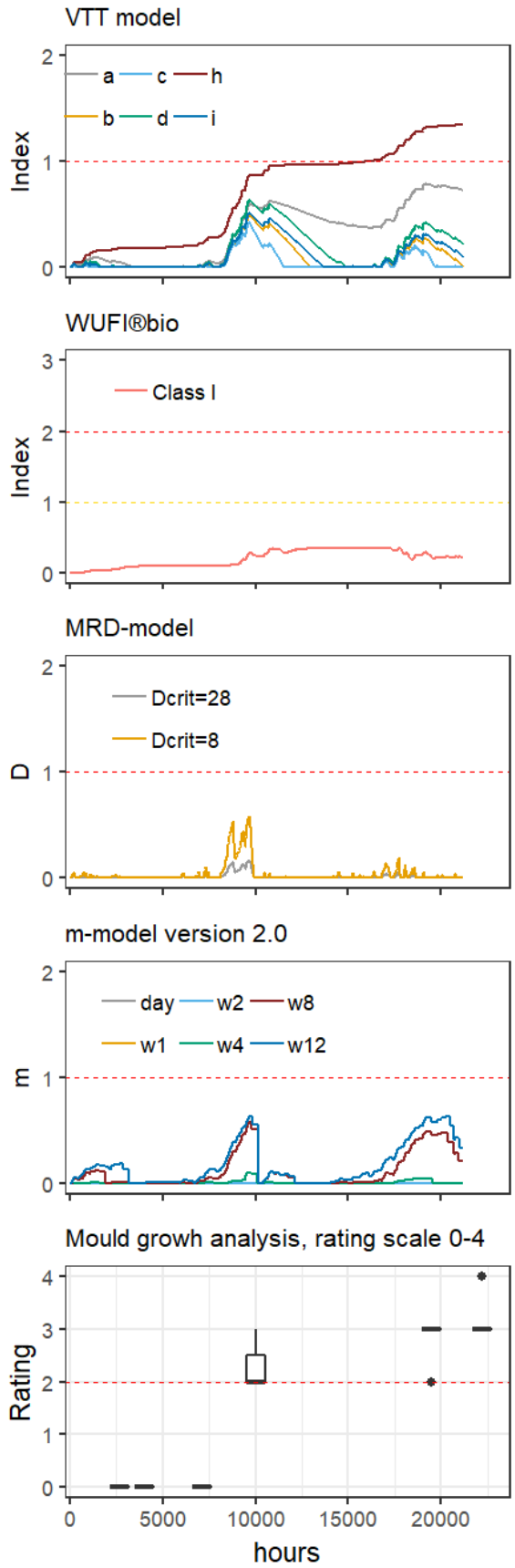

Climate3, Chipboard

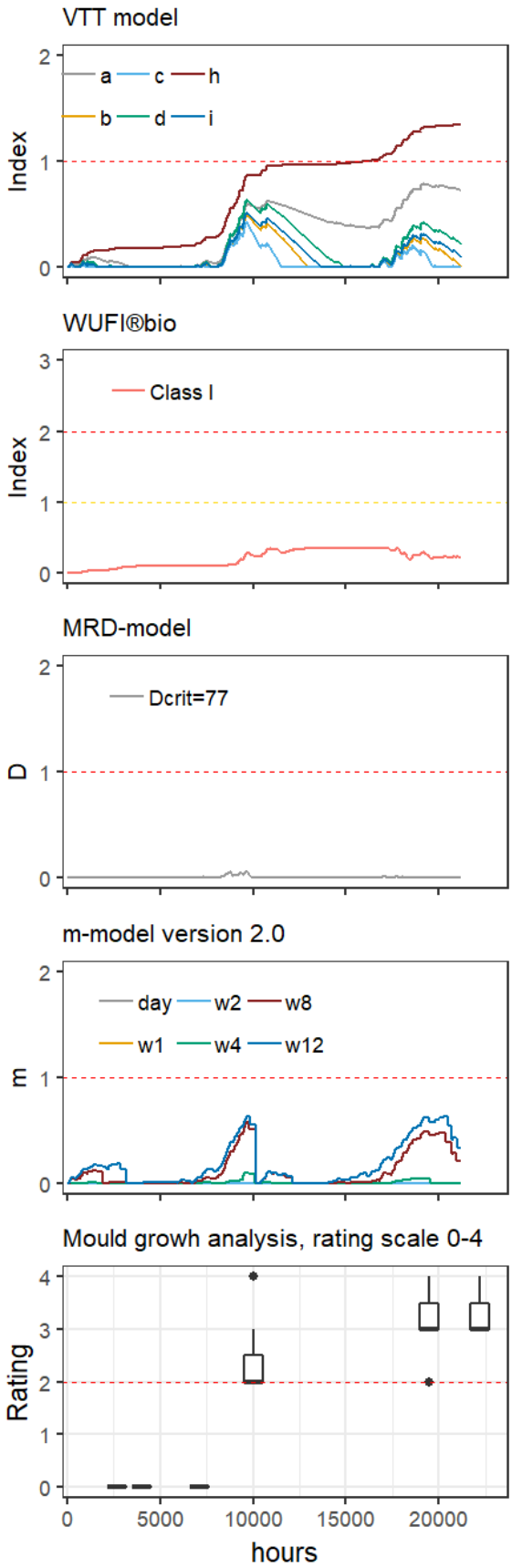

Climate3, Thin hardboard

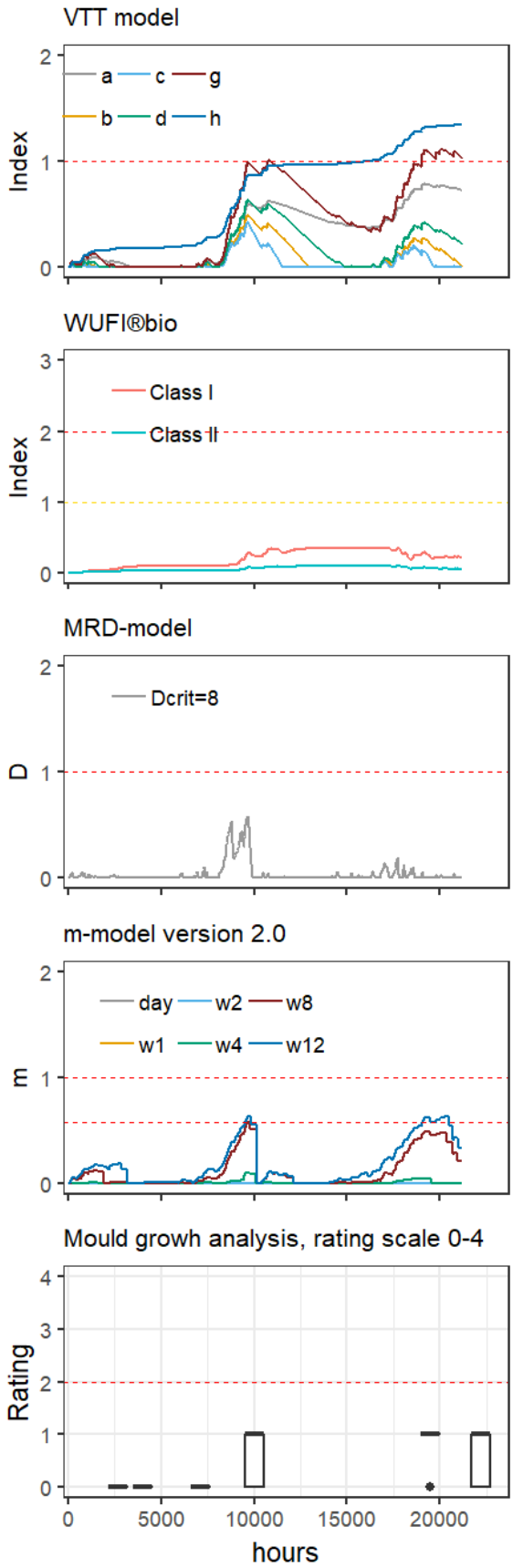

Climate3, Gypsum board

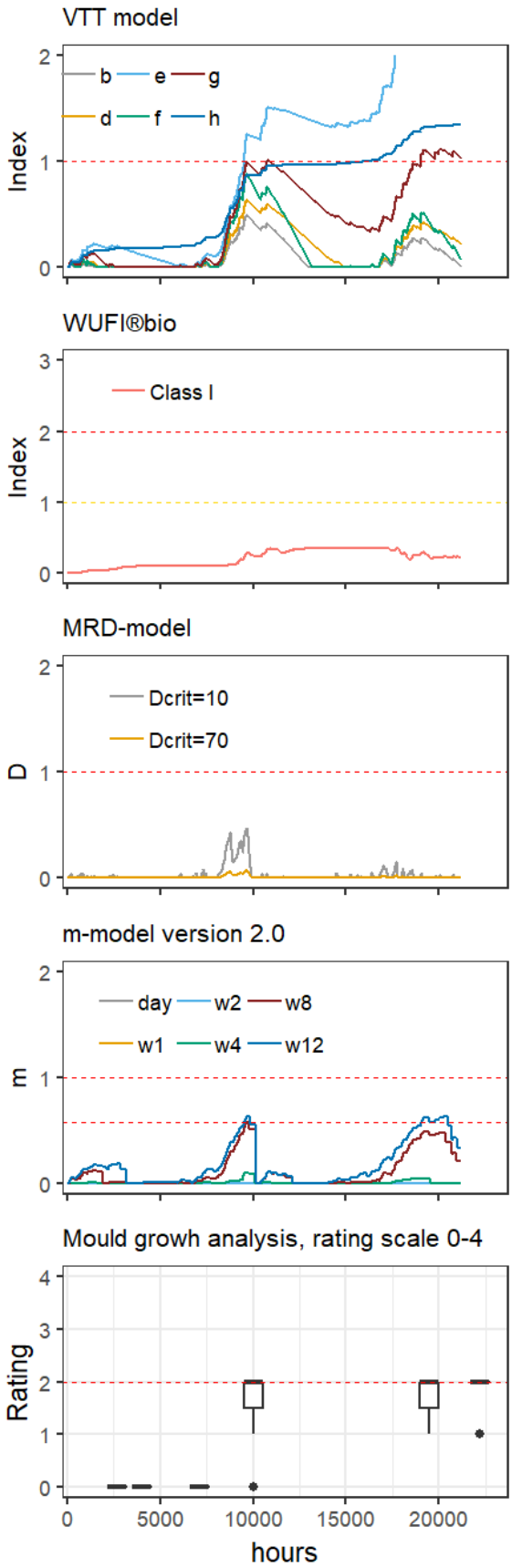

Climate3, Spruce

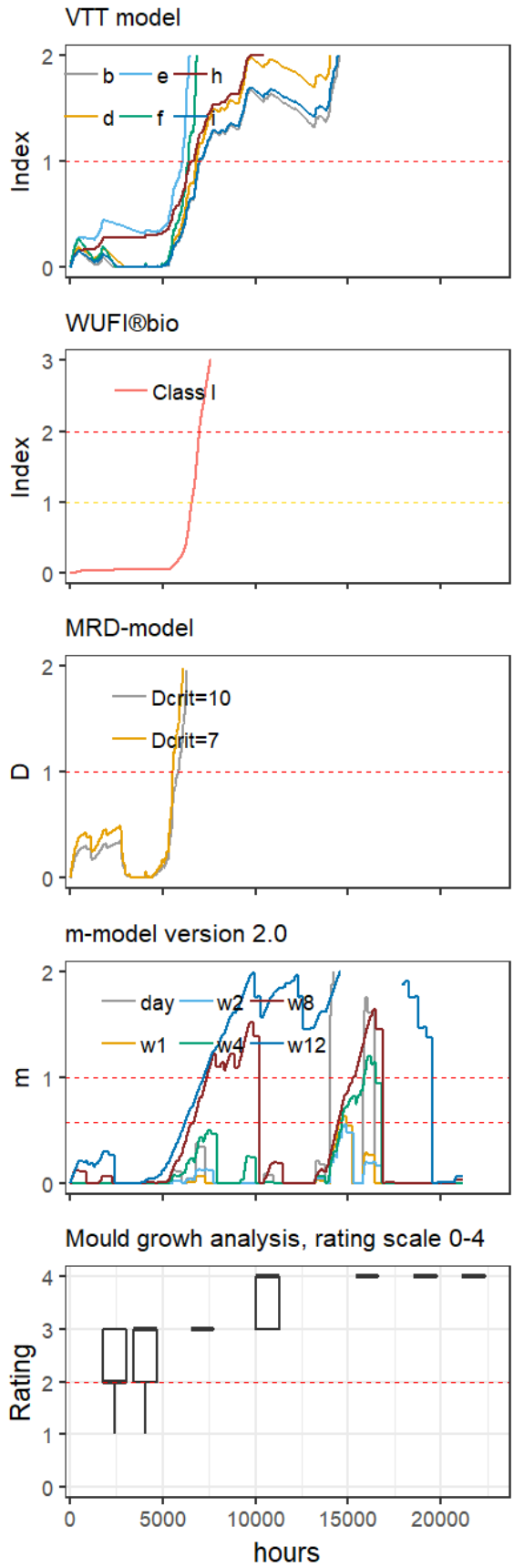

Climate5, Plywood

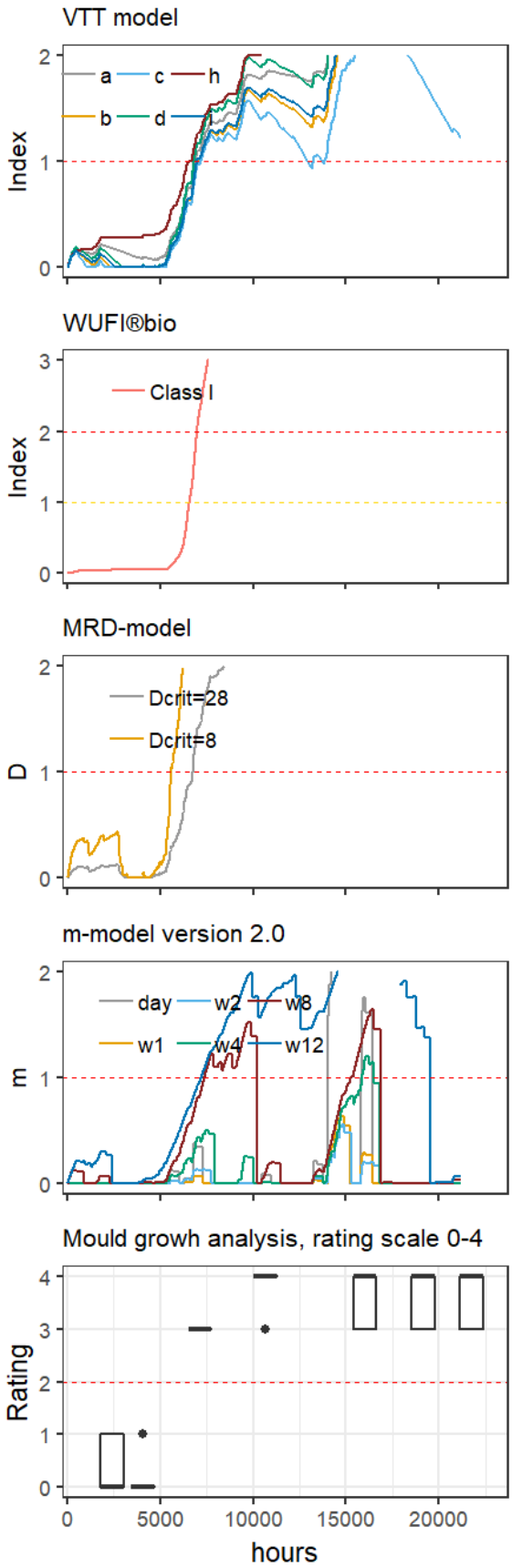

Climate5, Chipboard

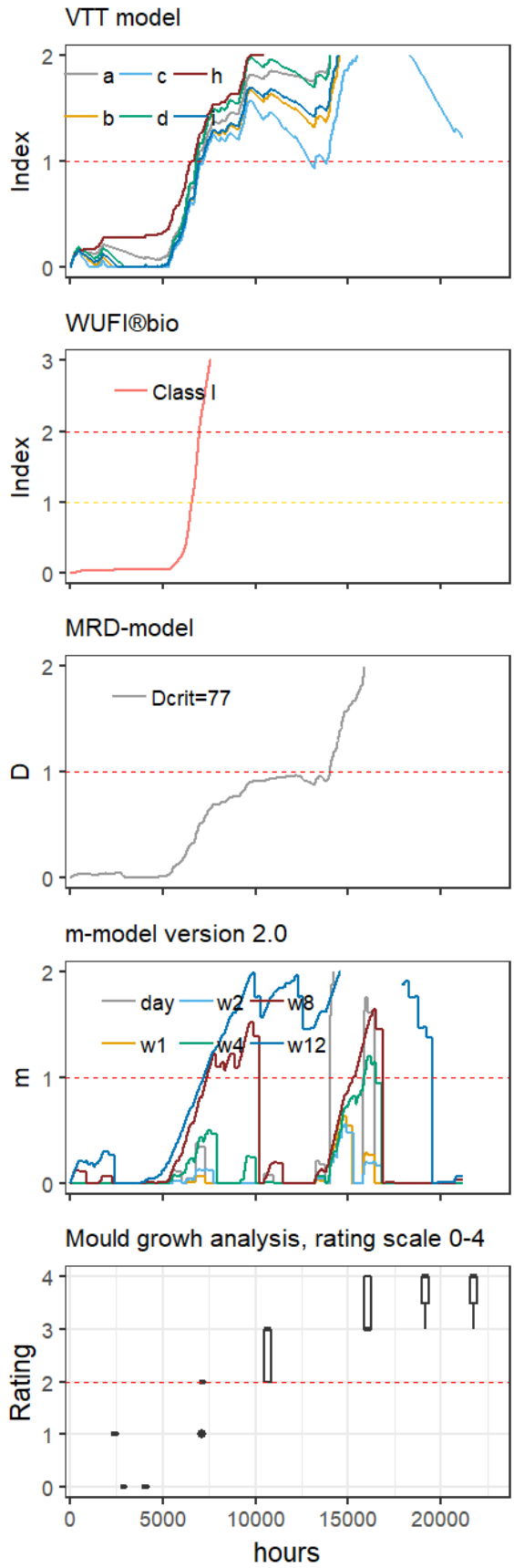

Climate5, Thin hardboard

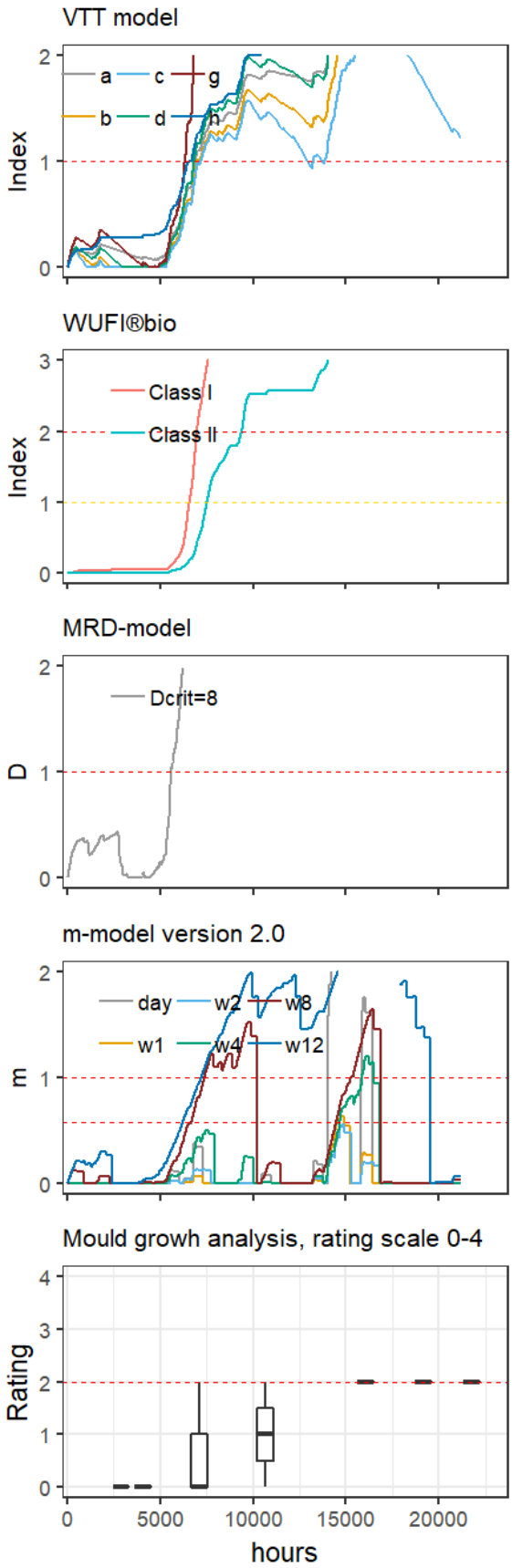

Climate5, Gypsum board

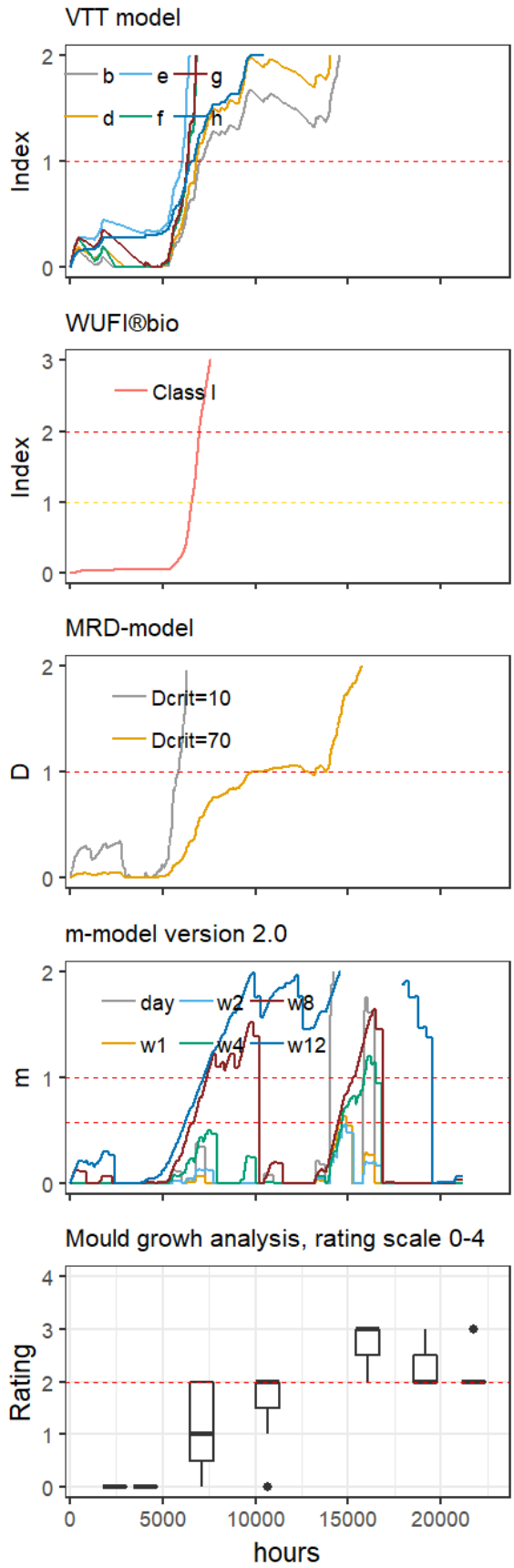

Climate5, Spruce

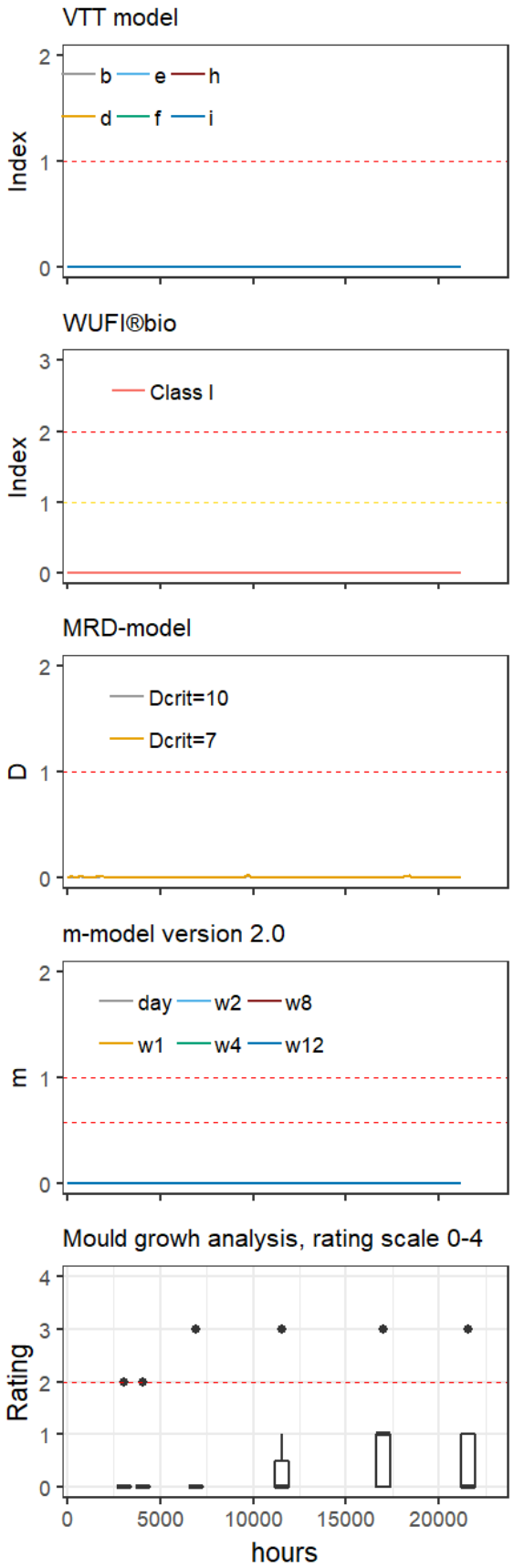

Climate 6, Plywood

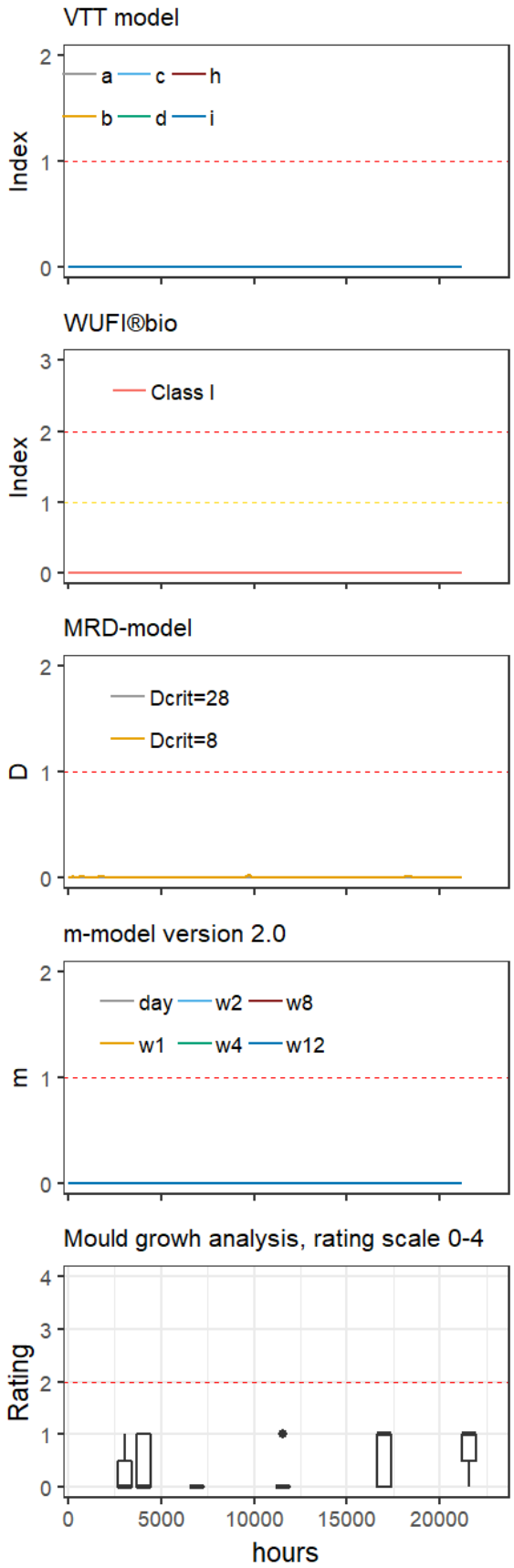

Climate6, Chipboard

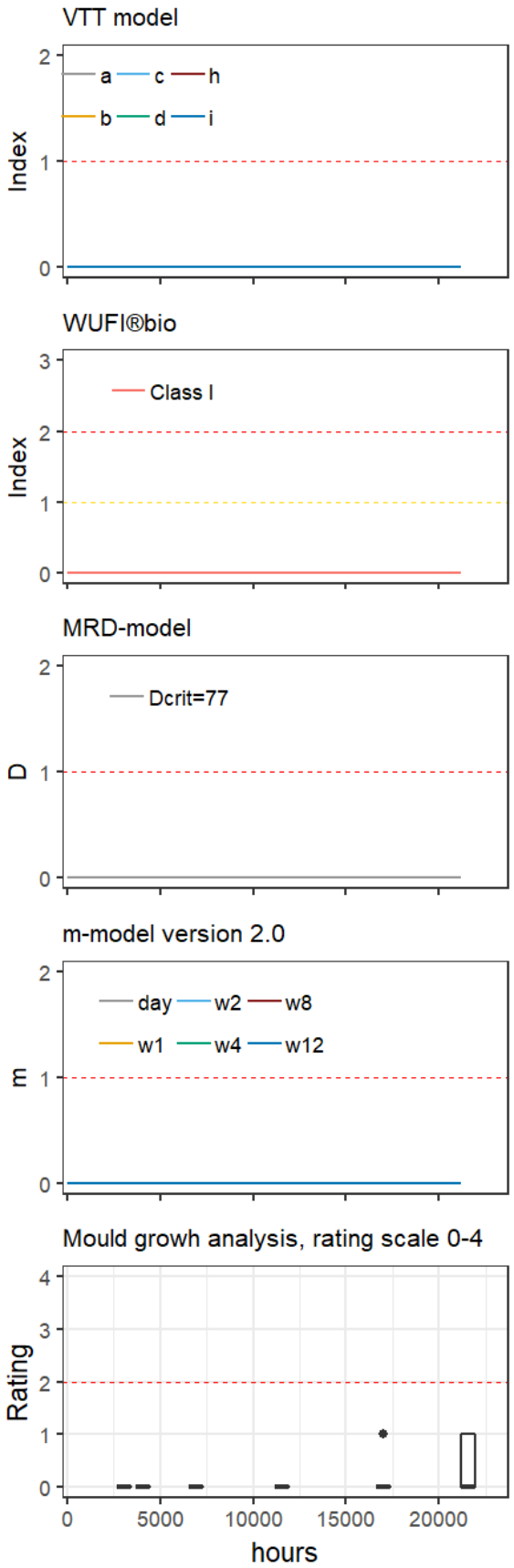

Climate6, Thin hardboard

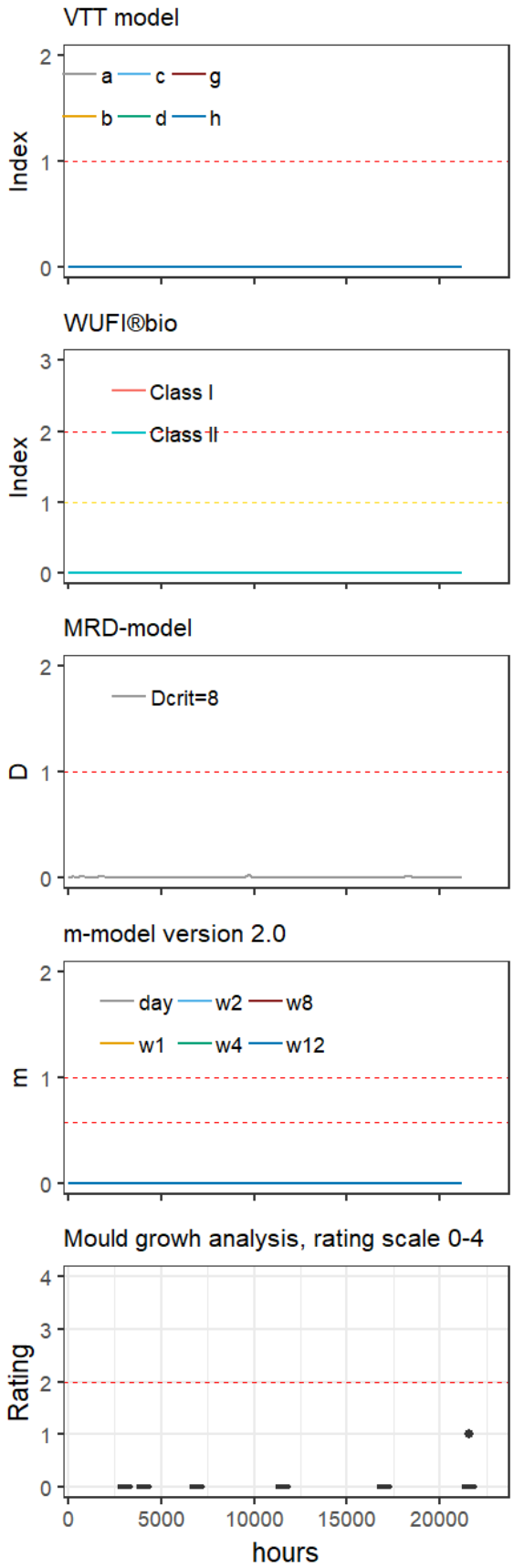

Climate6, Gypsum board

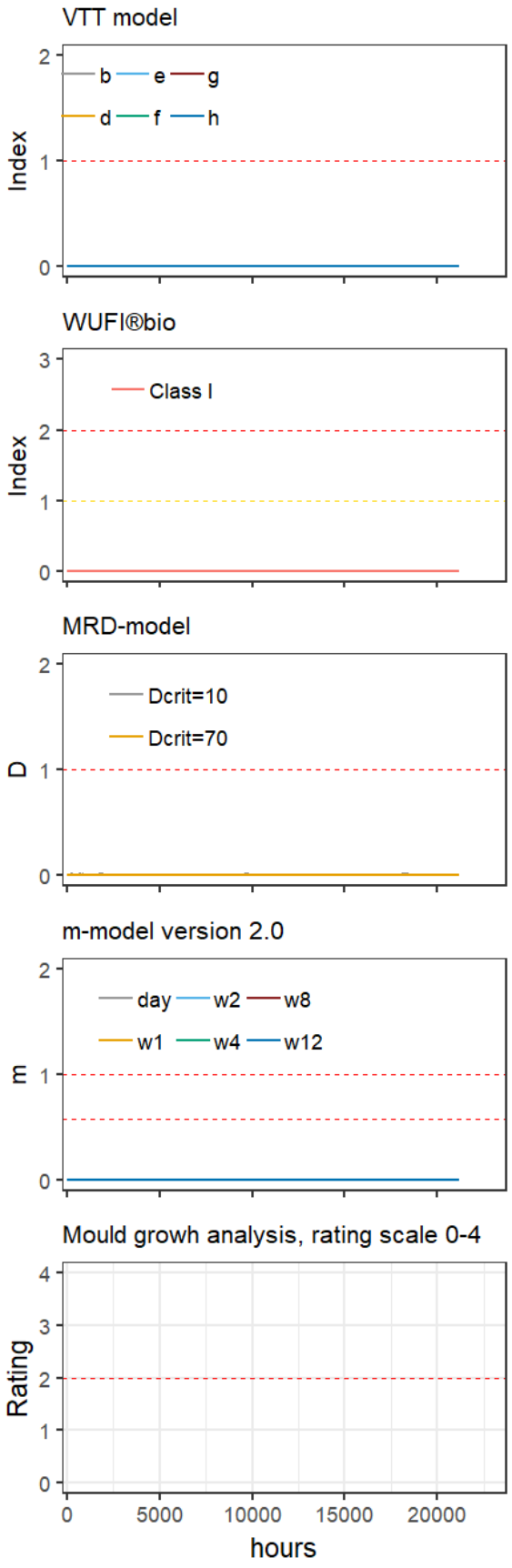

Climate6, Spruce

Appendix 3. Comparison of outcome of static mould models and field results

In this appendix, all results from running the static mould models are presented as graphs. In the left graph, the PJ-model is presented and in the centre the Sedlbauers LIMcurve is presented. The models are described in section 7.1.4.5 and 7.1.4.6. If the measured RH is above the red limit curve, mould growth is predicted in both models. If it is above the yellow line($RH_{critlow}$) in the pj-model there is also possible risk for mould growth. The right graph describes mould growth analysis in the end of the field study. The mould growth was assessed and rated according to Table 6.3. The median is represented with a blue square. If the median is at or above 2 (represented by the dotted horizontal line) mould growth is considered established.

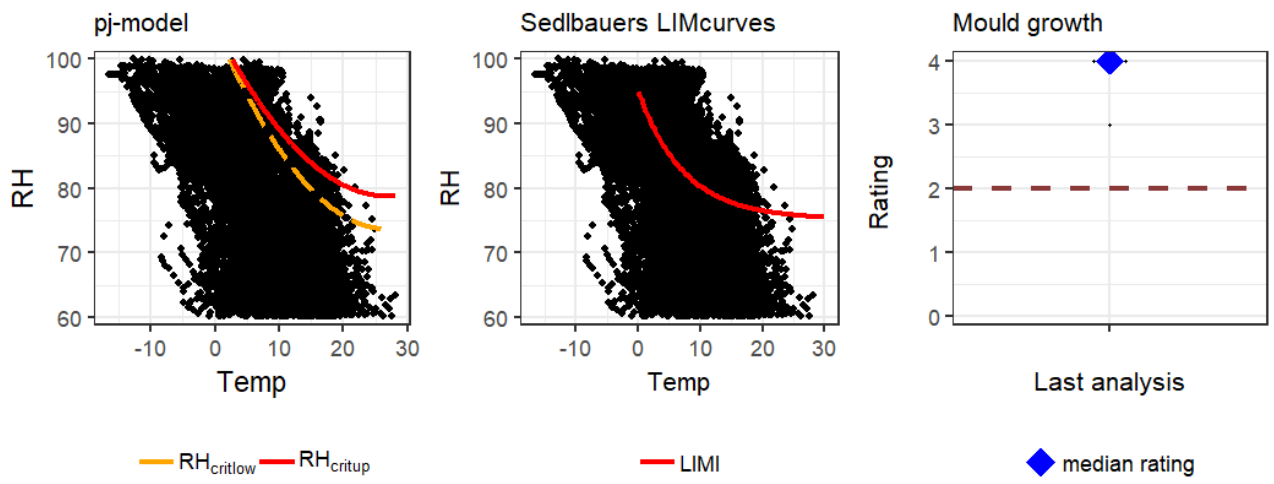

Climate 1, Plywood

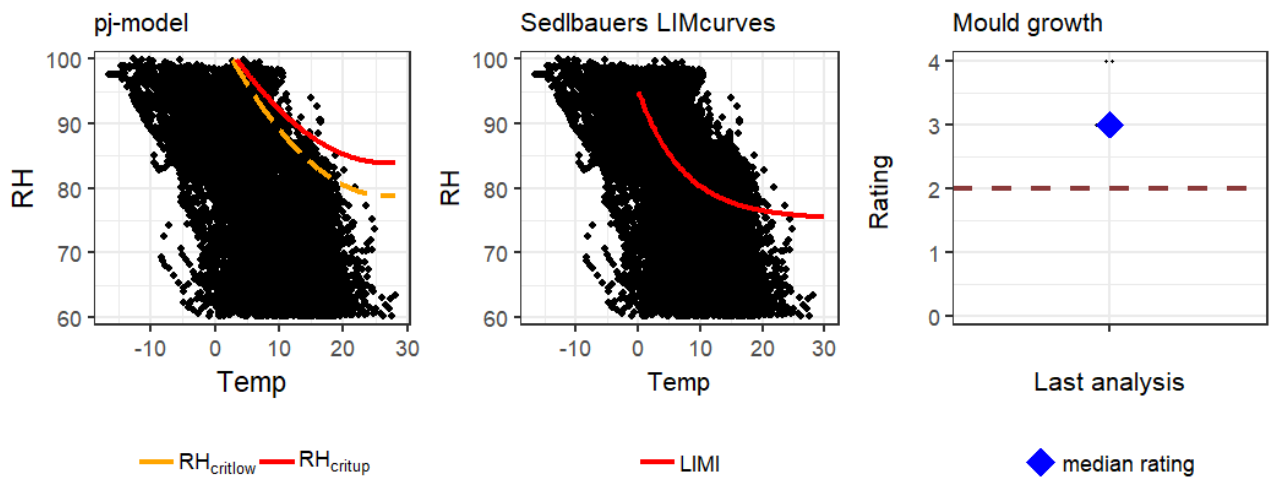

Climate1, Chipboard

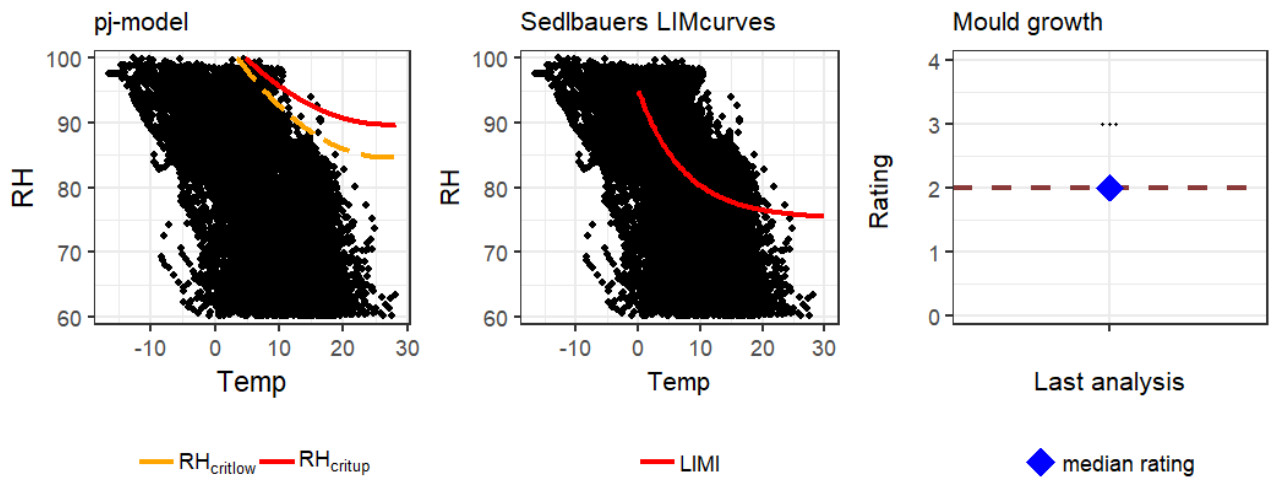

Climate1, Thin hardboard

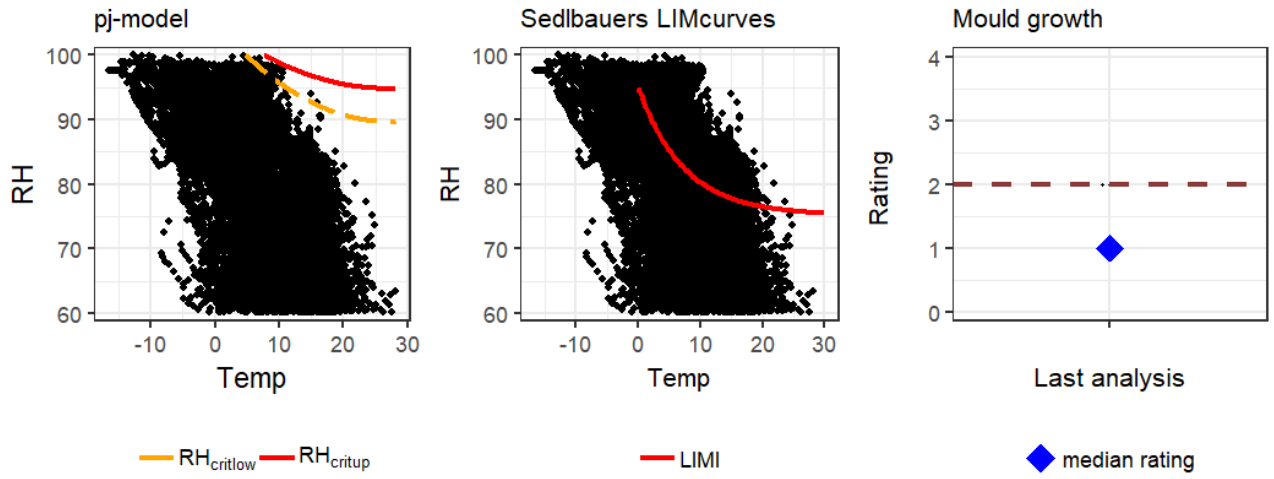

Climate1, Gypsum board

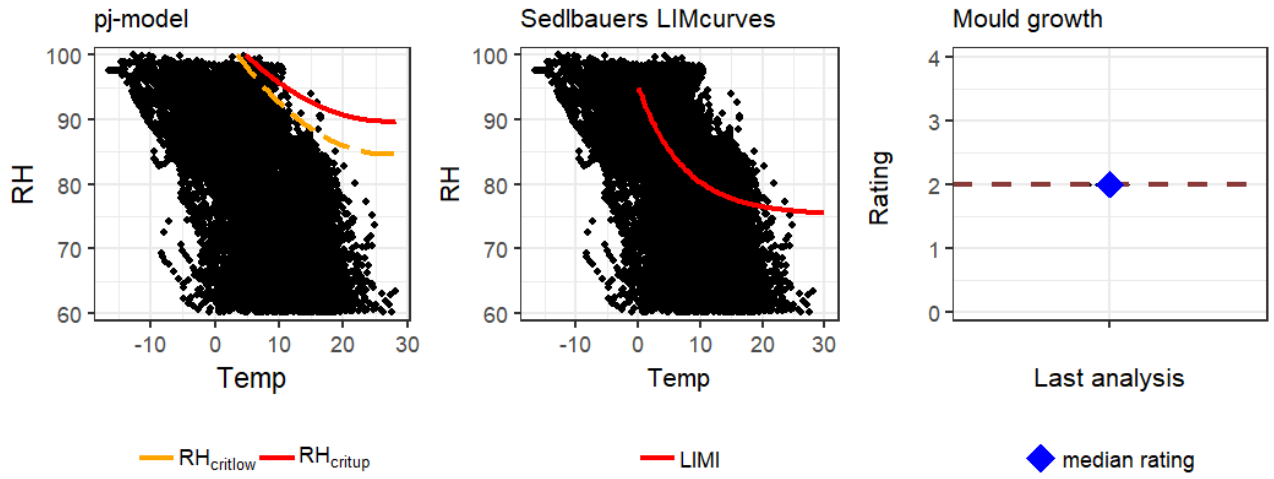

Climate1, Spruce

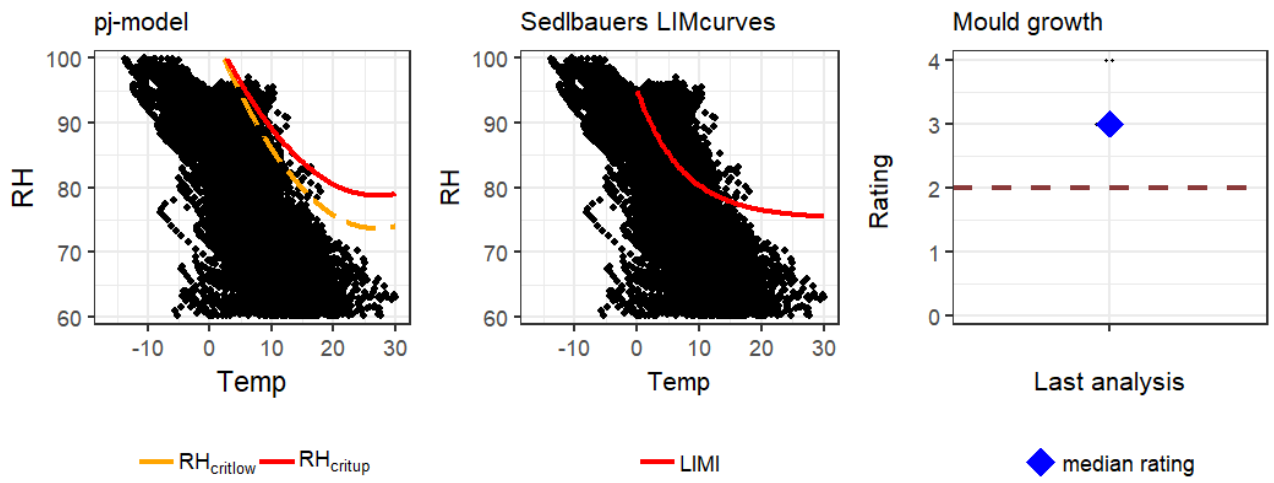

Climate2, Plywood

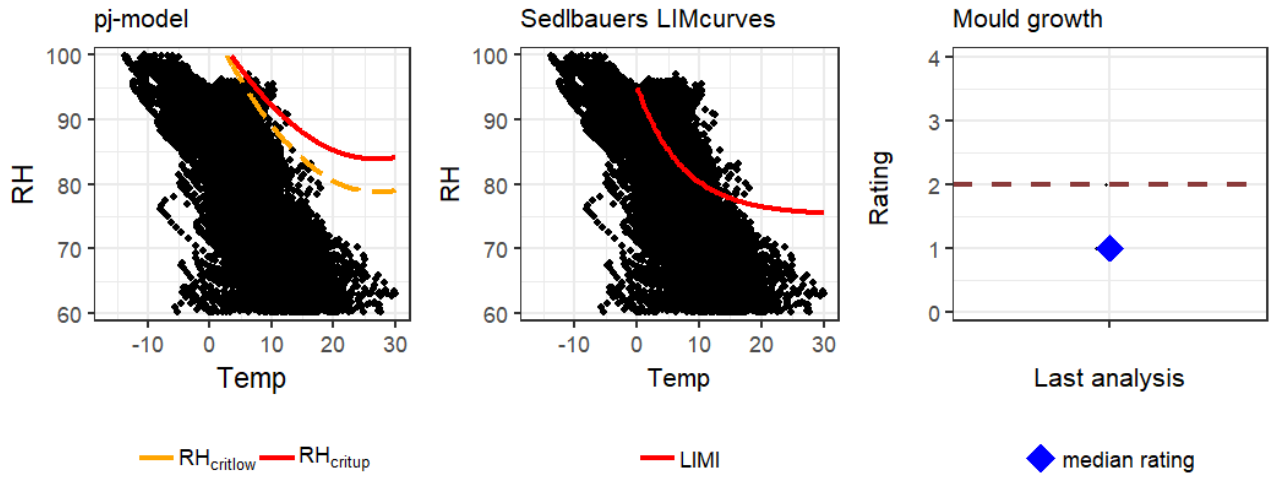

Climate2, Chipboard

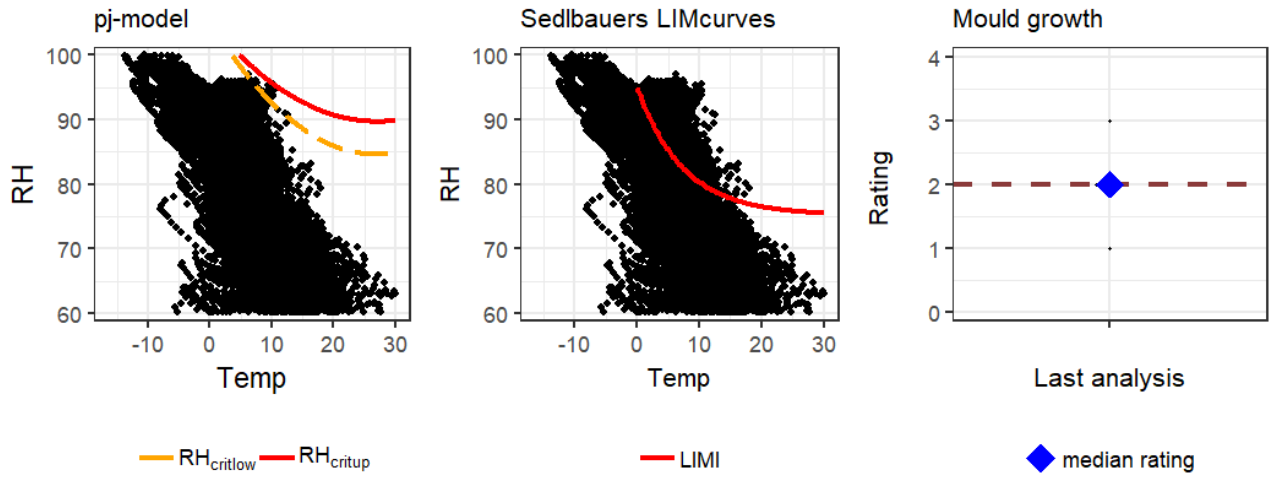

Climate2, Thin hardboard

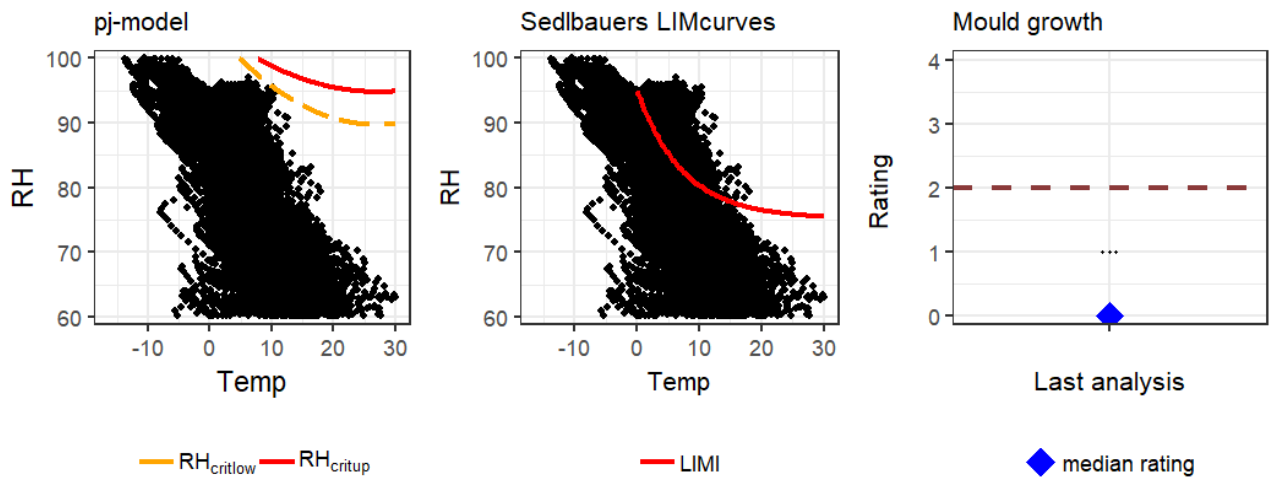

Climate2, Gypsum board

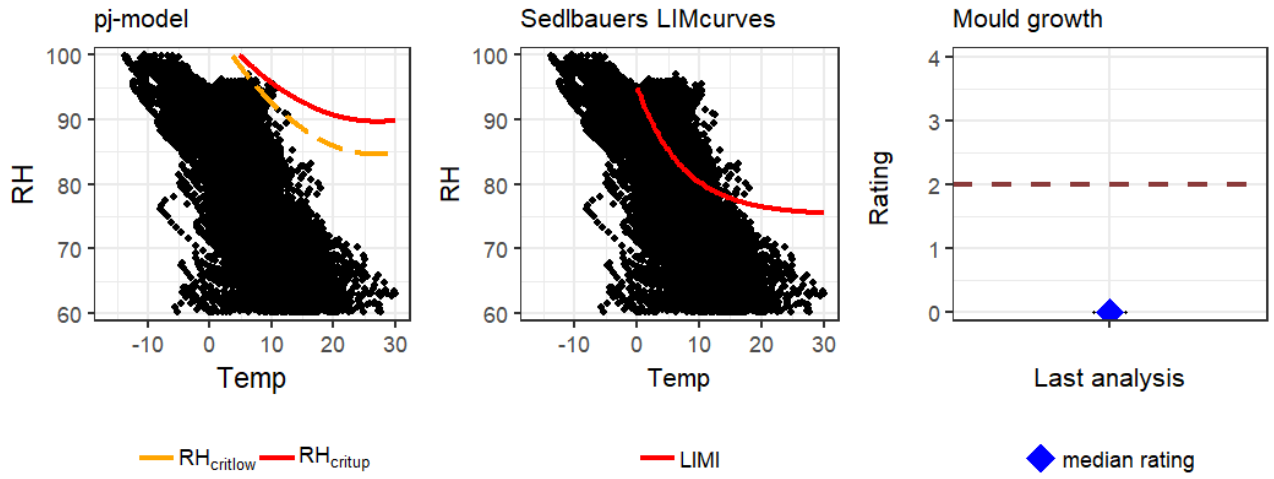

Climate2, Spruce

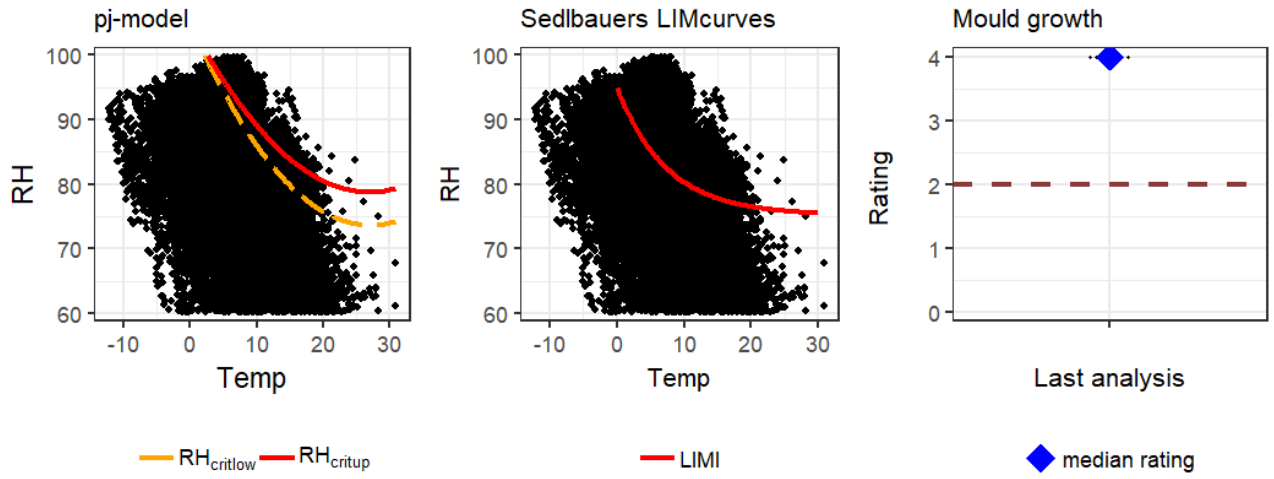

Climate 3, Plywood

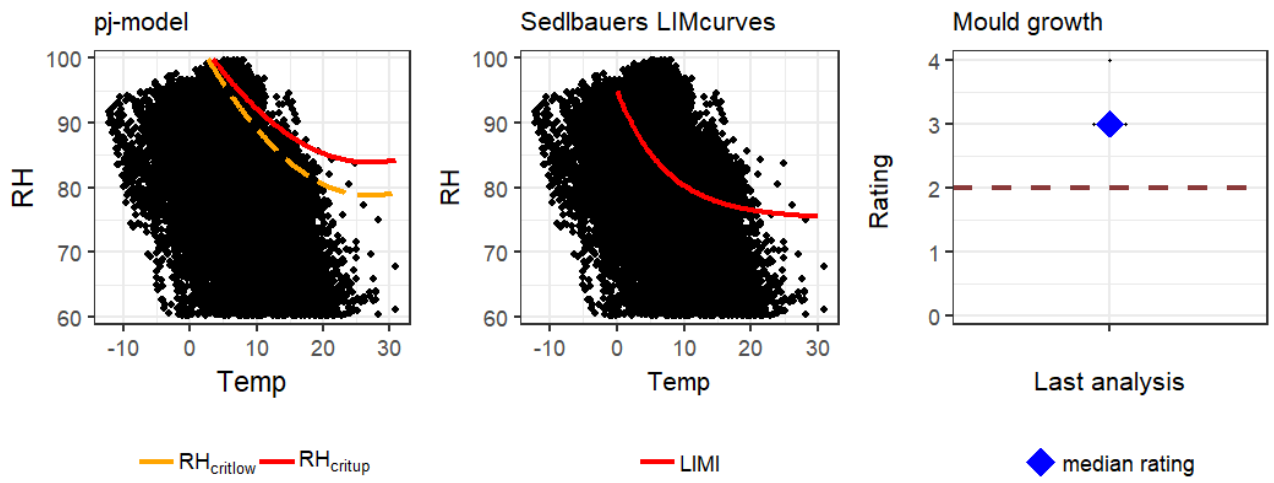

Climate3, Chipboard

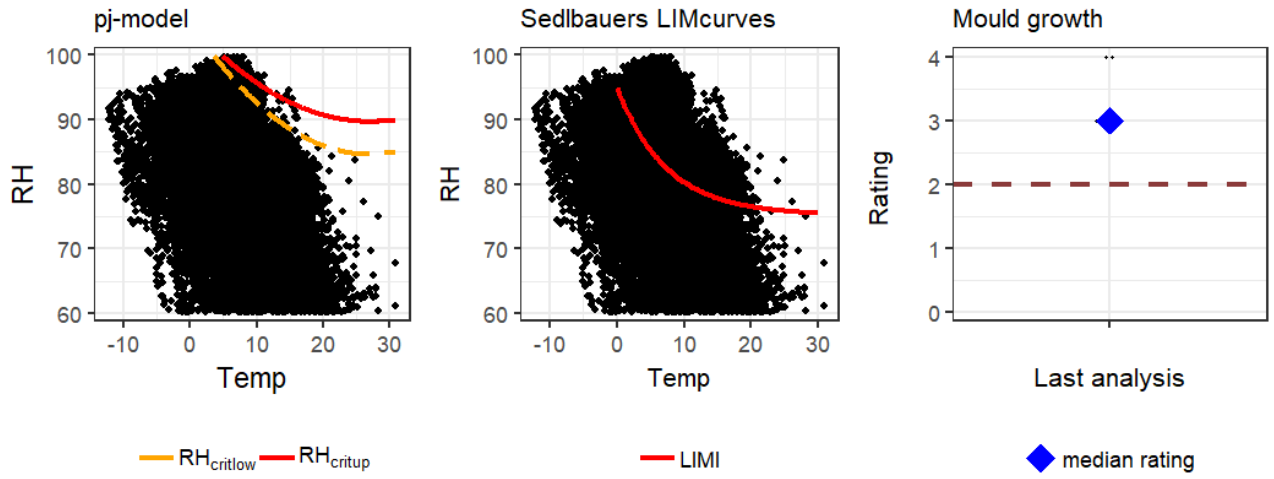

Climate3, Thin hardboard

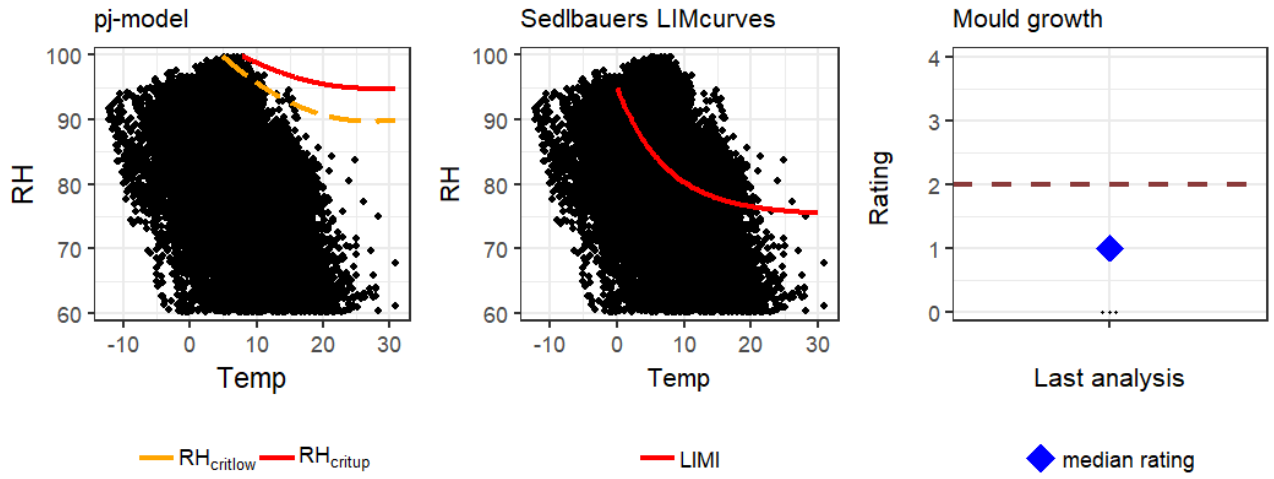

Climate3, Gypsum board

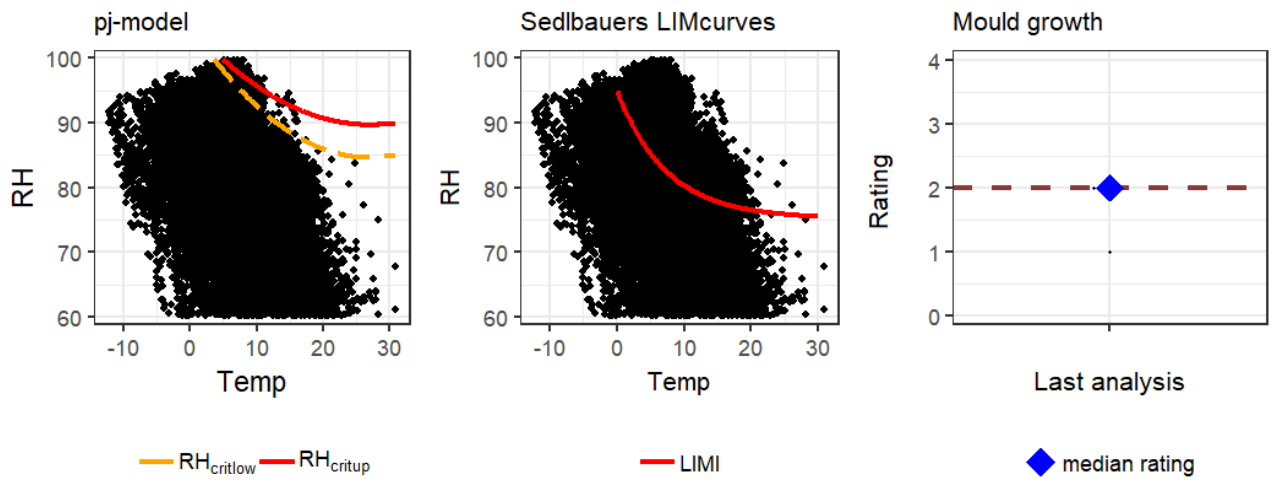

Climate3, Spruce

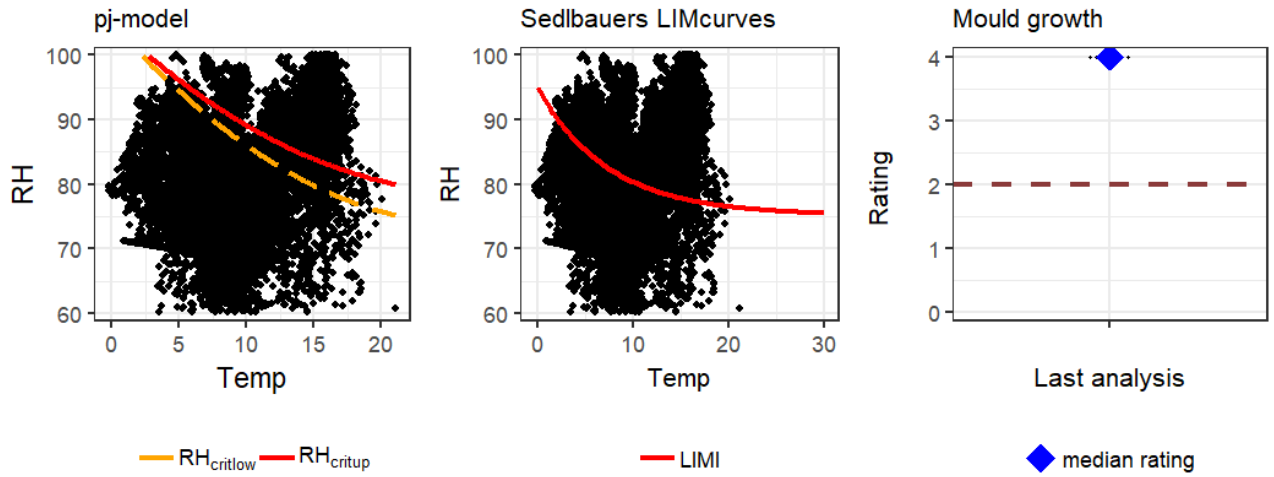

Climate5, Plywood

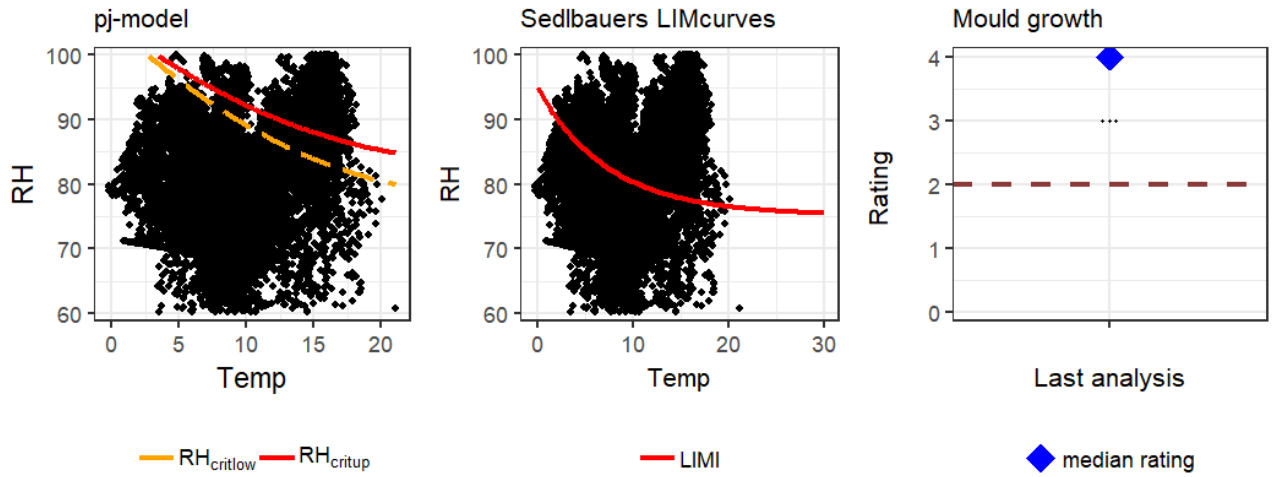

Climate5, Chipboard

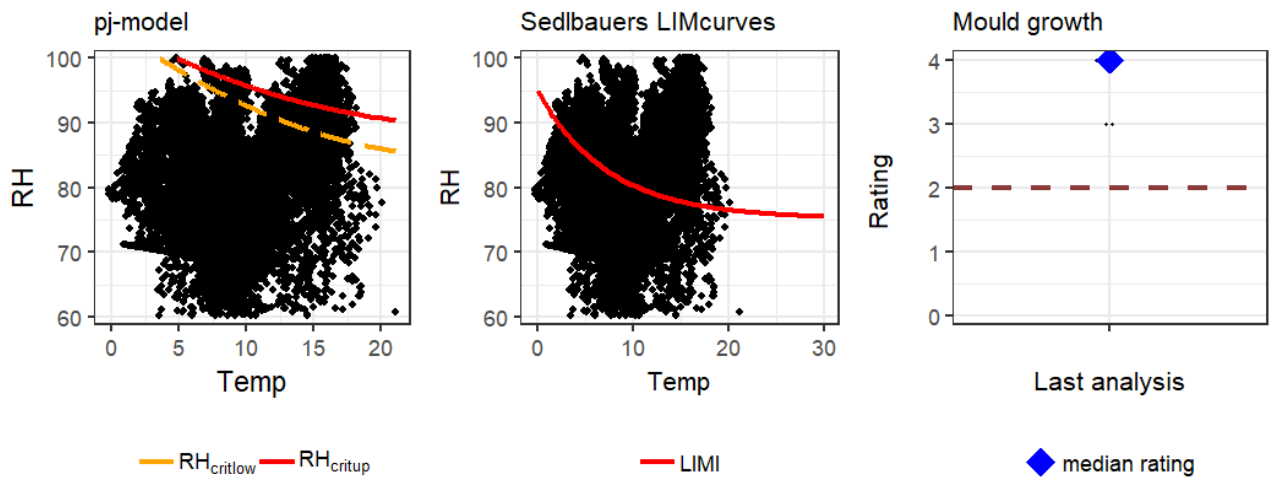

Climate5, Thin hardboard

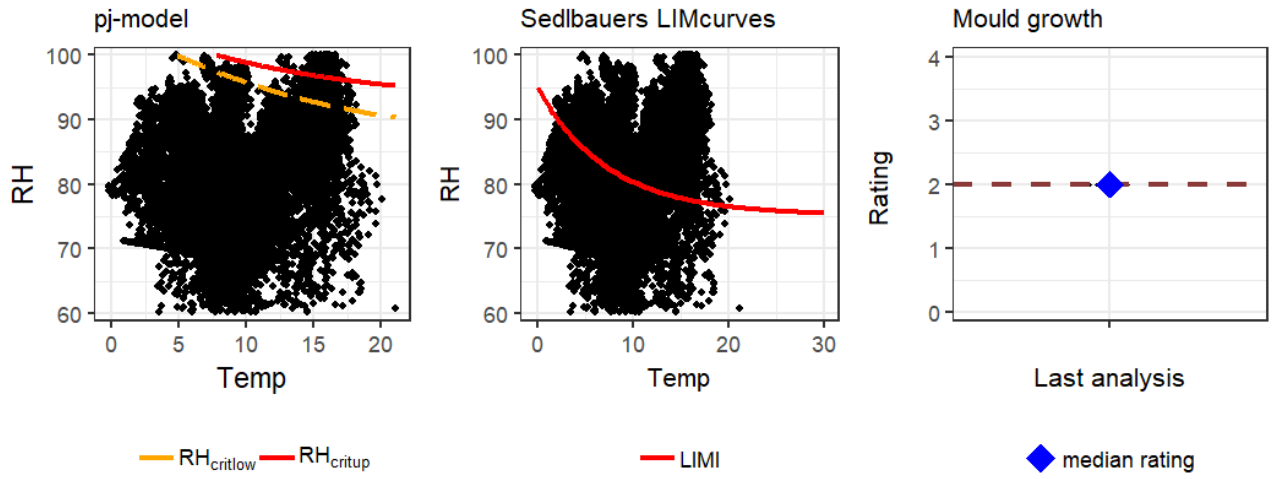

Climate5, Gypsum board

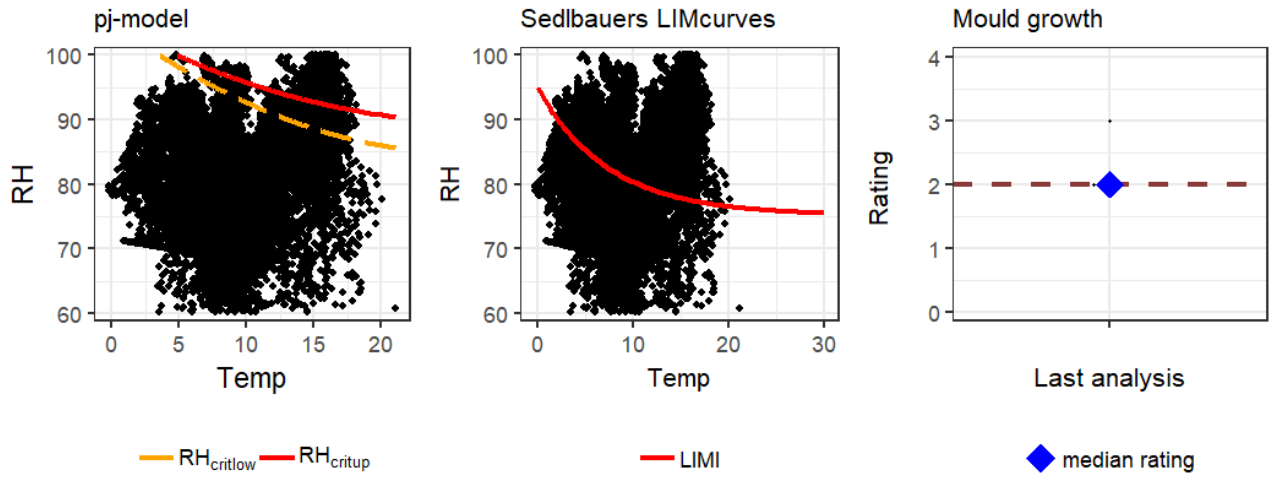

Climate5, Spruce

Appendix 4. Salt in wall

A4.1 Introduction

Before deciding whether the external wall is suitable for internal insulation, it should be clarified what kind of damage the building owner should look for and what failure criteria should be set for each kind of damage. Salt has been considered as one possible damage. There are generally very few data including the effect of salt in materials and there is a lack of measurements on salts in building materials. Collecting data would require many extra measurements. Including salts in the hygrothermal simulations would also complicate things. From an academic point of view, they should be included. However, as there are many different mixtures of salt, it is outside the scope of this project from a practical point of view.

Should we accept that the tool in WP6 could not be used if salt can cause a problem? But how often is salt the cause of problems? In Denmark, salt can often cause a problem, especially in basements and in ground floors of multi-storey residential buildings. These lower walls could then be treated in a different way. There also exist offer mortars for extraction of salts, but this takes time.

A4.2 Summary of questionnaire in Denmark

To qualify whether salt should be regarded as a problem, a number of people within the Danish building sector and at Danish research institutes where contacted by telephone. This included the Brick Masonry Centre at the Danish Technological Institute, The National Museum of Denmark, a consulting engineer, and architects being or having been Royal Building Inspectors (i.e. they are/were involved in renovation of buildings for the Danish Agency for Culture and Palaces).

In summary, all the interviewed persons could refer to specific cases where salt seemed to be a problem as it could affect the behaviour of the external wall, but the interviews gave no overall picture of whether salt should be regarded as a problem. There were different opinions of the size of the problem, although it was the general opinion that salt within brick masonry is difficult to remove. Also that the problem is not increasing. However, the architects seldom got the chance to follow-up on their renovation project, e.g. to see whether the use of a certain type of plaster was effective or not, as it could be another company that did the follow-up.

One of the interviewees mentioned that more than 1-2 % by weight of salt in brick masonry is problematic but was not able to tell how often this is the case. In addition, the type of salt is important, as not all types are equally damaging; a chemical analysis is needed to detect the type. Another one mentioned that measuring the salt content is important in any case as the presence of salt will affect moisture measurements and how they should be evaluated. He also mentioned that salt in relation to internal insulation should not be a problem. It takes time for salt to enter and typically, the salt concentration is low, even over a longer time span.

His experience is that the type of raw materials used for brick and mortar and the history (use) and construction of the building, e.g. the foundation of the building or whether it has a moisture barrier in the external wall, is more important than geography. The fact that the problem still exists can partly be explained by loss of knowledge on how to compose a strong, workable mortar.

Other interviewees however mentioned that buildings located at west oriented coasts in Denmark are more exposed to salt and gave specific examples of that, and also that it could take very long time of exposure, e.g. 100 years, before damages appeared as a result of accumulation of salt.

For Denmark a "salt map" exists, see Figure A4.1, based on information from the Danish Meteorological Institute, edited by Danish Technological Institute.

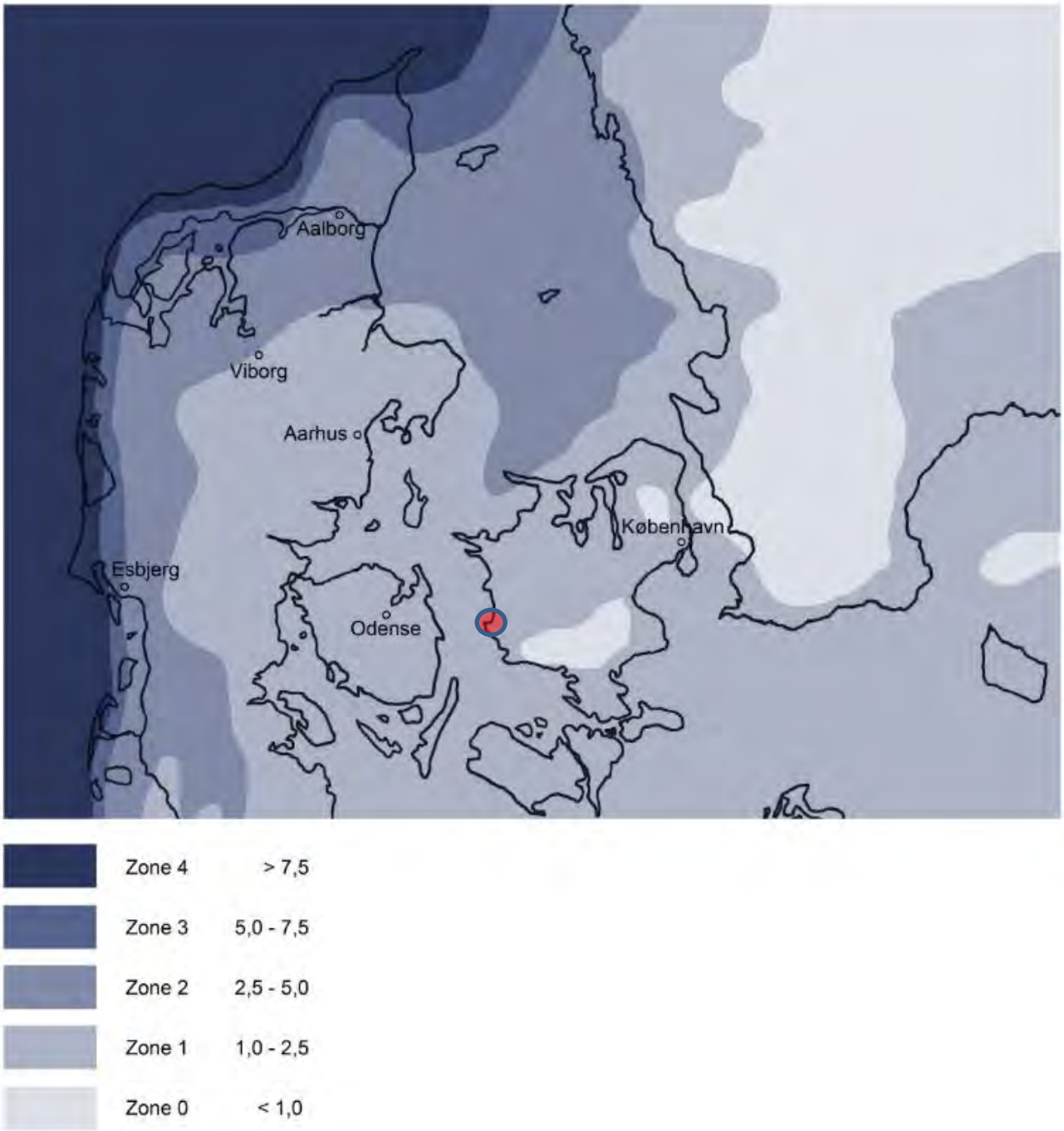

Figure A4.1. "Salt map" illustrating the load of salt expressed as deposition of Na-ions in tons/km^2/year. At specific locations the load may be higher than indicated, e.g. at Korsør (the red dot). A building located in zone 2-4 should refer to exposure class MX4 unless it is protected within an area of single-family houses, a town or other kind of shelter. According to Eurocode 6 (EN 1996, 2005-2006), brick masonry must be placed in one of five exposure classes (MX1-MX5) of which MX4 covers 'exposure for salt saturated air, sea water or de-icing salt'. Examples are brick masonry in coastal areas or brick masonry close to roads that are de-iced with salt during winter. Source: Danish Technological Institute and (MURO, 2016).

Several of the interviewees mentioned medieval churches as heavily exposed, especially bell towers, probably as churches are the oldest brick masonry buildings in Denmark. Further, one of the interviewees mentioned that masonry made of red bricks was more prone to salt related damage than masonry made of yellow bricks, and that buildings made of limestone or sand stone were less prone. Meaning the damage caused by salt is probably most pronounced in countries with a high percentage of external walls of red brick masonry.

Impregnation of external walls could be a way to avoid further salt transport into the wall as it would slow down moisture uptake from the surrounding air, but this has not been properly investigated at present. In some specific cases a special plaster, that can take up more salt than usual plasters, has been used to protect the masonry without hindering moisture diffusion outwards.

Problems related to salt will depend on the moisture content; only when the external wall has a lower relative humidity than the equilibrium moisture content of the type of salt present in the wall, the salt will crystallize and may cause problems.

In recent years, salt used to remove snow and ice on roads and pavements has become more important, especially when snow slings afterwards throw the snow towards buildings. Or salt brought into garages by cars, from where it travels into the masonry. In addition, the increased use of diffusion open materials can risk being a problem as it allows moisture to diffuse without the salt that crystallizes, thereby the salt concentration in the material increases.

A4.3 Conclusion

Salt complicates DELPHIN simulations by affecting the moisture content, and the characterization model does not include a parameter to describe salt storage capacity. Furthermore, it was not possible to get a clear picture of the number of damages related to presence of salt or locate it to specific types of buildings. Therefore, to be on the safe side, it was decided within RIBuild not to include salt in the simulations and for the WP6 web tool not to recommend the use of internal insulation if visual inspection could detect (unwanted) presence of salt.

A4.4 References

Eurocode 6: Design of masonry structures, EN 1996-1-1:2005, EN 1996-1-2: 2005, EN 1996-2:2006, EN 1996-3:2006.

MURO (2016). Murerhåndbogen. Prepared by Technological Institute, Department for Masonry, for MURO. Copenhagen.

Appendix 5. Control and prevention of mould growth for internal post-insulation. Laboratory based investigations of the materials' water activity and pH relative to mould growth (DTU)

A5.1 Introduction

At the Department of Civil Engineering at the Technical University of Denmark (DTU), a laboratory experiment was constructed to investigate the application of several internal insulation systems. 17 test walls were assessed, and the investigated insulation systems included: 1) Calcium silicate boards, 2) Lightweight mineral insulation boards, 3) Polyurethane foam boards with calcium silicate channels, 4) Phenolic foam insulation boards, and 5) Cork and lime based insulating render.

A5.1.1 Objective

The objective of the study is to find the causes and conditions that lead to mould growth between the existing wall and the installed insulation material, and suggest solutions to prevent mould growth. The study examines whether the alkaline environment (pH> 9), which may occur in the adhesive glue joint between the existing wall and the installed insulation is sufficient to prevent mould growth, even if the moisture (water activity (a_w)) at the interface exceeds the levels (a_w> 0.75) commonly considered critical for mould growth (Brandt et al., 2013; Sedlbauer, 2002). Furthermore, the mould species found in the interface will remain mapped to determine their toxic potential.

A5.1.2 Background

Several different insulation systems on the market consists of an insulation material and an adhesive glue mortar. According to the producers, these systems prevent mould growth from occurring by means of combining an inorganic insulation material with and a high pH adhesive glue mortar creating an environment where mould cannot survive. However, experiments at the Technical University of Denmark have shown that growth may occur in the experimental setups for some insulation systems.

Furthermore, preliminary experimental results indicate, that it is not possible to keep the moisture level down in some constructions with internal post-insulation, one must secure them against mould growth in other ways. This can be done by ensuring that all organic residues (e.g. glue and tape residues), from which mould can live off, have been removed before installation of the insulation system. Another option is to apply mould-inhibiting agents before installation. In both cases, it is of interest to know if a highly alkaline environment in the adhesive glue joint can help prevent mould growth, and, if so, the extent to which the alkaline environment in adhesive glue joint can be maintained.

A5.2 Method and materials

A5.2.1 The experimental setup

Preparation of test walls

The experimental setup consisted of 17 masonry test walls with the dimensions (LxWxH): 350 mm x 350 mm x 180 mm. The height of 180 mm included 10 mm internal render. The test walls were originally constructed in 2015, and the mortar joints were assumed carbonized. The study was performed in three parts: 1) material testing, 2) mould decontamination methods, and 3) internal insulation on solid masonry walls. The latter two were carried out using two sizes of plastic boxes; the smaller box with the exterior dimensions (LxWxH): 600 mm x 400 mm x 100 mm, and the large (LxWxH): 780 mm x 560 mm x 440 mm.

During the experiments, each test wall was sealed on the sides using a primer (DANA LIM;, 2018) and wet room membrane (LIP, 2018). The test wall was then placed inside the smaller box on a plastic grate, keeping the test wall above the demineralized water inside the box. The joint between test wall and box lid was sealed using silicone sealant, while the joint between box and lid was sealed using tight vapour barrier tape. An Ø100 mm hole was made in the lid in order to refill water into the small box, and the opening was tightened using a rubber plug. After assembly, the small boxes with test walls were placed inside the large boxes, sensors were installed inside the large box (during mould decontamination part) and later at the interface between masonry and insulation system (during internal insulation part). The joint between the large box and lid was then sealed using rubber sealing strips, and secured using tightening clamps, see Figure A5.1.

The experiment was performed at the indoor test facilities at the Department of Civil Engineering at DTU in Kongens Lyngby, Denmark. The indoor climate of the test facility was kept at 20 °C, with a relative humidity of around 30-40 %. The desired relative humidity in the small box was >96%, which should ensure favourable moisture levels for mould growth at the interface.

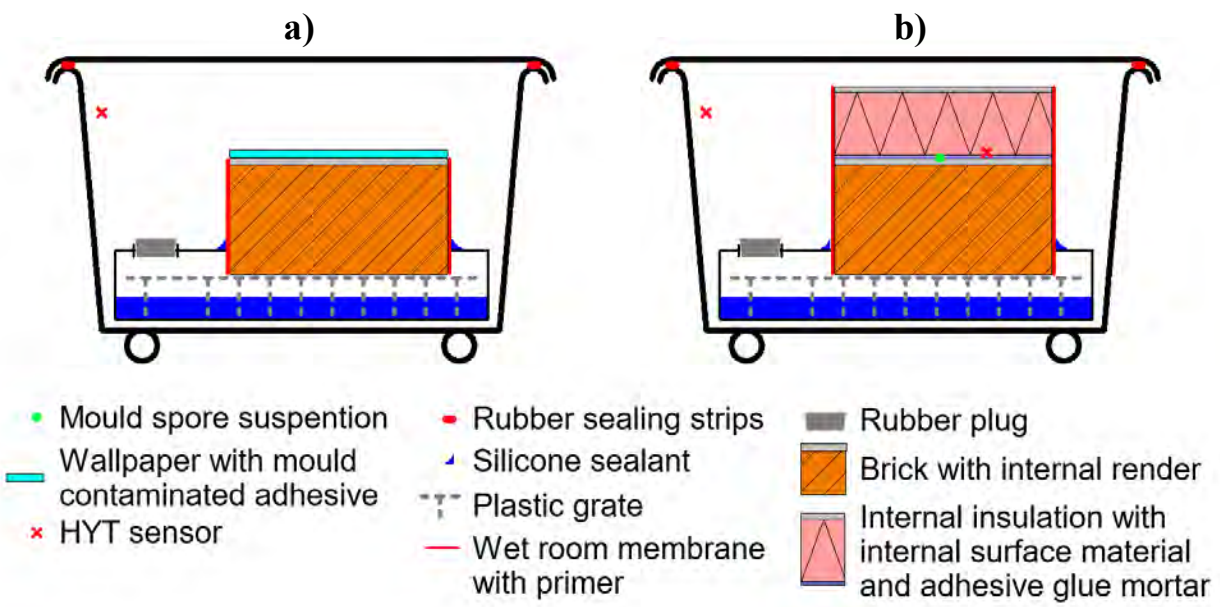

Figure A5.1: Experimental setup. (a) Mould decontamination methods and (b) Internal insulation on solid masonry

Measurement setup

Temperature and relative humidity were measured manually every 1-2 weeks throughout the experimental periods with mould decontamination and testing of internal insulation. Measurements were carried out using digital HYT221 sensors by Innovative Sensor Technology IST AG (IST, 2017), which were calibrated using saturated salt solutions prior to installation. During the mould decontamination period, sensors were installed only inside the large boxes, while during testing of internal insulation sensors were installed inside the boxes, at the interface between masonry and insulation, and two sensors for the indoor climate of test facility. The accuracy of the HYT221 sensors were 0.2 K at 0 - 60 °C for temperature, and 1.8 % at 23 °C at 0 - 90 % RH for relative humidity. The measurement range was -40 - 125 °C for temperature, and 1 - 100 % RH for relative humidity.

A5.2.2 Material testing

In order to better identify the risk of mould growth and determining governing factors for the systems assessed in the internal insulation experiment, it was necessary to perform material testing to determine the moisture transport properties of the adhesive glue mortar and verify the values for the insulating render system. Furthermore, the water vapour diffusion resistance was determined for the wet room membrane. Table 5.1 show the materials used in the internal insulation experiment, and the main properties if available. Note that no material properties were found in datasheets for the latter five products. However, these will be determined over the course of this study and will be presented in the results.

Table A5.1: Utilized materials and their properties. *marked values were obtained from datasheets, other values from material testing by Technische Universität Dresden

Material	Density, ρ [kg/m^3]	Thermal conductivity, λ_{dry} [W/(m·K)]	Water vapor diffusion resistance factor, μ_{dry} [-]	Water absorption coefficient, Aw [kg/(m^2 ·s^{½})]
Yellow soft-moulded brick	1643	0.600	16.9	0.2782
7.7% lime adjusted mortar, grain size 1-4 mm (air lime)	1243.3	0.440	22.43	0.39
CalsithermKalk	185*	0.059*	3.6	0.765*
Ytong Multipor	98.5	0.038	6.73	0.0060
IQ-Therm	45	0.031	27	0.0129
Kingspan	35.5	0.020	113.73	0.0089
Diasen Diathonite Thermactive.037	250*	0.037*	3*	0.1291*
Ytong Multipor Lightweight mortar	830	0.155	13	0.0031
IQ-Fix adhesive mortar	1313	0.497	18.75	0.0051
IQ-Top render	725	0.147	11.73	0.1070
Saint-Astier mineral lime mortar				
LIP Multi Fliseklæb				
Rødvig Juramørtel KKH 35/65/500 (Natural hydraulic lime mortar)				
LIP VS 30 (wet room membrane)				
DANA LIM Væggrunder Gele Ekstra 228 (wall primer)				

Water vapour diffusion resistance factor

The water vapour diffusion resistance factor, μ was determined through cup experiment (wet cup), according to DS/EN ISO 12572 – Hygrothermal performance of building materials and products – Determination of water vapour transmission properties – Cup method ("DS/EN ISO 12572:2016, Hygrothermal performance of building materials and products – Determination of water vapour transmission properties – Cup method, 2. edition," 2016). The water vapour diffusion resistance factor was determined for the adhesive glue mortars, Diasen Diathonite Thermactive.037, and the LIP VS 30 wet room membrane. This was done by sealing the test samples inside a test cup containing a saturated salt solution to obtain stable conditions inside the cup, in this case KNO_2 (94% relative humidity). The test cup was placed in a climate chamber with controlled temperature and relative humidity. Due to a difference in water vapour pressure on each side of the test sample, a vapour flow through the sample occurred. Through periodical weighting of the test cup, the rate of water vapour transmission was determined. Three samples of each product were tested. The sample size was Ø80 mm, and a sample thickness of the full product (5-10 mm for the glue mortars and 40 mm for the insulating render). For the LIP VS 30 wet room membrane, the test was performed with the membrane applied to a 12.5 mm gypsum board as well as test of the gypsum board without the membrane.

Water absorption coefficient

The rate of water absorption by capillary action was determined by partial immersion according to DS/EN ISO 15148:2003 – Hygrothermal performance of building materials and products – Determination of water absorption coefficient by partial immersion ("DS/EN ISO 15148:2003, Hygrothermal performance of building materials and products – Determination of water absorption coefficient by partial immersion, 1. edition," 2003). The water absorption coefficient was determined by measuring the mass of partial immersed test samples, where the bottom surface was in contact with water for an extended period. The sides of the samples were sealed against water intrusion. "Hanging" water droplets (not absorbed by the test sample) were removed through blotting with a damp sponge before weighting the samples. The experiment was carried out for the adhesive glue mortars and the Diasen Diathonite Thermactive.037 insulating render. Three samples of each product were tested, with a total contact surface of more than 300 cm^2 per product.

pH-value

There has been an increased focus on pH-value of the adhesive glue mortars, as the manufacturers of insulation systems for internal retrofitting claim the glue mortars maintain a high pH-value over an extended period of time, creating unfavourable growing conditions for mould at the interface.

Drillings of the core samples were made in the internal insulation experiment for determination of mould growth, and from these samples the adhesive glue mortars were separated from the insulation layer and placed in separate sealed containers. The adhesive glue mortars were crushed into powder, and 5 g of the powder was then mixed with 12.5 ml demineralized water in small plastic flasks. The mixtures were then shaken for 60 min using a Promax 2020 (Heidolph, 2019) with an act speed of approximately 260-270 revolutions per minute. Hereafter the flasks were standing of 10 min for the mixtures to settle before carrying out the measurements. The pH measurement were carried out using a Sension+ MM374 (HACH, 2019), and the measuring stick was flushed with demineralized water before each measurement. The pH-value was also determined from the fresh glue mortar samples upon installation of the insulation systems, and from glue mortar samples exposed to high doses of CO_2 for rapid carbonization. The carbonization of the glue mortar samples was tested using phenolphthalein.

Susceptibility to mould growth
The insulation materials and adhesive glue mortars were investigated for their susceptibility to mould growth. Previous research by DTU Bioengineering (Andersen et al., 2017) have shown that some building material contain embedded mould spores from the production process, which grow out when the moisture conditions are favourable. Sterile water was added to all the materials, and they were then incubated at 20 °C in darkness, in plastic boxes with high relative humidity (> 96 %). If spores were present in the materials, they would grow out. In additional, the materials were also tested by inoculating the samples with known mould spores and treated as mentioned above. In case of sufficient organic nutrition (dust and dirt from the environment) in the materials, mould growth would occur. All materials were assessed for mould growth every 14 days for three months.

A5.2.3 Mould testing

This section describes the procedures used to test for mould growth in the air and the test walls. Air samples were taken before taking samples for the test walls. Mould samples for the test walls were obtained by drilling out one core sample for each test walls using a 100 mm wide hole saw (without pilot bit). The core samples were taken from the internal surface to the interface between the existing wall and adhesive glue mortar. The entire saw was disinfected using ethanol before each drilling to avoid contamination, and the core samples were placed in sealed containers immediately after each drilling. After each drilling, two Mycometer Surface samples and two swab samples were taken at the interface. Note that the mould testing procedures described in this section are preliminary and may be subject to change as the experiments progress.

Tape samples
Tape samples were taken at prior to mould decontamination, on the internal surface of the contaminated test walls (on the woodchip wallpaper) before removing the wallpaper and testing the decontaminating methods. This was done to determine if the mould species found on the test walls were the same as the ones mixed into the adhesive for the wallpaper in the mould decontamination experiment. The samples were taken by placing the sticky side of a tape piece on the area being sampled and pressing gently to make contact. The tape piece was then removed and placed on a sterile glass slide, and then immediately placed in a sealed container. Two samples were taken per test wall. In the laboratory, the mould species were determined under microscope.

Air samples
Air samples were taken inside each of the large experimental boxes and for the indoor climate of the test facility in order to test if the mould species found in the air was the same as found inside the test walls. The air samples were carried out using a MAS-100 Eco (Merek, 2019). The device blew 100 l of air over an agar plate over a duration of 1 min. V8, and DG18 were used as growth media. In the laboratory, the media were incubated at 25 °C in darkness and the mould species determined under microscope.

Mycometer Surface
The Mycometer Surface test was carried out in order to determine the quantity of mould growth at the interface between the masonry and the adhesive glue mortar. The Mycometer method determines the amount of mould by measuring the fluorescent product released from the enzyme-substrate complex relating to the N-acetylhexosaminidase activity found in mould growth (Krause, 2003; Mycometer, 2012; Reeslev & Miller, 2000; Schrock et al., 2011).

The interface samples were taken using sterile cotton buds. The cotton buds were wetted in sterile water, and the samples were taken within the self-adhesive measurement area (of approximately 9 cm^2) placed at two different locations at the interface (within the drilling hole). During sample taking, the cotton bud was held at a low angle to the measurement surface, and the bud was rotated to utilized as much as possible of the cotton. The cotton buds were placed in sealed containers immediately after sample taking (Mycometer, 2018c).

At the laboratory, the samples were analysed using the Mycometer Surface method (Mycometer, 2017, 2018b). Before each of the two testing rounds (after mould decontamination and at the end of the measurement period), the fluorometer was calibrated according to the test protocol (Mycometer, 2017). Before commencing the analysis, all chemicals had to have room temperature.

A reaction tube was prepared with 1 ml of Substrate and 1 ml of Activator for each of samples, and one additional tube for blind testing. A cuvette was prepared with 2 ml Developer for each of samples, and one additional for blind testing. The room temperature was noted and used to determine the reaction time. The sample cotton buds were placed in the reaction tubes and the timer started. At the end of the reaction time, the reaction liquids were stirred with the cotton buds before removing the buds. Immediately after removal of the cotton buds, 100 µl of reaction liquid was transferred to the cuvettes containing Developer and stirred using the transfer pipette. The cuvettes now containing Developer and reaction liquid were then analysed with the fluorometer to obtain the analyse values (AV). To obtain the blind value (BV), 100 µl of the mixture of Substrate and Activator in the additional reaction tube was transferred to the additional cuvette with Developer, and the cuvette was analysed with the fluorometer. Finally, to obtain the Mycometer value (MV), the following equation was used:

$$MV = AV - BV \qquad (1)$$

The following evaluation categories were used for the Mycometer values:

A = the measured value does not exceed normal background levels (MV ≤ 25)

B = the measured value does exceed normal background levels (25 ≤ MV ≤ 450)

C = the measured value is high due to active mould growth (MV ≥ 450)

Mycometer Material

The Mycometer Material test was carried out in order to determine the quantity of mould growth in different layers of the insulation system. Through this obtain knowledge about the potential for mould growth penetrating the insulation system and contaminate the indoor environment.

In the laboratory, the core samples were prepared for the Mycometer Material test using a hobby knife (disinfected before preparing each sample). The outer parts of the core sample were cut away (excess insulation, adhesive glue mortar and internal surface material), until we were left with the centre part of the core sample, as shown with green on Figure A5.2. A total of four pieces were made from the centre part, and the cut areas are shown with red. As shown, there were two samples near the interface, and two samples made from the remaining thickness of the insulation layer. After achieving the desired sample pieces, each piece was crushed into powder.

Same procedures were used for reaction time, blind testing and analysis with the fluorometer as for the Mycometer Surface test (section A5.2.3). However, instead of placing cotton buds into the reaction tube containing Substrate and Activator, a suitable (weighted) amount of material powder

was added to a tube, and the reaction time started. The same amount of material powder was used for all samples. After the reaction period, the material powder was filtered out of the reaction liquid, as the material powder could cause misleading results during the analysis with the fluorometer. From the outcome of the Mycometer Material test it was possible to determine the fluorescent product per mg of material powder (Mycometer, 2010, 2018a).

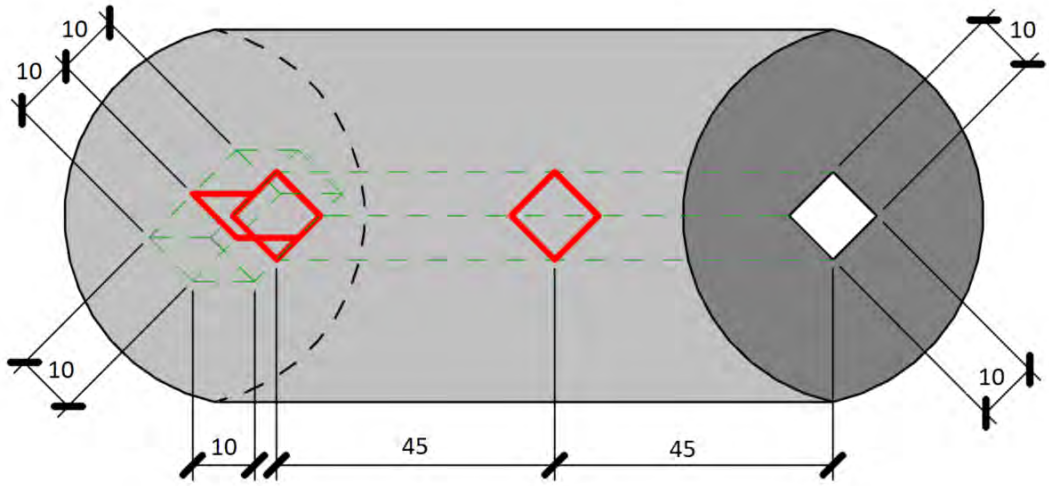

Figure A5.2: Illustration of a drilling core sample, and the material samples for the Mycometer Material test. Green lines indicate the parts of the core sample used in the test, and the red lines where the centre part of the core sample was separated

Swab test

The swab tests were carried out in order to determine the mould species growing inside the test walls, and if these species were the same as found in the indoor climate of the test facility. Following the Mycometer Surface swap tests, the swab samples were taken using sterile cotton buds at the interface between the masonry wall and the internal insulation systems. The cotton buds were placed in sealed containers immediately after each swab. At the laboratory, spores from the cotton buds were spread out on agar plates (V8, and DG18) through stroking. The agar plates were incubated at 25 °C in darkness, and the mould species were determined under microscope.

A5.2.4 Test of mould decontamination methods

After the material testing, three mould decontamination methods were investigated. For this experiment, 12 of the 17 existing masonry test walls (LxWxH: 35 cm x 35 cm x 18 cm) were used, four walls for each decontamination method. Woodchip wallpaper was applied to all 12 test walls, which was installed using wallpaper adhesive based on potato starch mixed with spores from four of the most common indoor climate moulds (Acremonium murorum, Aspergillus versicolor, Penicillium chrysogenum and Wallemia sebi). The small boxes were placed inside the large boxes, and the test walls were left for a period of three months (see Figure A5.1a). After three months the test walls were decontaminated for organic nutrition and mould growth using the following methods: 1) Hand-power: wallpaper, adhesive and mould were removed manually from the internal surface using a paint scraper, 2) Mechanical: wallpaper, adhesive, mould and internal render were removed manually using hammer and chisel (a new render layer was applied later), and 3) MicroClean: wallpaper and adhesive were removed manually using a paint scraper, while mould was removed using the MicroClean method (Bunch-nielsen, 2009; Hartung, 1996; SSG A/S, 2019). The method was carried out in four steps:

1. Vacuum the infected surface with a HEPA-filter.
2. Dry-steam cleaning with plate mouth piece, with a steam pressure of 8 atm and a temperature of 150-160 °C.
3. Dry-steam cleaning with a fibred cotton cloth mouth piece, with simultaneous vacuuming of denatured dissolved biomass. The cotton cloths were changed continually as they became saturated with moisture and biomass.
4. Vacuum the surface again with a HEPA-filter.

For the decontamination process, the small boxes were removed from the large boxes, to avoid potential contamination issues during the decontamination process. All large boxes, and the small boxes containing test walls for decontamination methods 1 and 2 were decontaminated using mould cleaning agents (Protox, 2019d, 2019c, 2019b, 2019a), meanwhile the small boxes for decontamination method 3 were decontaminated using the MicroClean method. After decontamination of test walls and boxes, the small boxes with test walls were placed back inside the large boxes, and the test walls were again exposed to the wet climate inside the small box (>96% RH) for 14 days. Finally, to test the effectiveness of the decontamination methods, the amount of mould present on the test walls was determined using the Mycometer Surface method (section A5.2.3).

A5.2.5 Test of insulation systems on solid masonry test walls

The 12 decontaminated test walls and the five uncontaminated test walls were given a spore solution contained the mould species described in section A5.2.4. The solution was given at the centre of the interface surface area of each test wall. Hereafter four different insulation systems (all except Diasen insulating reader) were installed according to the manufactures instructions, on 16 of the test walls so that each insulation system would be installed for each of the decontamination methods as well as on the uncontaminated walls (see A5.2). On the 17th (uncontaminated) test wall, the Diasen Diathonite Thermactive.037 was installed.

Table A5.2: Parameter variations in the internal insulation experiment

	Mould decontamination method			
	Contaminated			Uncontaminated
Material	Manual	Mechanical	Dry steam	No decontamination
CalsithermKalk	X	X	X	X
Ytong Multipor	X	X	X	X
IQ-Therm	X	X	X	X
Kingspan	X	X	X	X
Diasen Diathonite Thermactive.037				X

The insulation systems were installed with the following materials and thicknesses, on the internal side of the existing test walls with 10 mm render:

- CalsithermKalk: 10 mm Saint-Astier mineral lime mortar, 100 CalsithermKalk, and 8 mm Saint-Astier mineral lime mortar.
- Multipor: 8 mm Ytong Multipor Lightweight mortar, Ytong Multipor, and 8 mm Ytong Multipor Lightweight mortar.
- IQ-Therm: 10 mm IQ-Fix, 80 mm IQ-Therm, and 10 mm IQ-Top.
- Kingspan: 10 mm LIP Multi Fliseklæb, and 100 mm Kingspan Kooltherm K118 (with perforated aluminum foil on external side, and unperforated aluminum foil and 12.5 mm gypsum board on internal side).

- Diathonite Thermactive: 40 mm Diasen Diathonite Thermactive.037, and 10 mm Rødvig Juramørtel KKH 35/65/500 (NHL).

After installation, the small boxes containing the test walls were placed inside the large boxes, and the test walls were again exposed to the wet climate inside the small box (>96% RH) for three months (see Figure A5.1.b). After the experimental period, mould air samples were takes inside the large boxes and for the indoor climate according to section A5.2.3 and through the insulation systems were determined according to sections A5.2.3. The pH-value of the adhesive glue mortars was determined (according to section A5.2.2) with specimens from the core samples.

A5.3 Results

At the time of writing the report, only a few results were available as the experiment with internal insulation on solid masonry walls had just started up. Furthermore, the data for the previous parts had not yet been analysed. Results from the study will be included in the updated version of deliverable D2.2.

A5.4 References

Andersen, B., Dosen, I., Lewinska, A. M., & Nielsen, K. F. (2017). Pre-contamination of new gypsum wallboard with potentially harmful fungal species. *Indoor Air*, *27*(1), 6–12. https://doi.org/10.1111/ina.12298

Brandt, E., Bunch-Nielsen, T., Christensen, G., Gudum, C., Hansen, M. H., & Møller, E. B. (2013). *SBi-Anvisning 224 - Fugt i Bygninger (Danish)* (2nd ed.). Hørsholm, Denmark: Statens Byggeforskningensinstitut, Aalborg University.

Bunch-nielsen, T. (2009). Skimmelsanering (Danish). Retrieved November 26, 2018, from https://www.teknologisk.dk/_/media/37592_skimmelsaneringsprocessen - Tommy Bunch-Nielsen.pdf

DANA LIM; (2018). Væggrunder Gele Ekstra 228 (Danish). Retrieved November 1, 2018, from https://s3-eu-west-1.amazonaws.com/denoteit.com/danalim/produktinformation/dk/228.pdf

DS/EN ISO 12572:2016, Hygrothermal performance of building materials and products – Determination of water vapour transmission properties – Cup method, 2. edition. (2016). Charlottenlund, Denmark: Dansk Standard/Danish Standards.

DS/EN ISO 15148:2003, Hygrothermal performance of building materials and products – Determination of water absorption coefficient by partial immersion, 1. edition. (2003). Charlottenlund, Denmark: Dansk Standard/Danish Standards.

HACH. (2019). Sension+ MM 374 GLP 2 channel Laboratory Meter for pH, ORP, ISE and Conductivity. Retrieved January 16, 2019, from https://www.hach.com/sension-mm-374-glp-2-channel-laboratory-meter-for-ph-orp-ise-and-conductivity/product?id=7640520232

Hartung, A. (1996). Tør damp dræber skimmel (Danish). Retrieved January 11, 2019, from https://ing.dk/artikel/tor-damp-draeber-skimmel-15627

Heidolph. (2019). Promax 2020 Shakers & Mixers. Retrieved January 16, 2019, from

https://heidolph-instruments.com/en/products/Shakers-Mixers/Promax-2020~p1206

IST. (2017). HYT 221 Module. Retrieved May 10, 2018, from https://www.ist-ag.com/sites/default/files/DHHYT221_E.pdf

Krause, J. D. (2003). Analytical Instrument Performance Criteria Application: Application of a Fluorometric Method for the Detection of Mold in Indoor Environments. *Applied Occupational and Environmental Hygiene*, *18*(7), 1–5. https://doi.org/10.1080/10473220301457

LIP. (2018). LIP VS 30 Vandtætningsmembran (Danish). Retrieved November 1, 2018, from http://www.lip.dk/media/536145/0905_lip-vs-30-vandtaetningsmembran.pdf

Merek. (2019). MAS-100 Eco. Retrieved January 16, 2019, from http://www.merckmillipore.com/DK/en/product/MAS-100-Eco,MM_NF-C150448?ReferrerURL=https%3A%2F%2Fwww.google.com%2F

Mycometer. (2010). *ANALYSE AF MATERIALEPRØVER MED MYCOMETER ® -TESTEN (Danish)*. Hørsholm, Denmark.

Mycometer. (2012). mycometer surface: On-site fungal contamination assessment. Retrieved from http://cdn.mycometer.com/fileadmin/user_upload/Pdf/Mycometer-Surface_Flyer__2012_.pdf

Mycometer. (2017). Mycometer ® -surface Bulk Hurtigprotokol (Danish).

Mycometer. (2018a). BULK SAMPLING (porous materials). Retrieved November 21, 2018, from https://www.mycometer.com/products/mycometer-surface/bulk-sampling-porous-materials/

Mycometer. (2018b). ONSITE QUANTIFICATION OF MOULD ON SURFACES IN LESS THAN AN HOUR. Retrieved November 16, 2018, from https://www.mycometer.com/products/mycometer-surface/about-mycometer-surface/

Mycometer. (2018c). SURFACE SAMPLING. Retrieved November 16, 2018, from https://www.mycometer.com/products/mycometer-surface/surface-sampling/

Protox. (2019a). ProtoxHysan - Produktdata (Danish). Retrieved January 16, 2019, from https://protox.dk/produkter/hysan/hysan-produktdata/

Protox. (2019b). ProtoxHysan (Danish). Retrieved January 16, 2019, from https://protox.dk/produkter/hysan/?gclid=CjwKCAiA99vhBRBnEiwAwpk-uGpWXc1QcfT5mf6uoVhp9mYppECLCxL4hWOL7SxzanU93tAmeLba7xoCddYQAvD_BwE

Protox. (2019c). ProtoxSkimmel - Produktdata (Danish). Retrieved January 16, 2019, from https://protox.dk/produkter/protoxskimmel/protoxskimmel-produktdata/

Protox. (2019d). ProtoxSkimmel (Danish). Retrieved January 16, 2019, from https://protox.dk/produkter/protoxskimmel/

Reeslev, M., & Miller, M. (2000). The MycoMeter-test. A new rapid method for detection and quantification of mold in buildings. *Proceedings of Healthy Buildings*, *1*, 589–590.

Schrock, M., Riffle, C., Dindal, A., Mckernan, J., & Enriquez, J. (2011). *Environmental Technology*

Verification Report: Mycometer ®-test Rapid Fungi Detection and Bactiquant ®-test Rapid Bacteria Detection Technologies.

Sedlbauer, K. (2002). Prediction of Mould Growth by Hygrothermal Calculation. *Journal of THERMAL ENV. & BLDG. SCI.*, *25*(4), 321–336. https://doi.org/10.1106/109719602024093

SSG A/S. (2019). Micro Clean ®-metoden. Retrieved January 16, 2019, from https://www.building-supply.dk/supplement/view.html?id=6632